Interim Report for Phase II – Task 3 of the Comprehensive Study to Understand Longitudinal ERW Seam Failures

"Defect Characterization: Types, Sizes, Shapes, and Idealizations"

Authors

Bruce A. Young, Jennifer M. O'Brian, and Richard Olson

Battelle Memorial Institute
505 King Avenue
Columbus, OH 43201

Prepared for

U.S. Department of Transportation
Pipeline and Hazardous Materials Safety Administration
1200 New Jersey Ave., SE
Washington DC 20590

Contract No. DTPH56-11-T-000003
Battelle Contract No. G006084
Battelle Project No. 100004552

May 2017

Battelle does not engage in research for advertising, sales promotion, or endorsement of our clients' interests including raising investment capital or recommending investments decisions, or other publicity purposes, or for any use in litigation.

Battelle endeavors at all times to produce work of the highest quality, consistent with our contract commitments. However, because of the research and/or experimental nature of this work the client undertakes the sole responsibility for the consequence of any use or misuse of, or inability to use, any information, apparatus, process or result obtained from Battelle, and Battelle, its employees, officers, or Directors have no legal liability for the accuracy, adequacy, or efficacy thereof.

Acknowledgments

Useful discussions during this phase of the project with B.N. Leis of B.N. Leis, Inc. and D.J. Shim of EMCC are acknowledged. Likewise, the preparation of Attachment A on Stress Intensity Factor Solutions, by D.J. Shim eta al. of EMCC is acknowledged.

Executive Summary

On November 1, 2007 a liquid propane pipeline operated by Dixie Pipeline Company ruptured near Carmichael, Mississippi, which several pipeline industry experts collaboratively indicated the origin was likely a defect in the longitudinal ERW seam, with the ensuing fracture running along that joint into portions of the adjacent pipes. These experts also noted that a seam-integrity assessment did not prevent the failure, as this failure came 2 years after an in-line inspection (ILI) with a sophisticated crack-detection tool; and 23 years after a hydrostatic test to a hoop stress level greater than 1.25 times the maximum operating hoop stress level. Following the NTSB's public report, the NTSB issued Recommendation P-09-1, which called upon the PHMSA to conduct a comprehensive study to identify actions that can be used by operators to eliminate catastrophic longitudinal seam failures in pipe, and indicated the required scope. This led to the PHMSA issued a research announcement (RA) that targeted Recommendation P-09-1 in the form of BAA Solicitation DTPH56-11-RA-000001. That Solicitation sought a Comprehensive Understanding of Longitudinal ERW Seam Failures.

In response to that Solicitation, Battelle, as the prime contractor, proposed a two-phase project to work to develop the understanding sought by the research announcement in resolving Recommendation P-09-1.

The Phase I final report was issued in January 2014 and can be found at the following website: https://primis.phmsa.dot.gov/matrix/PrjHome.rdm?prj=390. Phase II has five tasks including:

- Task 1: Hydrotest protocols
- Task 2: ILI and ITDM Inspection Assessment
- Task 3: Defect Characterization: Types, Sizes, Shapes, and Idealizations
- Task 4: Model Validation
- Task 5: Software Development for Integrity Management of Long Seam Welds.

This report focuses on the results obtained during the work completed under Phase II, Task 3 which includes the development of analytical stress intensity solutions for various defect types, sizes, and shapes. Details of the finite element analysis (FEA)

methods used in the development are provided along with a summary of the results. The results of this task are implemented in the software development task (Task 5).

Contents

List of Figures

List of Tables

Acronyms

PipeAssess PI™	Battelle's Cracking Assessment for Pipeline Software
ERW	Electric Resistance Welded
FW	Flash Welded
HAZ	Heat Affected Zone
ID	Inner Diameter
ILI	Inline Inspection
ITDM	In the Ditch Method
KAI	Kiefner and Associates, Inc.
LF	Low Frequency
OD	Outer Diameter
SIF	Stress Intensity Factor
TW	Through-Wall
OD	Outer Diameter of Pipe
t	Wall thickness of Pipe
d	Weld cap height
a	Crack depth through the thickness of pipe
2c	Total crack length along the pipe axis for surface cracks
2W	Width of the weld in the circumferential direction
a1	Depth of the selective seam corrosion
2c1	Width of the selective seam corrosion cracking at the OD (or tope of the weld cap)
2c2	Width of the general corrosion for selective seam weld corrosion cracking
a2	Depth of the general corrosion for selective seam weld corrosion cracking
a3	Crack depth for the crack portion for selective seam weld corrosion cracking

Introduction

Work under Phase I followed a scope identified from National Transportation Safety Board (NTSB) Recommendation P-09-1 that developed understanding of longitudinal Electric Resistance Welded (ERW) seam failures by: 1) generating a database that quantified the industry and Government experience in regard to hydrotest and in-service failures, 2) completing a full-scale project that empirically quantified ERW seam failure behavior and resistance, and 3) developing technology to assess susceptibility to selective seam corrosion. Phase II builds on that understanding by establishing the viability of condition monitoring technology that relies on hydrotesting, in-line non-destructive inspection, and in-the-ditch nondestructive inspection along with the development of the engineering tools to translate condition into viable metrics of defect severity and re-inspection interval specific to ERW seam defects. Viability in all aspects will be assessed and demonstrated through use of full-scale burst tests that address the range of defects characteristics across that seen in the database developed in the initial phase of this of project. Management tools will be developed for use by pipeline operators as part of their integrity management plan to assure that their ERW pipelines are safe. This report focuses on the results obtained during the work completed under Phase II, Task 3.

Phase II, Task 3

This activity characterizes defect size and shape by defect type, defining a consistent basis to quantify these key inputs to the predictions of defect severity, and the timeline for operator response and re-inspection. The key parameter of concern here is the crack stress intensity factor (SIF) for typical ERW crack geometries. Because errors in depth can, in some cases, cause predictions of failure behavior to error by a factor of ten or more, this activity addresses the necessary accuracy for these parameters relative to their practical significance, from both an analytical and measurement perspective. Analytically, this activity addresses the fact that size and shape, as typically seen in the field, are poorly represented by the library of stress intensity factors previously available

in predictive models, by using finite element analysis to bridge this gap. Basically, new stress intensity factor solutions have been developed for pipe/defect geometries likely to be found in Flash Weld (FW) and Electric Resistance Weld (ERW) pipe, using advanced finite element analysis techniques. This activity bridges the measurement gap relative to the how ILI and In-the-Ditch-Methods (ITDM) must quantify and report size and shape to be useful in defect sensitivity analysis, identifying what sizing accuracy is needed, and the conditions under which adjacent axial planar defects interact.

The objective of this activity is to bridge technology gaps in defect characterization in regard to types, sizes, shapes, and analytical idealizations relevant to the FW and ERW processes by generating a catalogue of new stress intensity factor solutions for crack shapes and sizes likely to be encountered in FW and ERW pipe. This activity increases pipeline safety by critical improvements to the tools necessary to implement both ILI and hydrotesting, and demonstrating their viability. Realizing that autogenously generated upset-welds formed by FW, Low Frequency (LF) ERW and High Frequency (HF) ERW processes all share the same dependence on heat and pressure to create a forged bond line and lead to similar types of features, this activity will bridge the technology gaps in terms of two groups of effectively planar defects – located either in the bond line, the upset, or the Heat Affected Zone (HAZ). Activities have considered drivers for failure of each defect type, relative to how the weld-process, the steel, and the service conditions affect that failure. For purposes of improved predictive modeling, each defect type was characterized relative to its axial through-wall (TW) appearance as flat and planar (as for cold welds and simple hook cracks and selective seam weld corrosion (SSWC)) versus non-planar and complex (as occurs for other hook cracks and SSWC). SSWC can be further quantified relative to its transverse cross-section that reduces the net-section – either symmetrically or asymmetrically. Finally, this activity will idealize each defect type relative to its local properties, and modes of failure, such that predictive models can be established along with improved/new test methods/practices. It is anticipated that a range of idealized geometries will be needed to capture reality from the simple through quite complex shapes observed.

As indicated previously, this activity addresses the fact that, analytically, size and shape, as typically seen in the field, are poorly represented by the library of stress intensity factors available in predictive models. Attachment A provides an overview of the finite element methods used to obtain the results reported. Appendix A provides the summary plots for the various defects types.

Defect Types

Cold Weld

Elliptical Surface Flaw

Surface-breaking, semi-elliptical cold welds are idealized as shown in Figure 1. An example of an actual cold weld that this would represent is provided in Figure 2. Finite element methods were employed to determine the stress intensity factors (SIF) of single finite length anomalies either on the pipe inner diameter (ID) or outer diameter (OD). Solutions were also determined for infinitely long anomalies. These solutions are available in Attachment B. For use of SIFs within the software developed in Task 5, SIF solutions for finite flaws were ensured to have asymptotic solutions consistent with infinitely long flaws such that cracks can transition continuously from finite to "infinite" length, provided they do not become surface-breaking prior to the asymptotic solution. Once an anomaly becomes through-wall and thus represents a leak, PipeAssess PI™ considers it a failure.

If an anomaly does not become surface-breaking by the time its half-length reaches 50 times the crack depth at the center of the crack (i.e., c/a = 50), the length is considered sufficiently "infinite" and the respective infinite surface-crack SIFs are assumed. The SIF solutions approach the infinitely-long solution before c/a = 50 and often begin this plateau-like behavior at smaller c/a ratios. At infinite length, all through-thickness SIFs have plateaued and are constant at a given though-thickness value regardless of subsequent growth in the length direction. This asymptote was determined by evaluating the finite and infinitely long SIFs crack solutions side-by-side and observing when one would smoothly transition to the other as the crack grows. This was verified for both large diameter, intermediate thickness pipe (36" diameter, 0.382"

thickness) through small diameter, thin wall (8", 0.180" thickness) pipe. A conservative threshold was chosen to ensure the crack length grows sufficiently to reach the asymptotic SIF. This asymptote varies as the crack grows in depth, which is accounted for in PipeAssess PI™.

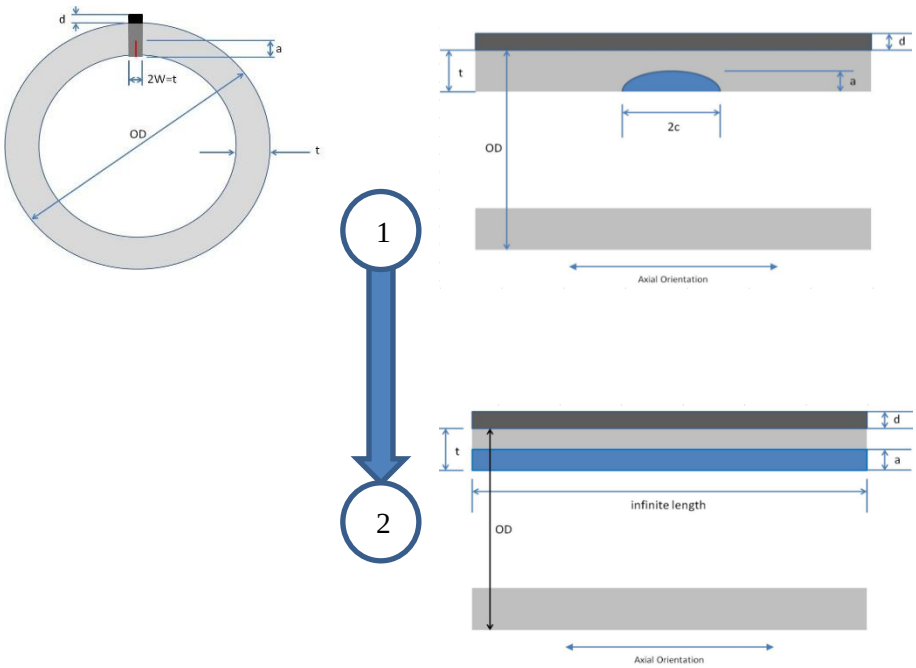

Figure 1: ID Semi-Elliptical Flaw SIF Evolution: Beginning Flaw (1) Grows, Which Includes Growth to Infinite Length (2) if Does Not Reach Through-Wall Before Failure

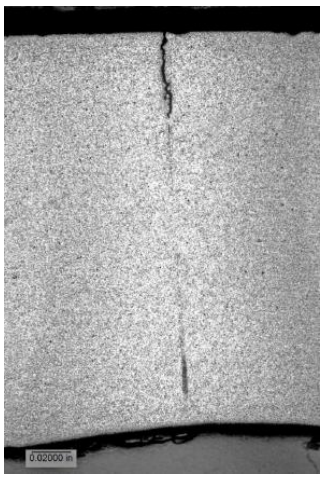

Figure 2: Example of Part-Through Wall OD Cold Weld in LF-ERW Pipe [1]

For finite length, part-through-wall, the SIFs were determined at both the deepest point in the idealized anomaly as well as at the crack tips at the pipe surface. This is important when PipeAssess PI™ grows cracks in fatigue, as it may grow at a different rate in the length direction versus the through-wall direction. These differences are incorporated with unique SIFs solutions; one is denoted "deep" for the through wall-direction and the other "surface" for the crack tip at the pipe surface. These locations are pointed out in Figure 3. In the event of multiple cracks in close proximity, the single crack solution is used for each anomaly and multiple crack coalescence is defined per British Standard 7910. Bond line stitching, an example of multiple cracks in proximity, is shown in Figure 4. A summary of SIF solution bases for elliptical surface flaws in PipeAssess PI™ is presented in Table 1.

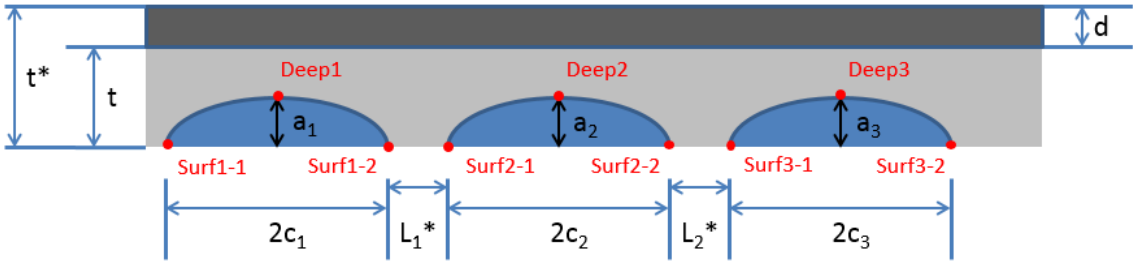

Figure 3: SIF Location Definition of Surface versus Deep and for Multiple Anomalies in Proximity to One Another [2]

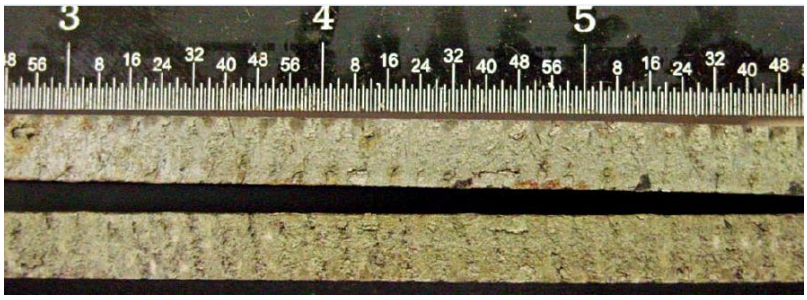

Figure 4: Example of Stitching Along a LF-ERW Bondline [1]

Table 1: SIF Solution Base by EMC^2 That Are Implemented Into PipeAssess PI™ for *Semi-Elliptical* Cold Weld Flaws

Anomaly Type & SIF Location	SIF Solution Base
Semi-Elliptical **ID** Cold Weld, K **Deep**	1.6 CW_E_ID_PTWC_S_3D_Deep + 1.1 CW_IL_ID_PTWC_S_2D_Deep
Semi-Elliptical **ID** Cold Weld, K **Surface**	1.6b CW_E_ID_PTWC_S_3D_Surf
Semi-Elliptical **OD** Cold Weld, K **Deep**	1.7 CW_E_OD_PTWC_S_3D_Deep + 1.2 CW_IL_OD_PTWC_S_2D_Deep
Semi-Elliptical **OD** Cold Weld, K **Surface**	1.7b CW_E_OD_PTWC_S_3D_Surf

Rectangular Surface Flaws

Surface-breaking, rectangular cold welds can be idealized as shown in Figure 5. An example of an artificially generated rectangular cold weld is provided in Figure 6. As depicted, the rectangular defect grows in a semi-elliptical fashion in fatigue and eventually, evolves into a well-developed semi-elliptical flaw. Finite element method solutions were not available for the transition from a rectangular geometry to an elliptical geometry. Thus, an elliptical geometry solution is assumed as an approximation. Specifically, a semi-ellipse geometry with the same cross-sectional area and maximum depth as the rectangular input is used. Identical to the underlying elliptical anomalies, SIFs for finite and infinitely long flaws were joined to cover a broader range of crack lengths. This transition scheme is depicted in Figure 5. A summary of SIF solution bases for rectangular flaws in PipeAssess PI™ is given in Table 2.

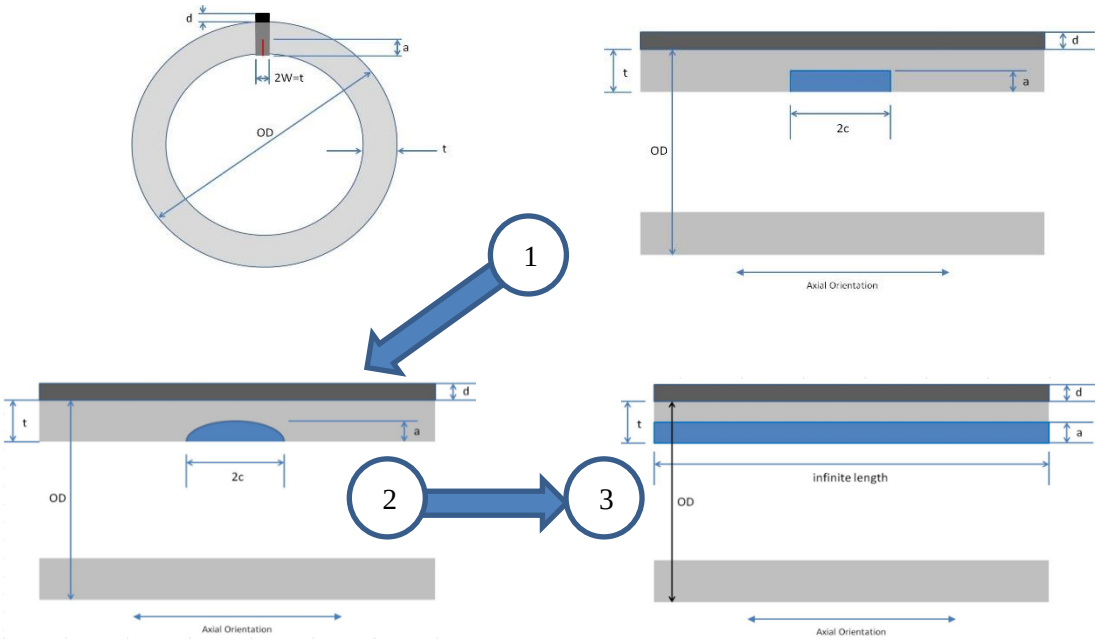

Figure 5: ID Rectangular Flaw SIF Evolution: Beginning Flaw (1) is Converted to ID Semi-Elliptical Flaw (2) for Semi-Elliptical Growth, which Includes Growth to Infinite Length (3) if Not Through-Wall Before Failure

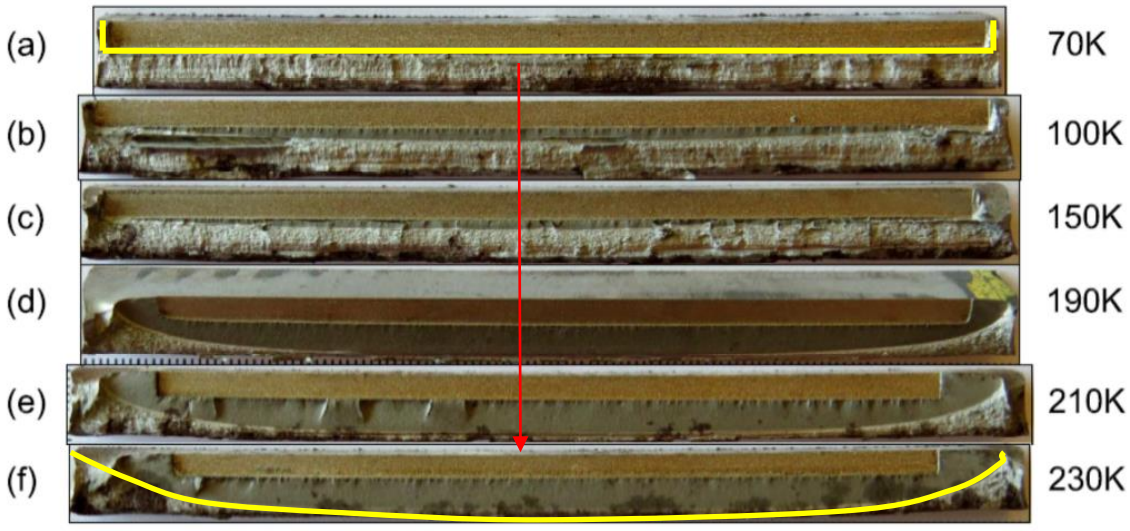

Figure 6: Initial EDM Rectangular Flaw Grows as Semi-Ellipse Under Fatigue [3]

Table 2: SIF Solution Base by EMC^2 that are Implemented in PipeAssess PI™ for *Rectangular* Cold Welds

Anomaly Type & SIF Location	SIF Solution Base
Rectangular **ID** Cold Weld, K **Deep**	1.6 CW_E_ID_PTWC_S_3D_Deep + 1.1 CW_IL_ID_PTWC_S_2D_Deep
Rectangular **ID** Cold Weld, K **Surface**	1.6b CW_E_ID_PTWC_S_3D_Surf
Rectangular **OD** Cold Weld, K **Deep**	1.7 CW_E_OD_PTWC_S_3D_Deep +1.2 CW_IL_OD_PTWC_S_2D_Deep
Rectangular **OD** Cold Weld, K **Surface**	1.7b CW_E_OD_PTWC_S_3D_Surf

Selective Seam Weld Corrosion

V-Notch Flaw

V-notch selective seam weld corrosion (SSWC) is idealized as shown in Figure 7, Figure 8, and Figure 9. In each scenario, two finite element SIF solutions were merged such that a seam corrosion pit can seamlessly transition to a corrosion pit with a growing crack at the bottom in the PipeAssess PI™ software. Note that the corrosion pit does not grow in the model, only the crack.

An example of V-notch SSWC in the field is provided in Figure 10. Note that these are 2D geometry models and as such, anomaly axial length and SIFs for the crack tips at the surface are not applicable. SIF solution bases for V-notch SSWC defects are summarized in Table 3.

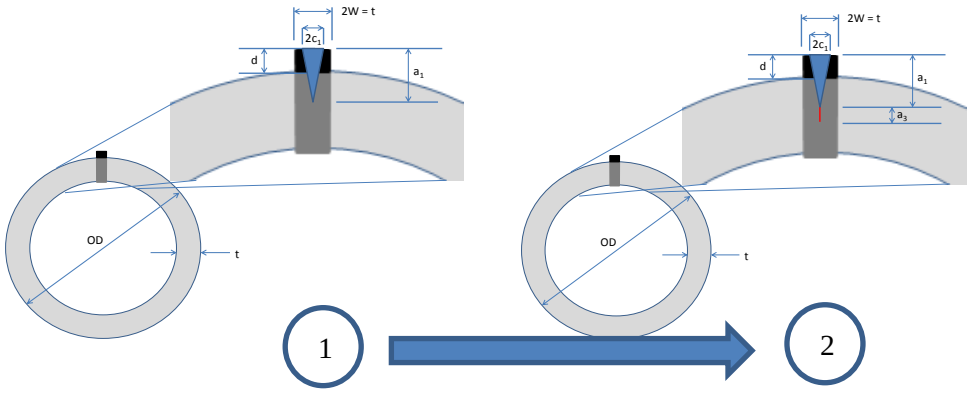

Figure 7: SSWC V-Notch (Solution 2.1; Shown Left) Was Joined with V-Notch with Crack (Solution 2.4; Shown Right)

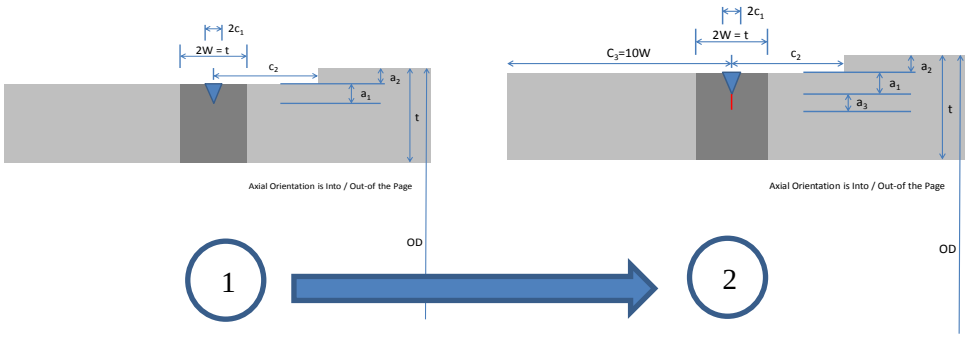

Figure 8: SSWC V-Notch with Asymmetric General Corrosion (Solution 2.3; Shown Left) Was Joined with Equivalent SSWC with a Crack (Solution 2.6; Shown right)

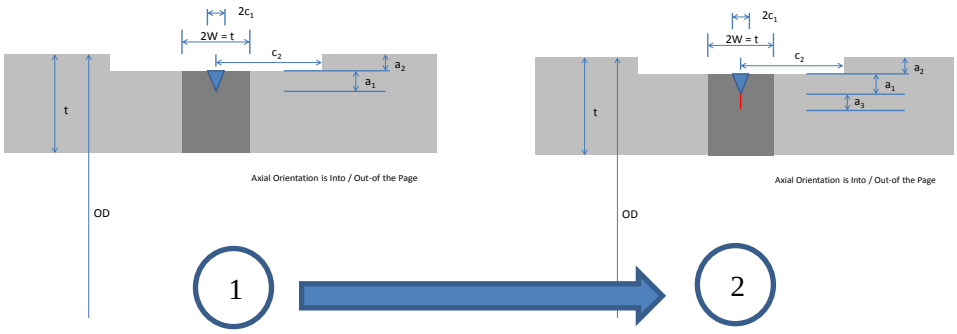

Figure 9: SSWC V-Notch with Symmetric General Corrosion (Solution 2.2; Shown Left) Was Joined with Equivalent SSWC with a Crack (Solution 2.2; Shown Right)

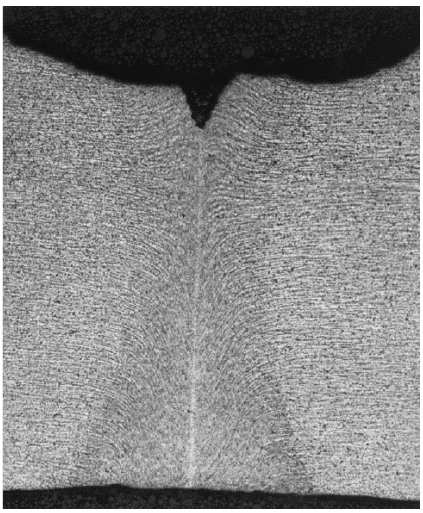

Figure 10: Example of SSWC with V-Shaped Selective Corrosion [1]

Table 3: SIF Solution Base by EMC2 That Are Implemented in PipeAssess PI™ for V-Notch SSWC

Anomaly Type & SIF Location	**SIF Solution Base**
V-Notch SSWC with **No General Corrosion**, K **Deep**	2.1 SSWC_V_2D_N_N_Deep + 2.4 SSWC_V_2D_N_Y_Deep
V-Notch with **Symmetric General Corrosion**, K **Deep**	2.2 SSWC_V_2D_S_N_Deep + 2.5 SSWC_V_2D_S_Y_Deep
V-Notch with **Asymmetric General Corrosion**, K **Deep**	2.3 SSWC_V_2D_A_N_Deep + 2.6 SSWC_V_2D_A_Y_Deep

U-Notch Flaw

U-notch selective seam weld corrosion (SSWC) can be idealized as shown in Figure 11 and Figure 12. In each scenario, two finite element SIF solutions were merged such that a seam U corrosion pit can seamlessly transition to a corrosion pit with a growing crack at the bottom in the PipeAssess PI™ software. Because the U-notch with symmetric corrosion was not analyzed with a crack, the SIF of the equivalent V-notch geometry was overlaid and modified to mate with the U-notch solution. This is pictorially represented in Figure 11. Note that these are 2D geometry models and as such, anomaly axial length and SIFs for the crack tips at the crack surface tips are not applicable.

A field example of a U-notch SSWC is provided in Figure 13. SIF solution bases for U-notch SSWC defects are summarized in Table 4.

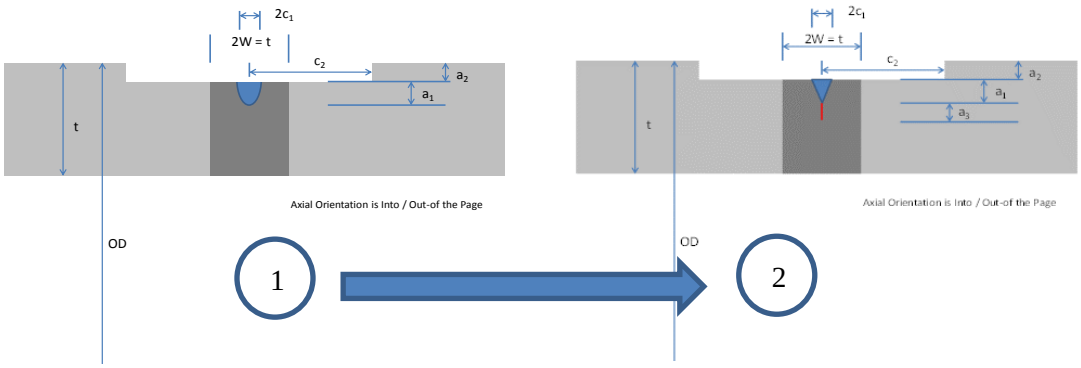

Figure 11: SSWC U-Notch with Symmetric General Corrosion (Solution 2.8; Shown Left) Was Joined with Closest Available SSWC Solution with a Crack (Solution 2.5; Shown Right)

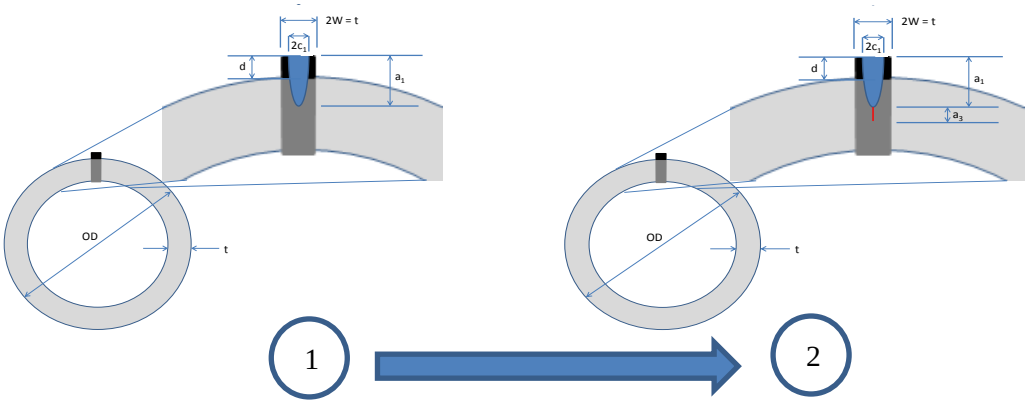

Figure 12: SSWC U-Notch (Solution 2.7; Shown Left) Was Joined with Equivalent SSWC Solution with a Crack (Solution 2.9; Shown Right)

Figure 13: SSWC Example with U-Shaped Selective Corrosion [1]

Table 4: SIF Solution Base by EMC2 That Are Implemented in PipeAssess PI™ for U-Notch SSWC

Anomaly Type & SIF Location	**SIF Solution Base**
U-Notch with **Symmetric General Corrosion**, K **Deep**	2.8 SSWC_U_2D_S_N_Deep + 2.5 SSWC_V_2D_S_Y_Deep
U-Notch with **No General Corrosion**, K **Deep**	2.7 SSWC_U_2D_N_N_Deep + 2.9 SSWC_U_2D_N_Y_Deep

Hook Cracks

A hook crack is typically a manufacturing defect that follows the flow lines of the material in FW/ERW pipe as the edges of the skelp are upset. Examples of hook cracks found in the field are shown in Figure 14 through Figure 17. Hook cracks can be either surface-breaking or fully embedded. They can hook up or down, and the innermost tail of the hook can be at any distance through the pipe wall thickness.

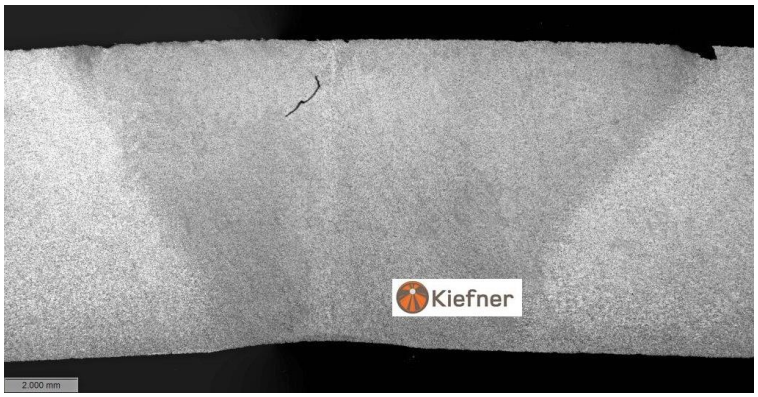

Figure 14: Example of Embedded Hook Crack Curtesy of Kiefner and Associates Inc. (KAI)

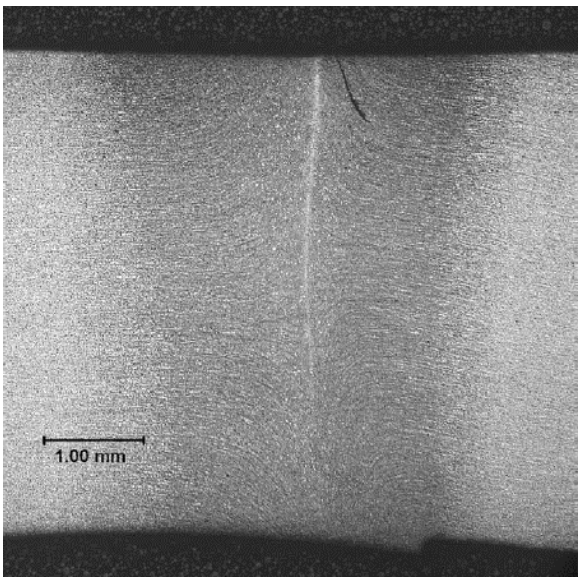

Figure 15: Example of Surface-Breaking Hook Crack Near a LF-ERW Seam [1]

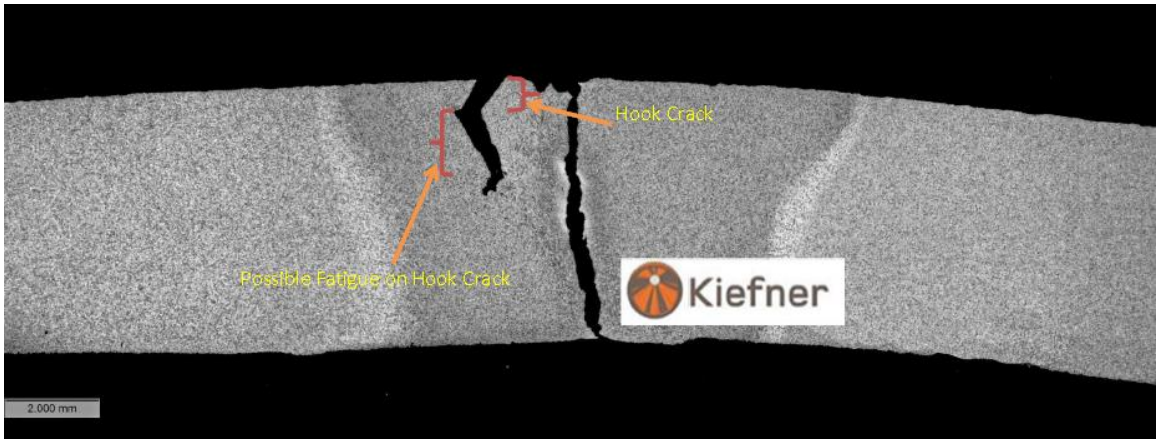

Figure 16: Example of Surface Breaking Hook Crack with Fatigue, Curtesy of KAI

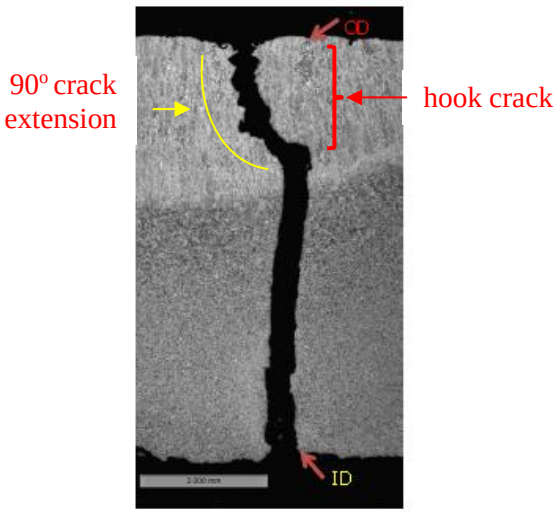

Figure 17: Cross Section of Hook Crack in Battelle Joint 16-36. Hook Crack Curvature Clearly Observed.

A common characteristic of hook cracks is that the crack tips tend to only grow perpendicular to the hoop stress field, i.e., more or less, radially. This observation is supported by field experience as well as theoretical fracture mechanics considerations. Furthermore, if both tips of the hook crack are embedded, the hook crack will have a much reduced SIF from a crack that extends to the ID or OD surface of the pipe.

Although the images shown in Figure 14, through Figure 17 clearly show the curvature of the "hook", current ILI and traditional ITDMs are unable to resolve this level of detail for hook cracks. Upcoming ITDMs such as inversed wave extrapolation (IWEX) have recently been able to determine if an indication is angled or not, but quantifying the amount of curvature of a hook crack is still beyond the inspection technology capability today. An example of the inspection resolution for hook cracks between technologies is illustrated in the following figures; an example IWEX output is provided in Figure 18, PAUT and TOFD in Figure 19, and ILI in Figure 20.

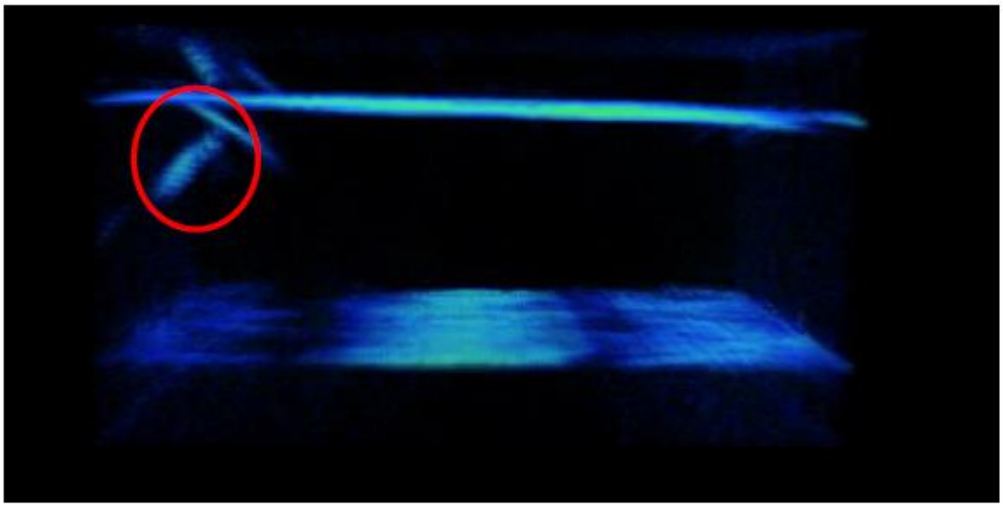

Figure 18: IWEX 3D Image of Hook Crack in Battelle Joint 16-36. Indication Visibly Angled but Extent of Hook Crack Curvature Unknown.

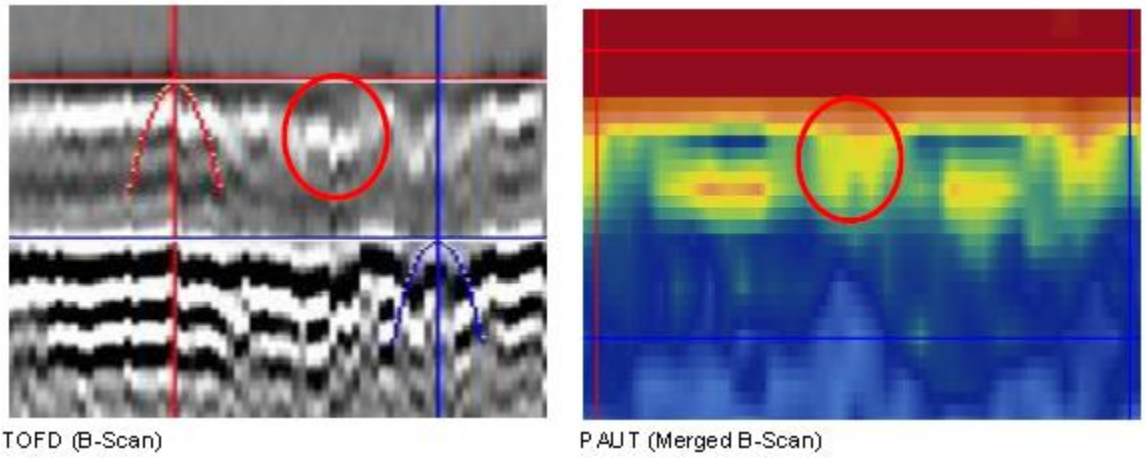

Figure 19: TOFD and PAUT Image of Hook Crack in Battelle Joint 16-36. Crack Type and Thus Also Extent of Crack Curvature Unknown in these Images.

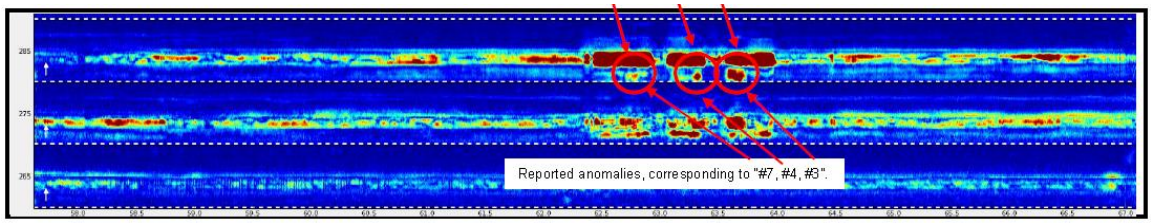

Figure 20: ILI Image of Hook Cracks in Battelle Joint 16-36. Crack Type and Thus Also Extent of Crack Curvature Unknown in these Images.

In light of the extremely wide range of possible innermost hook tail locations, hook heights, and hook widths, the need to respect the fact that crack tips will extend parallel to the hoop stress, and the fact that crack growth must be tracked at two crack tips, it is not practical to perform the tens of thousands of finite element analyses needed to make a generalized hook crack SIF solution. Furthermore, because current inspection technology cannot resolve the geometry of hook cracks consistent with a model based on a known curvature, an approach to estimating the SIF for hook cracks has been adopted that: a) does not demand crack geometry information that simply is not known, and b) respects the fact that an embedded hook crack has a relatively low SIF with respect to surface breaking cracks.

The SIF solution for hook cracks implemented in PipeAssess PI™ is rooted in the API 579-1/ASME FFS-1 infinitely long embedded crack in a pipe and infinitely long surface crack in a pipe solutions, adjusted to reflect the slanted nature of hook cracks and growth in the radial direction. Figure 21 shows the idealization of hook crack geometry used in PipeAssess PI™: The upper hook crack tip is characterized by a distance “h” from the pipe OD, the “height” of the hook crack is defined by “y”, the lateral extent of the hook is defined by “x”, and consistent with the fact that the curvature of the hook simply is not known, the crack is assumed to be a linear feature from the upper tip to the lower tip as shown in the yellow dotted line. The most general case of an embedded hook crack is shown in Figure 21, but distance “h” could be zero. Likewise, cracks can as easily hook downward or left as well as right using the three defining parameters. As limitations, no weld cap is permitted for hook crack solutions and the hook cracks are assumed to be infinite in length.

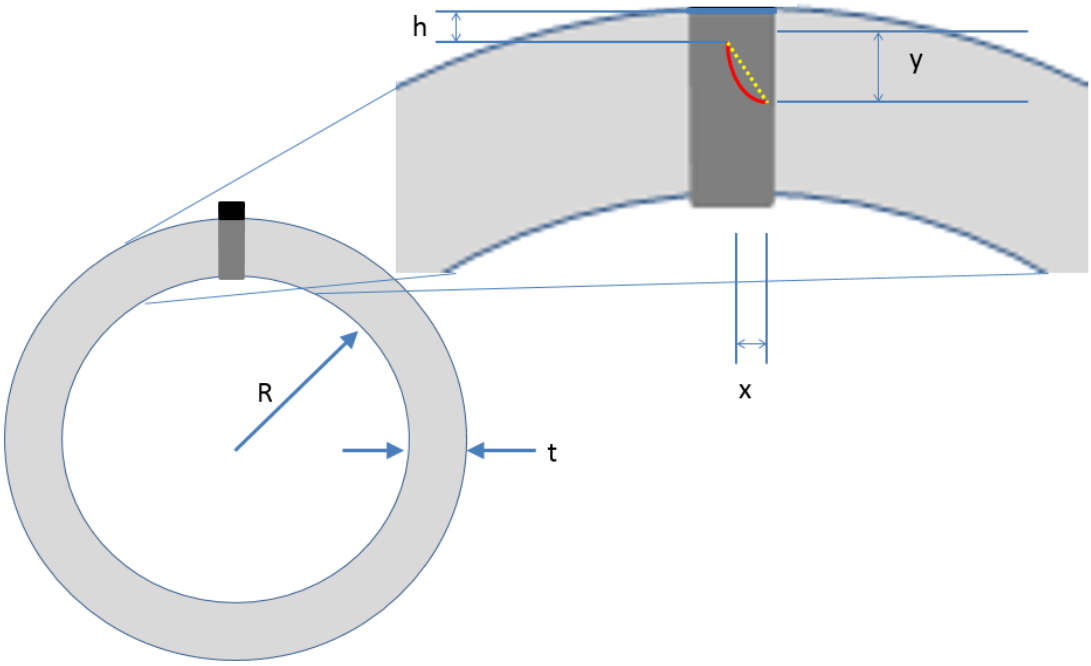

Figure 21: PipeAssess PI™ Hook Crack Geometry Idealization.

The available API579 embedded crack solution is for a radially oriented embedded flaw as shown in Figure 22. This is not the geometry shown in Figure 21, except for the special case of a crack that has "y"=0. Fortunately, some elementary fracture mechanics can be used to account for the slant shown in Figure 21, length of the slant, and crack growth in the radial direction.

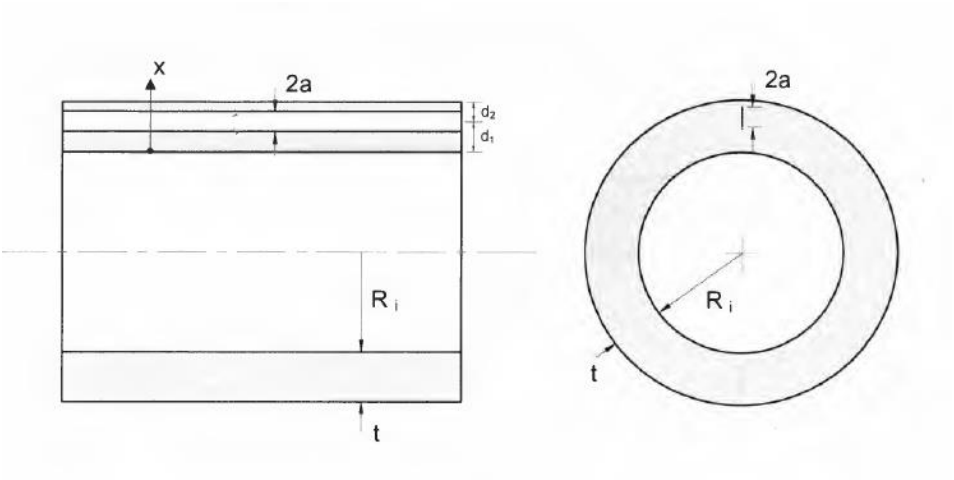

Figure 22: API579 Embedded Pipe Crack Solution Geometry. [4]

From basic fracture mechanics given in Reference [5], given the Mode I (crack opening) SIF of a crack when the stress is applied perpendicular to the crack, the Model I and Mode II (shearing) SIFs at the crack tips for the same crack at some angle β to the applied stress are (see Figure 23):

$$K_{I\beta} = K_{I0} \cos^2 \beta \tag{1a}$$

$$K_{II\beta} = K_{I0} \cos \beta \sin \beta \tag{1b}$$

Considering now a small "kink" at angle α at the crack tip of the crack that is at some angle β to the applied stress as shown in Figure 24, the local Mode I and Mode II SIFs at the tip of the kink are:

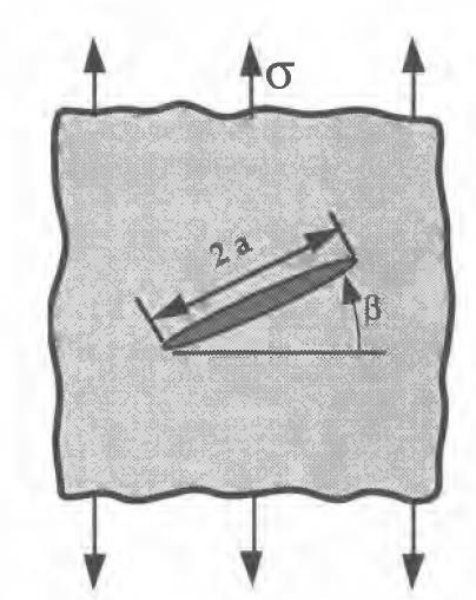

Figure 23: Crack at an Angle in a Uniaxial Stress Field. [5]

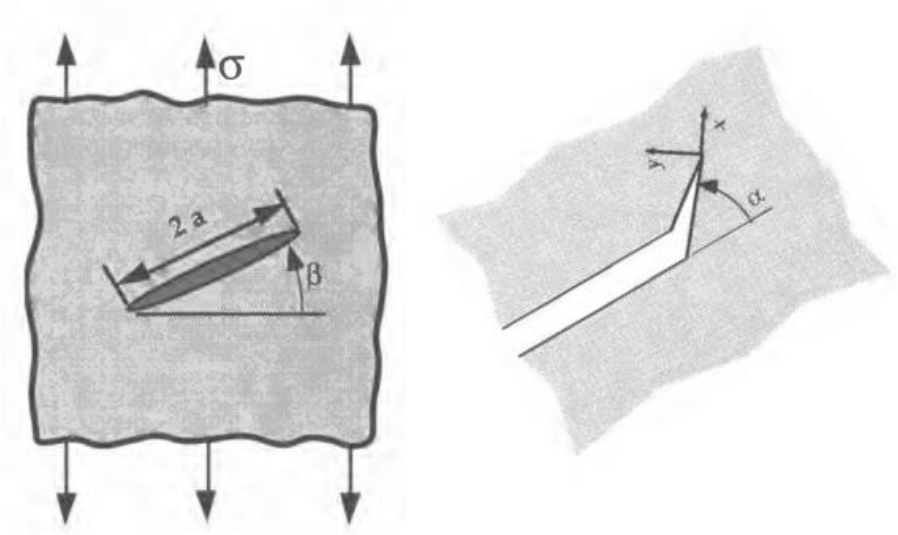

Figure 24: Kink at Angle α to Crack at Angle β. [5]

$$k_I(\alpha) = C_{11}K_{I\beta} + C_{12}K_{II\beta} \tag{2a}$$

$$k_{II}(\alpha) = C_{21}K_{I\beta} + C_{22}K_{II\beta} \tag{2b}$$

where

$$C_{11} = 0.75\cos\left(\frac{\alpha}{2}\right) + 0.25\cos\left(\frac{3\alpha}{2}\right) \tag{3a}$$

$$C_{12} = -0.75\left[\sin\left(\frac{\alpha}{2}\right) + \sin\left(\frac{3\alpha}{2}\right)\right] \tag{3b}$$

$$C_{21} = 0.25\left[\sin\left(\frac{\alpha}{2}\right) + \sin\left(\frac{3\alpha}{2}\right)\right] \tag{3c}$$

$$C_{22} = 0.25\cos\left(\frac{\alpha}{2}\right) + 0.75\cos\left(\frac{3\alpha}{2}\right) \tag{3d}$$

Accordingly, the energy release rate at the tip of the kink is

$$\mathcal{G}(\alpha) = \frac{k_I^2(\alpha) + k_{II}^2(\alpha)}{E} \tag{4}$$

If normalized energy release rate is plotted against kink angle for a range of crack angles, Figure 25, examination of the data indicates that the maximum energy release rate is, more or less, in the direction perpendicular to the applied stress. Furthermore, at this condition, the Mode II SIF is zero. Hence, a crack can only propagate at the angle of maximum energy release rate, i.e., perpendicular to the applied stress, a result completely consistent with field crack growth of hook cracks.

In practice, $\beta = \tan^{-1}\frac{x}{y}$, and it is a simple matter to find the angle α to maximize Equation 4 and thus, one can find corresponding $k_I(\alpha)$ for crack growth, given the Mode I SIF for the API579 radially oriented embedded crack, K_{I0}.

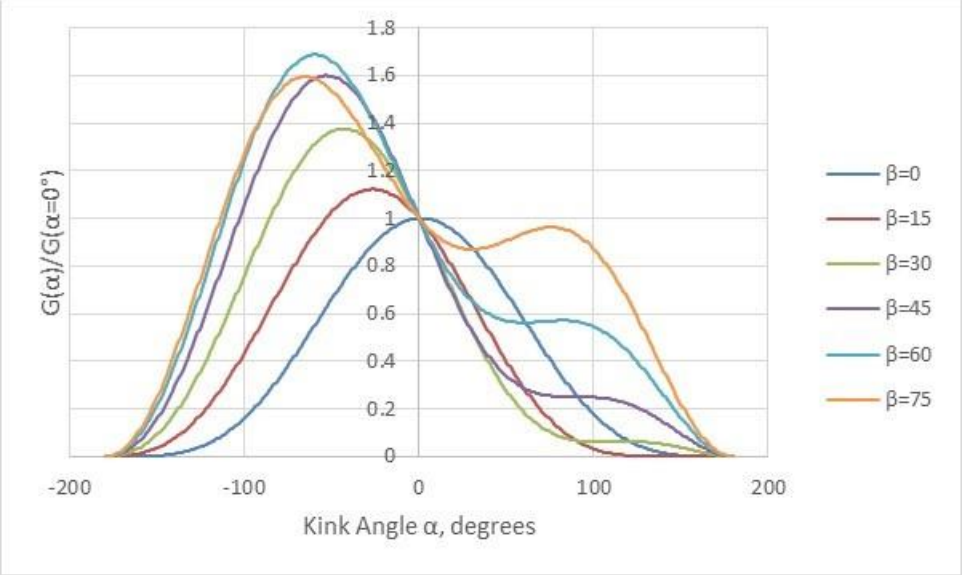

Figure 25: Energy Release Rate at the Tip of a Kinked Crack.

Consider now, the length of an embedded hook crack. By the geometry shown in Figure 21, the crack length = $\sqrt{x^2 + y^2}$. If x = 0, the crack will behave with crack length equal to y. In the case of a crack at the extreme of y = 0, the crack is no longer considered an axial crack and is more representative of a lamination, which is outside this project's scope. In other words, the actual crack could have a length greater than the pipe

wall thickness, even though the hoop stress provides no driving force (i.e. it behaves like the crack length is zero). Drawing from API579, effective embedded crack length can be taken as:

$$(2a)_{eff} = (2a)(cos^2\beta + 0.5sin\beta cos\beta) \quad (5)$$

where (2a) is the known hook crack slant length. This expression for effective crack length satisfies the known boundary conditions at x=0 and y=0, is continuous and provides a slight penalty for crack lengths from $0 < \beta < 27°$.

Putting the fracture mechanics together with the geometric description of the hook crack,

1. $\beta = \tan^{-1}\frac{x}{y}$
2. $(2a)_{eff} = (2a)(cos^2\beta + 0.5sin\beta cos\beta)$
3. Find the SIF (K_{I0}) at the crack tip(s) from the API579 solutions.
4. Find the Mode I and Mode II SIFs at the crack tip at angle β
    a. $K_{I\beta} = K_{I0}\cos^2\beta$
    b. $K_{II\beta} = K_{I0}\cos\beta\sin\beta$
5. Iteratively solve for the angle that maximizes the energy release rate at the crack tips
    a. $\mathcal{G}(\alpha) = \frac{k_I^2(\alpha)+k_{II}^2(\alpha)}{E}$
    b. $k_I(\alpha) = C_{11}K_{I\beta} + C_{12}K_{II\beta}$
    c. $k_{II}(\alpha) = C_{21}K_{I\beta} + C_{22}K_{II\beta}$
    d. $C_{11} = 0.75\cos\left(\frac{\alpha}{2}\right) + 0.25\cos\left(\frac{3\alpha}{2}\right)$
    e. $C_{12} = -0.75\left[\sin\left(\frac{\alpha}{2}\right) + \sin\left(\frac{3\alpha}{2}\right)\right]$
    f. $C_{21} = 0.25\left[\sin\left(\frac{\alpha}{2}\right) + \sin\left(\frac{3\alpha}{2}\right)\right]$
    g. $C_{22} = 0.25\cos\left(\frac{\alpha}{2}\right) + 0.75\cos\left(\frac{3\alpha}{2}\right)$
6. The SIF at the crack tip will be $k_I(\alpha_{\mathcal{G}=max})$

This solution strategy is the general solution which applies to both fully embedded and surface breaking hook cracks.

A summary of hook crack SIF solution bases used in PipeAssess PI™ is provided in Table 5. Note that these are 2D geometry models and as such anomaly axial length and SIFs for the crack tips at surface are not applicable.

Table 5: SIF Solution Base by API That Are Implemented Into PipeAssess PI™ for Hook Cracks

Anomaly Type & SIF Location	SIF Solution Base
Embedded Hook Crack,	API579 KCECLL
Surface Hook Crack,	API579 KCSCLL1

Discussion

This task determined the linear-elastic stress intensity factor values (i.e. K solutions) for cold welds, selective seam weld corrosion, and hook cracks typical to ERW and FW pipe. Prior to this work, these features were poorly represented in predictive models in that a one-size-fits-all approach was typically used, where all cracks are modeled as simple internal or external surface flaws. This SIF solution set is not only differentiated because of its various crack geometries, but also because it permits different pipe trim along the longitudinal seam. In particular, the SIF is now known for axial cracks in or covered by metallic trim of various heights. For simplicity, the trim width is idealized and constrained to double the wall thickness.

Overall, nearly two dozen crack geometries were modeled with finite element methods and their SIF solutions joined among themselves and smoothly transitioned to construct a full solution set. Joining occurred in two locations: First, finite and infinitely long cold weld solutions were merged to cover a wide range of crack lengths to ensure a continuous solution set as a given anomaly grows. Second, appropriate SSWC solutions were joined such that a general corrosion pit with no crack could smoothly evolve into the same pit but with a crack extending at the base of the pit. Smooth transitions were ensured at these interfaces as well as throughout the provided SIF data itself. In some

instances, the finite element method provided outliers that did not agree with the aggregate data set as cited in the conclusions section of Reference [6]. This was most common in the very shallow or near-through wall crack geometries, and it is theorized to be an artifact of the extended finite element method (XFEM) or chosen finite element mesh geometry. As a result, each SIF set went through a manual screening for these outliers. They were corrected with guidance from SIF values in the proximity or in some cases API 579's SIF solution set [4]. In this process, corrections were also verified to not disrupt the monotonically increasing or decreasing K slope behavior, whichever was the case.

The hook crack geometry is problematic for generating K solutions in that the possible geometries are extremely varied. Either an enormous number of finite element analyses must be run to provide a usefully large K solution space or else a simplified approach must be adopted to be able to make the problem tractable. The latter approach was adopted by utilizing existing API579 K solutions and applying well known fracture mechanics principles to approximate the expected behavior. From experience, it is known that embedded hook cracks have failure pressures well above comparable depth surface cracks. The embedded K solution methodology implemented herein is consistent with this field experience.

Recommendations

The stress intensity factor results reported herein are based on more than 2000 finite element solutions that examined various crack geometries (length, depth, internal, external), various corrosion geometries, (V and U pits, symmetric and asymmetric general corrosion), and various weld cap heights. In spite of the richness of the data set, there are still limitations which are enumerated as:

1) The multiple crack solution uses single crack SIF's and the BS 7910 Fitness-for-Service coalescence interaction rules,

2) The hook crack solutions are built from the API579 Fitness-for-Service radially-oriented embedded flaw solution and fracture mechanics considerations,

3) Hook cracks could consider the linear approximations rather than the actual curvature of the hook i,

4) Hook cracks do not consider various amounts of trim on the upset, and

5) The analysis space is limited for any of the solutions that were developed during this task.

Developing SIF's for the unanalyzed cases listed above using additional finite element analyses would take planning to generate meaningful and useful results. Considering the multiple crack case, the possibilities for crack depths, number of interacting cracks, and spacing between flaws is limitless. Likewise, for hook cracks, the possible geometries that may be encountered in practice are unbounded. The key to limiting the number of finite element analyses needed to improve the current SIF's would be to pick cases that would provide additional validity for the currently implemented SIF's and define the degree of conservatism in the present models, because it is unlikely that a large enough set of finite element analyses can be run to make a sufficiently generalized solution solely from FEA results.

Works Cited

[1] J. F. Kiefner and K. M. Kolovich, "Task 1.4: ERW and Flash Weld Seam Failures," task1_4-erw_and_flash_weld_seam_failures-kiefner-sept2012.pdf , 2012.

[2] EMC2, "Documentation and Development of Linear-Elastic Stress Intensity Factors for Various Axial Corrosion and Crack-Like Defects," (Note: This is Attachment A), Columbus, 2014.

[3] C. Taylor, "Fatigue Crack Growth of NPS20 Steel Oil Pipe at Varied Orientations," University of Windsor, Ontario, 2015.

[4] The American Society of Mechanical Engineers and the American Petroleum Insititute, "API 579-1/ASME FFS-1, Second Edition," 2007.

[5] T. L. Anderson, Fracture Mechanics: Fundamentals and Applications: 2nd Edition.

[6] D.-J. Shim and et al., "Application of Extended Finite Element Method (XFEM) to Stress Intensity Factor Calculations," Proceedings of the ASME 2015 Pressure Vessels & Piping Conference, Massachusetts, 2015.

Attachment A

Development of Linear-Elastic Stress Intensity Factors
for Various Axial Corrosion and Crack-Like Defects

Final Report

on

Documentation and Development of Linear-Elastic Stress Intensity Factors for Various Axial Corrosion and Crack-Like Defects

Emc^2 Project Number 14-G02-01

to

Battelle Memorial Institute

Columbus, Ohio

U.S.A.

by

Do-Jun Shim, Mohammed Uddin,
Sureshkumar Kalyanam, Frederick Brust

Engineering Mechanics Corporation of Columbus

3518 Riverside Drive, Suite 202

Columbus, OH 43221

Phone/Fax (614) 459-3200/6800

September 2014

EXECUTIVE SUMMARY

In this report, linear-elastic stress intensity factor values (K solutions) were calculated for various axial corrosion and crack-like defects in electric resistance welded (ERW) pipes. The stress intensity factors were calculated using the extended finite element method (XFEM). The work was divided into tasks based on the types of defects. The tasks were defined as:

- Task 1 - Cold weld cracks and lack of fusion cracks,
- Task 2 - Selective seam weld corrosion (SSWC) and SSWC with planar cracks, and
- Task 3 - Hook cracks.

For cold weld cracks, K solutions were provided for various types of cracks – infinitely long surface crack, rectangular surface crack, semi-elliptical crack, and through-wall crack. For all crack shapes, internal and external cracks were considered. In addition, K solutions were also provided for multiple crack cases.

For SSWC, both V-groove and U-groove shapes were considered. Furthermore, symmetric and asymmetric corrosion effects were included in the study. Cases with planar cracks were also included in the matrix.

For hook cracks, K solutions were provided for internal and surface-breaking hook cracks. Due to the geometry of the hook cracks, mixed-mode was observed at the crack-tips. Hence, K_I and K_{II} values were provided.

The K values for each case were provided in a separate Microsoft Excel spreadsheet. The K solutions developed in this work will be useful for assessments of various cracks in ERW pipes.

TABLE OF CONTENTS

LIST OF FIGURES

LIST OF TABLES

1 INTRODUCTION

In this report, linear-elastic stress intensity factor values (K solutions) were calculated for various axial corrosion and crack-like defects in electric resistance welded (ERW) pipes. The stress intensity factors were extracted from finite element analyses. The work was divided into tasks based on the types of defects. The tasks were defined as:

- Task 1 - Cold weld cracks and lack of fusion cracks,
- Task 2 - Selective seam weld corrosion (SSWC) and SSWC with planar cracks, and
- Task 3 - Hook cracks.

1.1 Task 1 – Cold Weld Cracks

In this task, stress intensity factors were developed for Cold Weld (CW) crack types, which include cracks of both Elliptical (E) and Rectangular (R) geometries for three dimensional analyses and infinitely long (IL) for two-dimensional analyses on both the inner-diameter (ID) and outer-diameter (OD) surface of the pipe. Both Through-Wall Cracks (TWC) and Part-TWC (PTWC) (aka surface cracks) were investigated in this task. Additionally, single cracks (S) and multiple cracks (M) (i.e. crack interaction) were considered along with two-dimensional (2D) and three-dimension (3D) finite element analyses. The nomenclature used to identify the unique description for these cases is TYPE_GEOMETRY_SURFACE_WALL_ NUMBER_DIMENSION. For example, if the crack can be characterized as Cold Weld, Infinitely Long, Outer-Diameter, Through-Wall-Crack, Single, and two-dimensional then the nomenclature would be CW_IL_OD_TWC_S_2D.

Table 1 outlines the efforts for this task where a total of 1014 cases are identified. Figures A1 through A12 in Appendix A of this report provide the visual representation of the geometries for Task 1.

1.2 Task 2 – Selective Seam Weld Corrosion (SSWC) and SSWC with Planar Cracks

In this task, stress intensity factors were developed for Selective Seam Weld Corrosion (SSWC) crack types, of both V-groove (V) and U-groove (U) geometries for an infinitely long (IL) defect on the outer-diameter (OD) surface of the pipe with two-dimensional (2D) and three-dimension (3D) finite element analyses. Only Part-TWC (PTWC) were investigated (since TWCs were investigated in Task 1). Additionally, symmetric (S) and asymmetric (A) general corrosion effects were considered. In addition, an investigation was conducted to understand the effect of the corrosion on planar defects in conjunction with the corrosion (PLANAR = Yes (Y) or No (N)). The nomenclature used to identify the unique description for these cases is TYPE_GEOMETRY_DIMENSION_SYMMETRY_PLANAR.

Table 2 outlines the efforts for this task where a total of 887 cases are identified. Figures B1 through B4 in Appendix B of this report provide the visual representation of the geometries for Task 2.

1.3 Task 3 – Hook Cracks

In this task, stress intensity factors were developed for Hook Crack (HC) types, for a plane strain (i.e. infinitely long defect) crack which follows the grain flow in an ERW weld. Only Part-TWC (PTWC) cases were investigated (since the grain direction changes at the mid-wall). These cracks can be characterized as internal (I) or surface breaking (S). For this study, only two dimensional stress intensity solutions were developed. The nomenclature used to identify the unique description for these cases is TYPE_GEOMETRY_ DIMENSION.

Table 3 outlines the efforts for this task where a total of 156 cases are identified. However, for 76 out of 156 cases, it was not possible to define the hook crack using the parameters provided in Table 3. This issue was identified to the Battelle program management team prior to conducting the FE analyses. Figures C1 and C2 in Appendix C of this report provide the visual representation of the geometries for Task 3.

Table 1 Analysis matrix for cold weld cracks (Task 1)

Case	Identifier	a/t*	c/a	d/t	L*/ c	Total Cases	Figure(s)[1]
1.1	CW_IL_ID_PTWC_S_2D	0.05, 0.10, 0.25, 0.50, 0.75, 0.90	N/A	0.00, 0.25, 0.50, 0.75, 1.00	N/A	30	A1
1.2	CW_IL_OD_PTWC_S_2D	0.05, 0.10, 0.25, 0.50, 0.75, 0.90	N/A	0.00, 0.25, 0.50, 0.75, 1.00	N/A	30	A2
1.3	CW_R_ID_PTWC_S_3D	0.05, 0.10, 0.25, 0.50, 0.75, 0.90	2, 3, 5, 10	0.00, 0.25, 0.50, 0.75, 1.00	N/A	120	A1,A5
1.4	CW_R_OD_PTWC_S_3D	0.05, 0.10, 0.25, 0.50, 0.75, 0.90	2, 3, 5, 10	0.00, 0.25, 0.50, 0.75, 1.00	N/A	120	A2,A6
1.5	CW_NA_NA_TWC_S_3D	1.00	2, 5, 10	0.00, 0.25, 0.50, 0.75, 1.00	N/A	15	A11
1.6	CW_E_ID_PTWC_S_3D	0.05, 0.10, 0.25, 0.50, 0.75, 0.90	2, 3, 5, 10	0.00, 0.25, 0.50, 0.75, 1.00	N/A	120	A1,A3
1.7	CW_E_OD_PTWC_S_3D	0.05, 0.10, 0.25, 0.50, 0.75, 0.90	2, 3, 5, 10	0.00, 0.25, 0.50, 0.75, 1.00	N/A	120	A2,A4
1.8	CW_R_ID_PTWC_M_3D	0.25, 0.50, 0.75	2, 5, 10	0.00, 0.50, 1.00	0.50, 1.0, 2.0	81	A1,A9
1.9	CW_R_OD_PTWC_M_3D	0.25, 0.50, 0.75	2, 5, 10	0.00, 0.50, 1.00	0.50, 1.0, 2.0	81	A2,A10
1.10	TWC_M_3D	1.00	2, 5, 10	0.25, 0.50, 0.75	0.50, 1.0, 2.0,	27	A12
1.11	CW_E_ID_PTWC_M_3D	0.25, 0.50, 0.75	2, 5, 10	0.00, 0.25, 0.50, 0.75, 1.00	0.50, 1.0, 2.0	135	A1,A8
1.12	CW_E_OD_PTWC_M_3D	0.25, 0.50, 0.75	2, 5, 10	0.00, 0.25, 0.50, 0.75, 1.00	0.50, 1.0, 2.0	135	A2,A7

Note 1. Figures are provided in Appendix A.

Table 2 Analysis matrix for selective seam weld corrosion with and without planar cracks (Task 2)

Case	Identifier	d/t	a_2/t	a_1/t*	a_3/t_2	$2c_1/2W$	$2c_2/2W$	Total Cases	Figure[1]
2.1	SSWC_V_2D_S_N	0.00,0.25, 0.50,0.75, 1.00	0	0.05,0.10, 0.25,0.50, 0.75,0.90	0**	0.10,0.25, 0.50,0.75, 1.0	0	150	B1
2.2	SSWC_V_2D_S_N	0.00	0.10, 0.25, 0.50	0.25, 0.5, 0.75	0**	0.25,0.50, 0.75	2.0, 3.0, 4.0	81	B4
2.3	SSWC_V_2D_A_N	0.00	0.10, 0.25, 0.50	0.25, 0.5, 0.75	0**	0.25,0.50, 0.75	2.0, 3.0, 4.0	81	B5
2.4	SSWC_V_2D_S_Y	0.25, 0.50, 0.75	0	0.25, 0.5, 0.75	0.10, .25, 0.50, 0.75	0.25,0.50, 0.75	0	108	B1
2.5	SSWC_V_2D_S_Y	0.00	0.10, 0.50	0.25, 0.75	0.10,0.25, 0.50, 0.75	0.25, 0.75	2.0, 4.0	64	B4
2.6	SSWC_V_2D_A_N	0.00	0.10, 0.50	0.25, 0.75	0.10,0.25, 0.50, 0.75	0.25, 0.75	2.0, 4.0	64	B5
2.7	SSWC_U_2D_S_N	0.00,0.25, 0.50,0.75, 1.00	0	0.05,0.10, 0.25,0.50, 0.75, 0.90	0**	0.10,0.25, 0.50,0.75, 1.0	0	150	B2
2.8	SSWC_U_2D_S_N	0.00	0.10, 0.25, 0.50	0.25, 0.5, 0.75	0**	0.25,0.50, 0.75	2.0, 3.0, 4.0	81	B3
2.9	SSWC_U_2D_S_Y	0.25, 0.50, 0.75	0	0.25, 0.5, 0.75	0.10,0.25, 0.50, 0.75	0.25,0.50, 0.75	0	108	B2

Note 1 Figures are provided in Appendix B.

Note ** Since a non-zero value was needed to calculate K, a_3/t_2=0.02 was used for these cases.

Table 3 Analysis matrix for hook cracks (Task 3)

Case	Identifier	d/t	a_1/t*	a_2/W	Total Cases	Figure[1]
3.1	HC_I_2D	0.00, 0.25, 0.50, 0.75, 1.00	0.10, 0.20, 0.30, 0.40, 0.45	0.10, 0.25, 0.50, 0.75, 0.90, 1.0	150	C1
3.2	HC_S_2D	0.0	0.50	0.10, 0.25, 0.50, 0.75, 0.90, 1.0	6	C2

Note 1 Figures are provided in Appendix C.

1.4 General Input Data and Requirements

As per the scope of work defined in Reference [1], the following input data were used for all the analyses:

1. Elastic material properties
    a. Modulus of elasticity : 29,000,000 psi
    b. Poisson's ratio : 0.3
2. Default geometric parameters for this study
    a. Pipe inner radius, R_i =7.5 inch
    b. Pipe wall thickness, t = 0.25 inch
    c. $R_i/t = 30$ ($D_o/t = 60$)
3. Internal pressure applied to pipe, p = 100 psi (including axial tension due to end-cap effect)
4. Crack face pressure
    a. 100% of internal pressure for internal surface cracks
    b. 50% of internal pressure for through-wall cracks
5. For 3D models, K values were provided at the surface and at the deepest points. For 2D models, K values at the crack tip were provided for surface breaking cracks. For embedded 2D cracks, K values at each crack tip were provided.
6. All cracks are considered to be idealized (no roughness, no kinks, etc.)

2 TECHNICAL APPROACH

2.1 Extended Finite Element Method (XFEM)

In this work, K solutions were calculated using the extended finite element method (XFEM) embedded in Abaqus [2]. The XFEM is an extension of the conventional finite element method based on the concept of partition of unity [3]. This allows the presence of discontinuities in an element by enriching degrees of freedom with special displacement functions. Hence, it does not require the mesh to match the geometry of the discontinuities. Note that the XFEM method is an extension of the 'embedded singular element' approached first developed in the 1970's.

Abaqus offers two different ways to evaluate the contour integral. The first approach is based on the conventional finite element method, which typically requires the user to match the mesh to the cracked geometry, to explicitly define the crack front, and to specify the virtual crack extension direction. Detailed focused meshes are generally required, and obtaining accurate contour integral results for a crack in a three-dimensional curved surface can be quite cumbersome. The XFEM alleviates these shortcomings since it does not require the mesh to match the cracked geometry. The presence of a crack is ensured by the special enriched functions in conjunction with additional degrees of freedom. This approach also removes the requirement for explicitly defining the crack front or specifying the virtual crack extension direction when evaluating the contour integral. The data required for the contour integral are determined automatically based on the level set for signed distance functions at the nodes in an element.

Prior to this work, preliminary calculations were conducted by Emc^2 to demonstrate the applicability of XFEM to calculate the K values for the present work. An initial example is a constant depth surface crack (a/t=0.5, where 'a' is the depth of the crack and 't' is the plate thickness) in a plate under tension. As shown in Figure 1, the planar crack is inserted on to the uncracked plate using only the cracked geometry. The opening mode stress contour in the plate is depicted in Figure 2. The K value at the center of the crack was calculated from the FE model and was compared to the handbook solution for a single-edge-notched tension (SENT) specimen [4] which showed agreement within 1% difference.

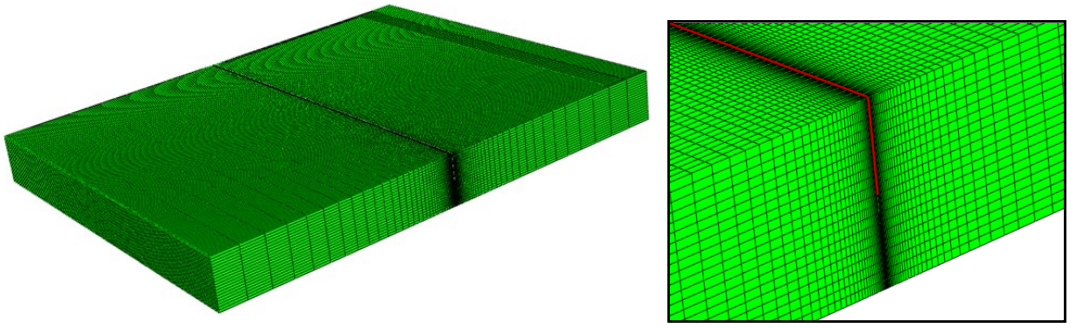

Figure 1 FE mesh for constant depth surface crack in a plate under tension

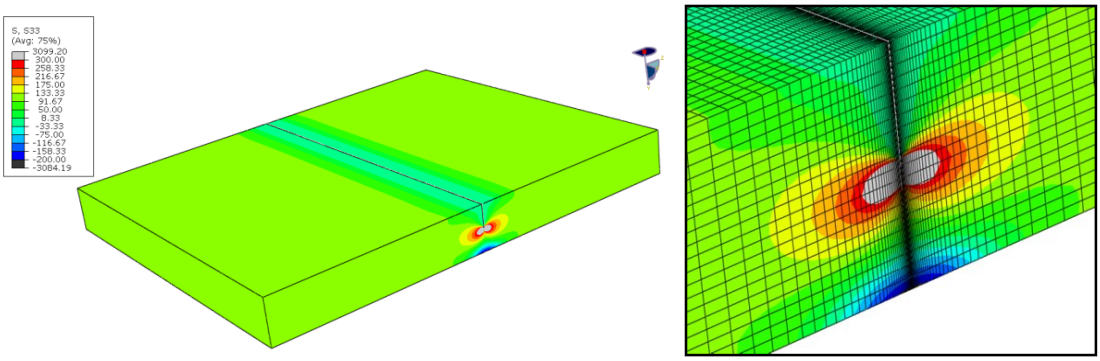

Figure 2 Opening mode stress contour for constant depth surface crack in a plate under tension loading

The next example is a semi-elliptical surface crack in a plate under tension as shown in Figure 3. In this example a/t=0.4, a/c=0.4 and w/c=4. Figure 4 illustrates the FE mesh for the surface cracked plate. Note that this mesh is the same as the one that was used in the previous example. The only difference is that the semi-elliptical surface crack has been inserted to the model using the cracked geometry[a]. Figure 5 shows the opening mode stress distribution of the plate under tension. The stress contour in the cracked plane is also shown in this figure. K_I values along the entire crack front were calculated from the FE analysis and these values were compared against the Raju-Newman solution [5] given as,

[a] Indeed, the ability to minimize the number of meshes required is an advantage of choosing the XFEM approach.

$$K_I = \sigma\sqrt{\pi a} \cdot \frac{F}{Q}$$

where

F is a dimensionless function of a/t, a/c and ϕ,
Q is the complete elliptical integral of the second kind.

Figure 6 shows a comparison of the F values obtained from the present FE analysis and the Raju-Newman solution. The FE results provided overall good agreement with the Raju-Newman solution. However, the XFEM results showed some oscillations along the crack front. As shown in Figure 6, a polynomial curve fit of the XFEM results showed good agreement with the Raju-Newman solution. Table 4 of this document compares the F values at the deepest and surface points where the results are comparable to conventional FE calculations results where focused crack tip meshing is used. Note that there are typical differences near the surface points between different methods used because of the 'vertex singularity' at this point, which is not square root [6].

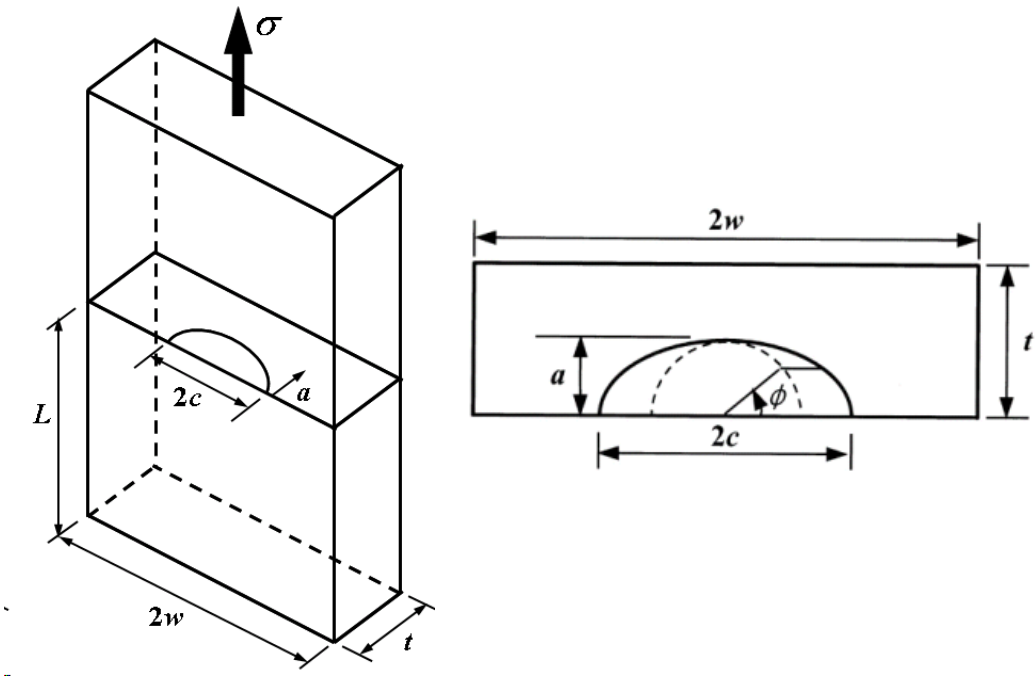

Figure 3 Geometry and dimensions of a semi-elliptical surface crack in a plate under tension loading

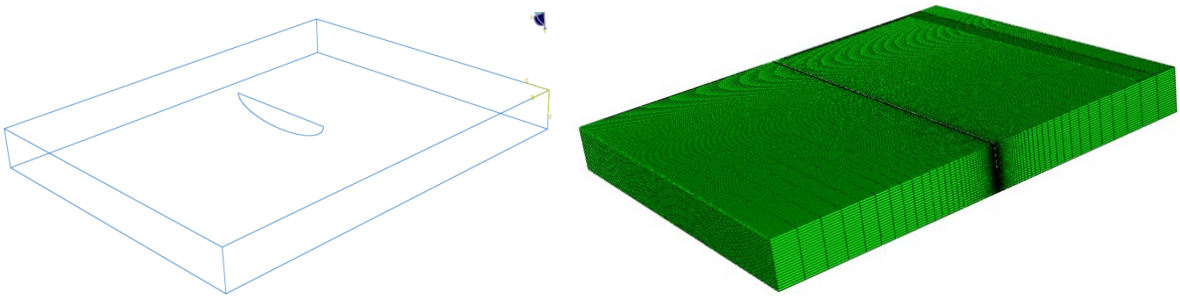

Figure 4 FE mesh for semi-elliptical surface crack in a plate under tension

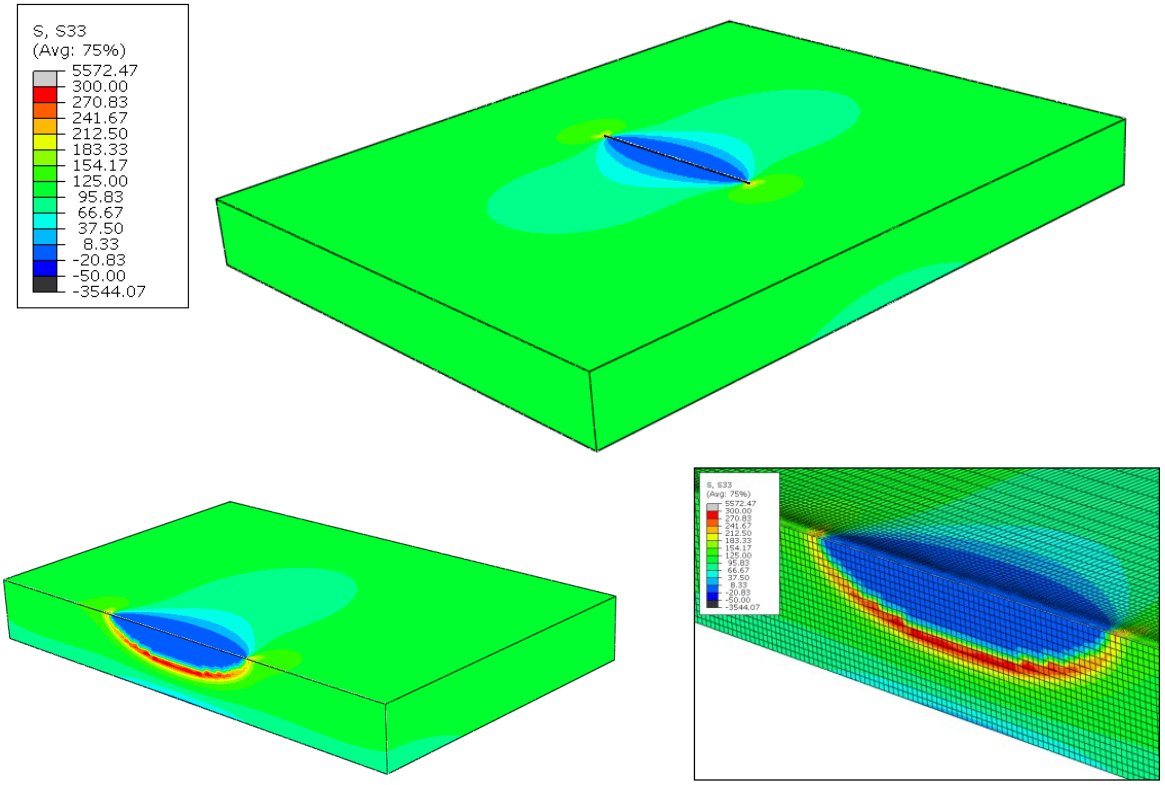

Figure 5 Opening mode stress contour for semi-elliptical surface crack in a plate under tension

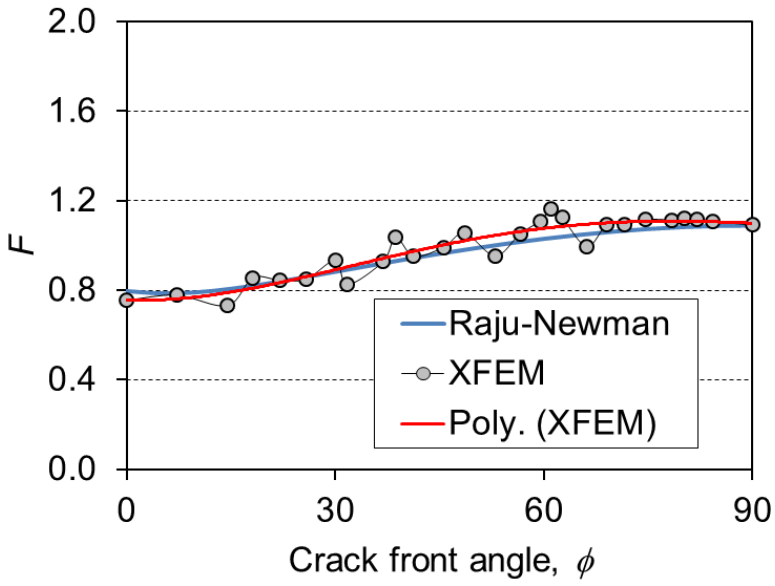

Figure 6 Comparison of F values along the crack front

Table 4 Comparison of F values at deepest and surface points

Location	XFEM	Raju-Newman	% Diff.
Deepest point	1.092	1.089	0.26
Surface point	0.755	0.796	5.13

These example cases demonstrated the applicability of the XFEM for the present work. As described in these examples, for a given pipe geometry, the same mesh can be used and the crack shape (e.g., constant depth, semi-elliptical and rectangular surface crack/through-wall crack) can be easily varied. In addition, the same mesh can be used for multiple crack cases.

2.2 Techniques Used for Verification of XFEM

In addition to the handbook calculations, limited FE analyses using the conventional FE method were carried out to verify the XFEM results. Emc^2's in-house software program, PipeFracCAE©, was used to generate Abaqus input files for 3D cracked pipes. K values calculated from the model generated by this software have been verified against various handbook solutions for the cracked pipe geometries that were considered in the present work. Recently, this software has been used to develop K solutions for the ASME BPV Section XI code. A screen capture of PipeFracCAE is shown in Figure 7 and example meshes generated by this software are provided in Figure 8.

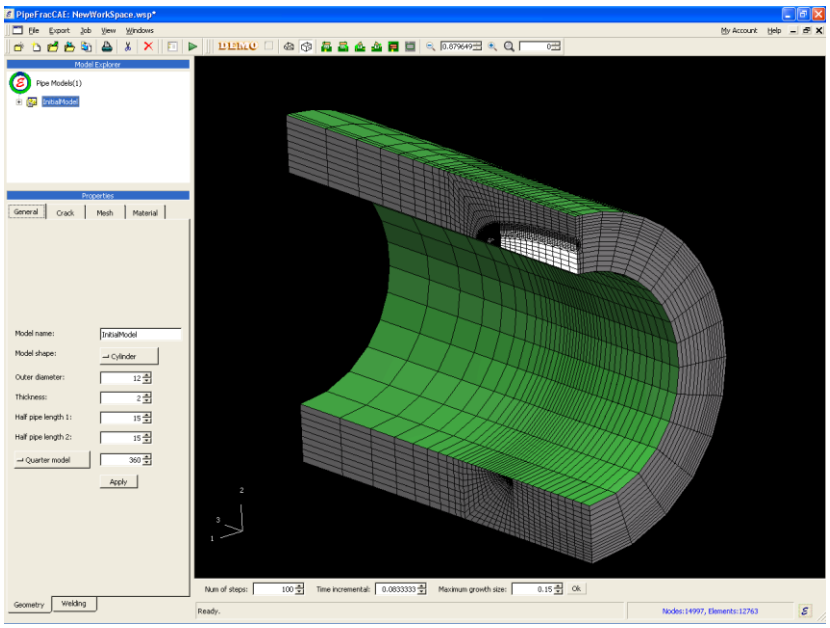

Figure 7 Screen capture of PipFracCAE

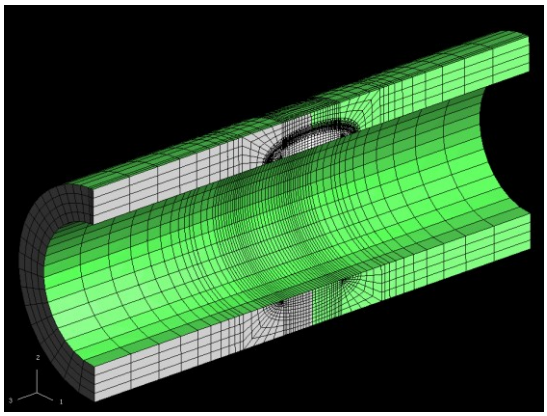

Axial semi-elliptical internal surface crack

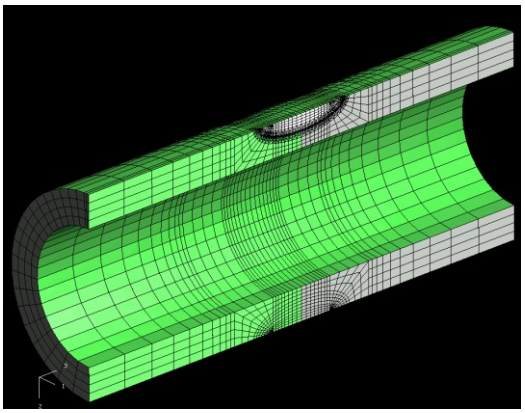

Axial semi-elliptical external surface crack

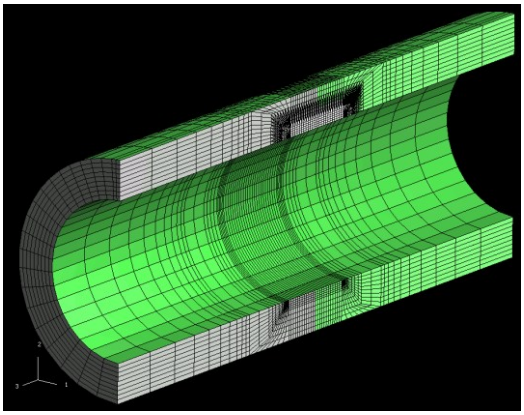

Axial rectangular internal surface crack

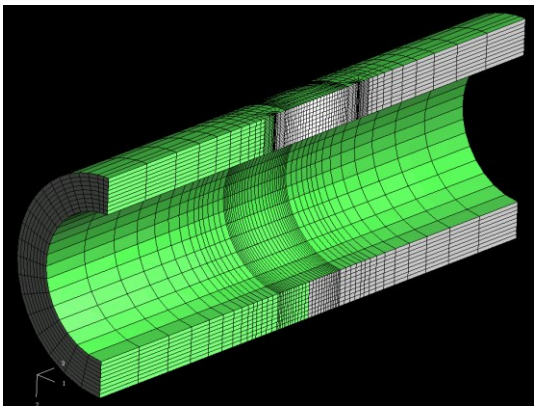

Axial through-wall crack

Figure 8 Example of FE meshes for various crack types generated using PipeFracCAE

In addition to the conventional FE calculations, the ALT3D software program was used by Emc^2 (which uses the finite element alternating method (FEAM) [7,8,9]) to verify the XFEM K calculations for single and multiple semi-elliptical crack cases. Similar to XFEM, the elegance of the FEAM employed by ALT3D lies primarily in the fact that the crack is not explicitly included in the finite element grid. This provides significant benefits over more direct finite element methods. The most important aspect of FEAM is that the same mesh can be used to obtain solutions for many different crack sizes, locations, and for multiple cracks [8,9] . Because the finite element stiffness matrix only needs to be reduced once regardless of the crack size, crack location, crack orientation, crack number (mixed mode conditions can be handled as well), etc., the method is extremely efficient. FEAM has been used extensively for crack growth analyses over the years including in the aerospace and nuclear communities. Figure 9 shows a schematic illustration of the finite element alternating method. An example K calculation for semi-elliptical cracks in a pipe is shown in Figure 10, where the FEAM results showed good agreement with the Raju-Newman solutions.

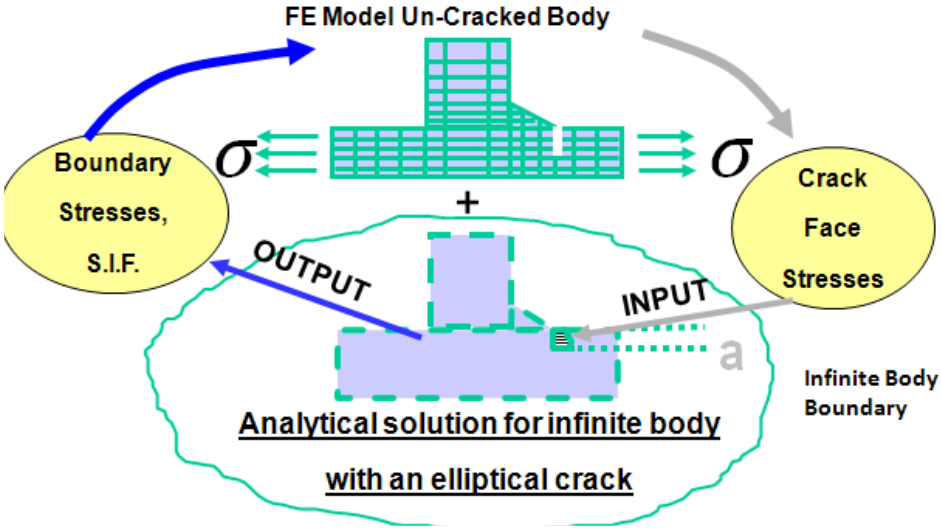

Figure 9 Illustration of finite element alternating method (FEAM)

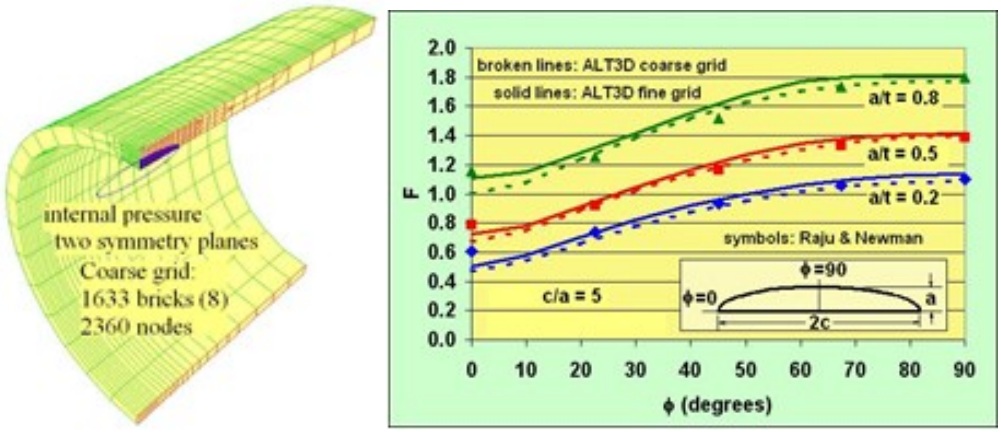

Figure 10 Example K calculation using FEAM

2.3 Automated FEA Procedure

Since the total number of cases defined in the Work Scope[1] was over 2,000, it was essential to automate (or semi-automate) the FE modeling and the analysis procedure. For this purpose, the Abaqus Scripting Interface (used to access the functionality of Abaqus from scripts) was employed for the FE analyses based on XFEM. The Abaqus Scripting Interface is an extension of the Python language and uses the syntax required by Python. In the present work, Python scripts were used to generate the models, vary the parameters in the model, run the FE model and extract data from the output files. As part of Emc^2's quality assurance protocols, random cases from the automated (or semi-automated) runs were checked to ensure that the automated procedure worked properly.

3 RESULTS AND VERIFICATION

3.1 Results for Cold Weld Cracks

The stress intensity factor (K) values calculated for cold weld cracks are provided in the Microsoft Excel spreadsheets that have been separately delivered. The spreadsheets are provided for all cases identified in Table 1. For example, results for Case 1.1 are provided in "Task1-Case-1-1-SIF-Results.xlsx."

The remainder of this section describes the efforts conducted to verify the XFEM results by comparing the present results with other available methods – handbook solution, traditional FEM, and FEAM.

3.1.1 Infinitely long surface cracks

Case 1.1 and Case 1.2 cover infinitely long axial surface cracks in pipes. To verify the XFEM results, traditional FE analyses were performed. In addition, the results were compared against solutions from API 579-1/ASME FFS-1[10][b]. Note that these comparisons were made for limited cases without upset (d/t=0.0).

Figure 11 shows an example comparison between FEM and XFEM for an ID surface crack with d/t=0.0 and a/t*=0.5. As shown in this figure the traditional FEM has the "spider-web" mesh near the crack-tip whereas the XFEM has no special meshing. The deformation and the stress distribution near the crack-tip are comparable.

More comparisons for ID surface cracks with various depths are provided in Figure 12. In this figure, solutions from API 579-1/ASME FFS-1 are also shown for comparison. The solutions from various methods showed good agreement. Similar comparison for OD surface cracks (d/t=0.0) are provided in Figure 13. For some OD surface cracks with upset (d/t≠0.0), there was compressive stress near the OD surface due to bending caused by the geometry effect. Hence, for relatively shallow OD surface cracks, the numerically calculated K values were negative (for

[b] API 579-1/ASME FFS-1 solutions are also based on conventional finite element analyses.

example, see Figure 14) especially for the surface point. These negative values were reported 'as is' in the spreadsheets.

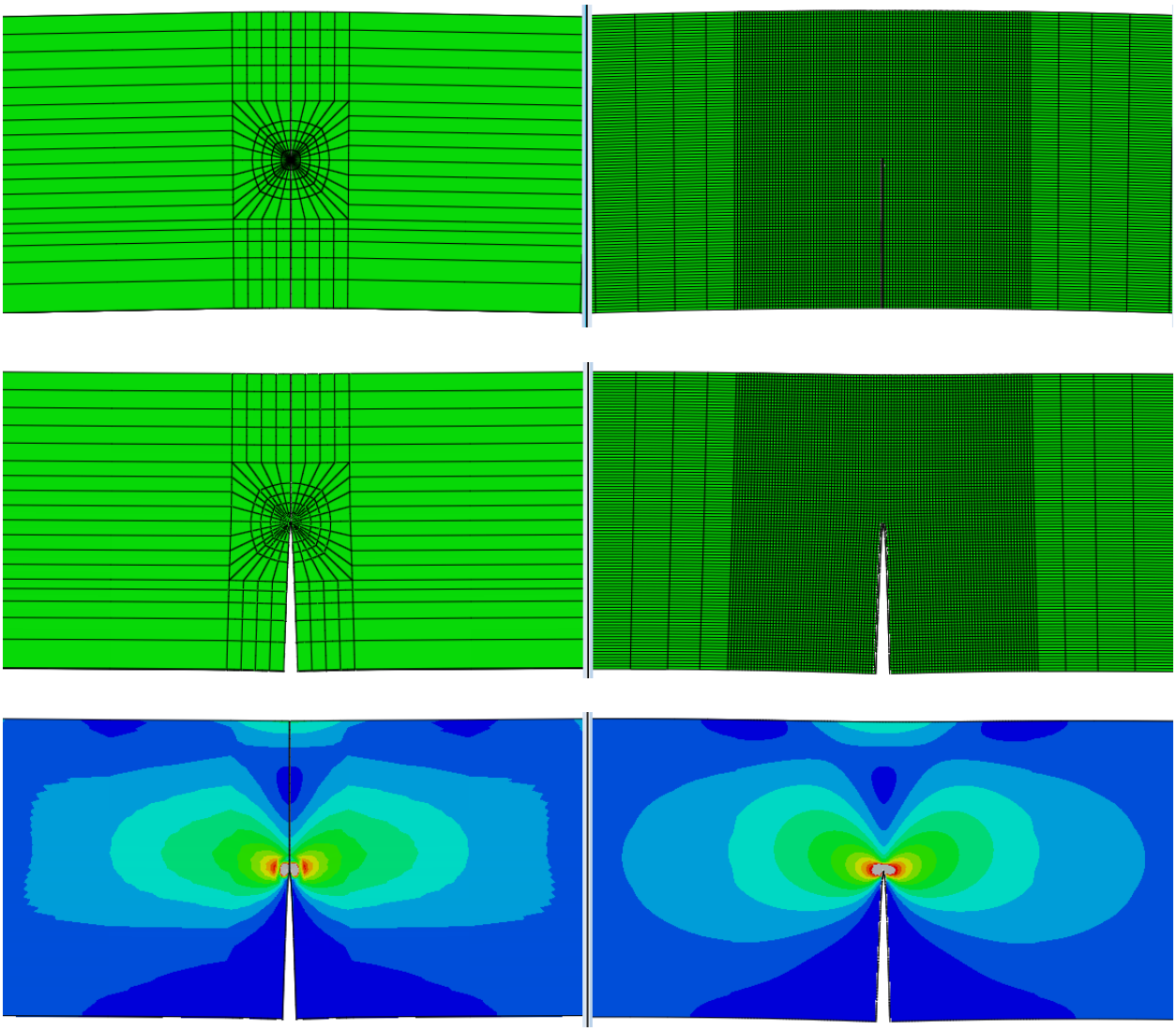

Figure 11 Comparison of FEM and XFEM results (d/t=0.0, a/t*=0.5)

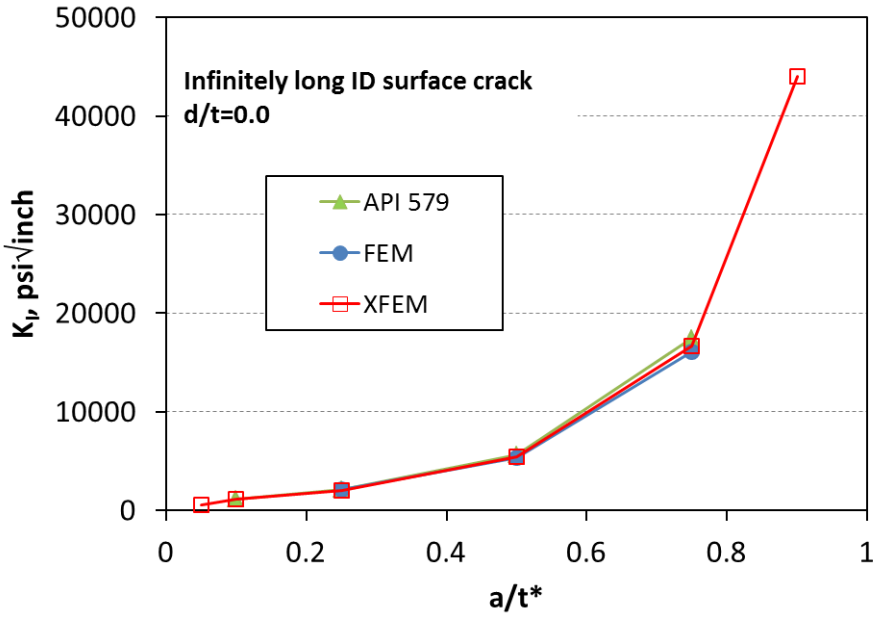

Figure 12 Comparison of various solutions for ID surface crack (d/t=0.0)

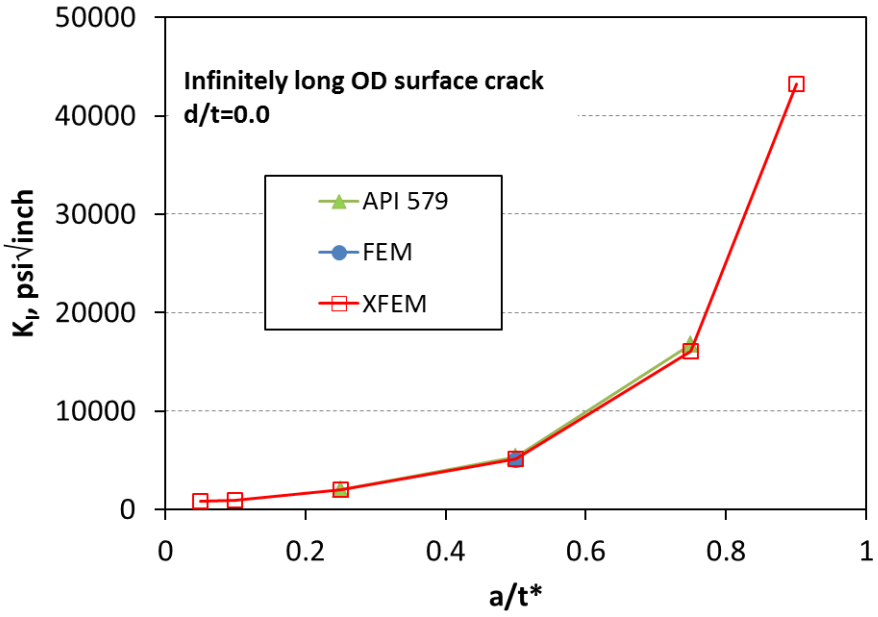

Figure 13 Comparison of various solutions for OD surface crack (d/t=0.0)

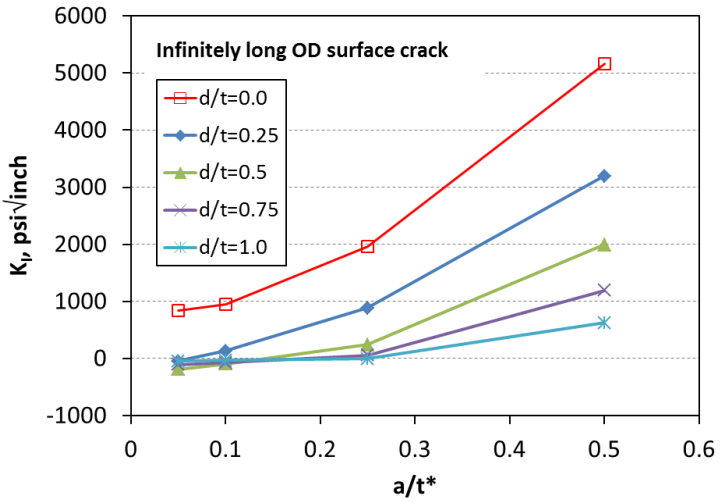

Figure 14 XFEM results for selected OD surface cracks

3.1.2 Single semi-elliptical surface cracks

Case 1.6 and Case 1.7 cover single semi-elliptical axial surface cracks in pipes. For these cases, the XFEM results were compared against handbook solutions, FEM, and FEAM.

Figure 15 shows example XFEM results for semi-elliptical ID surface cracks without upset (d/t=0.0). The K values along the crack fronts are provided in this figure. The XFEM results showed oscillations near the surface points, especially for larger a/t* values (similar to results shown in Figure 6). Hence, to obtain the K value at the surface points, the K values along the crack front were curve-fitted using a 4th order polynomial fit.

Comparisons between FEM and XFEM are provided in Figure 16 and Figure 17. The overall mesh and stress distributions are compared in Figure 16 whereas those from the crack planes are provided in Figure 17.

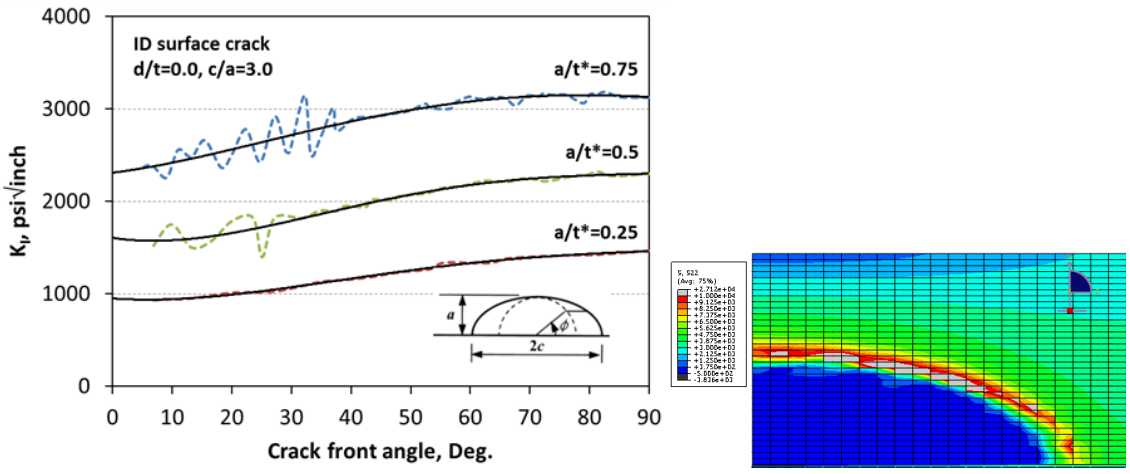

Figure 15 Example of XFEM results for semi-elliptical ID surface cracks

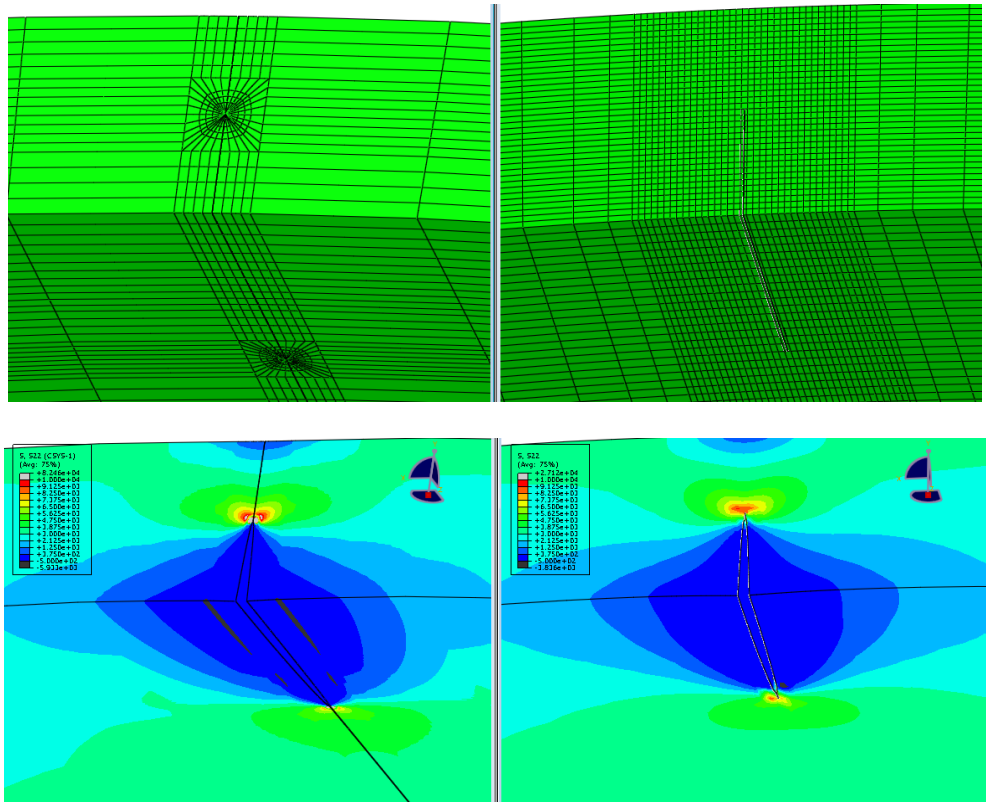

Figure 16 Comparison of FEM and XFEM results for ID semi-elliptical surface crack (d/t=0.0, a/t*=0.5, c/a=3.0)

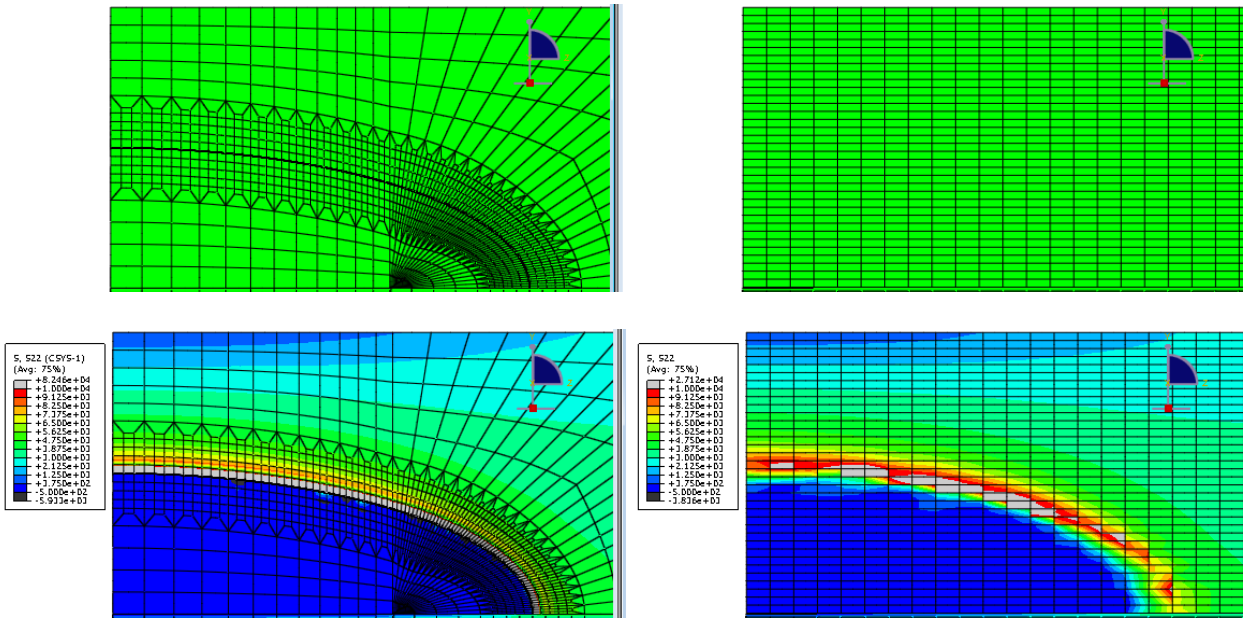

Figure 17 Comparison of crack front stress distribution from FEM and XFEM for ID semi-elliptical surface crack (d/t=0.0, a/t*=0.5, c/a=3.0)

Comparison of crack front K values from various solutions for ID semi-elliptical surface crack (d/t=0.0, a/t*=0.5, c/a=3.0) is depicted in Figure 18. The XFEM results (i.e. the 4th order polynomial curve fit) showed good agreement with the Raju-Newman solution [11] and FEM results along the entire crack front. The FEAM results showed good agreement near the deepest point but were slightly higher than the XFEM results near the pipe surface. Similar comparisons are provided for an OD semi-elliptical surface crack in Figure 19. Here again, XFEM results matched well with FEM results and the FEAM results were slightly higher than the other two results. Figure 20 and Figure 21 show a comparison between XFEM and FEAM results with various d/t values for ID and OD surface cracks, respectively.

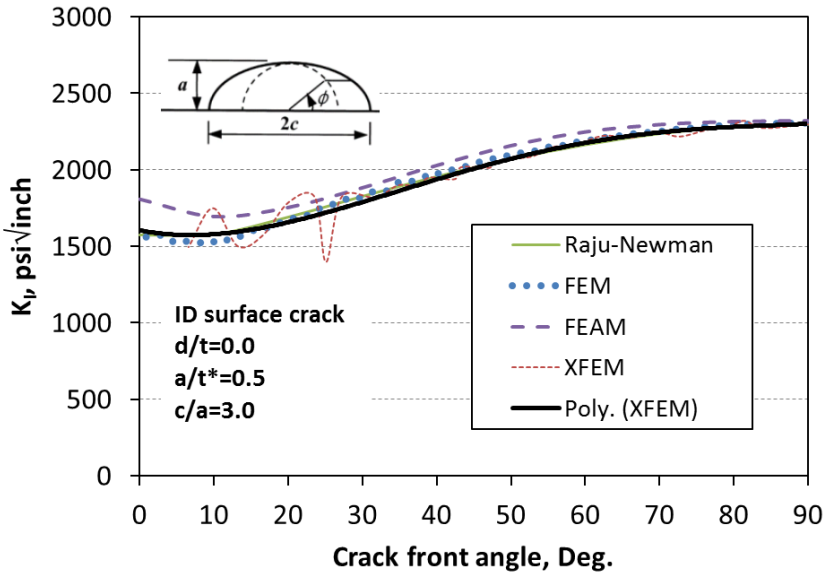

Figure 18 Comparison of various solutions for ID semi-elliptical surface crack (d/t=0.0, a/t*=0.5, c/a=3.0)

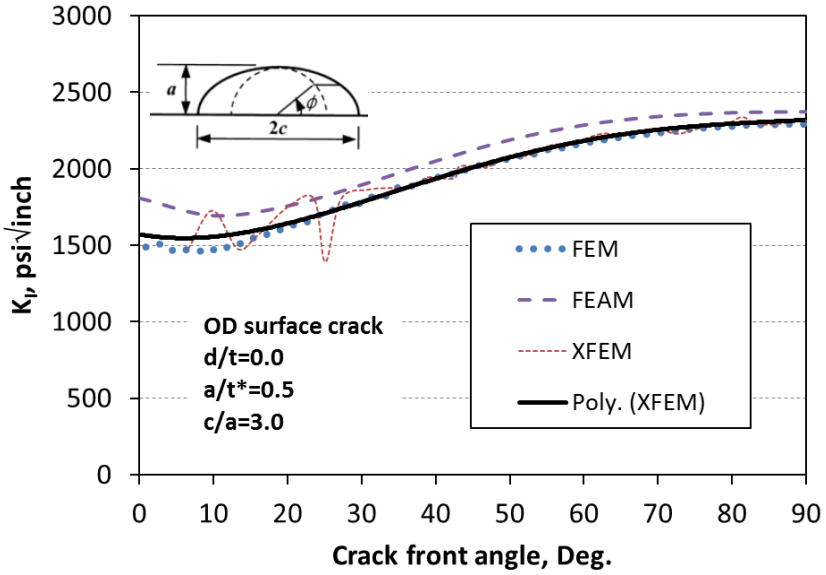

Figure 19 Comparison of various solutions for OD semi-elliptical surface crack (d/t=0.0, a/t*=0.5, c/a=3.0)

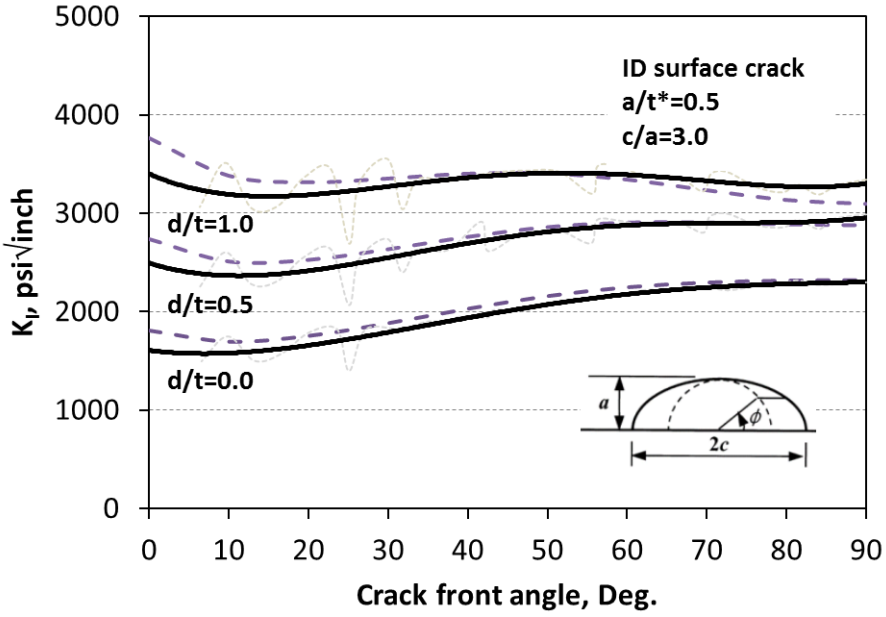

Figure 20 Comparison between XFEM and FEAM for various d/t values – ID surface crack

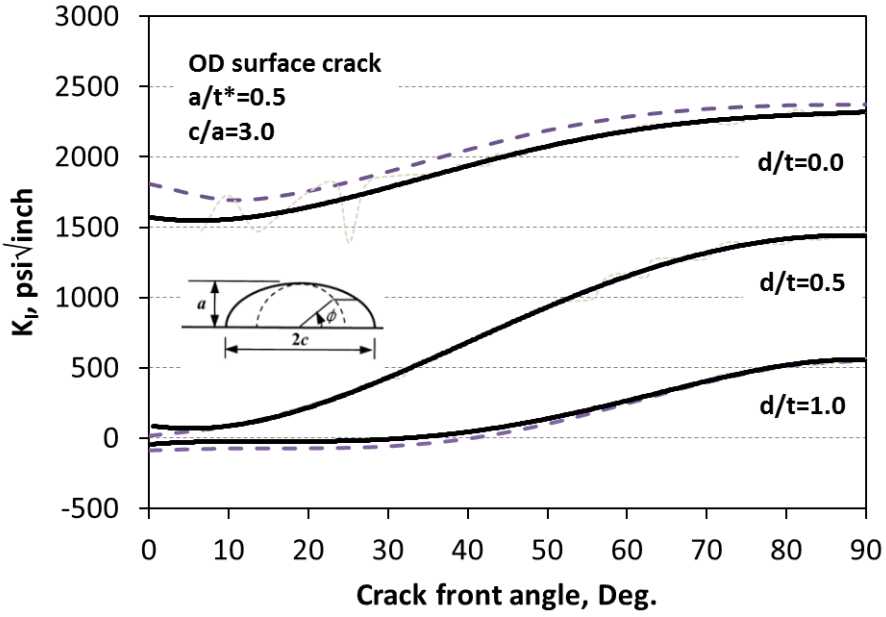

Figure 21 Comparison between XFEM and FEAM for various d/t values – OD surface crack

3.1.3 Single rectangular surface cracks

Case 1.3 and Case 1.4 cover single rectangular axial surface cracks in pipes. For these cases, the XFEM results were compared against FEM results. Figure 22 compares the K values along the rectangular crack front for selected ID and OD surface cracks (d/t=0.0, a/t*=0.5, c/a=3.0). For ID rectangular crack, the XFEM results provided higher K values along the entire crack front, especially near the surface point. On the other hand, the XFEM results for OD rectangular crack provided good agreement with the FEM results in the constant depth crack front region, but the values in the vertical portion of the rectangular crack showed overly conservative results (similar to ID crack results). After further investigation, it was identified that this was due to the limitation of the XFEM method embedded in ABAQUS, where unstable solutions can be provided when there is a discontinuity in the normal direction along the crack front. To avoid this issue, a fillet was inserted at the corner of the rectangular crack where the radius of the fillet (R) was determined as half of the crack depth (a). Figure 23 shows the XFEM results for rectangular cracks with rounded corners. As shown in these plots, the XFEM results provided good agreement with the FEM results (no rounded corner) along the constant depth region as well as near the surface point. As expected, some differences were shown near the corner which is not of a great interest for developing the K solutions. Similar results were obtained for OD rectangular cracks with rounded corners as illustrated in Figure 24. Note that the K value at the surface point was extracted from the XFEM results by using a 2nd order polynomial fit near the OD surface (as indicated in Figure 23 and Figure 24).

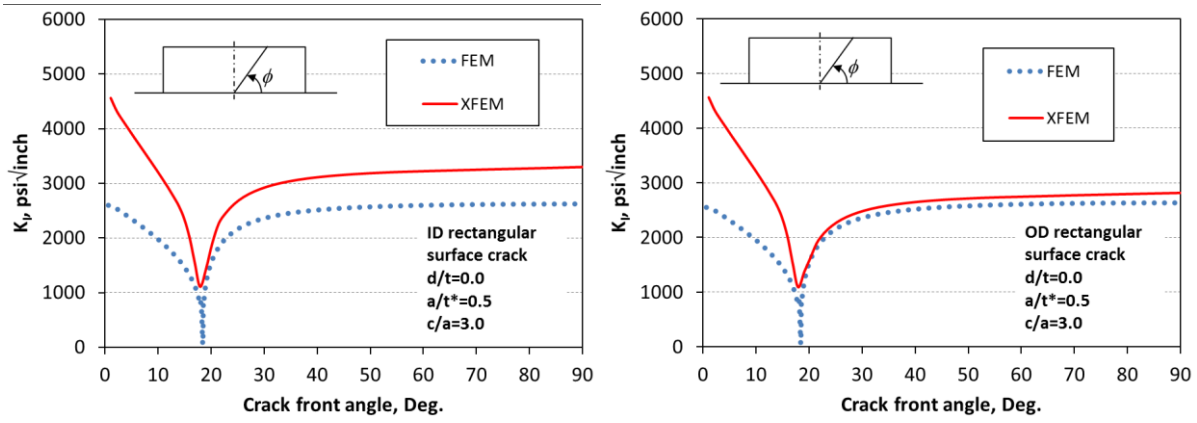

Figure 22 Comparison between XFEM and FEM results for ID and OD rectangular surface cracks (d/t=0.0, a/t*=0.5, c/a=3.0)

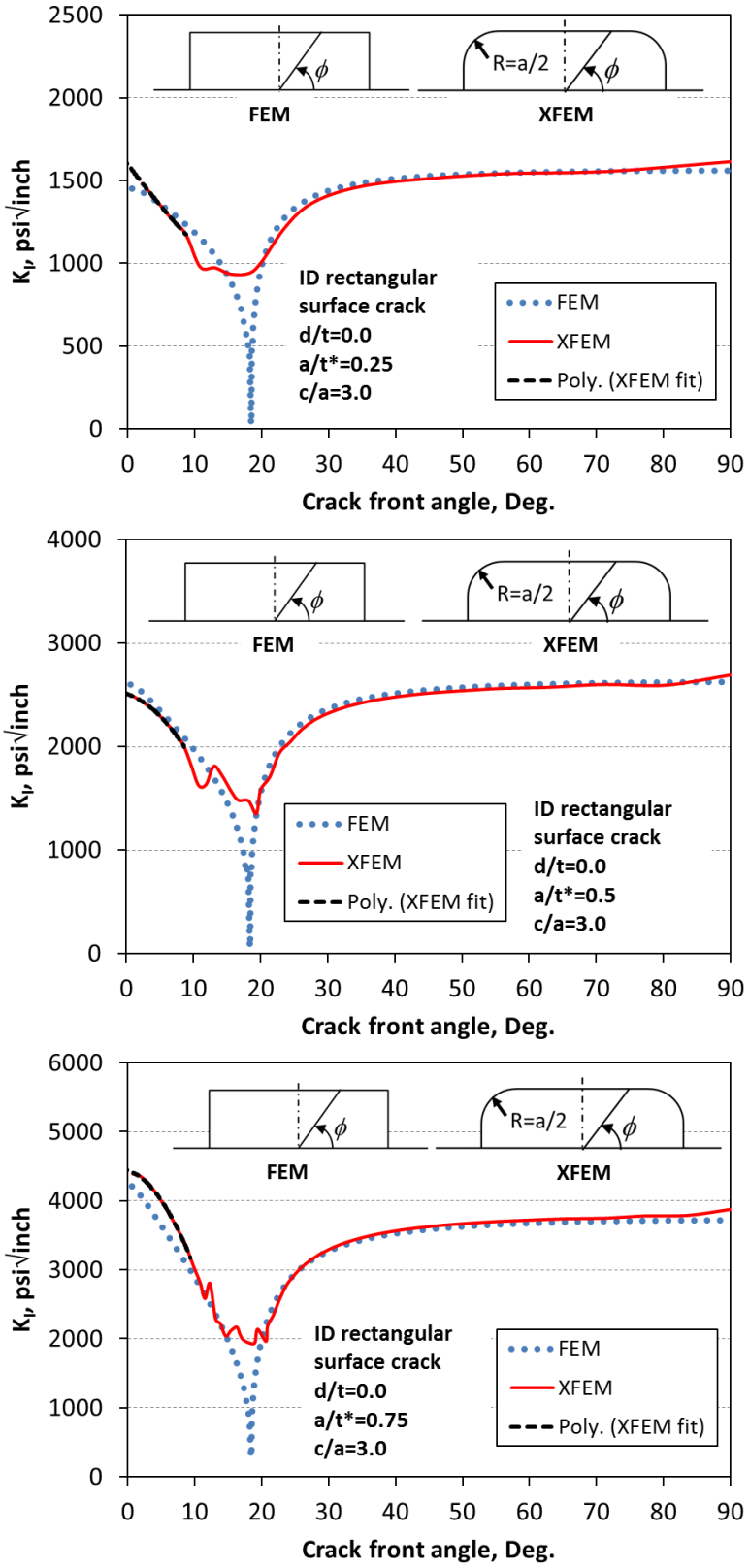

Figure 23 Comparison between XFEM and FEM results for ID rectangular surface cracks (d/t=0.0, a/t*=0.25, 0.5, 0.75, c/a=3.0)

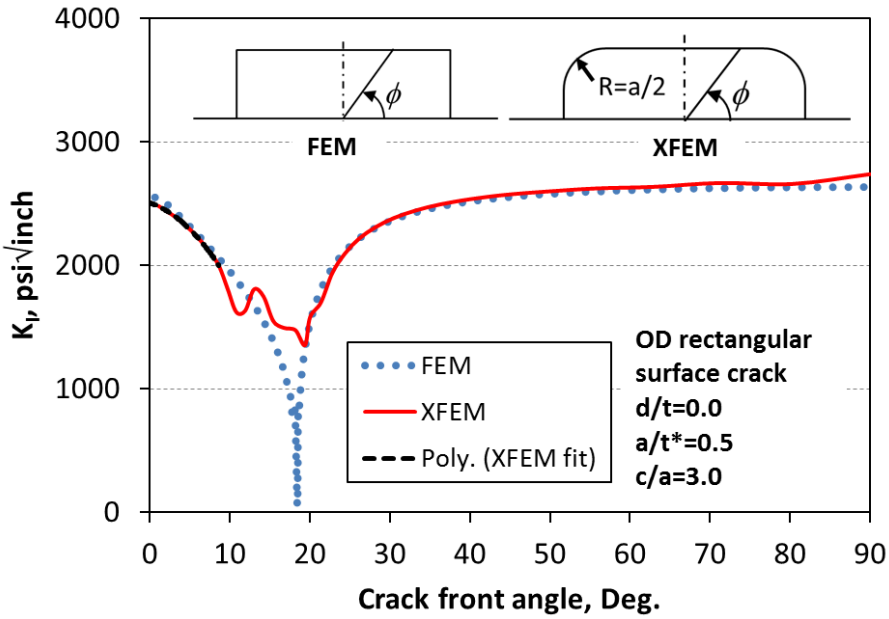

Figure 24 Comparison between XFEM and FEM results for OD rectangular surface crack (d/t=0.0, a/t*=0.5, 0.75, c/a=3.0)

3.1.4 Single through-wall cracks

Case 1.5 covers single through-wall cracks in pipes. For this case, the XFEM results were compared against handbook solutions (SINTAP solution[12]) and FEM results.

Comparisons between FEM and XFEM are provided in Figure 25 and Figure 26. The overall mesh and stress distributions are compared in Figure 25 whereas those near the crack planes are provided in Figure 26. The K values along the crack front from various solutions are compared in Figure 27. All solutions showed good agreement. The K values provided in the spreadsheet are the averaged value along the crack front. Figure 28 provides a comparison of averaged K values for various crack lengths (for d/t=0.0).

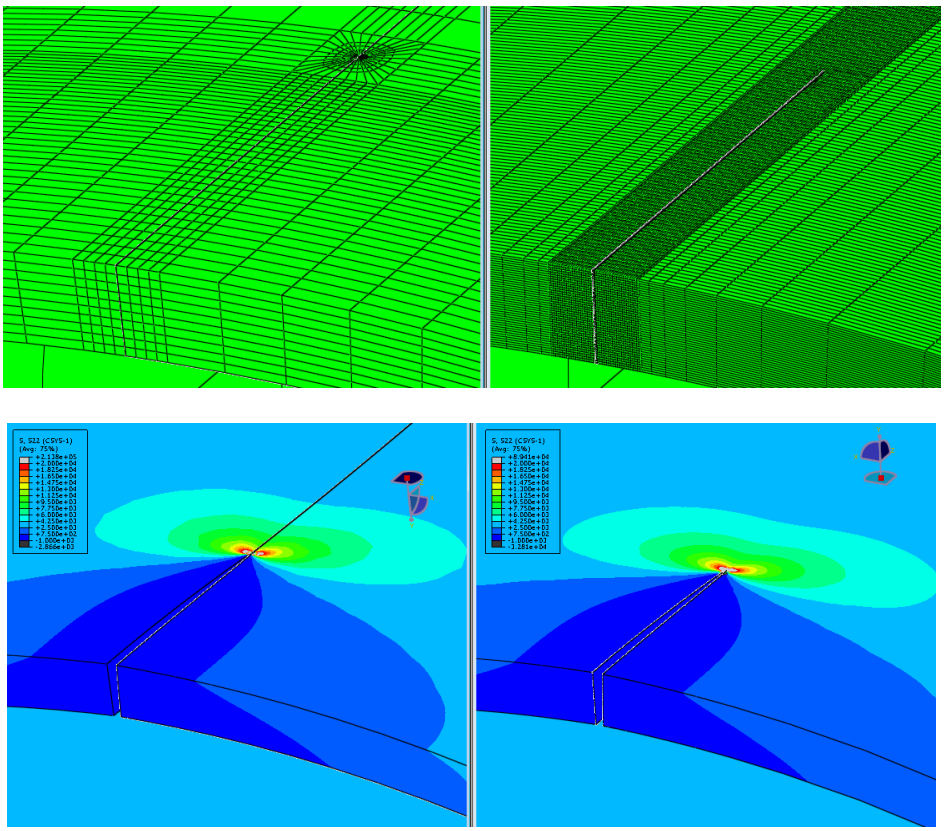

Figure 25 Comparison of FEM and XFEM results for through-wall crack (d/t=0.0, a/t*=1.0, c/a=5.0)

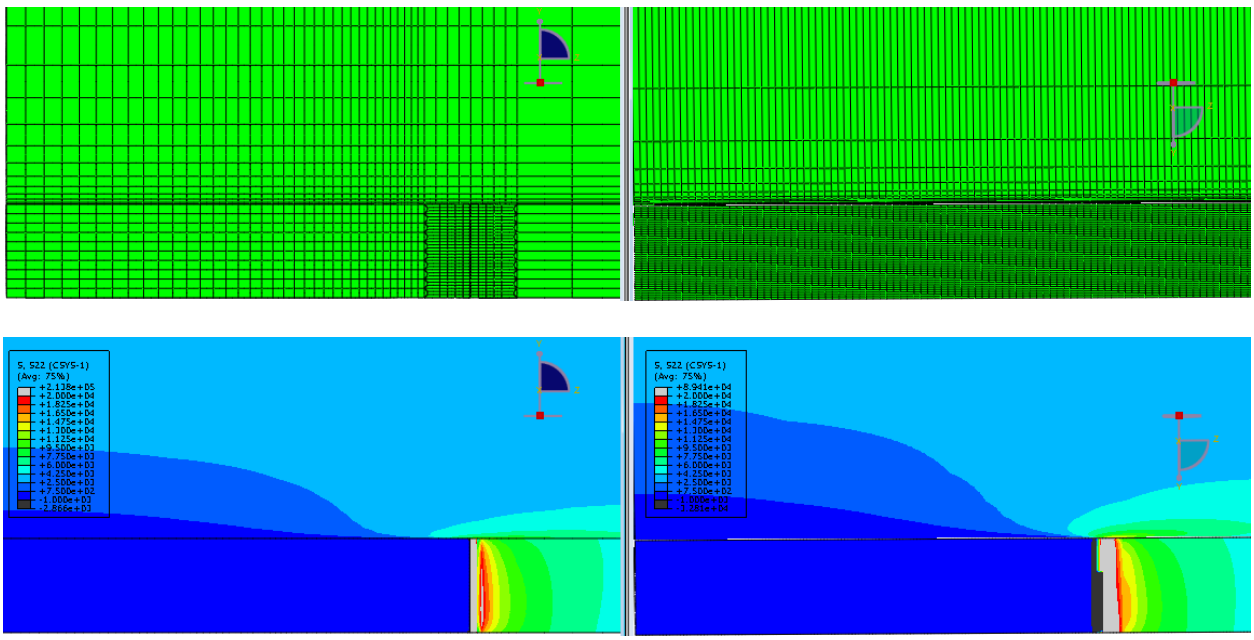

Figure 26 Comparison of crack front stress distribution from FEM and XFEM for through-wall crack (d/t=0.0, a/t*=1.0, c/a=5.0)

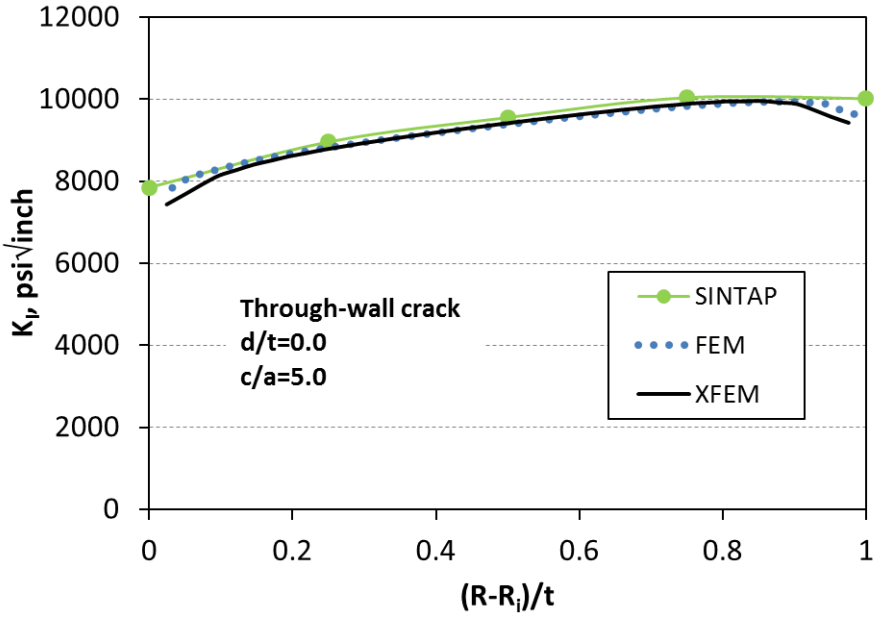

Figure 27 Comparison of crack front K values for through-wall crack (d/t=0.0, a/t*=1.0, c/a=5.0)

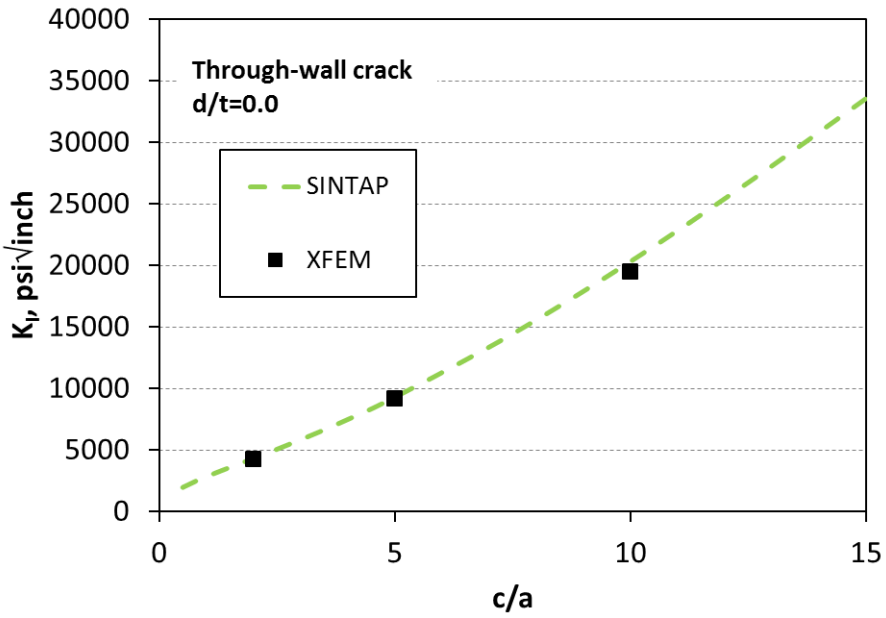

Figure 28 Comparison of various solutions for through-wall crack (d/t=0.0)

3.1.5 Multiple cracks

Case 1.8 through Case 1.12 cover multiple cracks (semi-elliptical surface crack, rectangular surface crack, and through-wall crack) in pipes. For verification of XFEM, only the multiple ID semi-elliptical surface crack case was compared against FEAM results. Figure 29 shows the comparison results for d/t=0.0, a/t*=0.5, c/a=5.0, and L*/c=1.0. Similar to the single crack cases, the FEAM results provided slightly higher K values along both crack fronts. For multiple crack cases, five K values are provided in the spreadsheets – at deepest and surface points of the crack in the center, two surface points and deepest points of the next crack. The surface point K values were extracted using a 4th order polynomial curve fit of the values from the deepest point towards the surface point (same as single crack case).

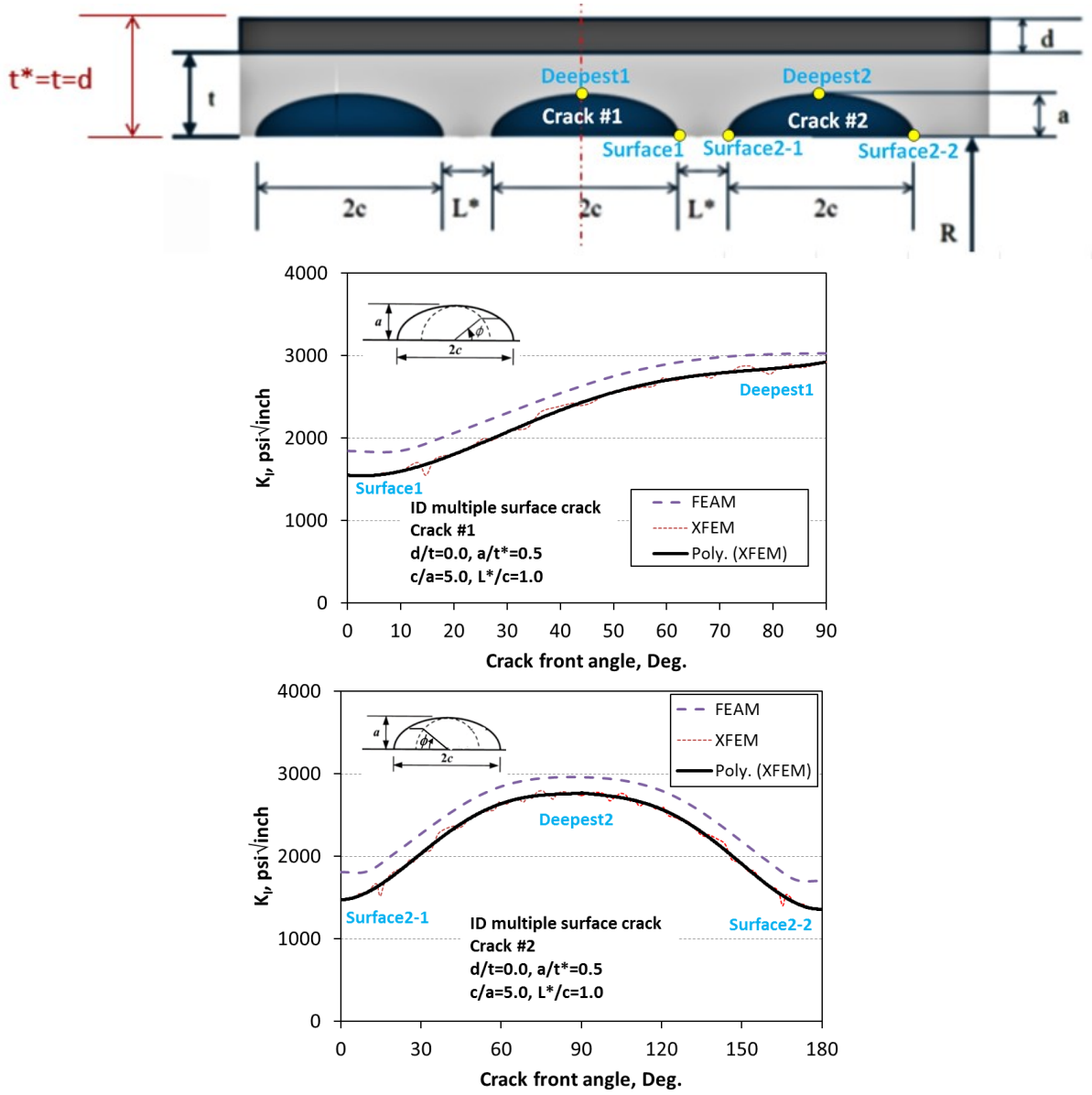

Figure 29 Comparison between XFEM and FEAM for multiple ID semi-elliptical surface cracks (d/t=0.0, a/t*=0.5, c/a=5.0, L*/c=1.0)

3.2 Results for Selective Seam Weld Corrosion with and without Planar Cracks

The stress intensity factor (K) values calculated for selective seam weld corrosion (SSWC) and SSWC with planar cracks are provided in the Microsoft Excel spreadsheets that have been separately delivered. The spreadsheets are provided for all cases identified in Table 2. For example, results for Case 2.1 are provided in "Task1-Case-2-1-SIF-Results.xlsx."

Since there are no existing solutions for crack shapes considered in this task, no comparison was provided. However, since the XFEM modeling method used in this task is similar to that used in Task 1 (Case 1.1 and Case 1.2), the results are expected to be reliable. As noted in Table 2, for cases where a_3/t_2=0.0 (i.e., no crack at tip of V-groove and U-groove) a very small crack (a_3/t_2=0.02) was inserted to calculate the K values. Figure 30 shows a comparison of stress distribution for SSWC with V-groove and U-groove. Example of XFEM result for SSWC with V-groove and symmetric general corrosion is provided in Figure 31.

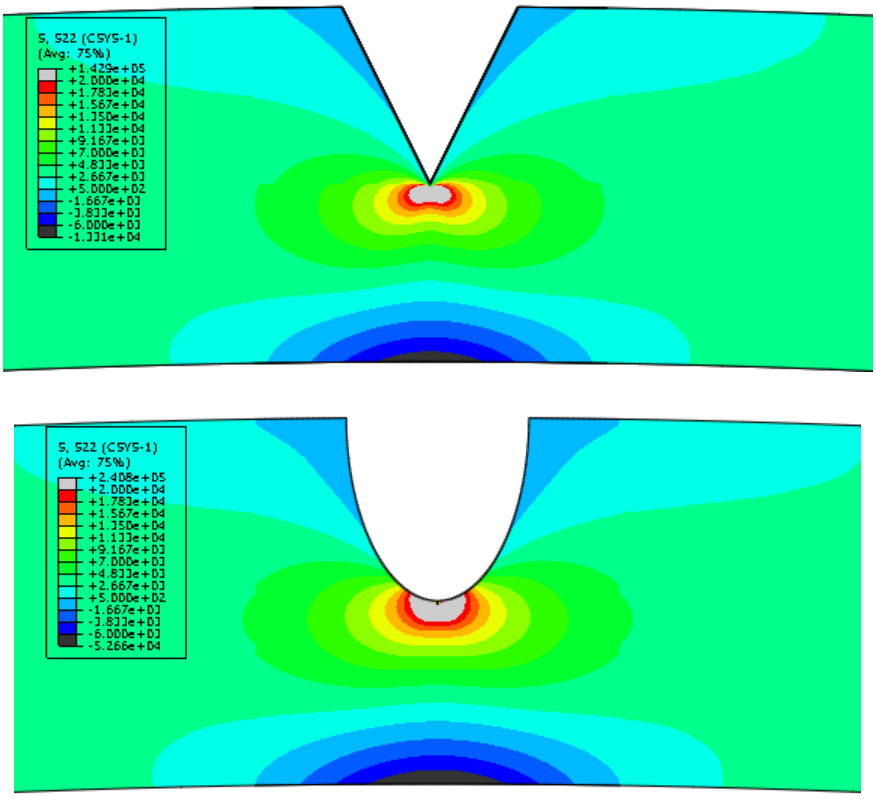

Figure 30 Example XFEM results for SSWC with V-groove and U-groove (d/t=0.0, a_1/t^*=0.5, a_3/t_2=0.02, c_1/W=0.5)

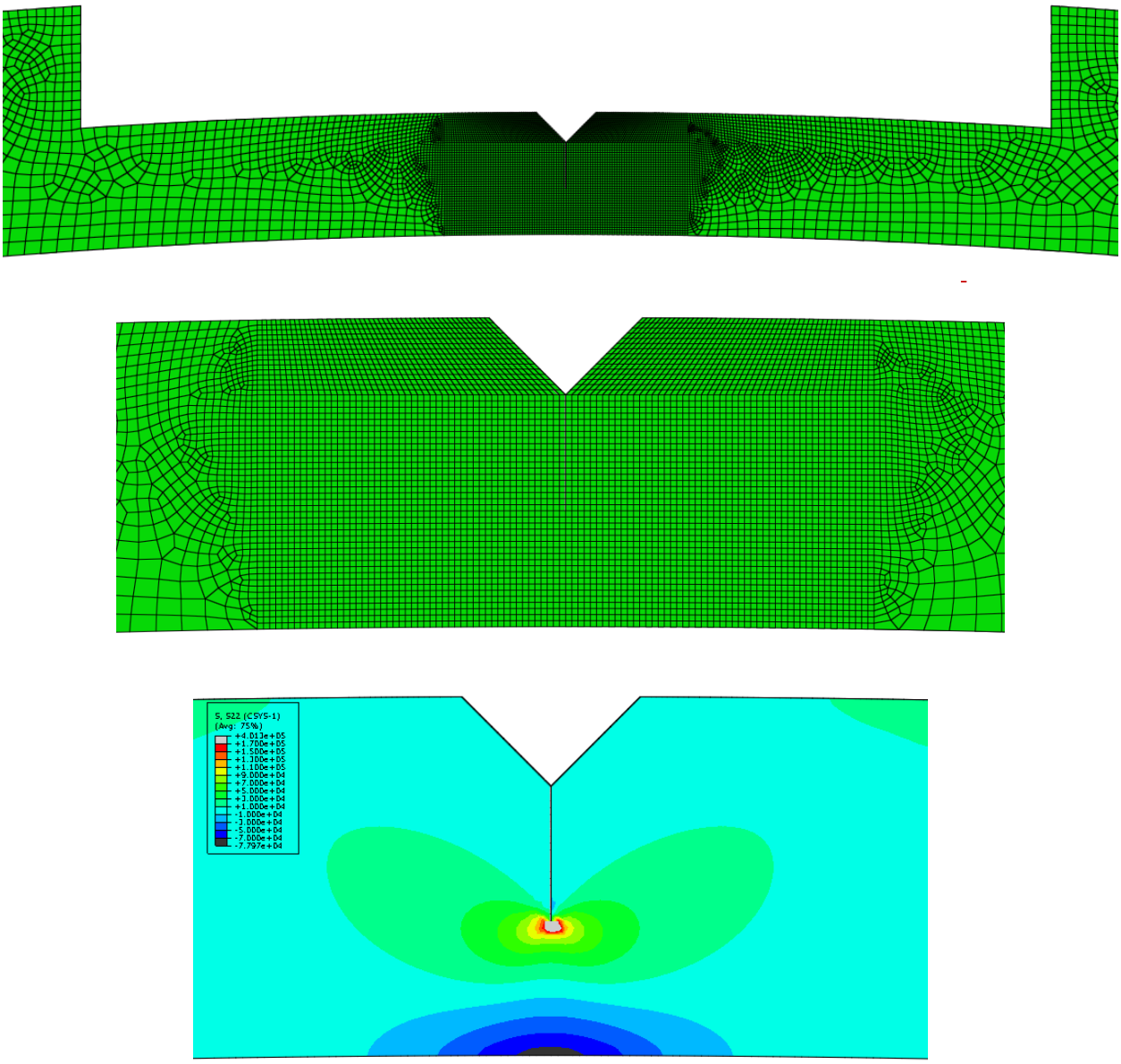

Figure 31 Example XFEM result for SSWC with V-groove and symmetric general corrosion (d/t=0.0, a_1/t^*=0.25, a_2/t=0.5, a_3/t_2=0.5, c_1/W=0.25, c_2/W=4.0)

3.3 Results for Hook Cracks

The stress intensity factor (K) values calculated for hook cracks are provided in the Microsoft Excel spreadsheets that have been separately delivered. The spreadsheets are provided for all cases identified in Table 3. For example, results for Case 3.1 are provided in "Task1-Case-3-1-SIF-Results.xlsx."

An example mesh and result (von Mises stress distribution) for an internal hook crack is shown in Figure 32. As depicted in this figure, there is mixed-mode observed at the two crack-tips.

Hence, K_I and K_{II} values were provided in the spreadsheet. Figure 33 shows similar results for a surface-breaking hook crack. Here again, due to mix-mode, K_I and K_{II} values were provided in the spreadsheet.

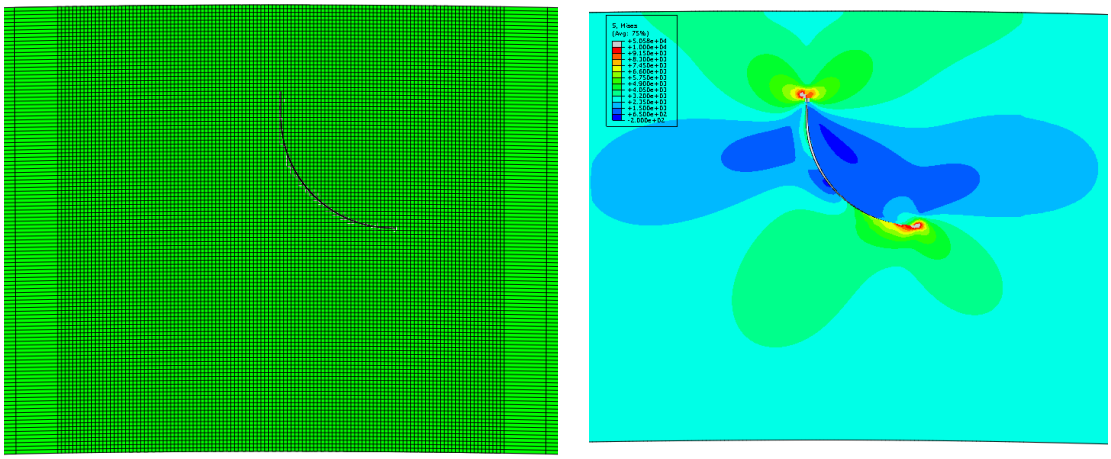

Figure 32 Example XFEM result for internal hook crack (d/t=0.0, a_1/t^*=0.3, a_2/W=0.5)

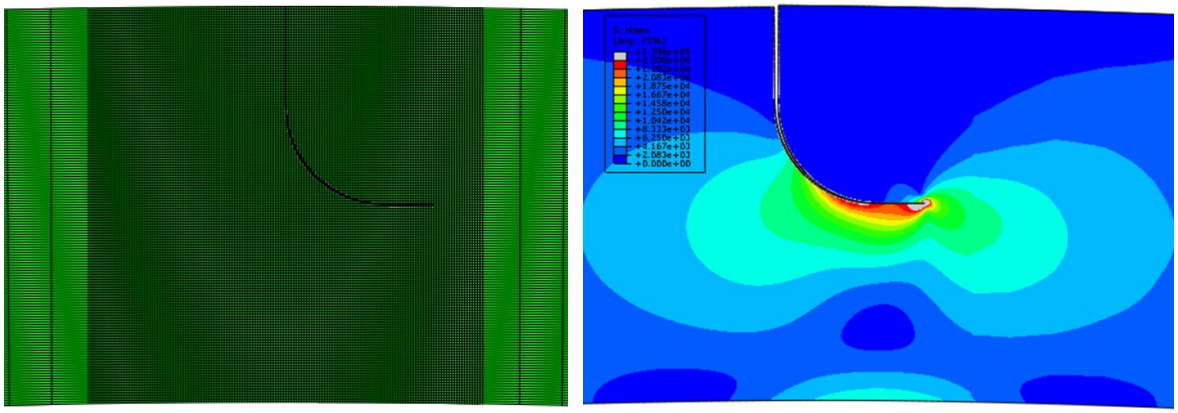

Figure 33 Example XFEM result for surface-breaking hook crack (d/t=0.0, a_1/t^*=0.5, a_2/W=0.75)

4 FUTURE WORK

Based on this initial study and observations during the calculations, some recommended tasks that can be conducted in the future include:

- Develop closed-form K solutions using the results provided in the present work.
- Extend the work to elastic-plastic fracture mechanics by conducting similar calculations to develop J-estimation schemes.
- Explore the possibility of using XFEM to conduct fatigue and/or corrosion crack growth calculations.

5 CONCLUSIONS

In this report, linear-elastic stress intensity factor values (K solutions) were calculated for various axial corrosion and crack-like defects in electric resistance welded (ERW) pipes. The stress intensity factors were calculated using the extended finite element method (XFEM).

For cold weld cracks, K solutions were provided for various types of cracks – infinitely long surface crack, rectangular surface crack, semi-elliptical crack, and through-wall crack. For all crack shapes, internal and external cracks were considered. In addition, K solutions were provided for multiple crack cases.

For selective seam weld corrosion (SSWC), both V-groove and U-groove shapes were considered. Furthermore, symmetric and asymmetric corrosions were included in the study. Cases with planar cracks were also included in the matrix.

For hook cracks, K solutions were provided for internal and surface-breaking hook cracks. Due to the geometry of the hook cracks, mixed-mode was observed at the crack-tips. Hence, K_I and K_{II} values were provided.

The K values for each case were provided in a separate Microsoft Excel spreadsheet. The K solutions developed in this work will be useful for assessments of various cracks in ERW pipes.

6 REFERENCES

[1] Competitive Request for Proposal (RFP) No. 2014-14-267: Phase-2, Task-3 of the DOT PHMSA ERW Project – Attachment 1 "Detailed Scope of Work for Partial Fulfillment of Objectives of Phase-2, Task-3 of the DOT PHMSA ERW Project," April, 2014.

[2] ABAQUS 6-13.2, SIMULIA, Providence, USA, 2014.

[3] Sukumar, N., Moes, N., Moran, B., Belytschko, T. (2000) "Extended finite element method for three-dimensional crack modelling," International Journal for Numerical Methods in Engineering, 48, 1549-1570.

[4] Murakami, Y., Aoki, S., Hasebe, N., Itoh, Y., "Stress Intensity Factors Handbook" Vol. 1, Pergamon Press, 1986.

[5] Raju, I.S. and Newman, Jr. J.C., "Stress Intensity Factors for a Wide Range of Semi-Elliptical Surface Cracks in Finite-Thickness Plates," Engineering Fracture Mechanics, Vol. 11, pp. 817-829, 1979.

[6] Shivakumar, K. N., an Raju, I. S., "Treatment of Singularities in Cracked Bodies", International Journal of Fracture, Vol. 45, No. 3, Oct. 1990, pp 159-178.

[7] Nishioka, T. And Atluri, S. N., "Analytical Solutions for Embedded Elliptical Cracks, and Finite Element Alternating Method for Elliptical Surface Cracks, Subjected to Arbitrary Loadings," Engineering Fracture Mechanics, Vol. 17, No. 3, pp. 247-268, 1983.

[8] Stonesifer, R. B., Brust, F. W., and Leis, B. N., "Mixed-Mode Stress Intensity Factors for Interacting Semi-Elliptical Surface Cracks in a Plate," Engineering Fracture Mechanics, Vol. 45, No. 3, pp. 357-380, 1993.
[9] Brust, F. W., Zhang, T., Shim, D-J, Wilkowski, G., and Rudland, D. L., "Evaluation of Fabrication Related Indications in Reactor Upper Head Penetrations", NRC report ML110410587, March, 2011.
[10] "Fitness-for-Service," API 579-1/ASME FFS-1 (API 579 Second Edition), American Petroleum Institute and American Society of Mechanical Engineers, 2007.
[11] Raju, I.S. and Newman, Jr. J.C., "Stress Intensity Factors for Internal and External Surface Cracks in Cylindrical Vessels" Journal of Pressure Vessel Technology, Vol. 104, pp. 293-298, 1982.
[12] Zang, W., "Stress Intensity Factor Solutions for Axial and Circumferential Through-Wall Crack in Cylinders," SINTAP/SAQ/02, SAQ Kontroll AB, Sweden, 1997.

APPENDIX A – COLD WELD CRACKS

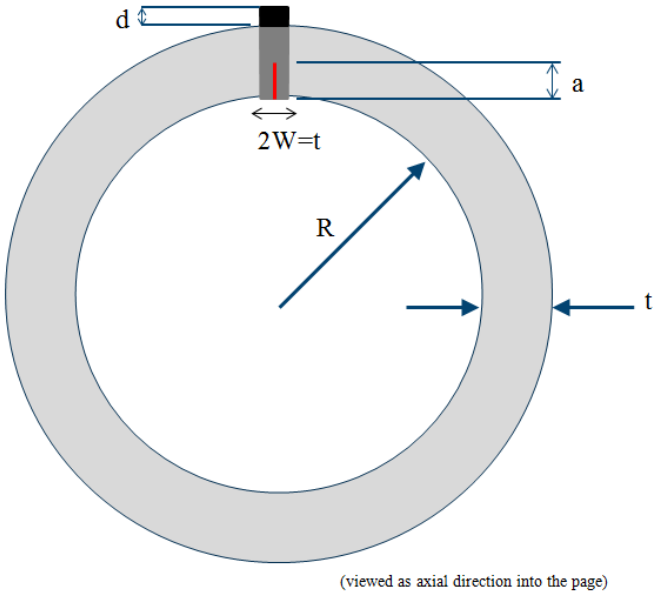

Figure A1 2D Planar Sketch of ID Crack

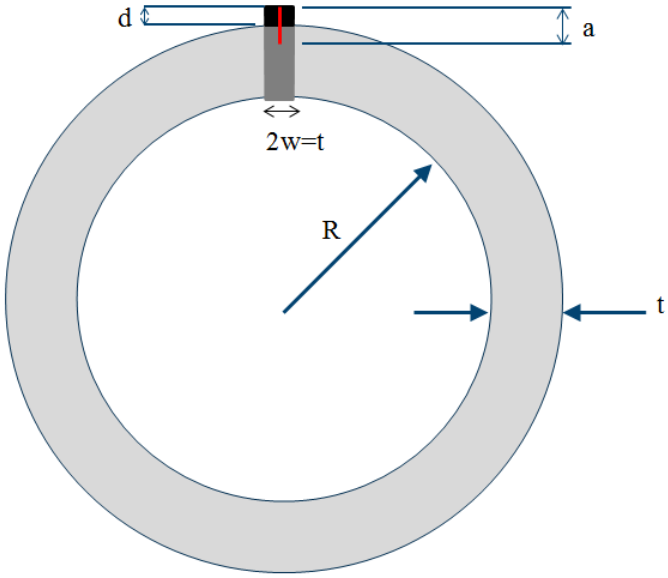

Figure A2 2D Planar Sketch of OD Crack

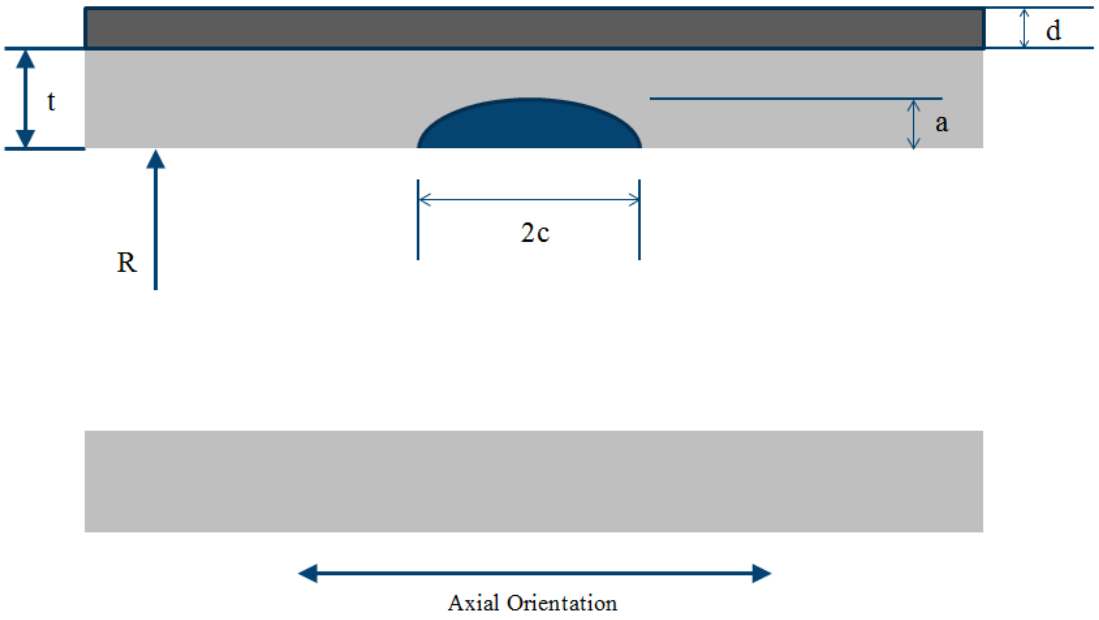

Figure A3 2D Planar Sketch of Axial, Elliptical, Part Through-Wall Crack on ID

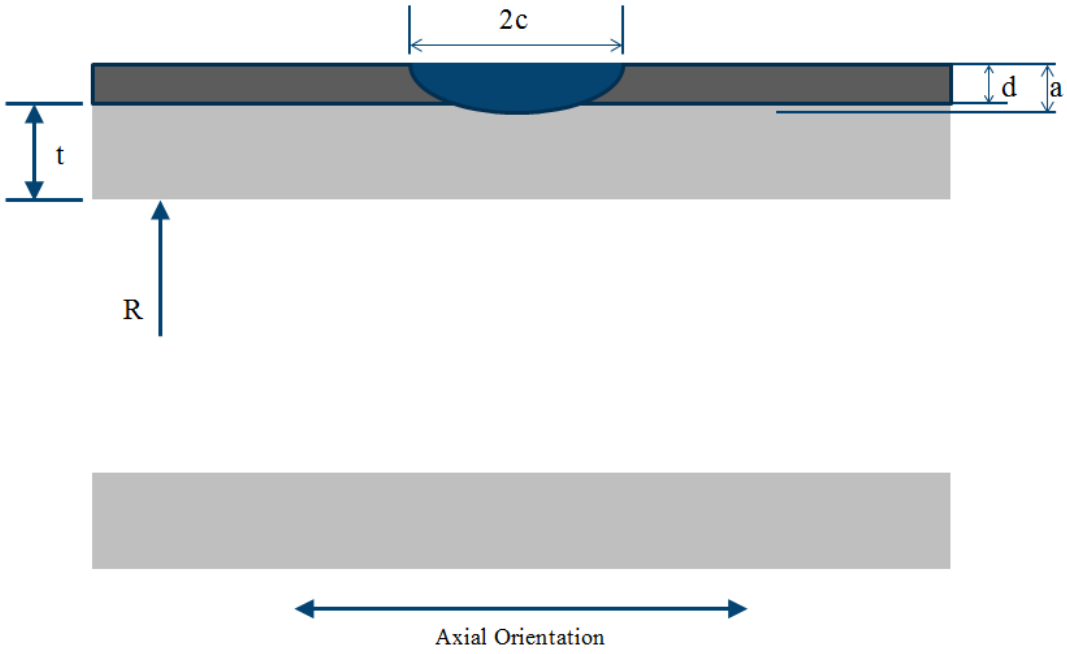

Figure A4 2D Planar Sketch of Axial, Elliptical, Part Through-Wall Crack on OD

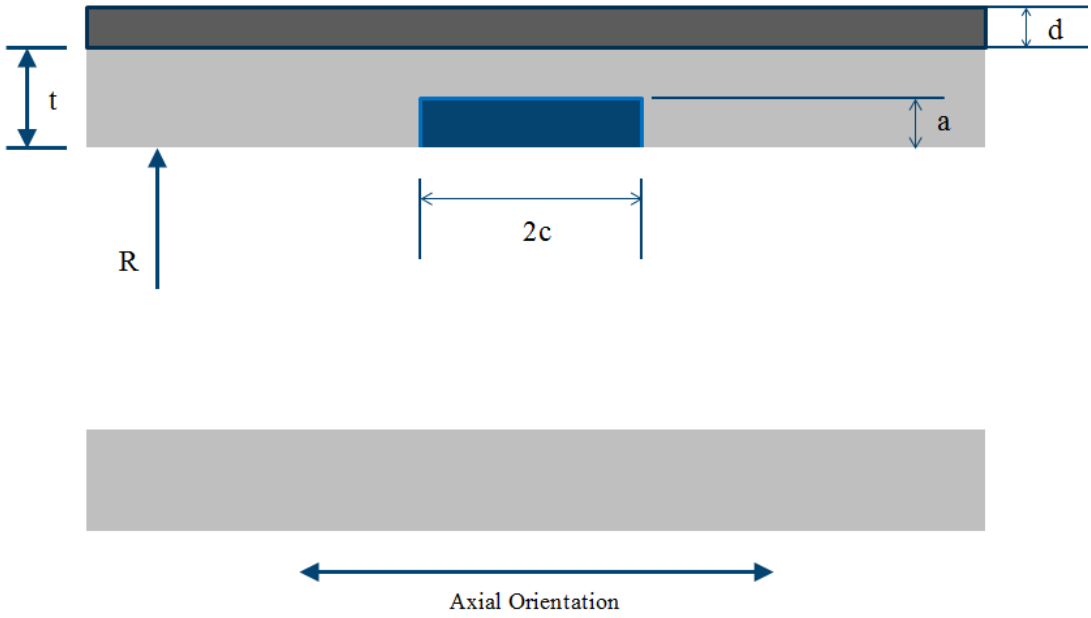

Figure A5 2D Planar Sketch of Axial, Rectangular, Part Through-Wall Crack on ID

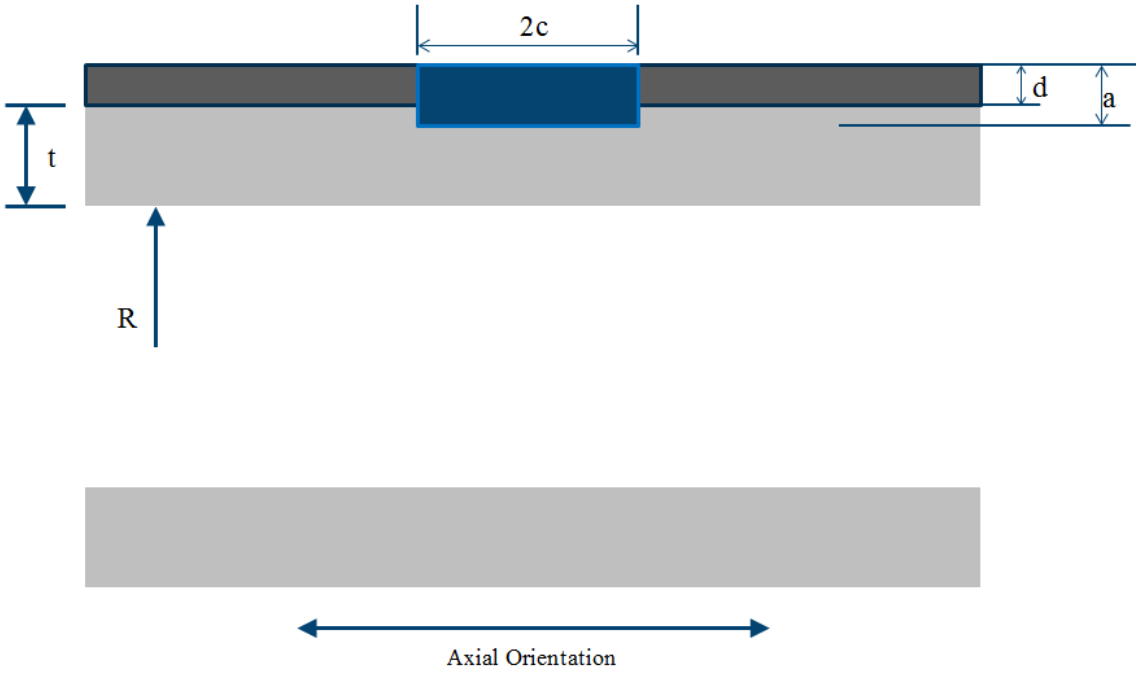

Figure A6 2D Planar Sketch of Axial, Rectangular, Part Through-Wall Crack on OD

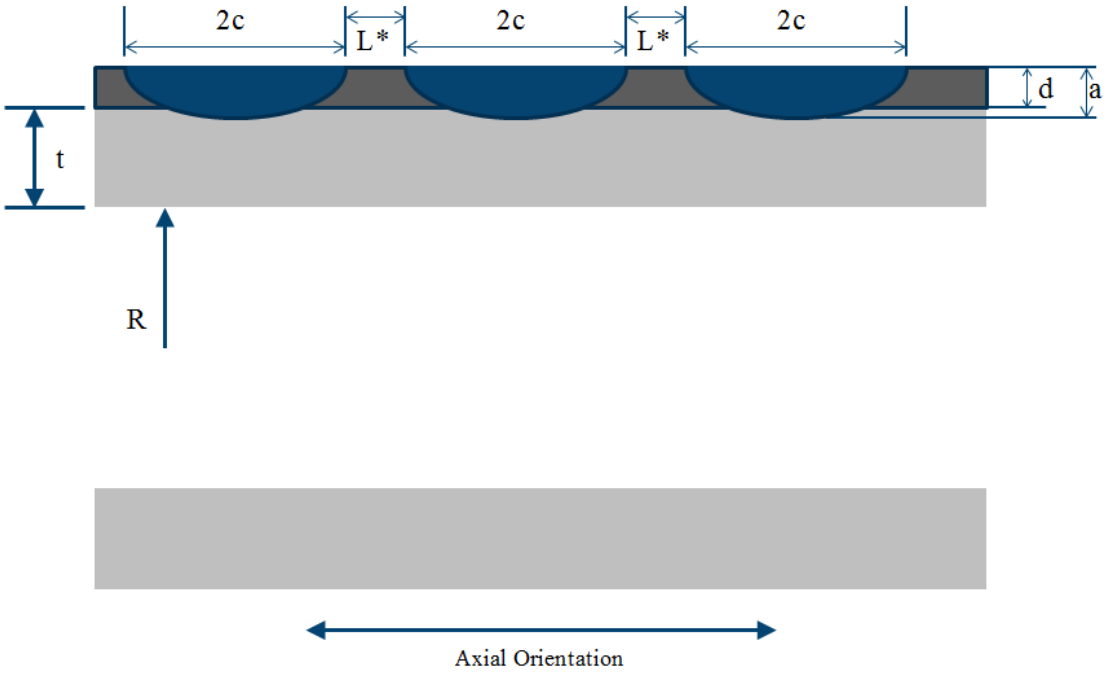

Figure A7 **2D Planar Sketch of Multiple, Axial, Elliptical, Part Through-Wall Cracks on OD**

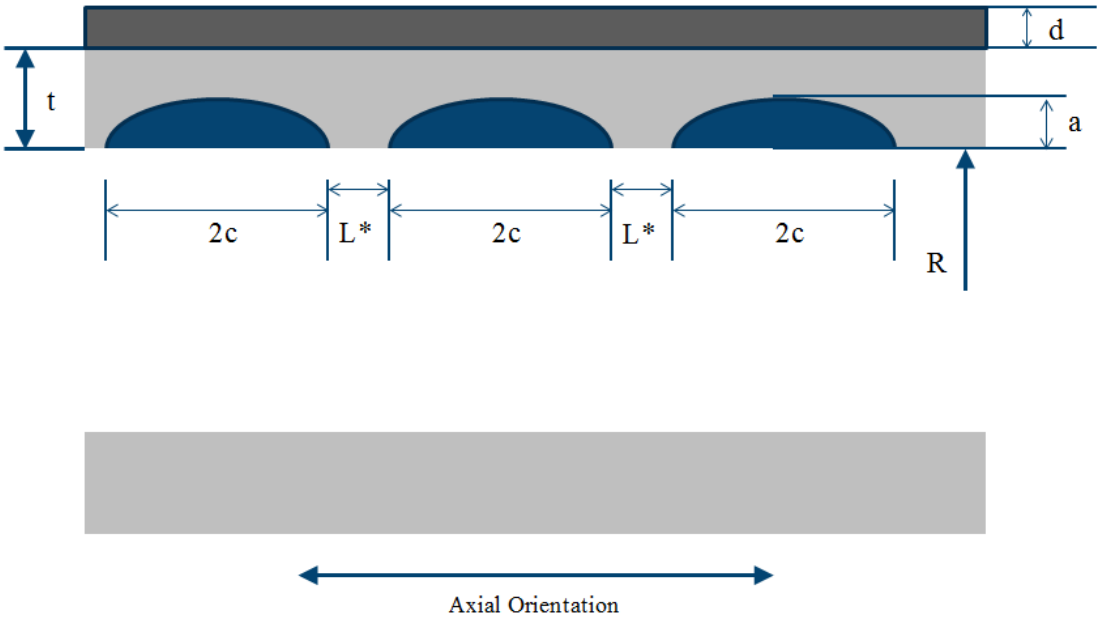

Figure A8 **2D Planar Sketch of Multiple, Axial, Elliptical, Part Through-Wall Cracks on ID**

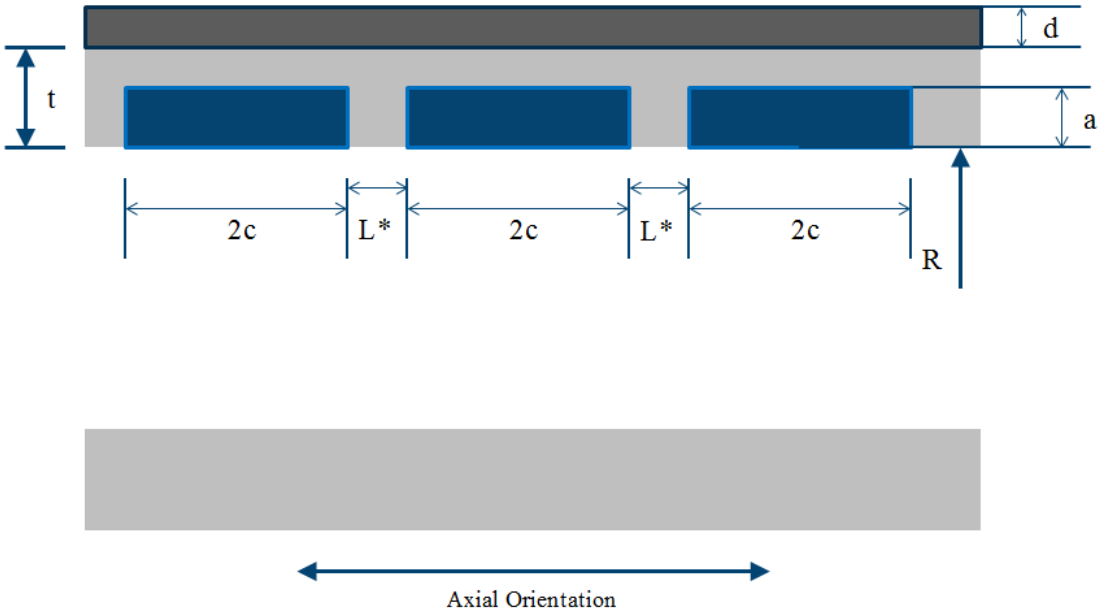

Figure A9 **2D Planar Sketch of Multiple, Axial, Rectangular, Part Through-Wall Cracks on ID**

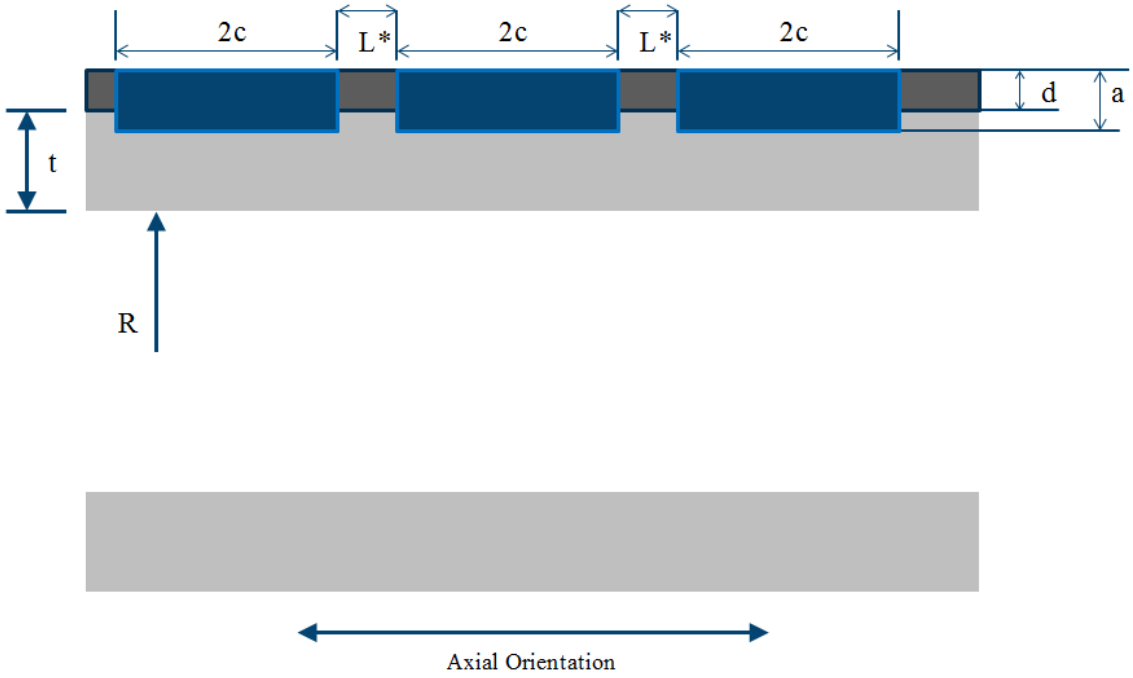

Figure A10 **2D Planar Sketch of Multiple, Axial, Rectangular, Part Through-Wall Cracks on OD**

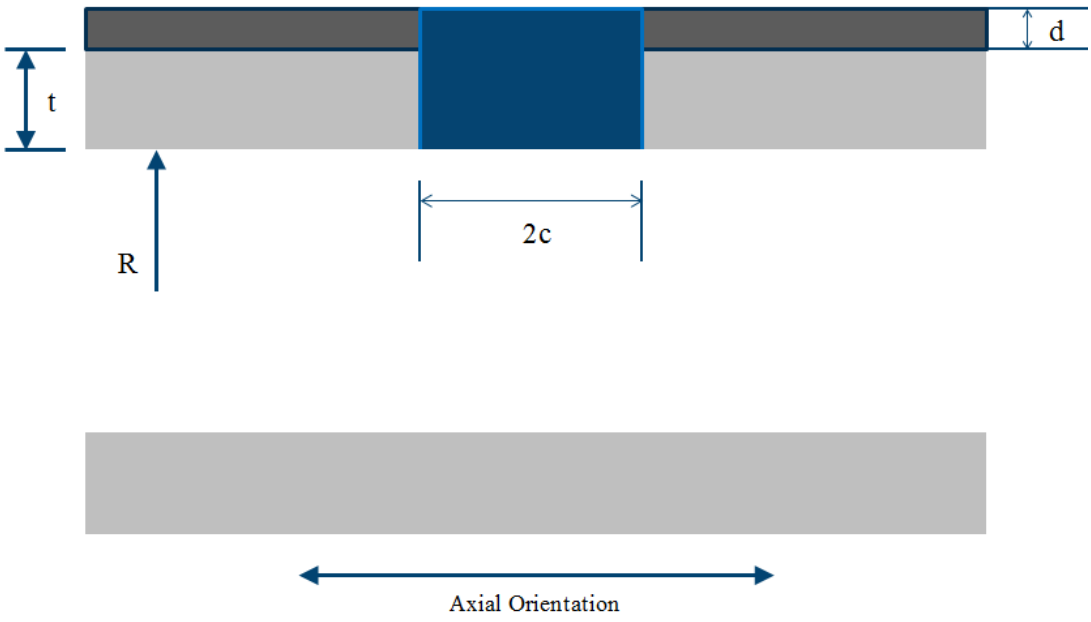

Figure A11 2D Planar Sketch of a Through-Wall Crack

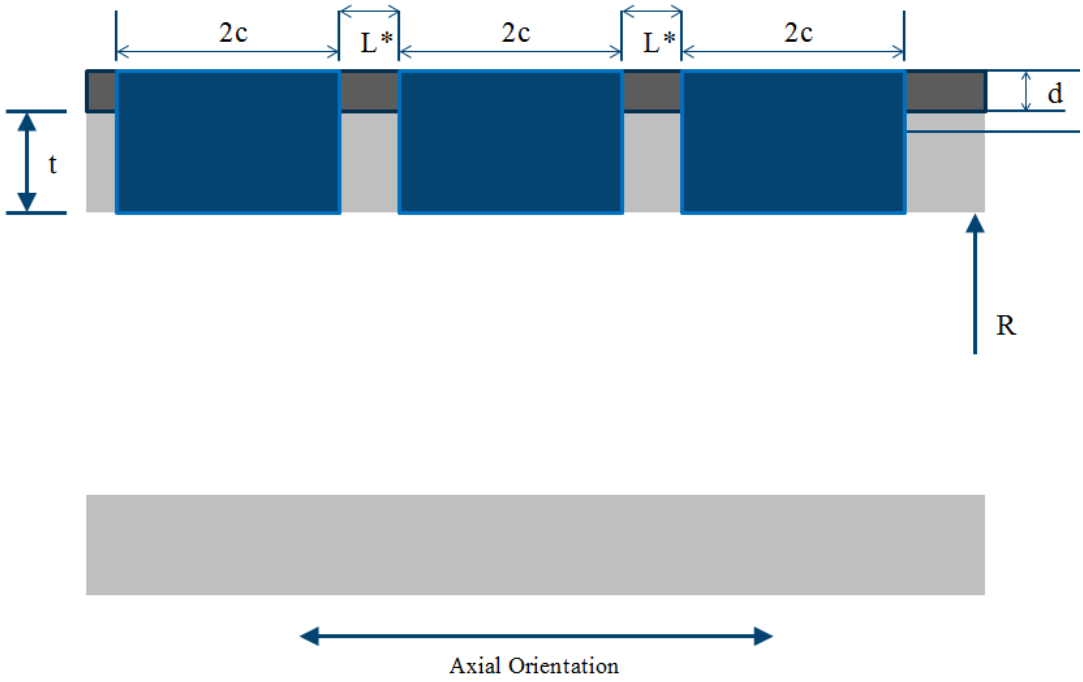

Figure A12 2D Planar Sketch of Multiple Through-Wall Cracks

APPENDIX B – SSWC AND SSWC WITH PLANAR CRACKS

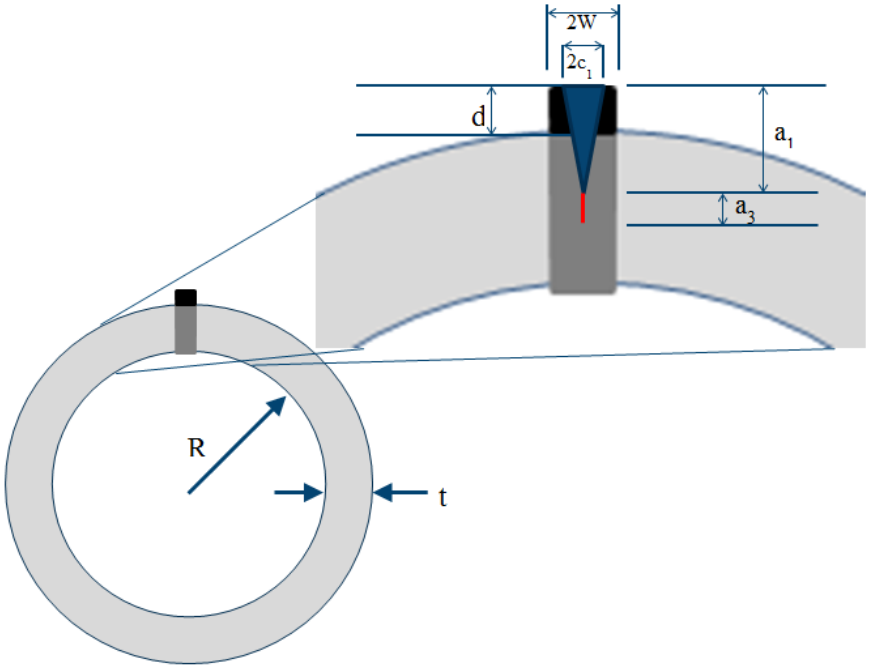

Figure B1 2D SSWC V-Groove Plane-Strain – No General Corrosion

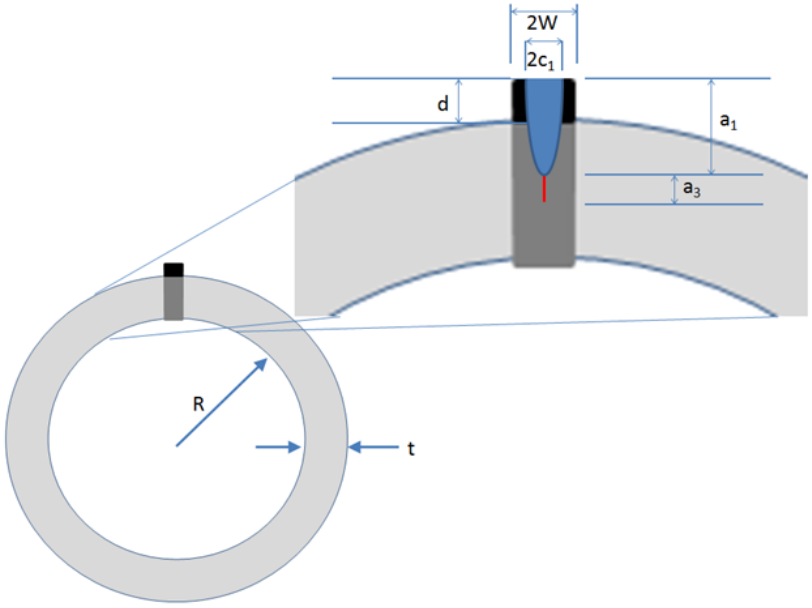

Figure B2 2D SSWC U-Groove Plane-Strain – No General Corrosion

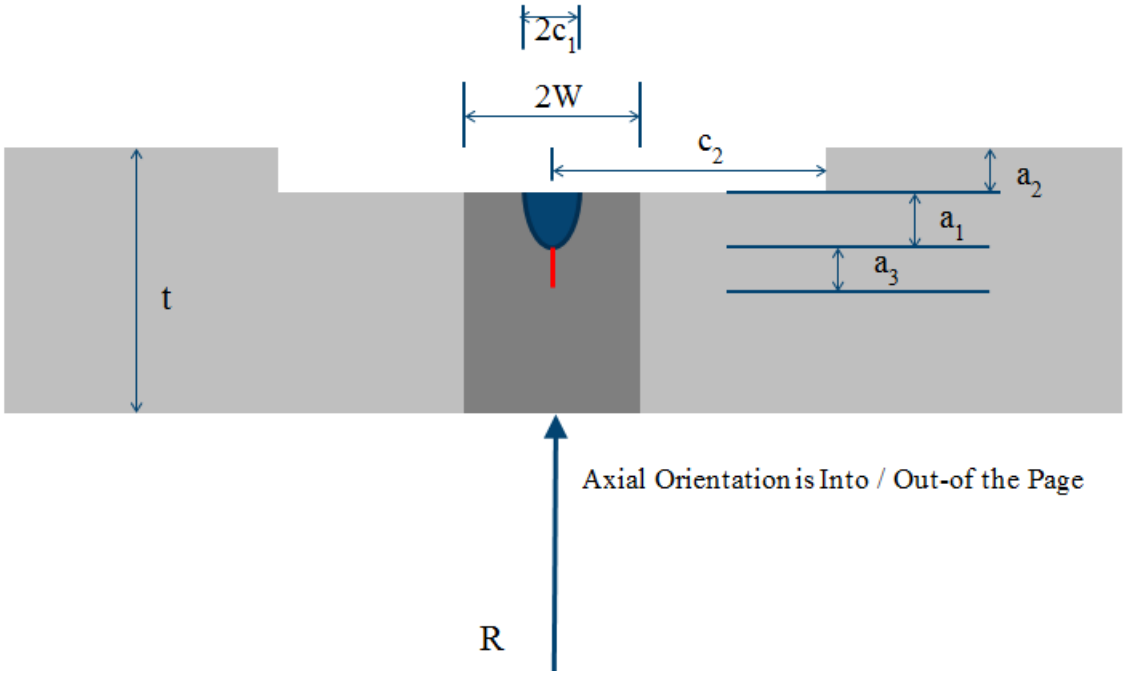

Figure B3 2D SSWC U-Groove Plane-Strain – Symmetric General Corrosion

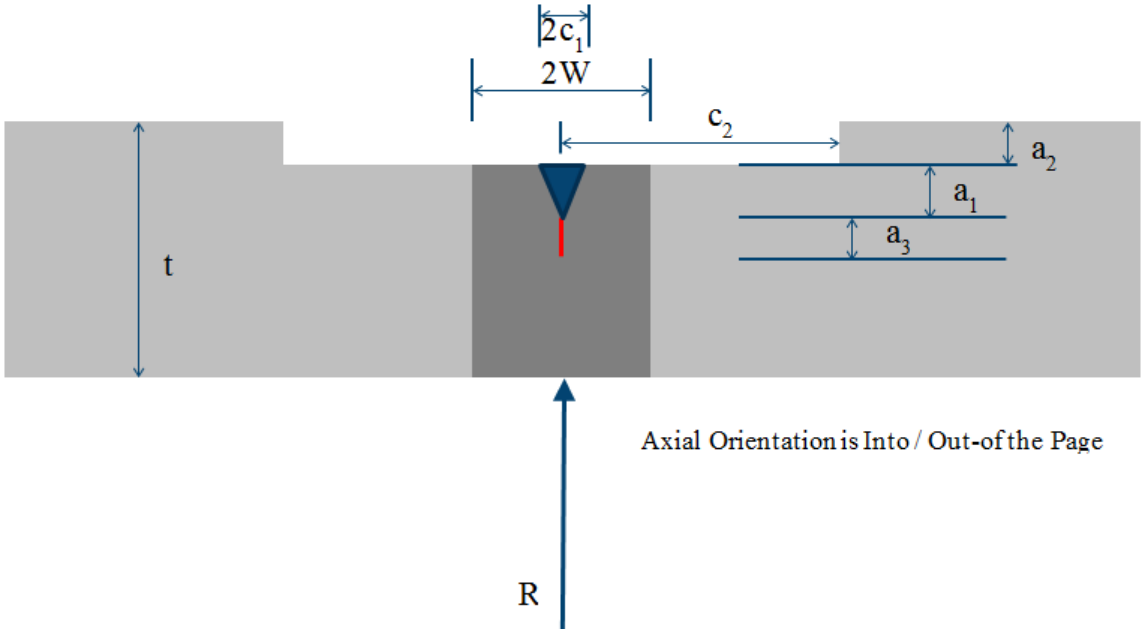

Figure B4 2D SSWC V-Groove Plane-Strain – Symmetric General Corrosion

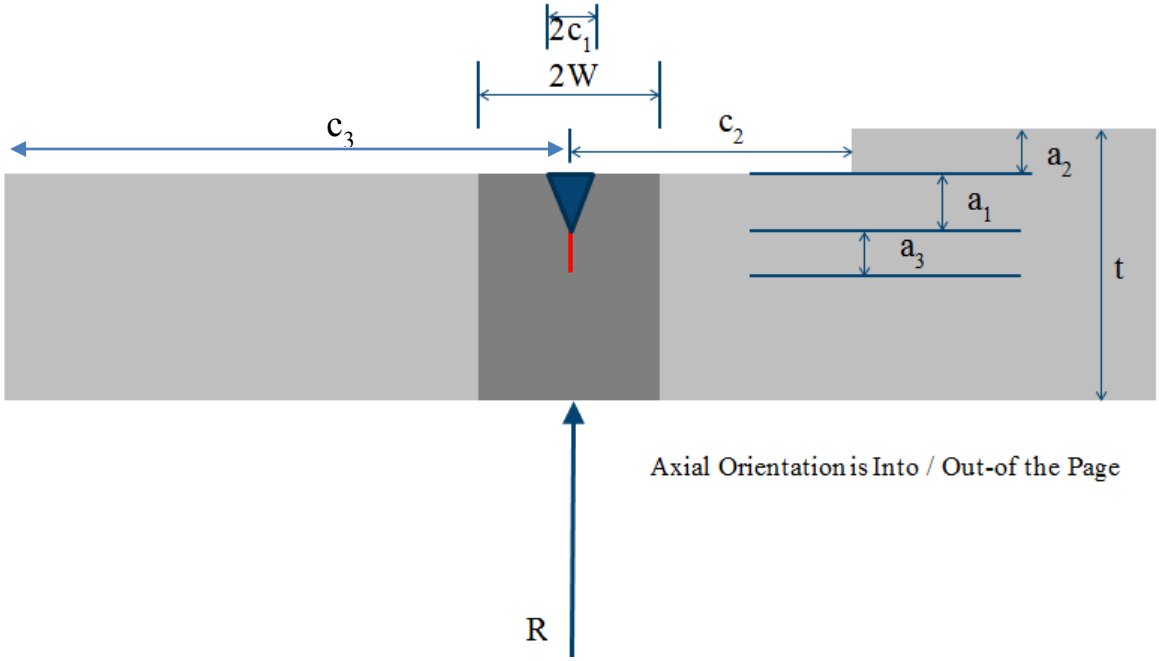

Figure B5 2D SSWC V-Groove Plane-Strain – Asymmetric General Corrosion

APPENDIX C – HOOK CRACKS

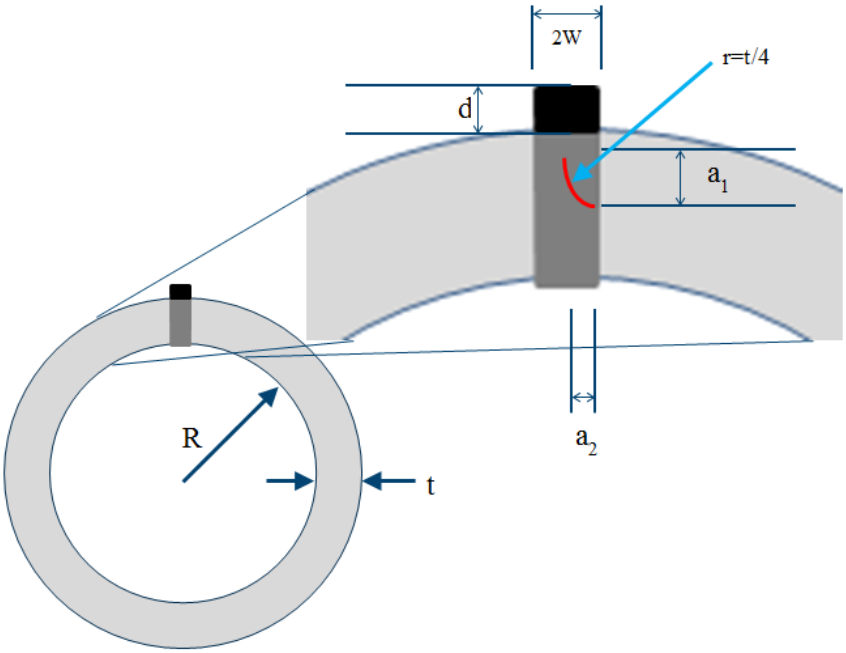

Figure C1 2D, Internal Hook Crack

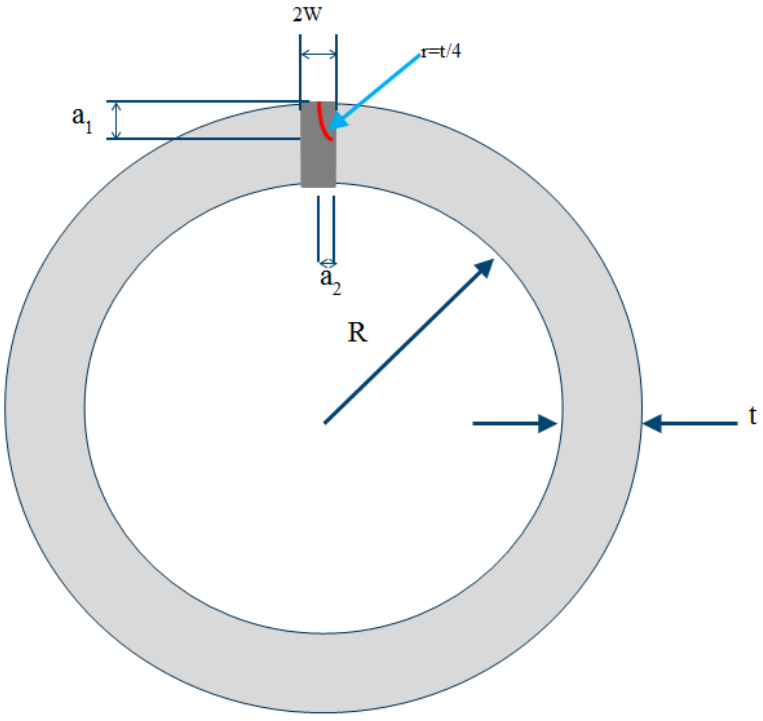

Figure C1 2D, Surface Hook Crack

Appendix A

Appendix A
Stress Intensity Factors

Overview

The stress intensity factor (K) for a crack is required for calculation of the strain energy release rate (J-integral) for ductile tearing and fatigue crack growth. K is dependent on pipe and crack geometry, as well as the applied load. For all but a few specialized geometry cases, K cannot be determined in closed form. Accordingly, finite element analysis (FEA) must be used to determine K analytically, as described in Attachment A. The resulting data are K as discrete points that are subsequently fitted with smooth, analytic functions that fully describe the relationship between the K and all relevant parameters over the design space of crack depth, crack length, and other relevant geometry parameters.

The FEA models used to generate K solutions simulated a pipe with an outer diameter of 15.5" and a thickness of 0.25", which, for all practical purposes, is prototypically thin walled. In the FE model, the pipe was pressurized to 100 psi. Because stress intensity factor scales linearly with remote (hoop) stress, the choice of 100 psi internal pressure for the loading is completely arbitrary. Normalizing the resulting stress intensity factors with respect to the mean hoop stress makes them applicable to all pipe sizes that are considered thin walled (diameter/thickness > 20).

Analytic Equation Fits

For a J-controlled tearing failure (in contrast to a net-section limit load failure), two J-related conditions must be satisfied:

$$J_{material} = J_{applied} \tag{1a}$$

$$\frac{dJ_{material}}{da} = \frac{dJ_{applied}}{da} \tag{1b}$$

where J is the J-integral, a is the crack size (depth). For the axial crack pipe problem, J is proportional to the stress intensity factor, K, and the size of the plastic zone at the tip of the crack. Thus, to calculate pipe internal pressure needed to cause a J-controlled tearing failure in PipeAssess PI™, the first derivative of K with respect to crack depth must be known.

Furthermore, K must be known from some starting crack depth to the depth that goes just through the pipe wall. Finally, from experience, discontinuities in the slope of the K versus crack size cause solution convergence issues, so performing numerical derivatives on relatively sparse, discrete-valued tables is problematic, even though sparse, discrete-valued tables is the native format for the FEA SIF solutions.

To ensure smoothness of K versus crack depth and to permit extrapolation to the fully through-wall condition, the relatively sparse, discrete-valued K tables from the FEA solutions are fitted with an analytic function using one of three forms:

$$\psi = A\left(\frac{a}{t}\right)^2 + B\frac{a}{t} + C \tag{2a}$$

$$\psi = e^{\left(A\frac{a}{t} + B\right)} + C \tag{2b}$$

$$\psi = A + B\frac{a}{t}\left(1 + e^{C\left(1 - \frac{a}{t}\right)}\right) \tag{2c}$$

where *A*, *B*, and *C* are fitting coefficients, *a* is crack depth, *t* is normalized wall thickness, and $K = \psi\sigma$. The first choice for the fitting function is always 2a, with 2b and 2c only used if the least squares fit quadratic form has an inflection in the range $0 \leq \frac{a}{t} \leq 1$. All three forms shown in Equation 2 are smooth and continuous over the range $0 \leq \frac{a}{t} \leq 1$, and they have closed-form derivatives with respect to *a*.

In most cases, there are more variables in addition to $\frac{a}{t}$ on which K depends. In such cases, simple linear interpolation is used sequentially on all variables up to $\frac{a}{t}$, with $\frac{a}{t}$ behavior fitted at the final stage per Equation 2 for use in determining the J-controlled tearing failure pressure.

Nomenclature

OD	Outer Diameter of Pipe
t	Wall thickness of Pipe
d	Weld cap height
a	Crack depth through the thickness of pipe
2c	Total crack length along the pipe axis for surface cracks
2W	Width of the weld in the circumferential direction
a1	Depth of the selective seam corrosion
2c1	Width of the selective seam corrosion cracking at the OD (or tope of the weld cap)
2c2	Width of the general corrosion for selective seam weld corrosion cracking
a2	Depth of the general corrosion for selective seam weld corrosion cracking
a3	Crack depth for the crack portion for selective seam weld corrosion cracking

Geometry Codes

Each type of pipe/crack geometry was assigned a descriptive code. The format of the code is dependent upon the type of flaw. The basic code takes the format TYPE_Param1_ParamN. The parameters vary by flaw type and are listed below.

If TYPE=**CW** (cold weld): TYPE_GEOMETRY_SURFACE_WALL_NUMBER_DIMENSION_(CRACK)_LOCATION	
	GEOMETRY: **IL**=infinitely long, **R**=rectangular flaw, **E**=semi-elliptical, **NA**=not applicable
	SURFACE: **ID**=crack on inner surface, **OD**=crack on outer surface, **NA**=not applicable
	WALL: **TWC**=through-wall crack, **PTWC**=part through-wall crack (surface crack)
	NUMBER: **S**=single crack, **M**=multiple cracks
	DIMENSION: **2D**=two dimensional analysis model, **3D**=three-dimensional analysis model
	CRACK: **Ckx**=crack number x (Used only when NUMBER=**M**)
	LOCATION: **Deep**=deepest point on crack, **Surf**=where the crack intersects the pipe surface, **Surfx** or **Sx**=where the crack x intersect the pipe surface (when NUMBER=M), **Avg**=average value
If TYPE=**SSWC** (selective seam weld corrosion): TYPE_GEOMETRY_DIMENSION_CORROSION_CRACK	
	GEOMETRY: **V**=v-groove, **U**=u-groove
	DIMENSION: **2D**=two dimensional analysis model
	CORROSION: **N**=none, **S**=symmetrical about seam weld, **A**=asymmetrical with respect to seam weld
	CRACK: **N**=no, **Y**=yes
IF TYPE=**HC** (hook crack): TYPE_GEOMETRY_DIMENSION_LOCATION_MODE	
	GEOMETRY: **I**=internal, **S**=surface breaking
	DIMENSION: **2D**=two dimensional analysis model
	LOCATION: **TOP**=tip at top of crack, **BOT**=tip at bottom of crack
	MODE: **KI**=mode I (opening), **KII**=mode II (in-plane shear)

Some of the geometry codes listed above are not part of the solution space examined as part of this task. In particular, the TWC, HC and M (multiple) codes have not been used. They are listed, however, because it is inevitable that they will eventually be analyzed.

Geometry Cases

The various pipe geometries for which K solutions were generated are described below.

Code: CW_IL_ID_PTWC_S_2D

Inputs: OD, t, d, a

Input Limitations: OD/t > 40 , a < t+d

Solution Bounds: 0.05 < a/(t+d) < 0.9, 0 < d/t < 1

Depth Normalizing Parameter: t*=d+t

Associated FEA Case: 1.2 CW_IL_OD_PTWC_S_2D_Deep

Description:

This geometry represents a cold welded pipe with a single infinitely long surface crack on the inner diameter of the pipe. The data were generated using a two-dimensional finite element model.

Diagram:

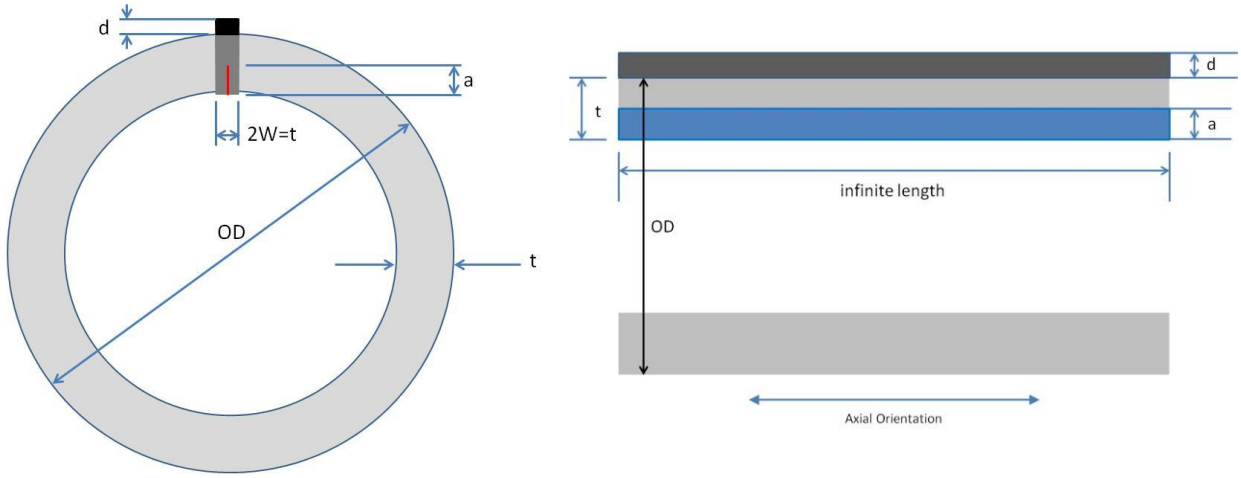

Figure 1: CW_IL_ID_PTWC_S_2D

Code: CW_IL_OD_PTWC_S_2D

Inputs: OD, t, d, a

Input Limitations: OD/t > 40 , a < t+d

Solution Bounds: 0.05 < a/(t+d) < 0.9, 0 < d/t < 1

Depth Normalizing Parameter: t*=d+t

Associated FEA Case: 1.2 CW_IL_OD_PTWC_S_2D_Deep

Description:

This geometry represents a cold welded pipe with a single infinitely long surface crack on the outer diameter of the pipe. The data were generated using a two-dimensional finite element model.

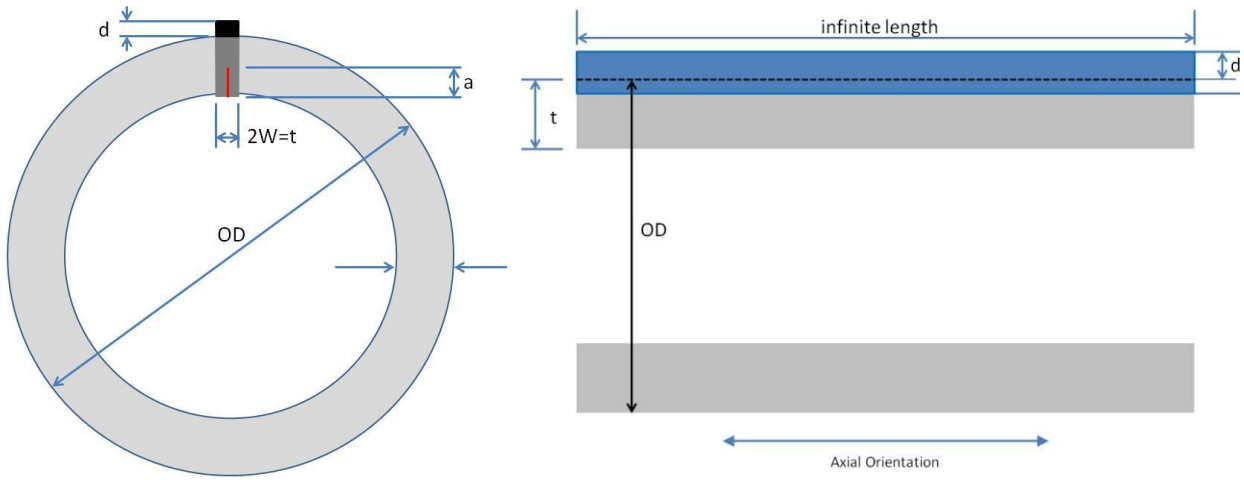

Figure 2: CW_IL_OD_PTWC_S_2D

Code: CW_E_ID_PTWC_S_3D

Inputs: OD, t, d, a, 2c

Input Limitations: OD/t > 40 , a < t+d

Solution Bounds: 0.05 < a/(t+d) < 0.9, 0 < d/t < 1, 2 < c/a < 10

Relevant Depth Normalizing Parameter: t*=d+t

Associated FEA Cases: 1.6 CW_E_ID_PTWC_S_3D_Deep, 1.6 CW_E_ID_PTWC_S_3D_Surf

Description:

This geometry represents a cold welded pipe with a single semi-elliptical surface crack on the inner diameter of the pipe. The data were generated using a three-dimensional finite element model.

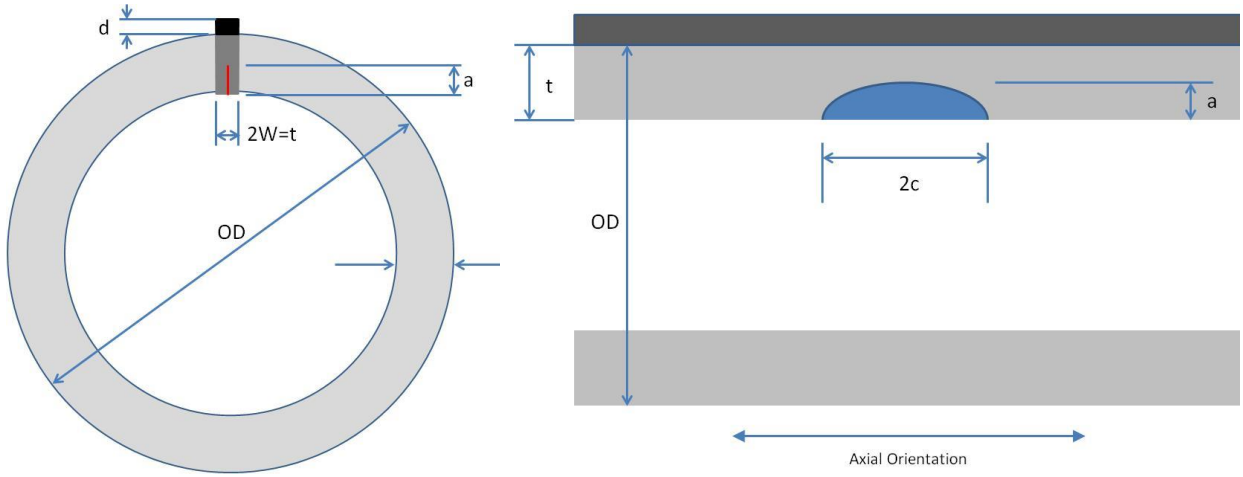

Figure 3: CW_E_ID_PTWC_S_3D

Code: CW_E_OD_PTWC_S_3D

Inputs: OD, t, d, a, 2c

Input Limitations: OD/t > 40 , a < t+d

Solution Bounds: 0.05 < a/(t+d) < 0.9, 0 < d/t < 1, 2 < c/a < 10

Depth Normalizing Parameter: t*=d+t

Associated FEA Cases: 1.7 CW_E_OD_PTWC_S_3D_Deep, 1.7 CW_E_OD_PTWC_S_3D_Surf

Description:

This geometry represents a cold welded pipe with a single semi-elliptical surface crack on the outer diameter of the pipe. The data were generated using a three-dimensional finite element model.

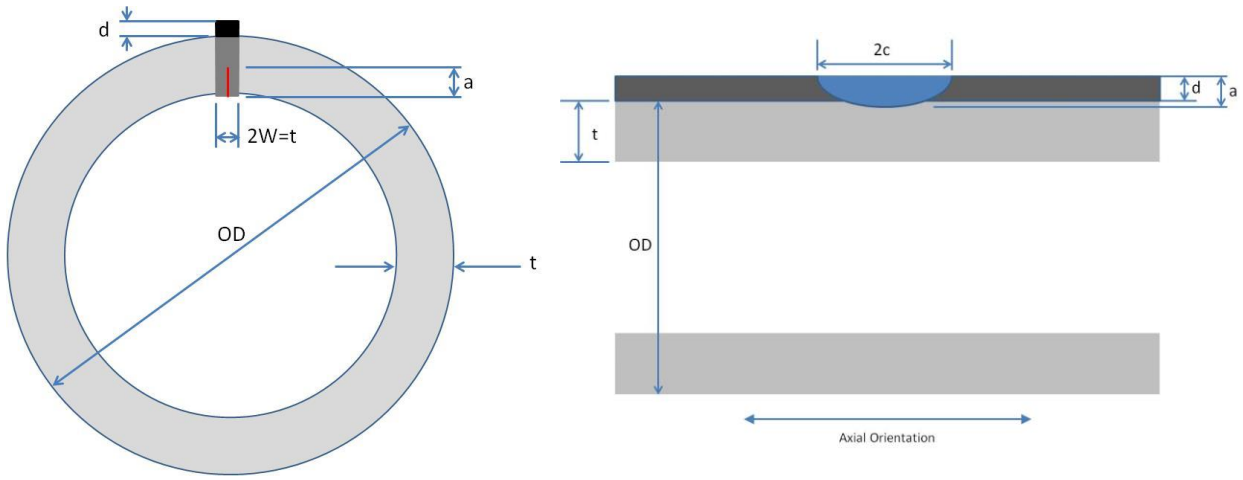

Figure 4: CW_E_OD_PTWC_S_3D

Code: SSWC_V_2D_N_N

Inputs: OD, t, d, a, 2c

Input Limitations: OD/t > 40, a1 < t+d, 2c1 < 2W

Solution Bounds: 0 < d/t < 1, 0.05 < a1/(d+t) < 0.9, 0.1 < 2c1/2W < 1

Depth Normalizing Parameter: t2=d+t-a1

Associated FEA Case: 2.1 SSWC_V_2D_N_N_Deep

Description:

This geometry represents a V-groove seam welded pipe with no crack. The data were generated using a two-dimensional finite element model.

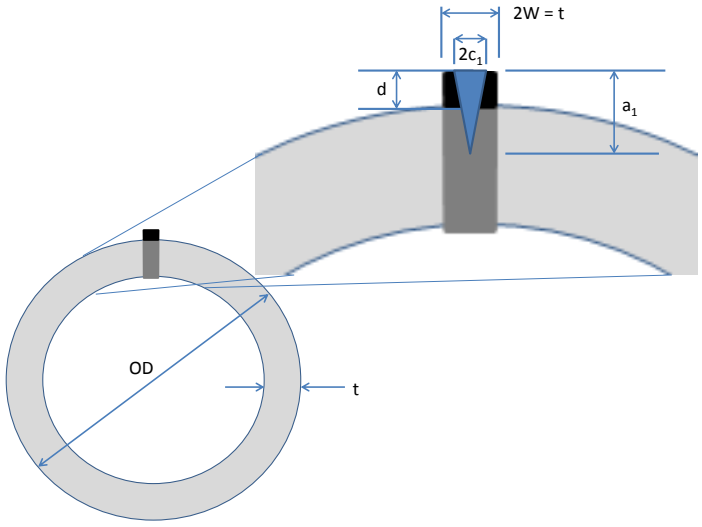

Figure 5: SSWC_V_2D_N_N

Code: SSWC_V_2D_S_N

Inputs: OD, d, t, a1, 2c1

Input Limitations: OD/t > 40, $a_1 + a_2 < t$

Solution Bounds: 0.25 < a1/(t-a2) < 0.75, 0.1 < a2/t < 0.5, 0.25 < 2c1/2W < 0.75, 2 < 2c2/2W < 4

Depth Normalizing Parameter: t2=t-a2-a1

Associated FEA Case: 2.2 SSWC_V_2D_S_N_Deep

Description:

This geometry represents a V-groove seam welded pipe with corrosion symmetrical about the weld. The data were generated using a two-dimensional finite element model.

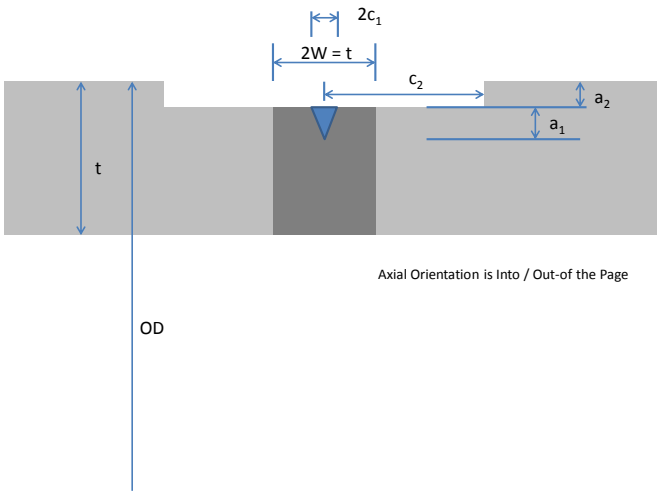

Figure 6: SSWC_V_2D_S_N

Code: SSWC_V_2D_A_N

Inputs: OD, t, a1, a2, 2c1, c2

Input Limitations: OD/t > 40, $a_1 + a_2 < t$

Solution Bounds: 0.25 < a1/(t-a2) < 0.75, 0.1 < a2/t < 0.5, 0.25 < 2c1/2W < 0.75, 2 < 2c2/2W < 4

Depth Normalizing Parameter: t2=t-a2-a1

Associated FEA Case: 2.3 SSWC_V_2D_A_N_Deep

Description:

This geometry represents a V-groove seam welded pipe with corrosion asymmetrical with respect to the weld. The data were generated using a two-dimensional finite element model.

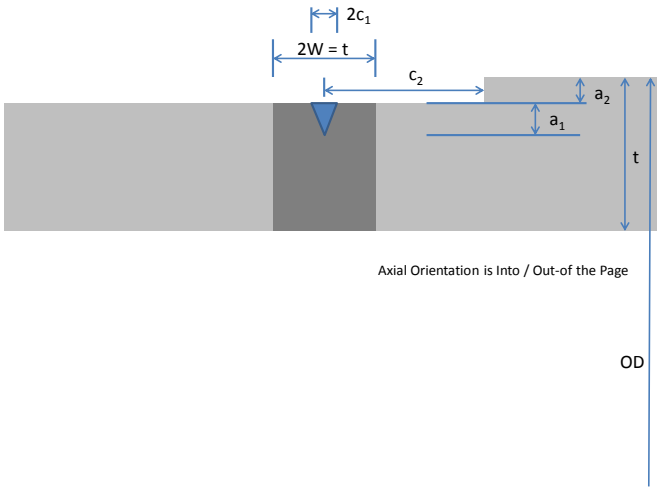

Figure 7: SSWC_V_2D_A_N

Code: SSWC_V_2D_N_Y

Inputs: OD, t, a1, a3, 2c1

Input Limitations: OD/t > 40, a1+a3 < t+d, 2c1< 2W

Solution Bounds: 0.25 < d/t < 0.75, 0.25 < a1/(d+t) < 0.75, 0.1 < a3/(d+t-a1) < 0.75, 0.25 < 2c1/2W < 0.75

Depth Normalizing Parameter: t2=d+t-a1

Associated FEA Case: 2.3 SSWC_V_2D_A_N_Deep

Description:

This geometry represents a V-groove seam welded pipe with a crack at the tip of the groove. The data were generated using a two-dimensional finite element model.

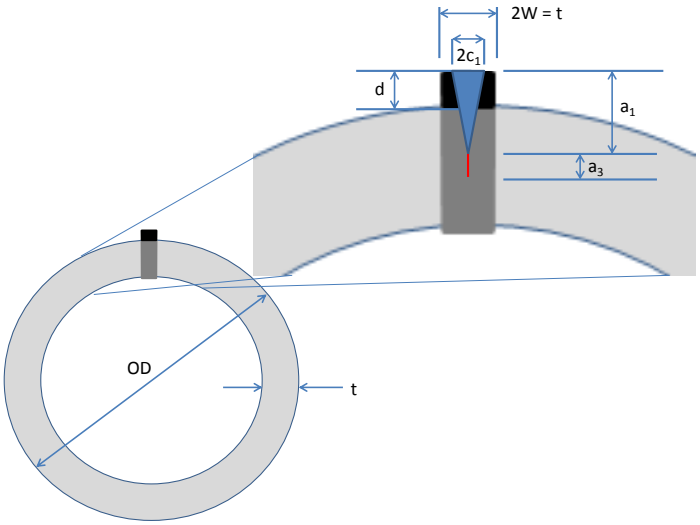

Figure 8: SSWC_V_2D_N_Y

Code: SSWC_V_2D_S_Y

Inputs: OD, t, a_1, a_2, a_3, $2c_1$, c_2

Input Limitations: $OD/t > 40$, $a_1+a_3 < t-a_2$, $2c_1 < 2W$

Solution Bounds: $0.25 < a1/(t-a2) < 0.75$, $0.1 < a2/t < 0.5$, $0.1 < a3/(t-a1-a2) < 0.75$, $0.25 < 2c1/2W < 0.75$, $2 < 2c2/2W < 4$

Depth Normalizing Parameter: $t2=t-a2-a1$

Associated FEA Case: 2.5 SSWC_V_2D_S_Y_Deep

Description:

This geometry represents a V-groove seam welded pipe with corrosion symmetrical about the weld and a crack at the tip of the groove. The data were generated using a two-dimensional finite element model.

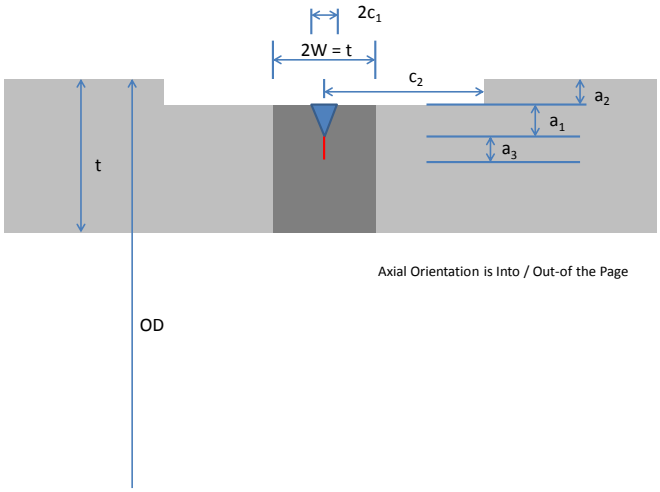

Figure 9: SSWC_V_2D_S_Y

Code: SSWC_V_2D_A_Y

Inputs: OD, t, a_1, a_2, a_3, $2c_1$, c_2

Input Limitations: $OD/t > 40$, $a_1+a_3 < t-a_2$, $2c_1 < 2W$

Solution Bounds: $0.25 < a1/(t-a2) < 0.75$, $0.1 < a2/t < 0.5$, $0.1 < a3/(t-a1-a2) < 0.75$, $0.25 < 2c1/2W < 0.75$, $2 < 2c2/2W < 4$

Depth Normalizing Parameter: t2=t-a2-a1

Associated FEA Case: 2.6 SSWC_V_2D_A_Y_Deep

Description:

This geometry represents a V-groove seam welded pipe with corrosion asymmetrical about the weld and a crack at the tip of the groove. The data were generated using a two-dimensional finite element model.

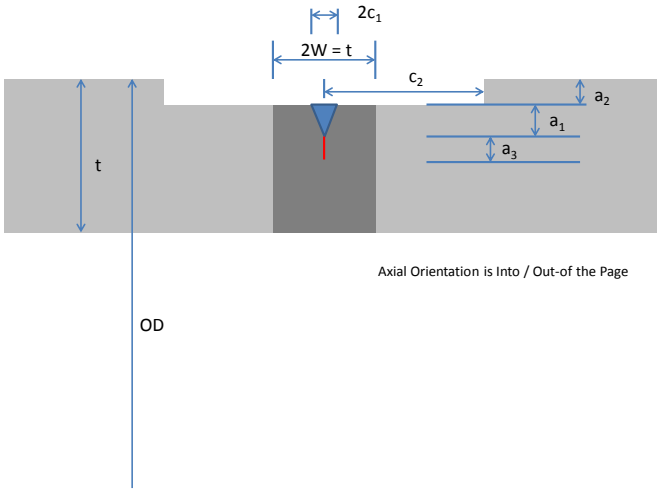

Figure 10: SSWC_V_2D_A_Y

Code: SSWC_U_2D_N_N

Inputs: OD, t, d, a1, 2c1

Input Limitations: OD/t > 40, a1 < t+d, 2c1 < 2W

Solution Bounds: 0 < d/t < 1, 0.05 < a1/(d+t) < 0.9, 0.1 < 2c1/2W < 1

Depth Normalizing Parameter: t2=d+t-a1

Associated FEA Case: 2.7 SSWC_U_2D_N_N_Deep

Description:

This geometry represents a U-groove seam welded pipe with no crack. The data were generated using a two-dimensional finite element model.

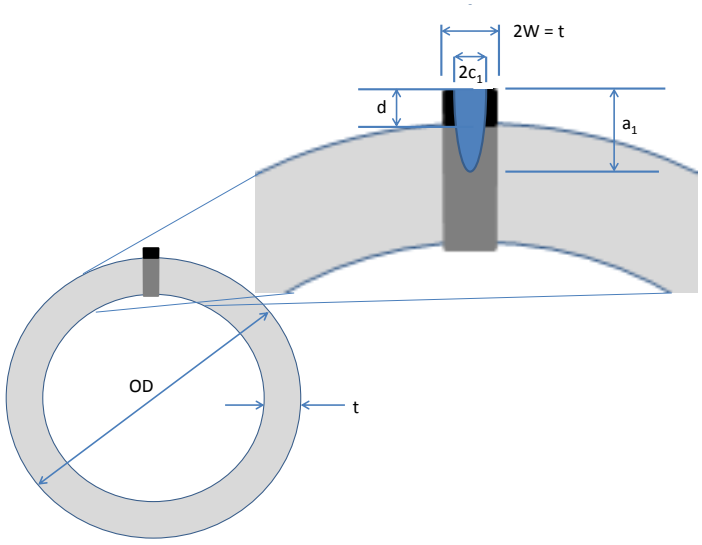

Figure 11: SSWC_U_2D_N_N

Code: SSWC_U_2D_S_N

Inputs: OD, t, a1, a2, 2c1, c2

Input Limitations: OD/t > 40, a1+ a2 < t

Solution Bounds: 0.25 < a1/(t-a2) < 0.75, 0.1 < a2/t < 0.5, 0.25 < 2c1/2W < 0.75, 2 < 2c2/2W < 4

Depth Normalizing Parameter: t2=t-a2-a1

Associated FEA Case: 2.8 SSWC_U_2D_S_N_Deep

Description:

This geometry represents a U-groove seam welded pipe with corrosion symmetrical about the weld and no crack. The data were generated using a two-dimensional finite element model.

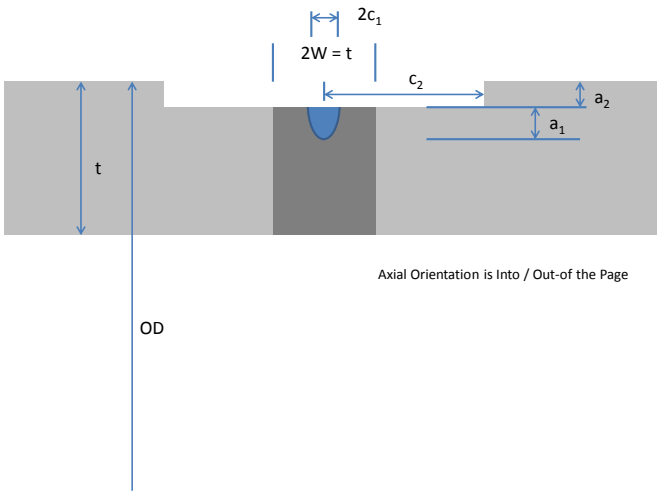

Figure 12: SSWC_U_2D_S_N

Code: SSWC_U_2D_N_Y

Inputs: OD, t, d, a1, a3, 2c1

Input Limitations: OD/t > 40, a1+a3 < t+d, 2c1 < 2W

Solution Bounds: 0.25 < d/t < 0.75, 0.25 < a1/(d+t) < 0.75, 0.1 < a3/(d+t-a1) < 0.75, 0.25 < 2c1/2W < 0.75

Depth Normalizing Parameter: t2=t-a2-a1

Associated FEA Case: 2.9 SSWC_U_2D_N_Y_Deep

Description:

This geometry represents a U-groove seam welded pipe with a crack at the tip of the groove. The data were generated using a two-dimensional finite element model.

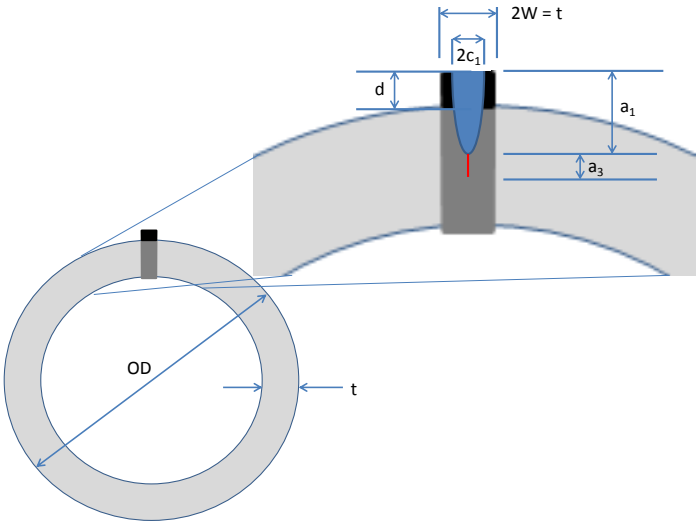

Figure 13: SSWC_U_2D_N_Y

Stress Intensity Factors

As indicated in the body of the report, limiting cases of geometry (infinitely long, for instance) have been absorbed into the basic crack cases (elliptical, for instance). Likewise, as discussed above, analytic functions have been fitted to variations in growth through the depth. The plots shown below indicate the raw data points as red dots, while the surface shows the smooth variation of the function in a/t space.

In general, the growth through the depth in the plots is denoted at a/t* or a3/t2 where t* is thickness plus weld cap height or t2 is the pipe wall thickness less the sum of the general corrosion height and V-groove or U-groove height.

Task 1 Stress Intensity Factors

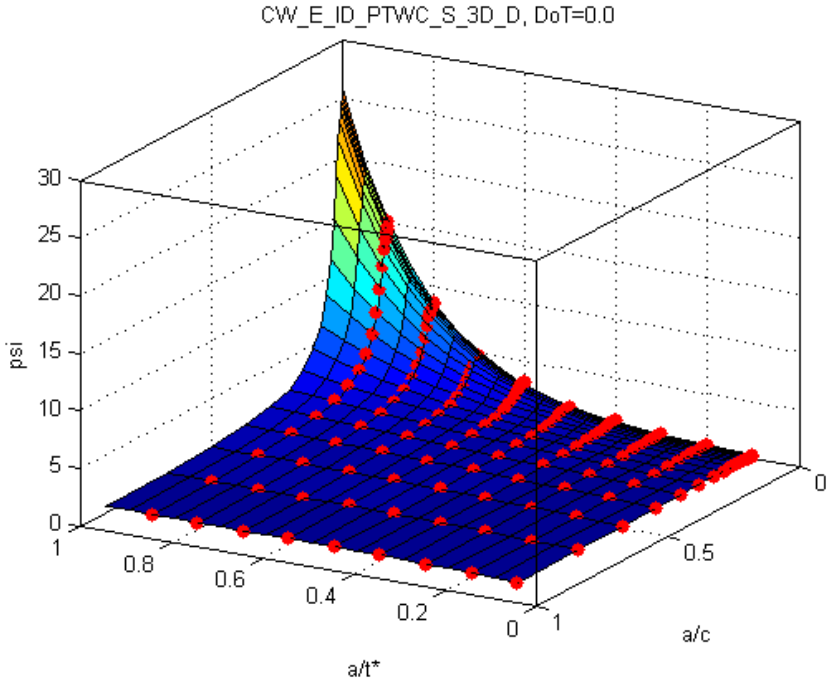

Figure 14: Cold Weld Semi-Elliptical ID Surface Crack at the Deepest Point, No Weld Cap

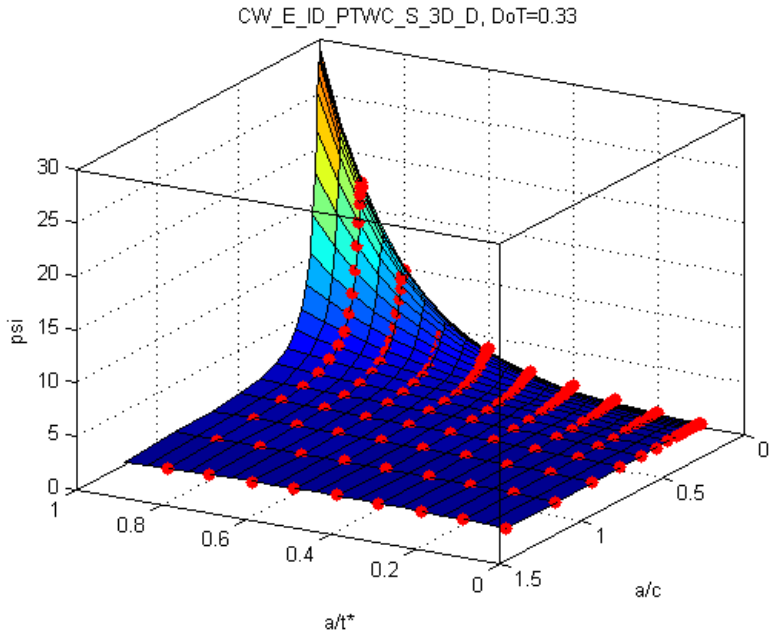

Figure 15: Cold Weld Semi-Elliptical ID Surface Crack at the Deepest Point, Weld Cap=0.33t

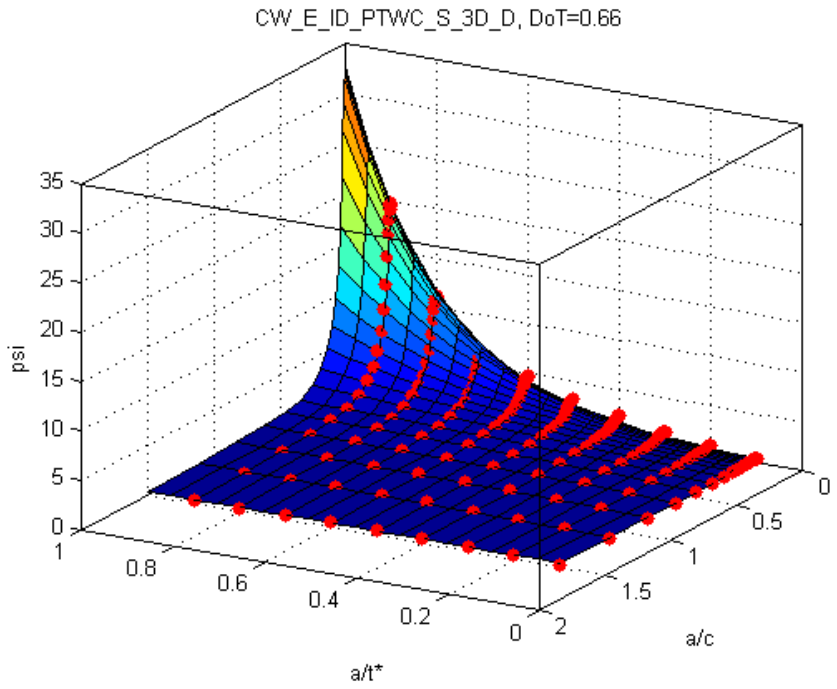

Figure 16: Cold Weld Semi-Elliptical ID Surface Crack at the Deepest Point, Weld Cap=0.66t

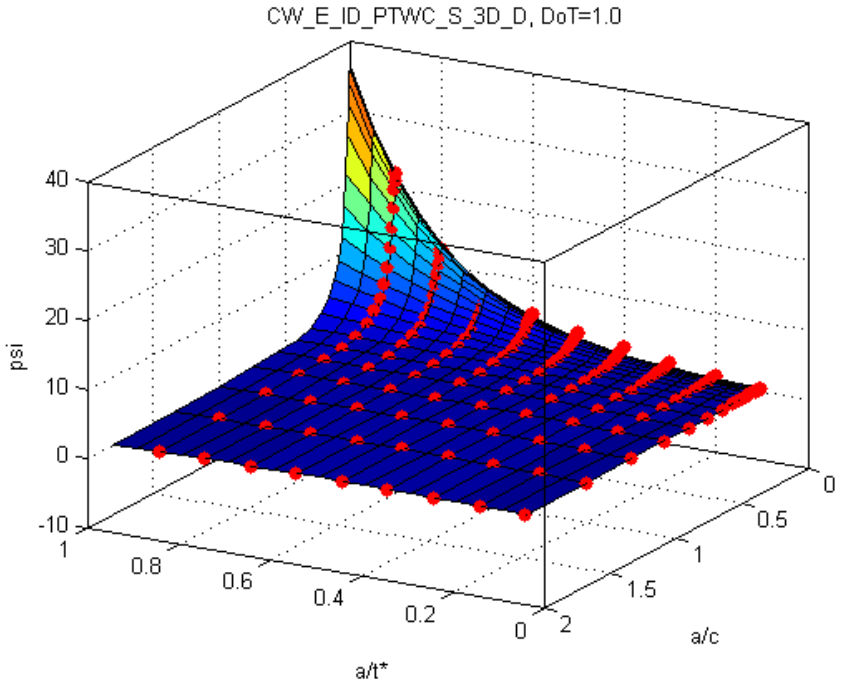

Figure 17: Cold Weld Semi-Elliptical ID Surface Crack at the Deepest Point, Weld Cap=1.0t

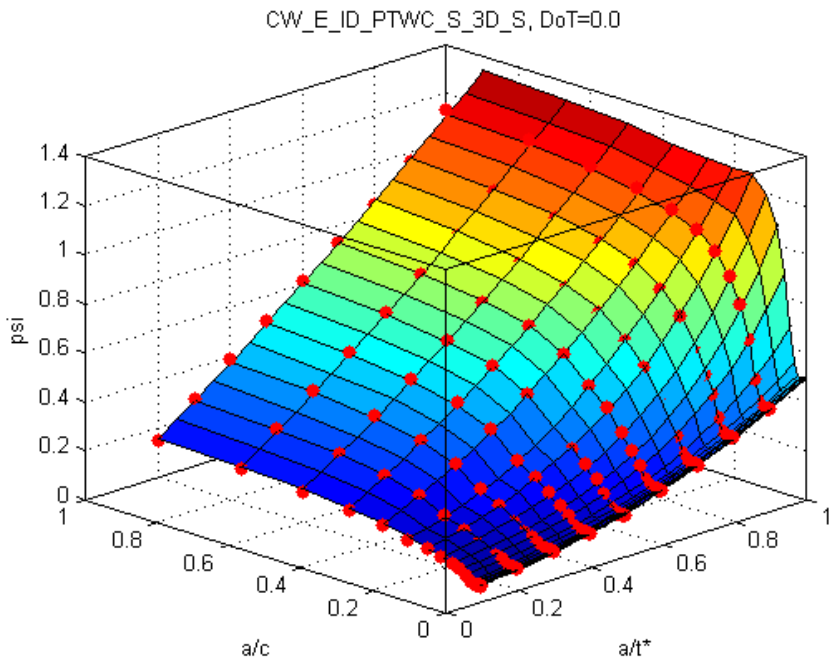

Figure 18: Cold Weld Semi-Elliptical ID Surface Crack at the Crack Tip, No Weld Cap

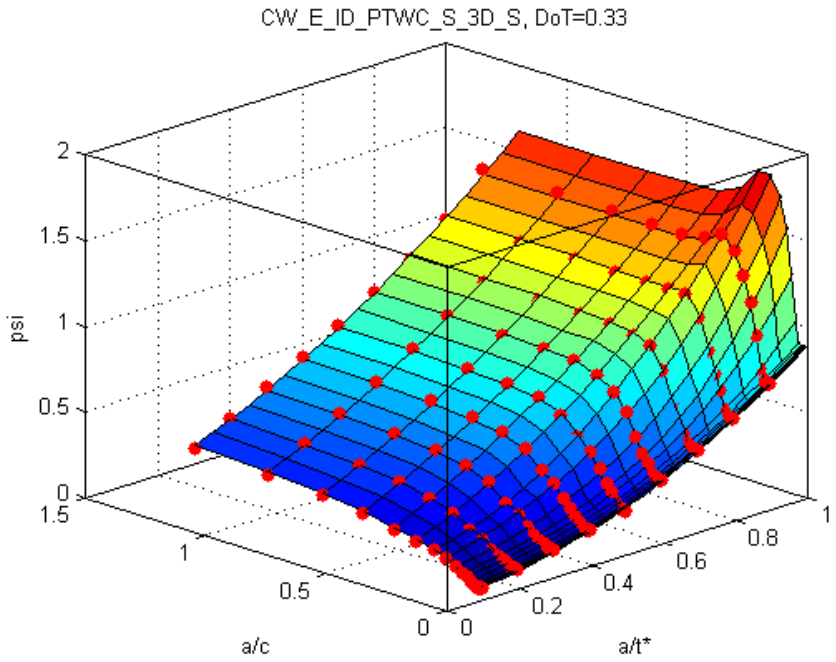

Figure 19: Cold Weld Semi-Elliptical ID Surface Crack at the Crack Tip, Weld Cap=0.33t

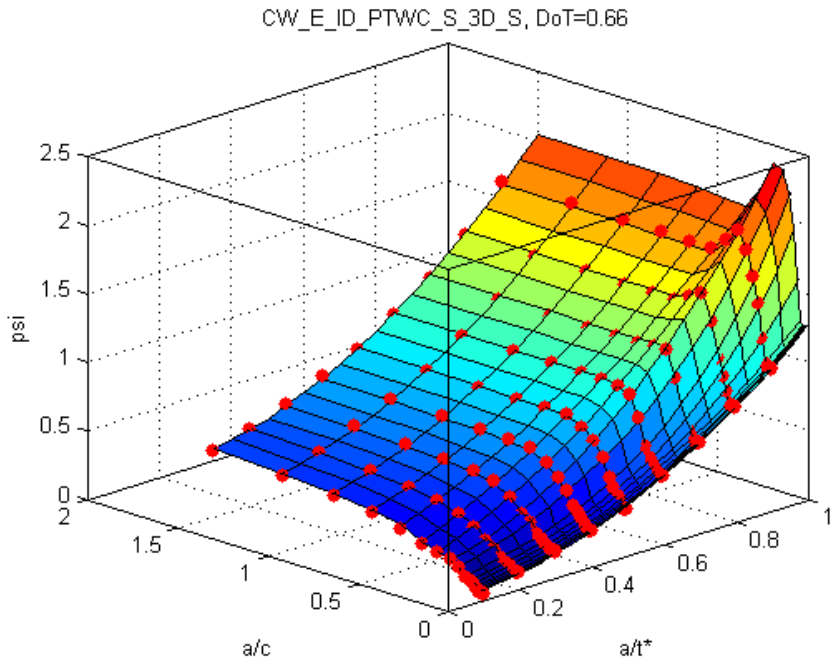

Figure 20: Cold Weld Semi-Elliptical ID Surface Crack at the Crack Tip, Weld Cap=0.66t

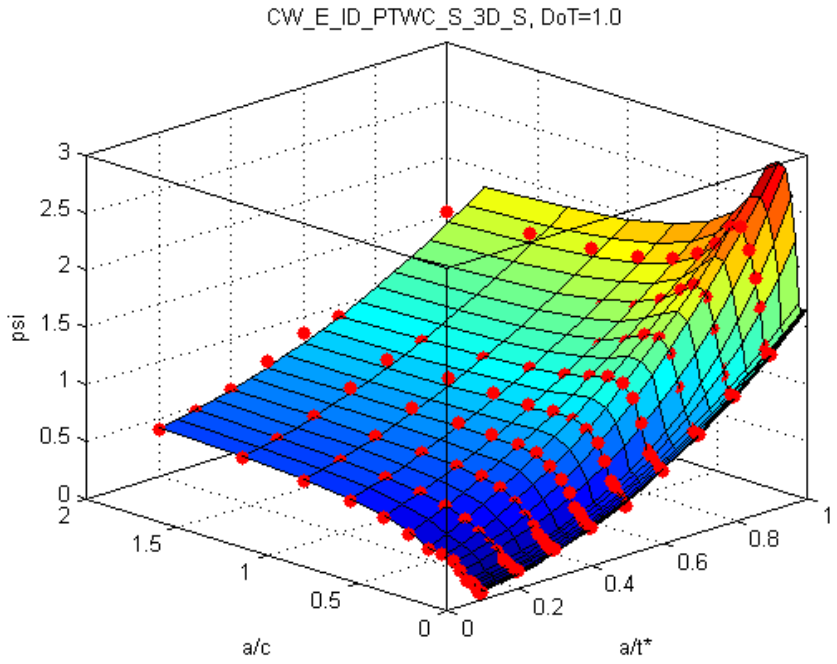

Figure 21: Cold Weld Semi-Elliptical ID Surface Crack at the Crack Tip, Weld Cap=1.0t

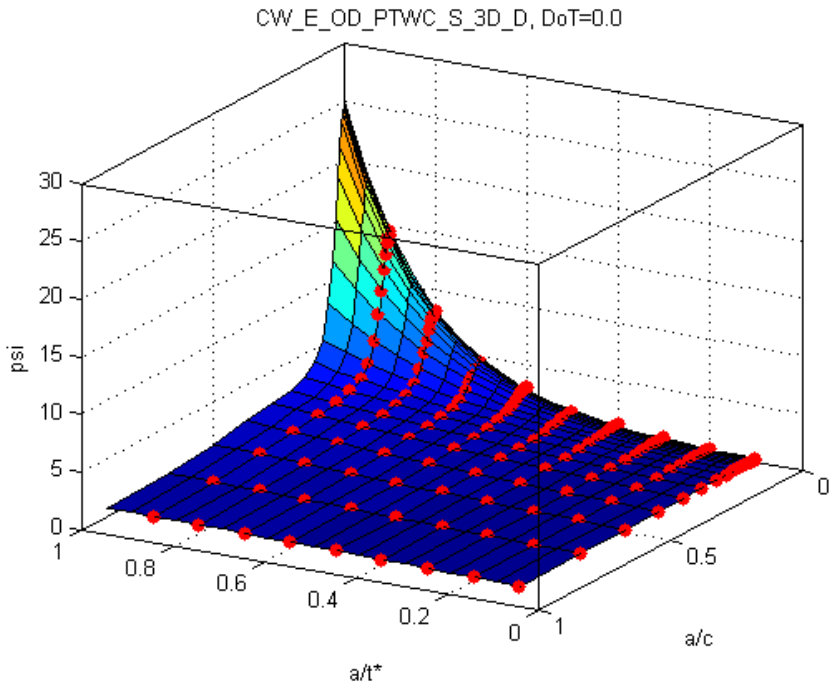

Figure 22: Cold Weld Semi-Elliptical OD Surface Crack at the Deepest Point, No Weld Cap

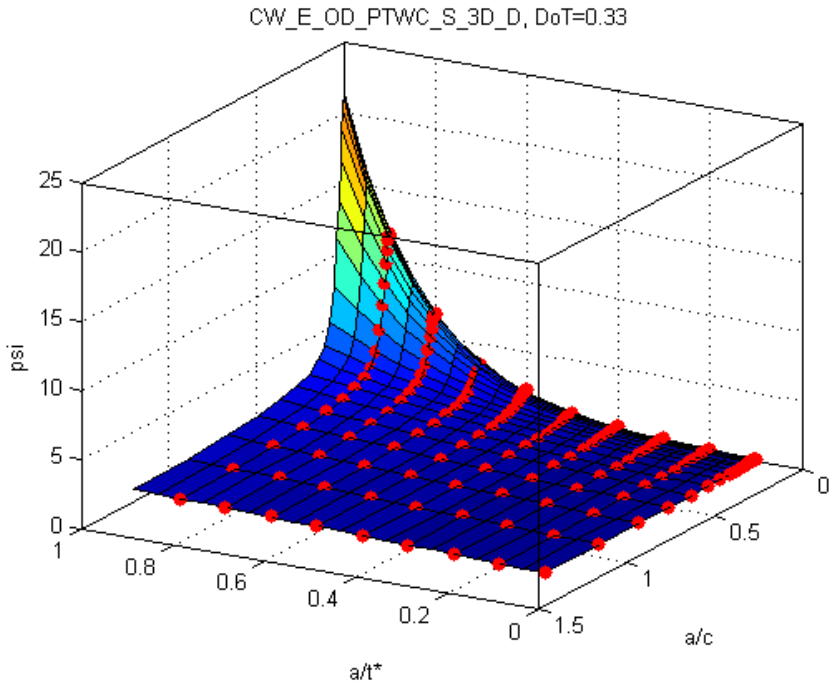

Figure 23: Cold Weld Semi-Elliptical OD Surface Crack at the Deepest Point, Weld Cap=0.33t

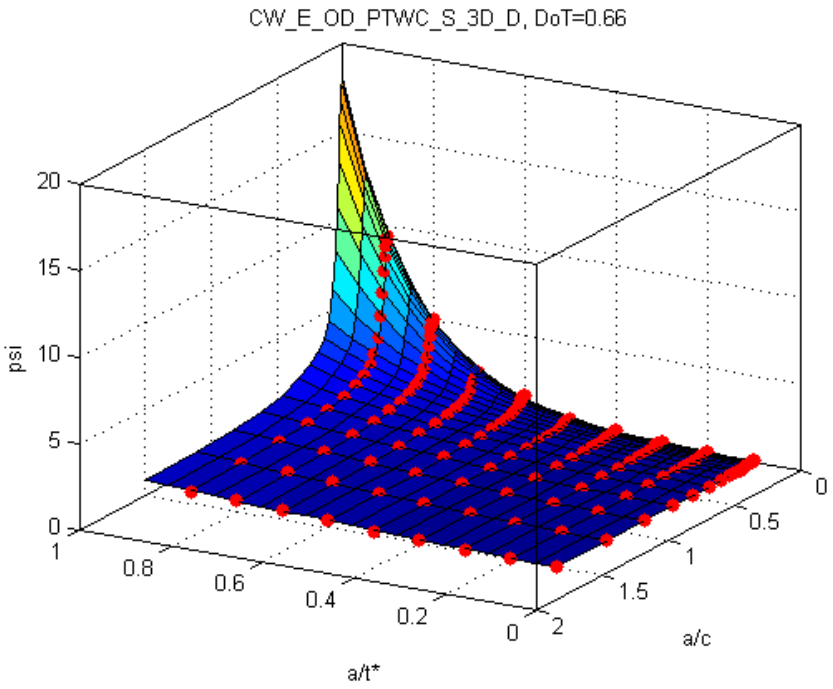

Figure 24: Cold Weld Semi-Elliptical OD Surface Crack at the Deepest Point, Weld Cap=0.66t

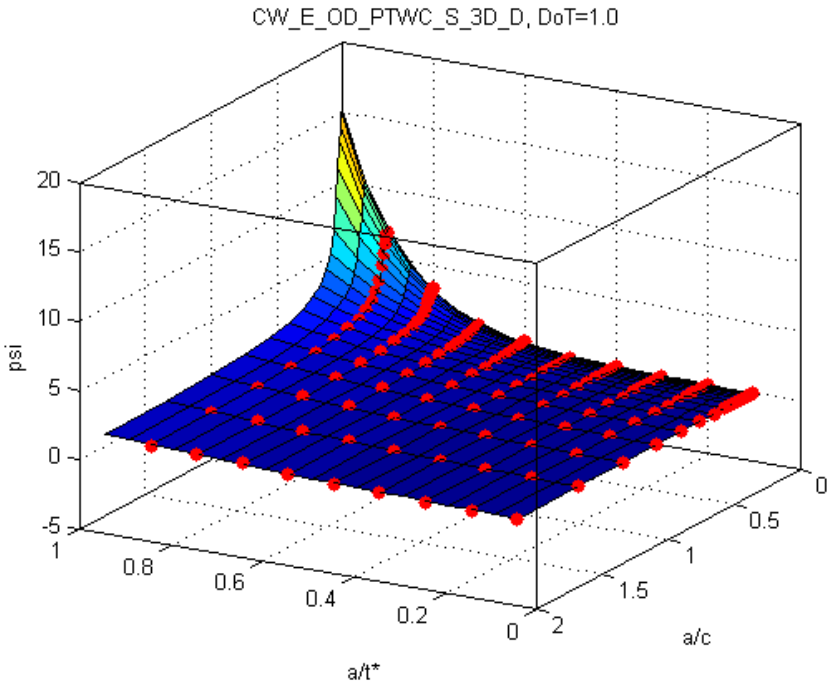

Figure 25: Cold Weld Semi-Elliptical OD Surface Crack at the Deepest Point, Weld Cap=1.0t

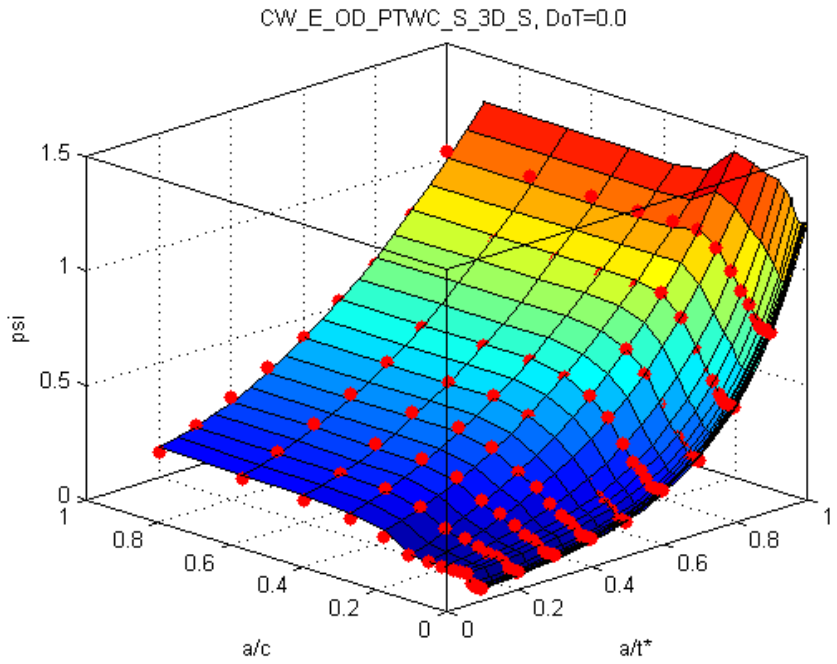

Figure 26: Cold Weld Semi-Elliptical OD Surface Crack at the Crack Tip, No Weld Cap

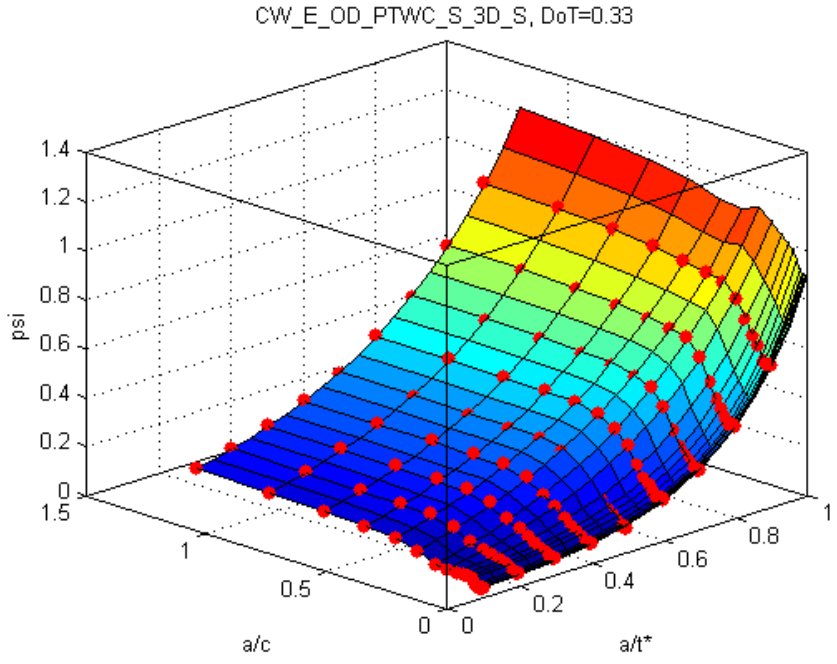

Figure 27: Cold Weld Semi-Elliptical OD Surface Crack at the Crack Tip, Weld Cap=0.33t

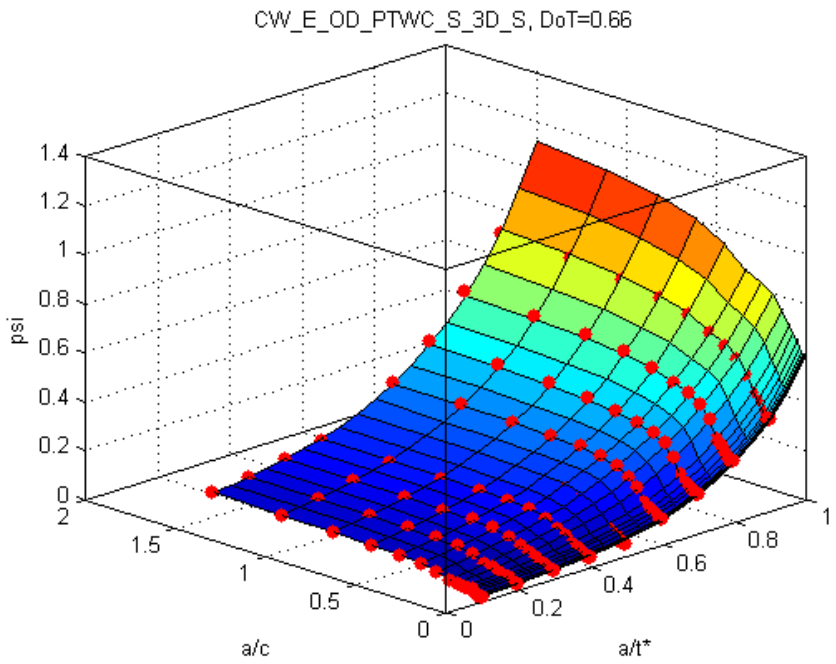

Figure 28: Cold Weld Semi-Elliptical OD Surface Crack at the Crack Tip, Weld Cap=0.66t

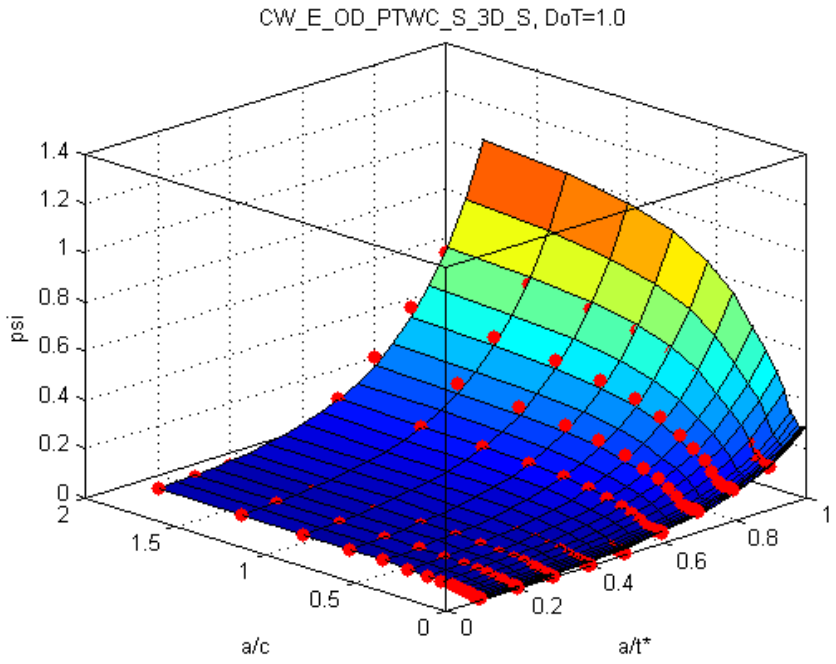

Figure 29: Cold Weld Semi-Elliptical OD Surface Crack at the Crack Tip, Weld Cap=1.0t

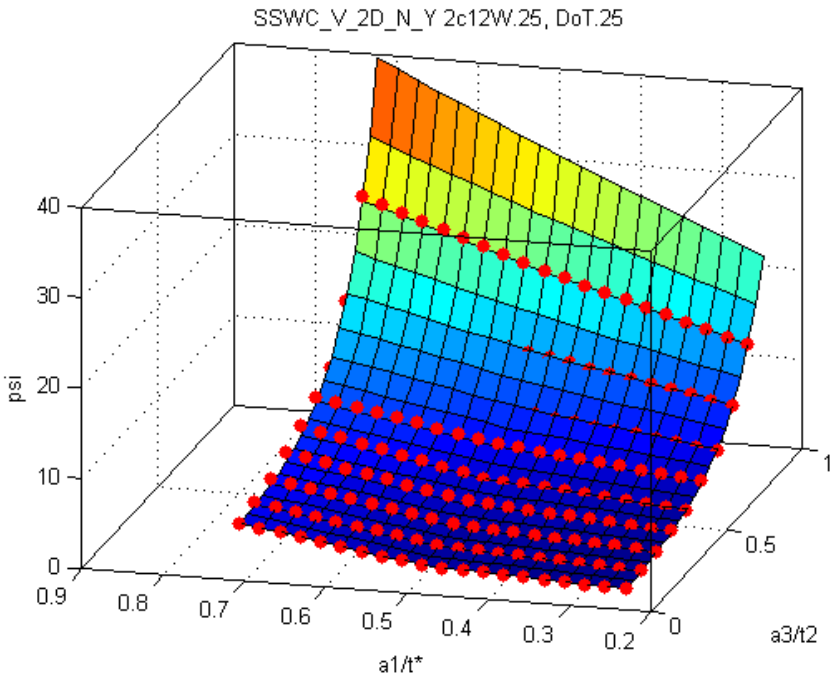

Figure 30: SSWC V-Crack with Width=0.25t, Weld Cap=0.25t and No General Corrosion

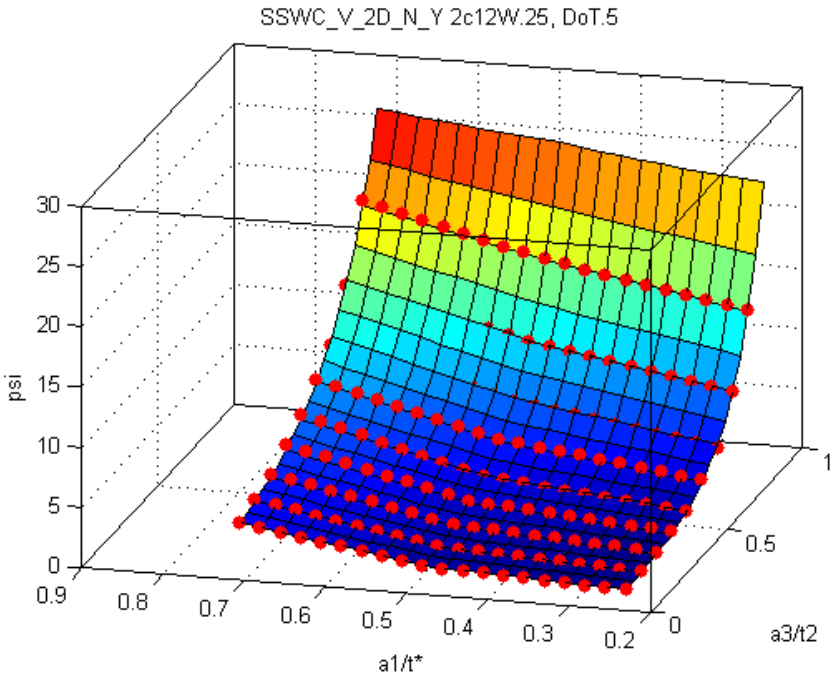

Figure 31: SSWC V-Crack with Width=0.25t, Weld Cap=0.5t and No General Corrosion

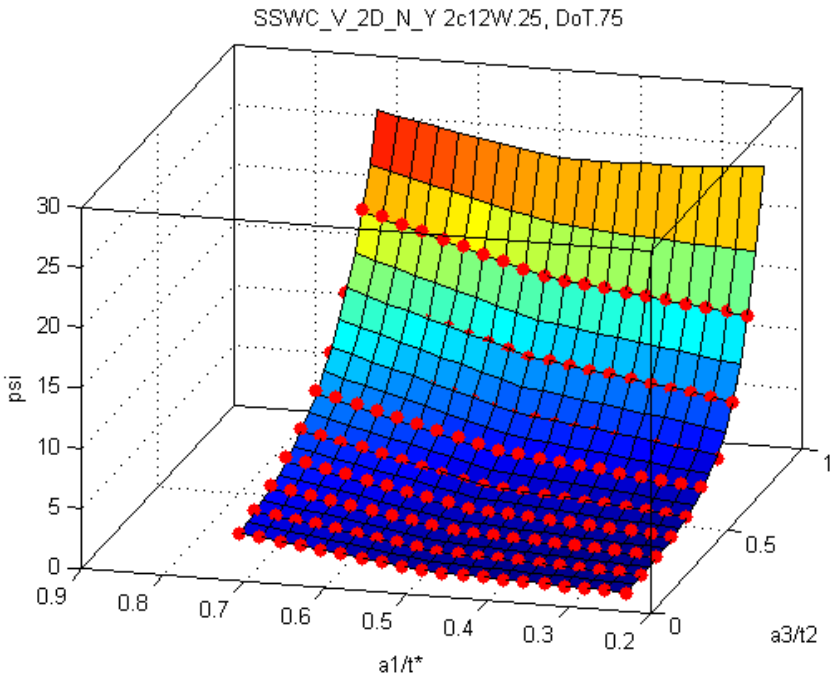

Figure 32: SSWC V-Crack with Width=0.25t, Weld Cap=0.75t and No General Corrosion

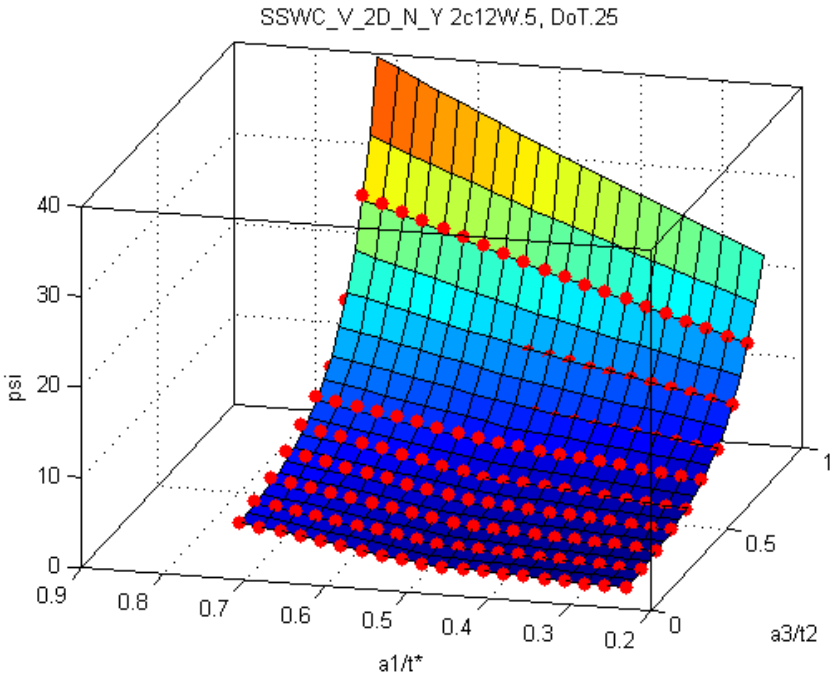

Figure 33: SSWC V-Crack with Width=0.5t, Weld Cap=0.25t and No General Corrosion

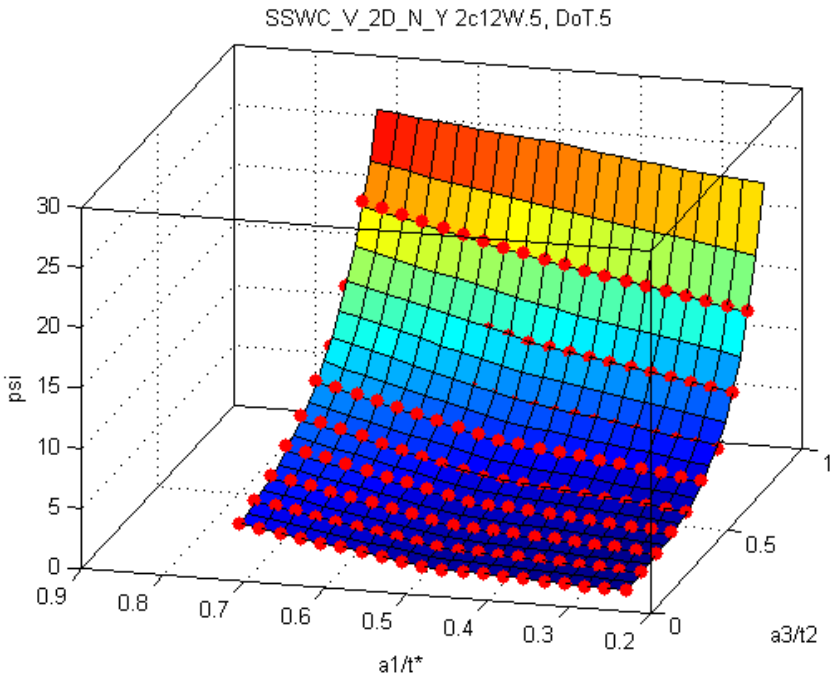

Figure 34: SSWC V-Crack with Width=0.5t, Weld Cap=0.5t and No General Corrosion

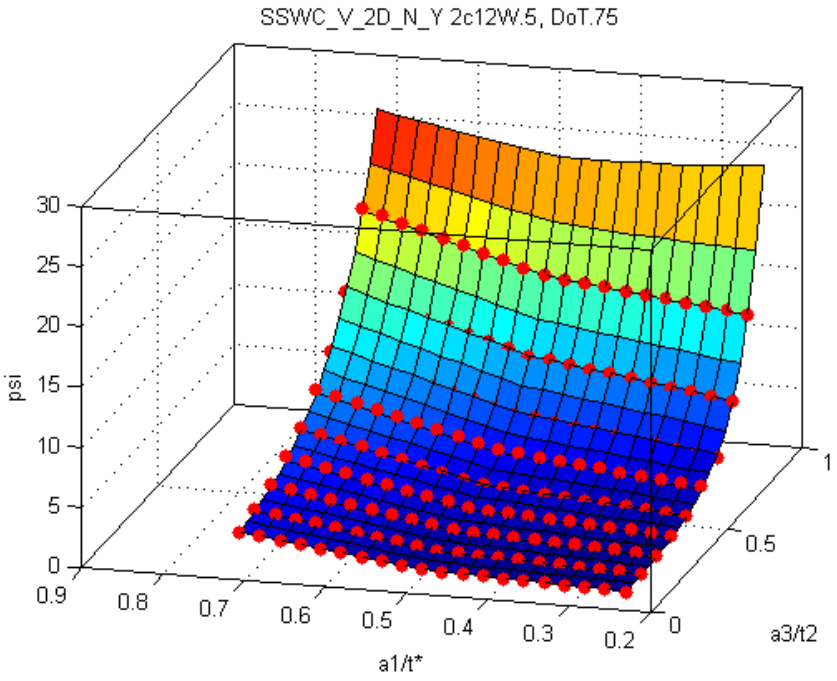

Figure 35: SSWC V-Crack with Width=0.5t, Weld Cap=0.75t and No General Corrosion

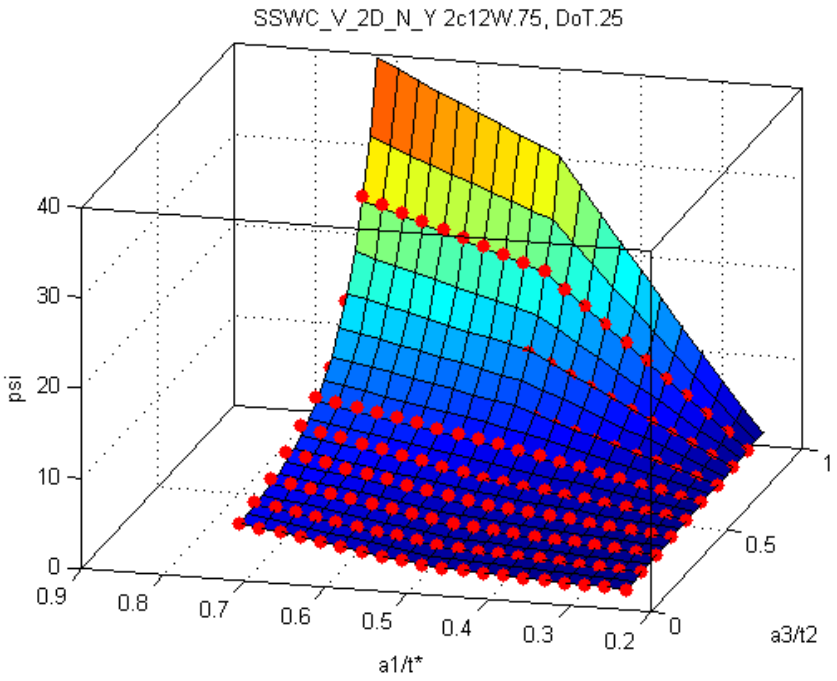

Figure 36: SSWC V-Crack with Width=0.75t, Weld Cap=0.25t and No General Corrosion

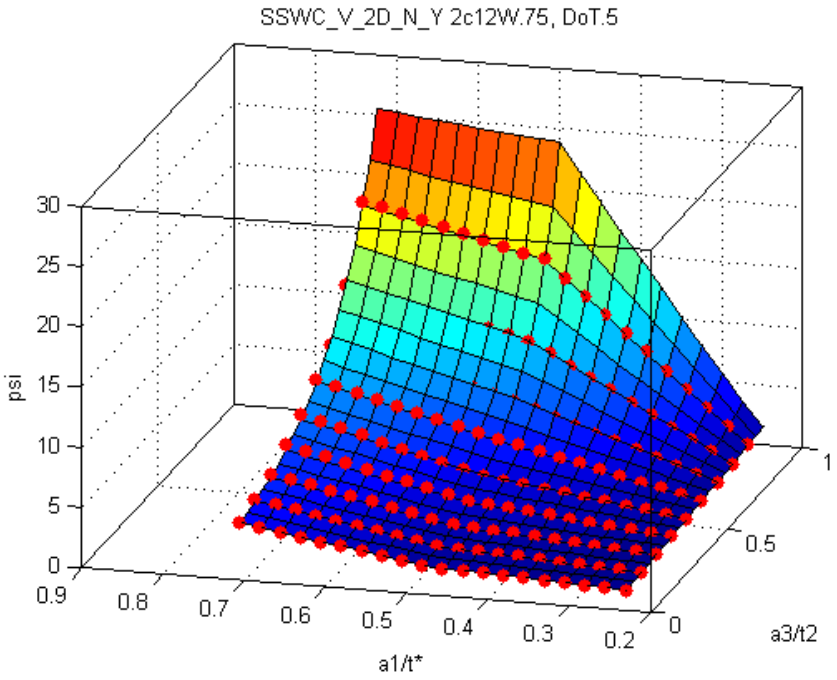

Figure 37: SSWC V-Crack with Width=0.75t, Weld Cap=0.5t and No General Corrosion

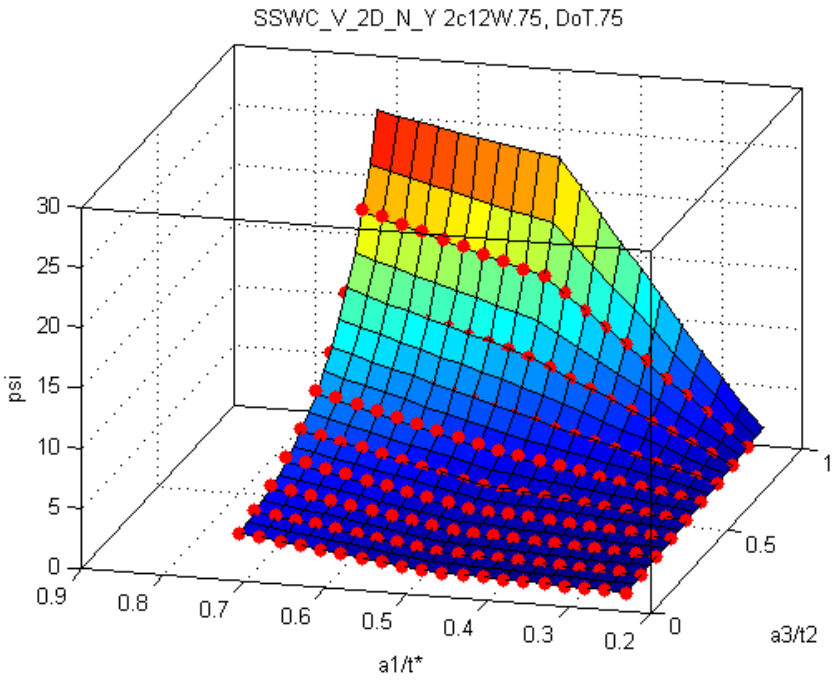

Figure 38: SSWC V-Crack with Width=0.75t, Weld Cap=0.75t and No General Corrosion

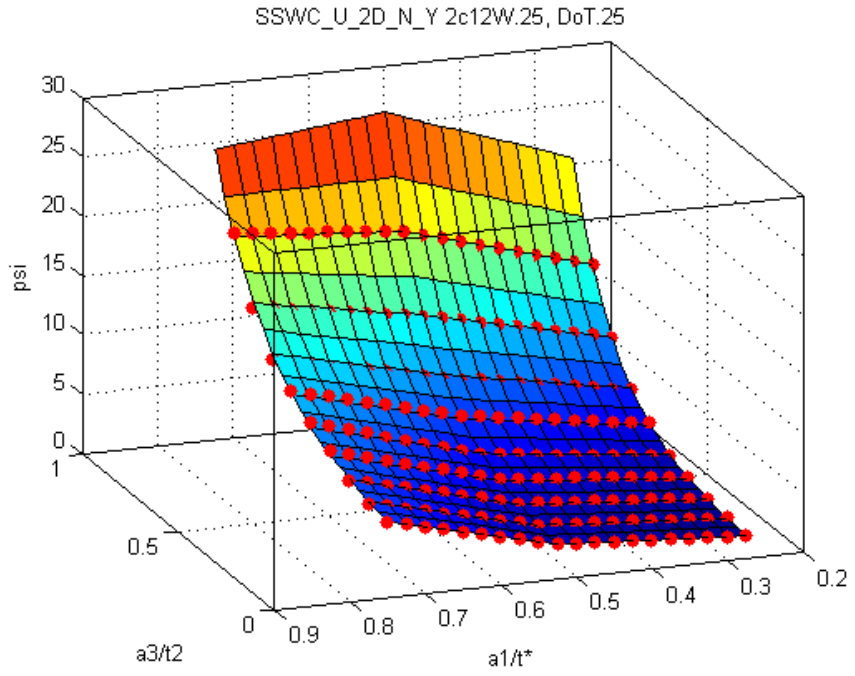

Figure 39: SSWC U-Crack with Width=0.25t, Weld Cap=0.25t and No General Corrosion

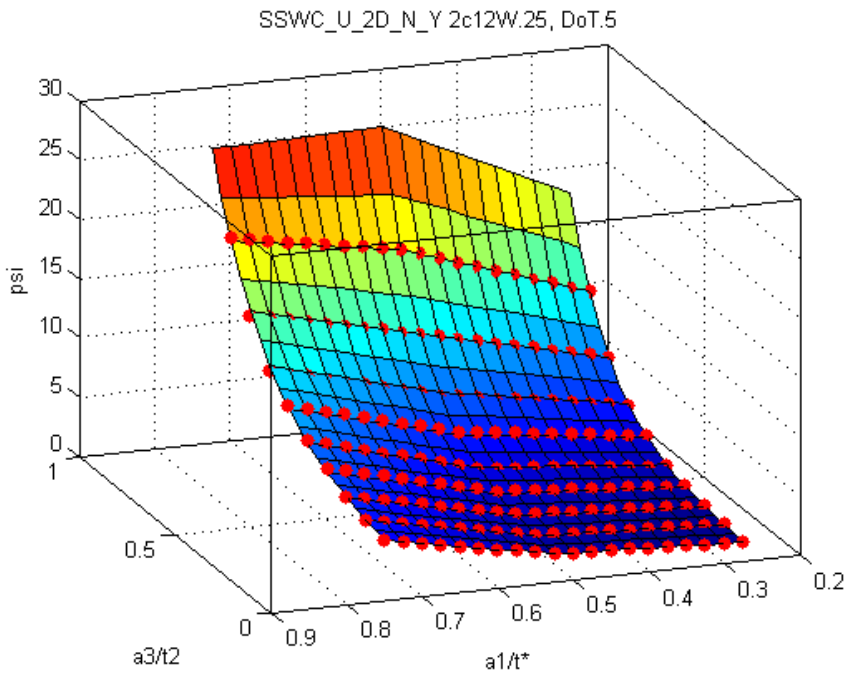

Figure 40: SSWC U-Crack with Width=0.25t, Weld Cap=0.5t and No General Corrosion

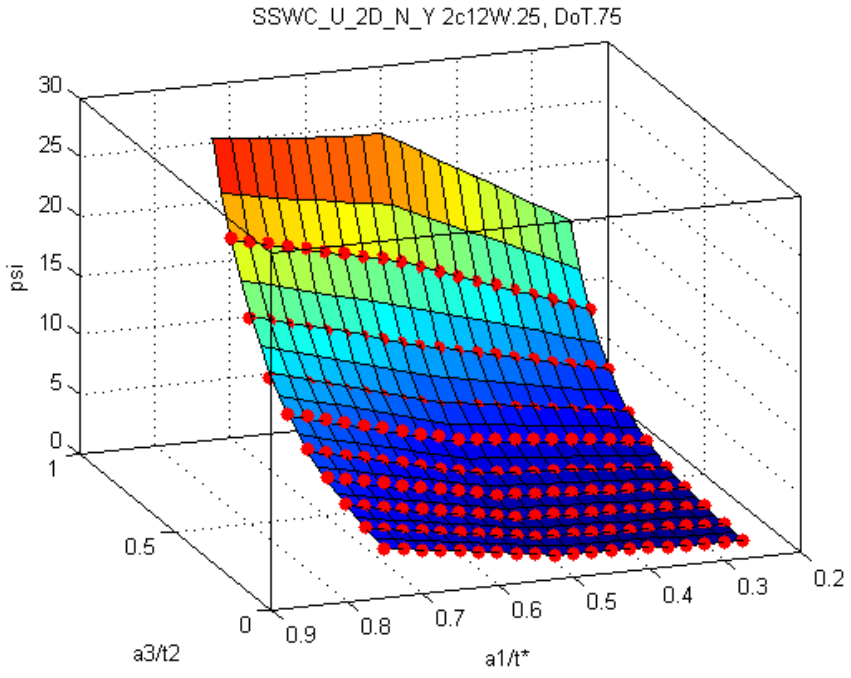

Figure 41: SSWC U-Crack with Width=0.25t, Weld Cap=0.75t and No General Corrosion

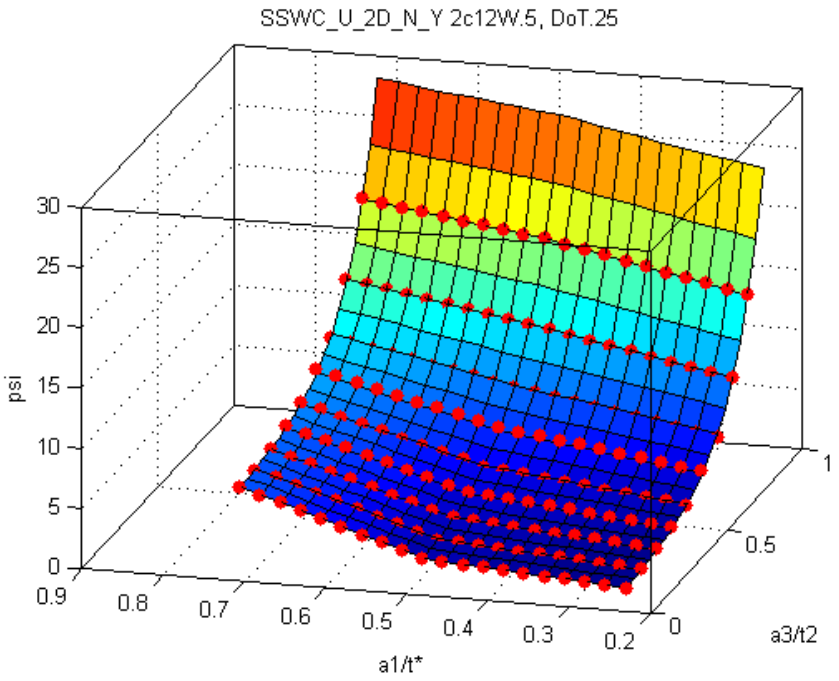

Figure 42: SSWC U-Crack with Width=0.5t, Weld Cap=0.25t and No General Corrosion

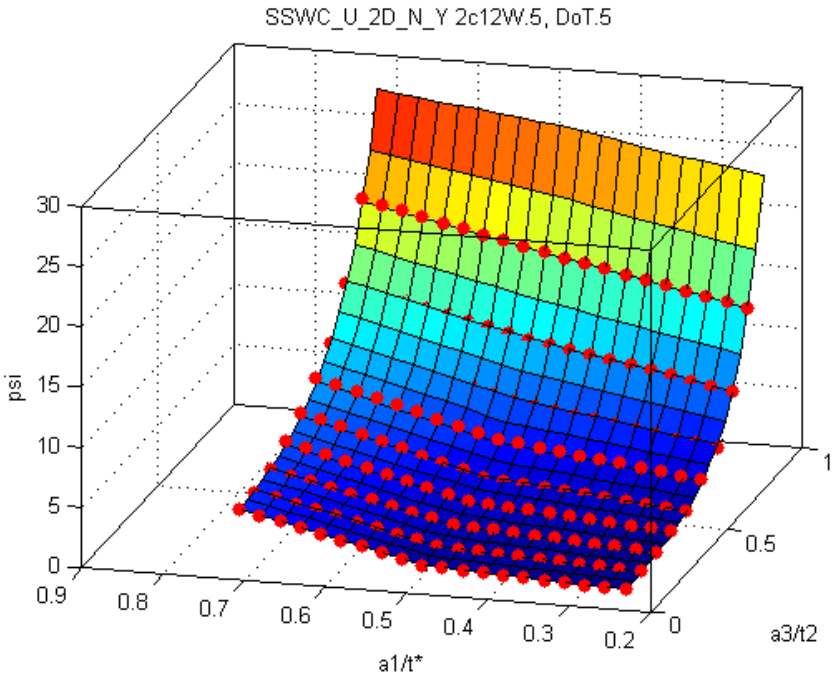

Figure 43: SSWC U-Crack with Width=0.5t, Weld Cap=0.5t and No General Corrosion

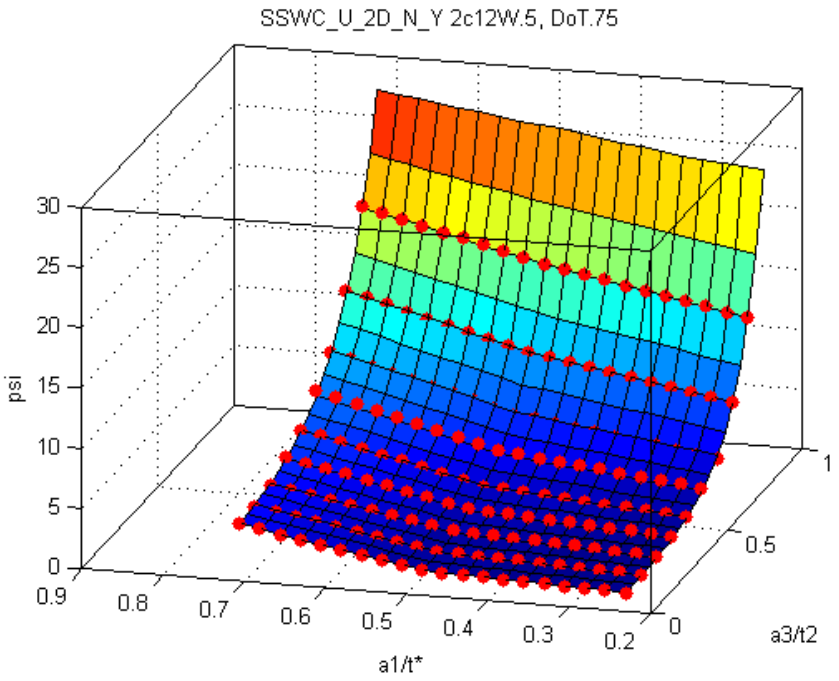

Figure 44: SSWC U-Crack with Width=0. 5t, Weld Cap=0.75t and No General Corrosion

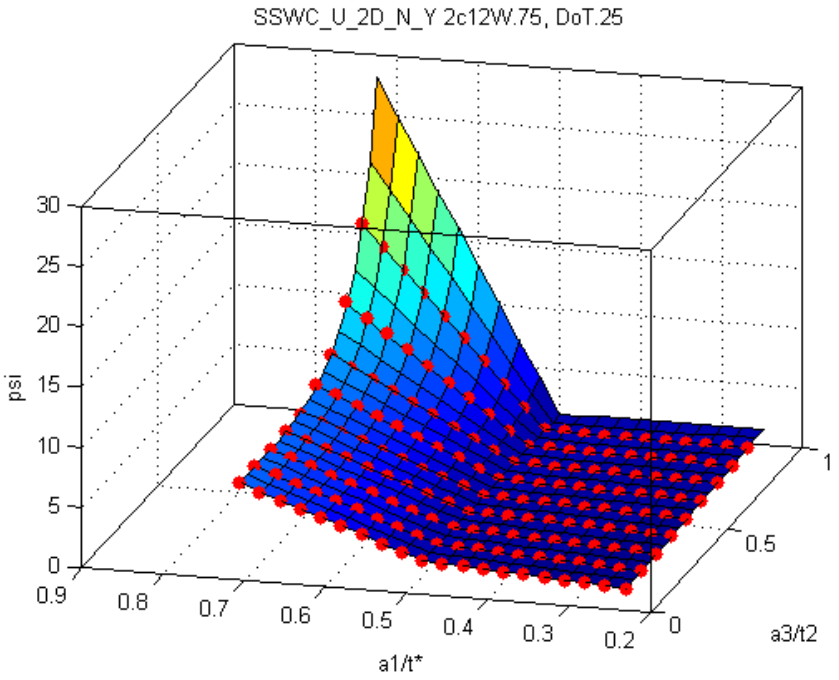

Figure 45: SSWC U-Crack with Width=0.75t, Weld Cap=0.25t and No General Corrosion

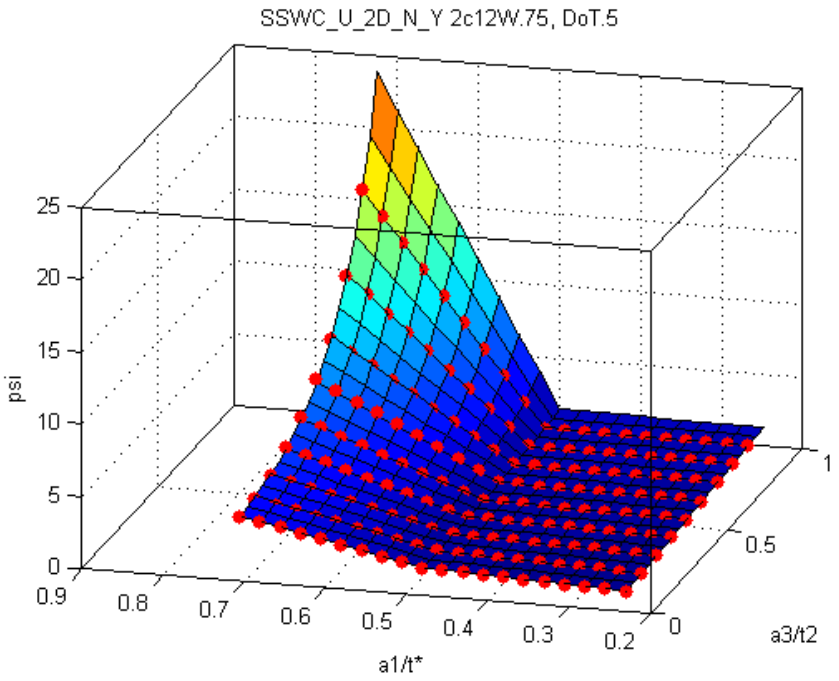

Figure 46: SSWC U-Crack with Width=0.75t, Weld Cap=0.5t and No General Corrosion

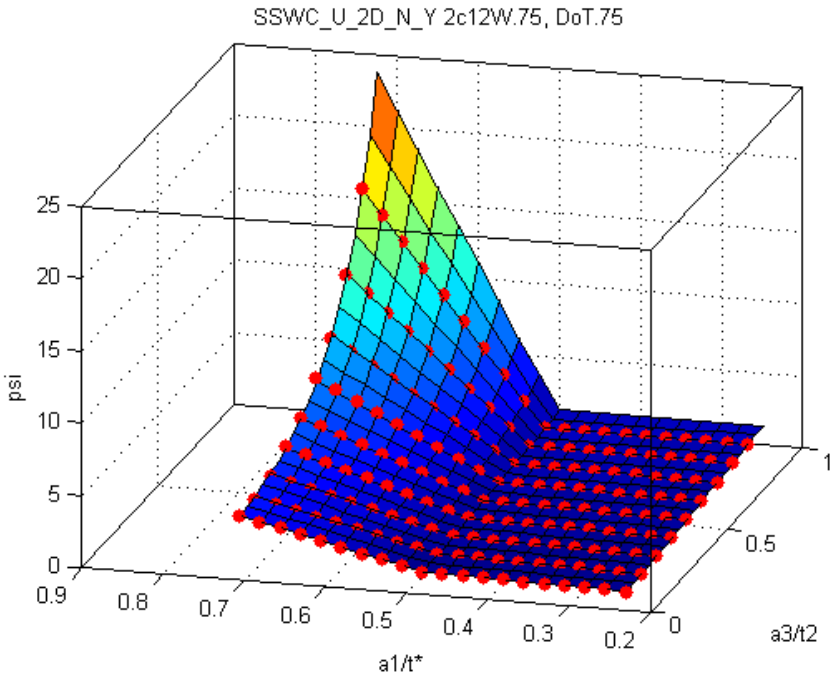

Figure 47: SSWC U-Crack with Width=0.75t, Weld Cap=0.75t and No General Corrosion

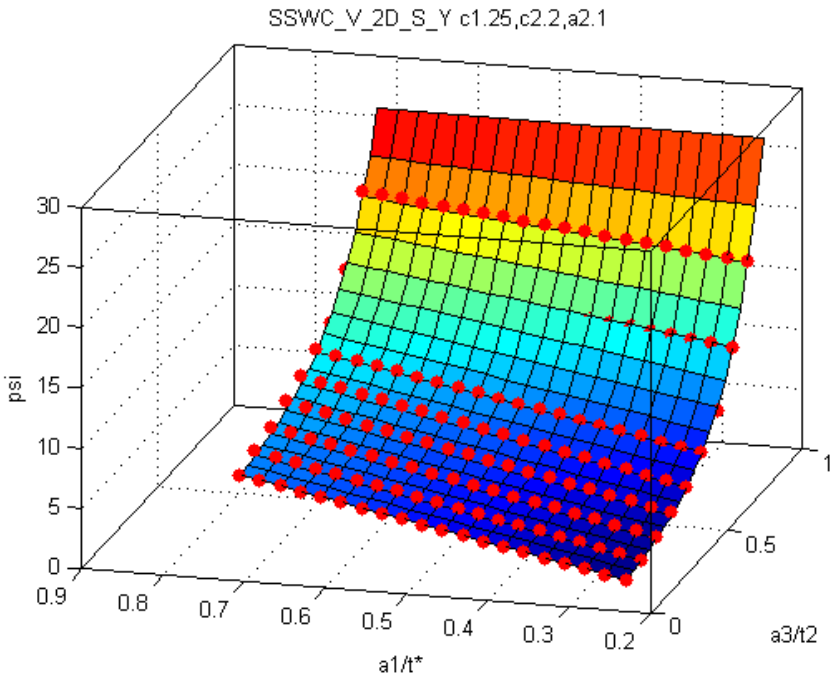

Figure 48: SSWC V-Crack with Width=0.25t, Symmetric General Corrosion Total Width=4t and Depth=0.1t

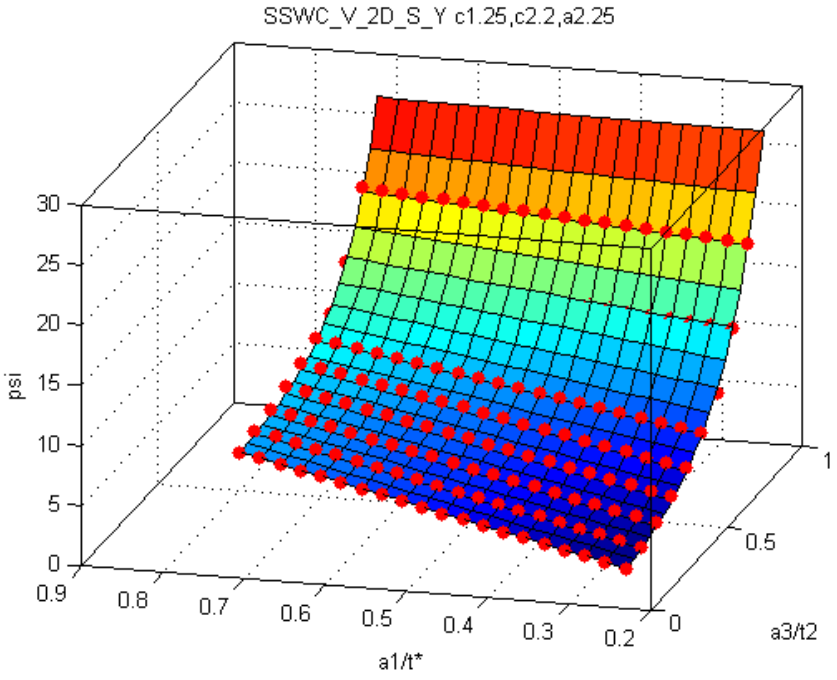

Figure 49: SSWC V-Crack with Width=0.25t, Symmetric General Corrosion Total Width=4t and Depth=0.25t

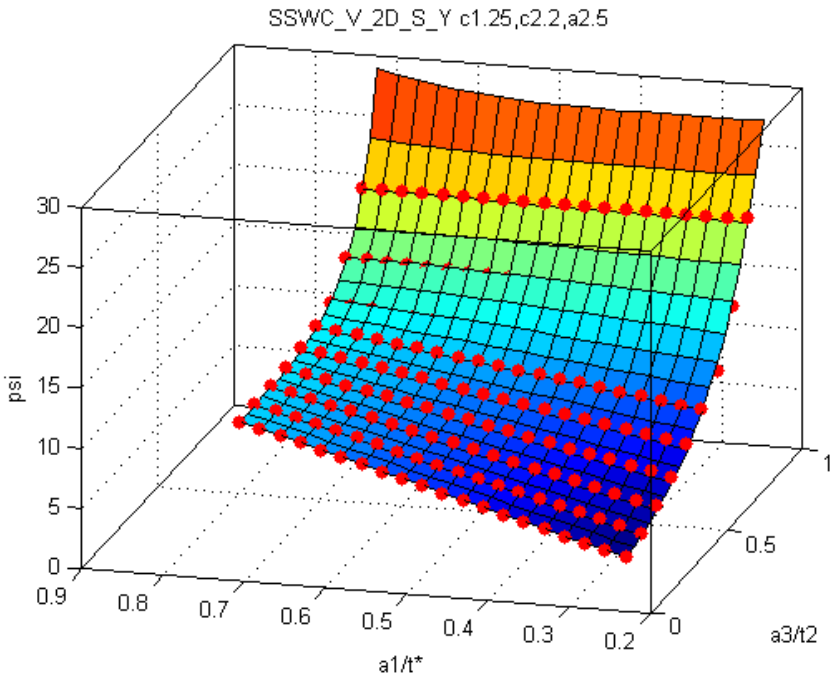

Figure 50: SSWC V-Crack with Width=0.25t, Symmetric General Corrosion Total Width=4t and Depth=0.5t

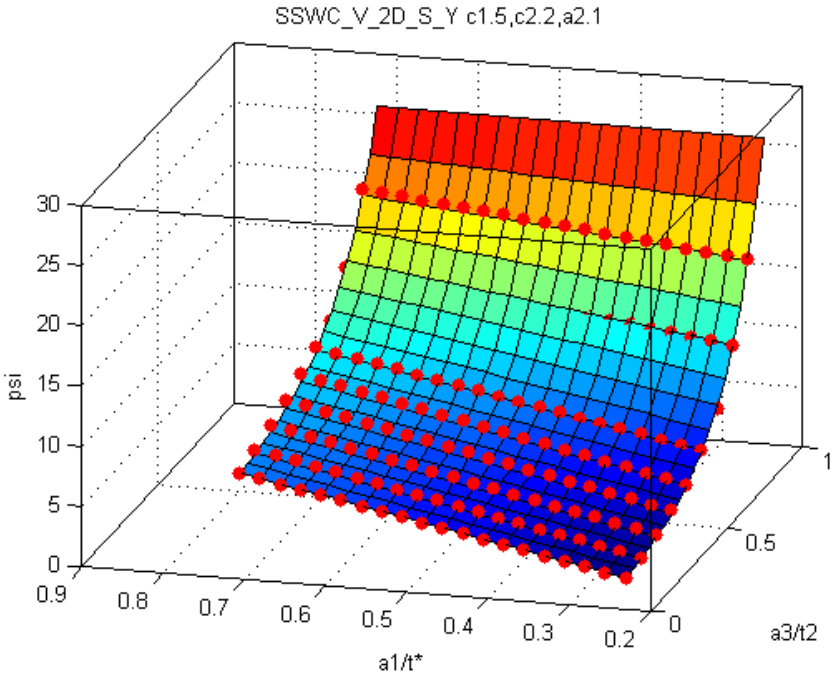

Figure 51: SSWC V-Crack with Width=0.5t, Symmetric General Corrosion Total Width=4t and Depth=0.1t

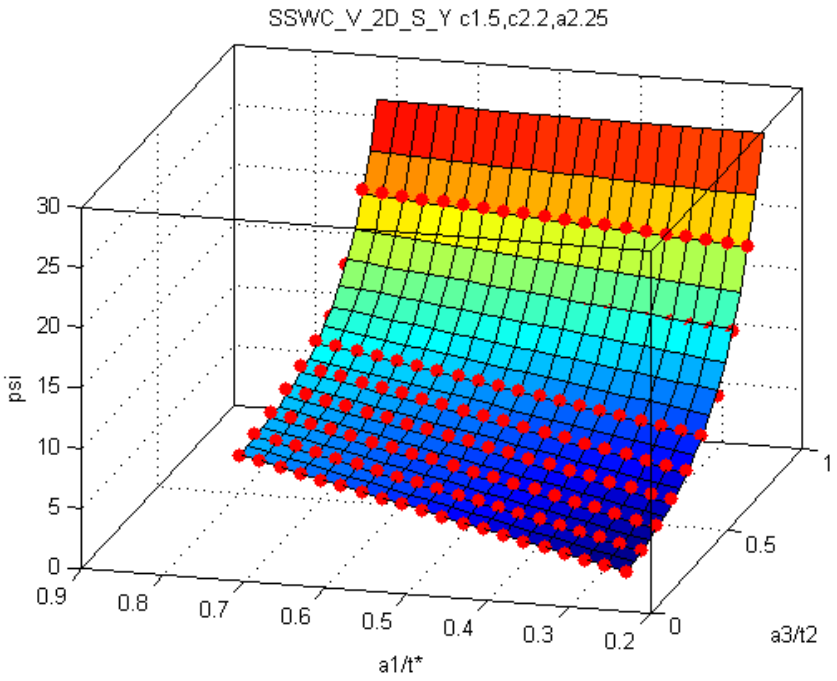

Figure 52: SSWC V-Crack with Width=0.5t, Symmetric General Corrosion Total Width=4t and Depth=0.25t

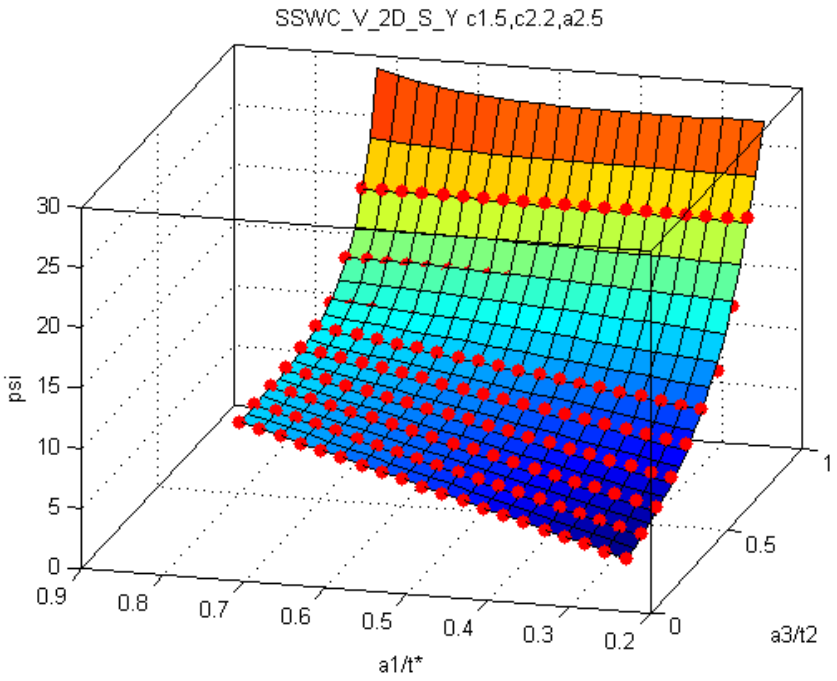

Figure 53: SSWC V-Crack with Width=0.5t, Symmetric General Corrosion Total Width=4t and Depth=0.5t

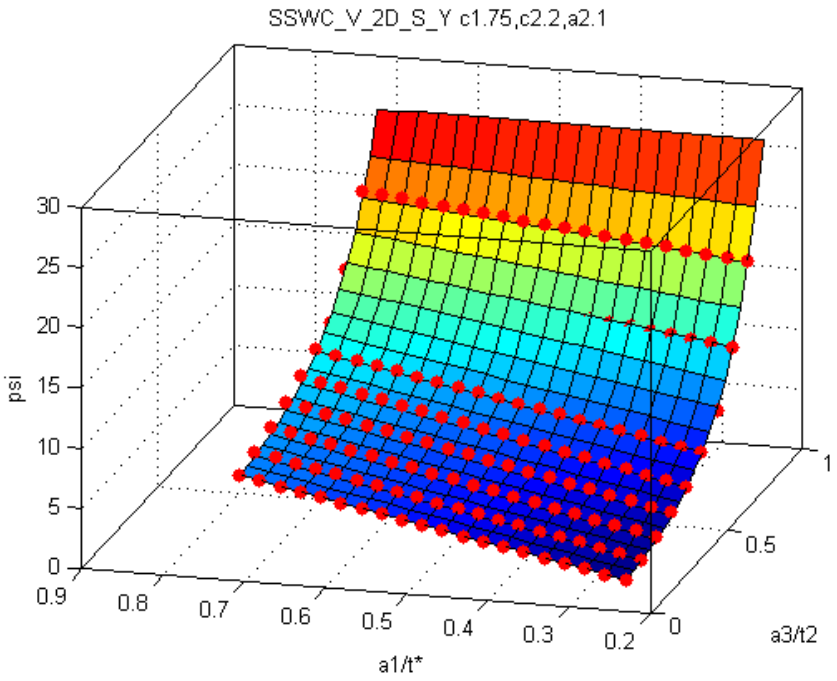

Figure 54: SSWC V-Crack with Width=0.75t, Symmetric General Corrosion Total Width=4t and Depth=0.1t

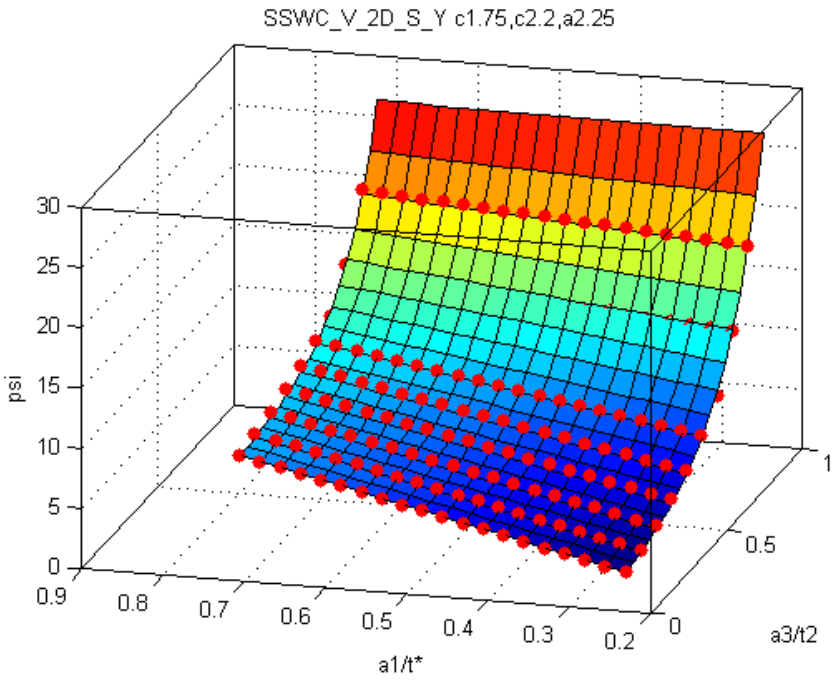

Figure 55: SSWC V-Crack with Width=0.75t, Symmetric General Corrosion Total Width=4t and Depth=0.25t

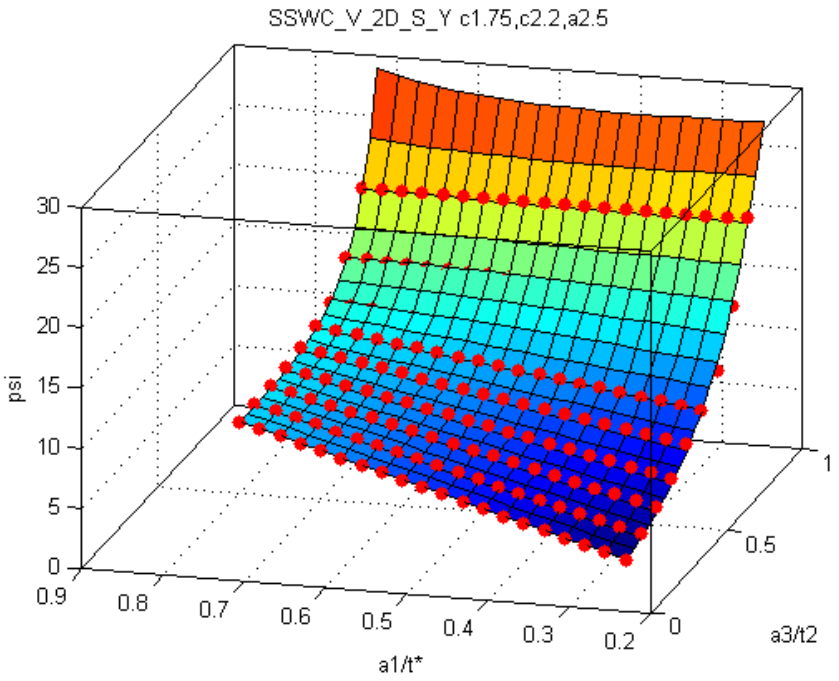

Figure 56: SSWC V-Crack with Width=0.75t, Symmetric General Corrosion Total Width=4t and Depth=0.5t

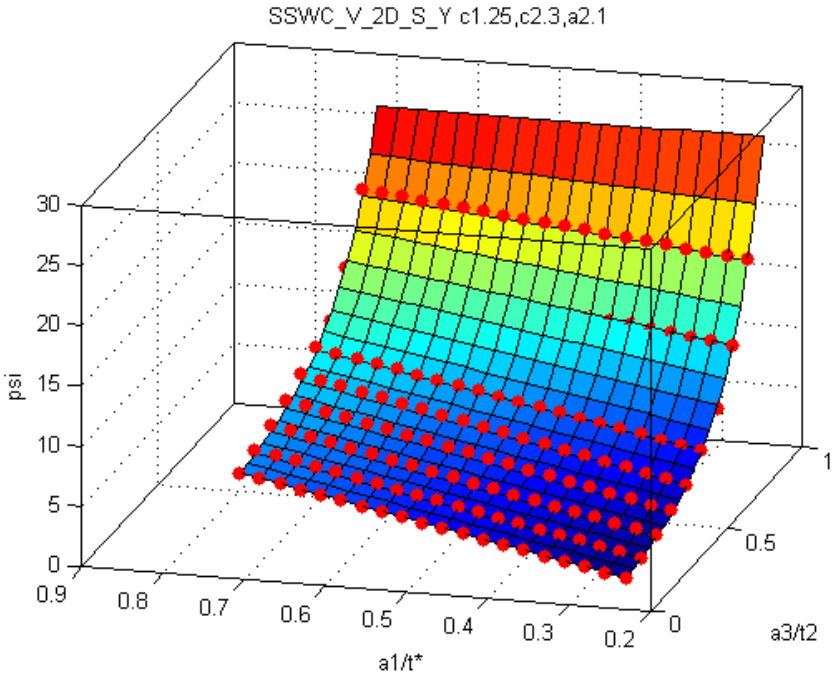

Figure 57: SSWC V-Crack with Width=0.25t, Symmetric General Corrosion Width=6t and Depth=0.1t

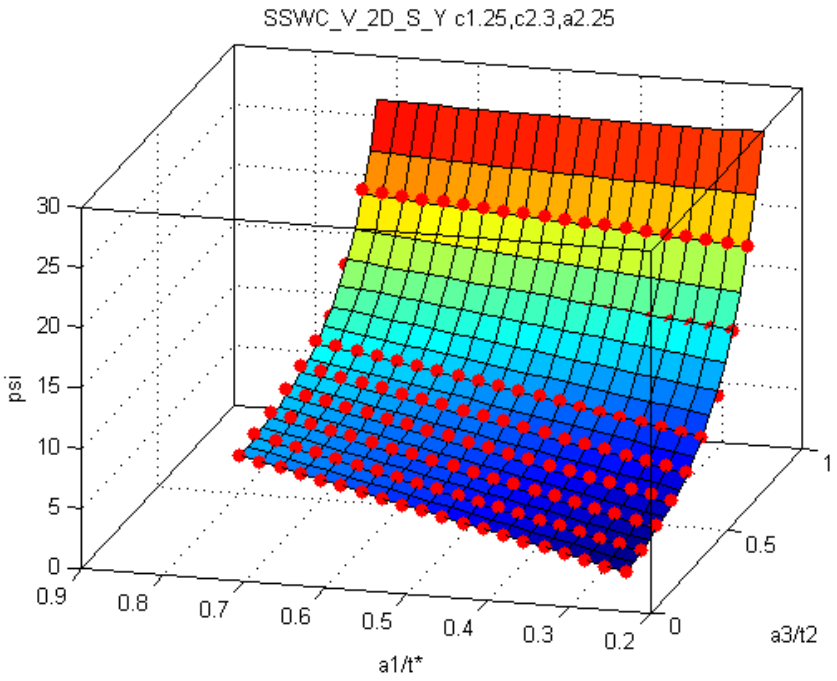

Figure 58: SSWC V-Crack with Width=0.25t, Symmetric General Corrosion Total Width=6t and Depth=0.25t

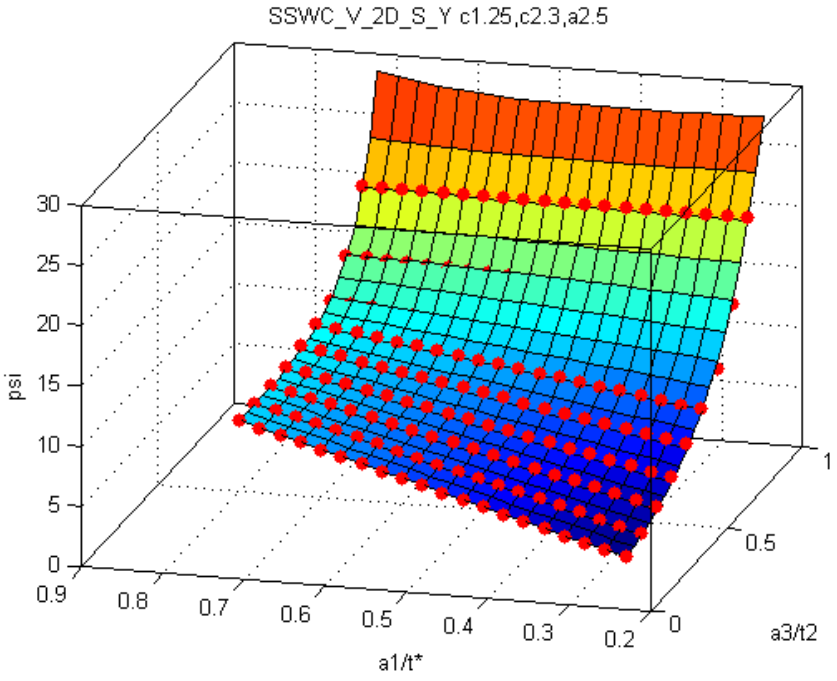

Figure 59: SSWC V-Crack with Width=0.25t, Symmetric General Corrosion Total Width=6t and Depth=0.5t

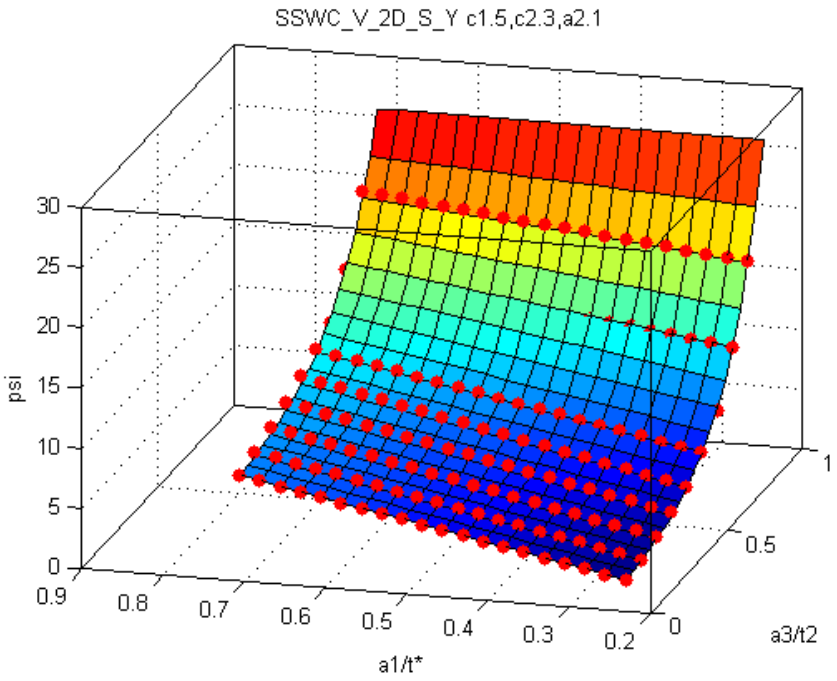

Figure 60: SSWC V-Crack with Width=0.5t, Symmetric General Corrosion Total Width=6t and Depth=0.1t

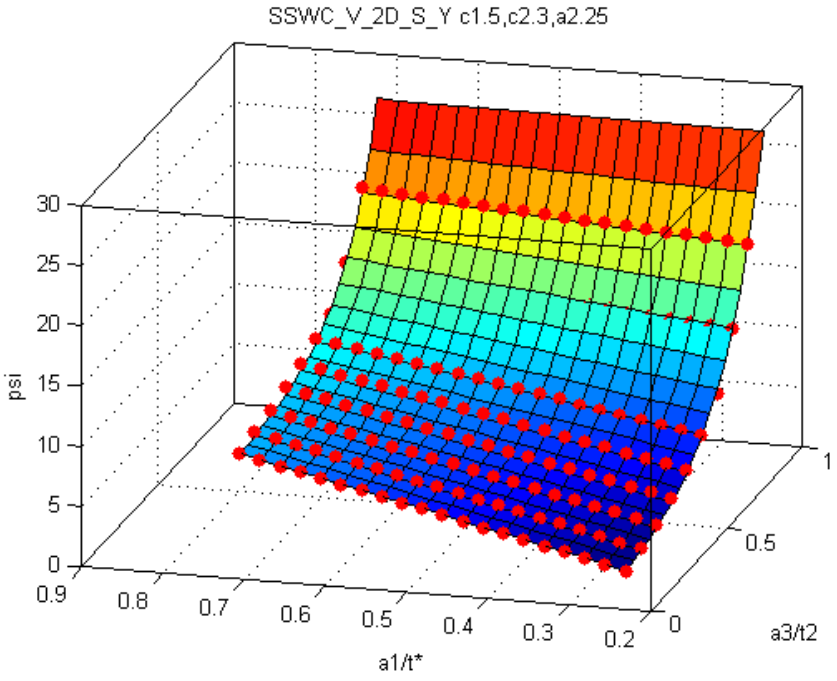

Figure 61: SSWC V-Crack with Width=0.5t, Symmetric General Corrosion Total Width=6t and Depth=0.25t

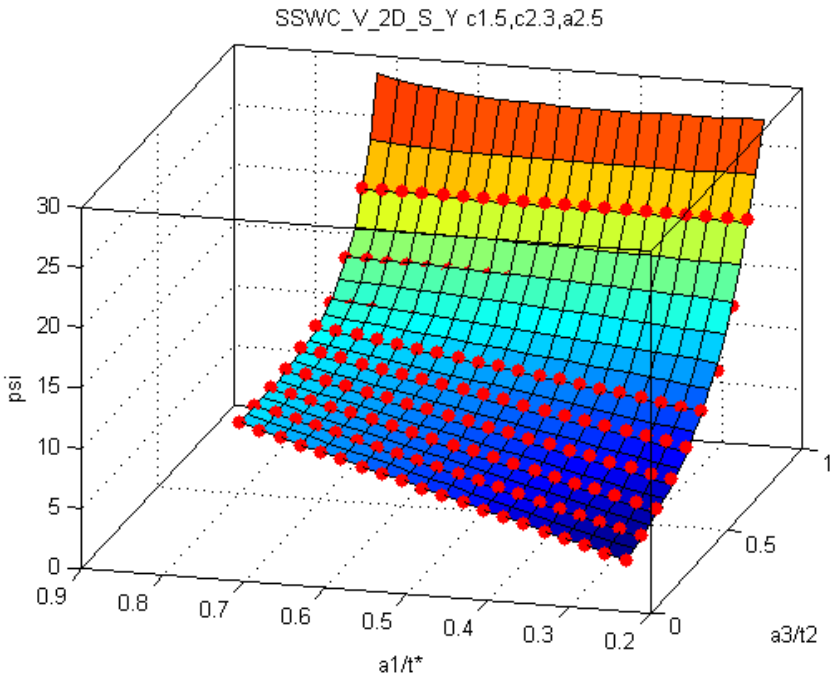

Figure 62: SSWC V-Crack with Width=0.5t, Symmetric General Corrosion Total Width=6t and Depth=0.5t

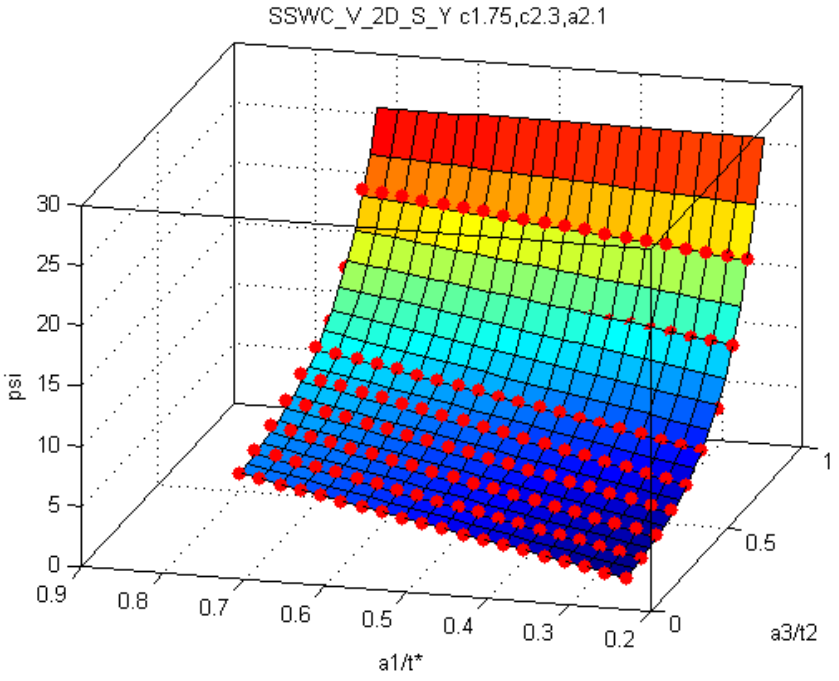

Figure 63: SSWC V-Crack with Width=0.75t, Symmetric General Corrosion Total Width=6t and Depth=0.1t

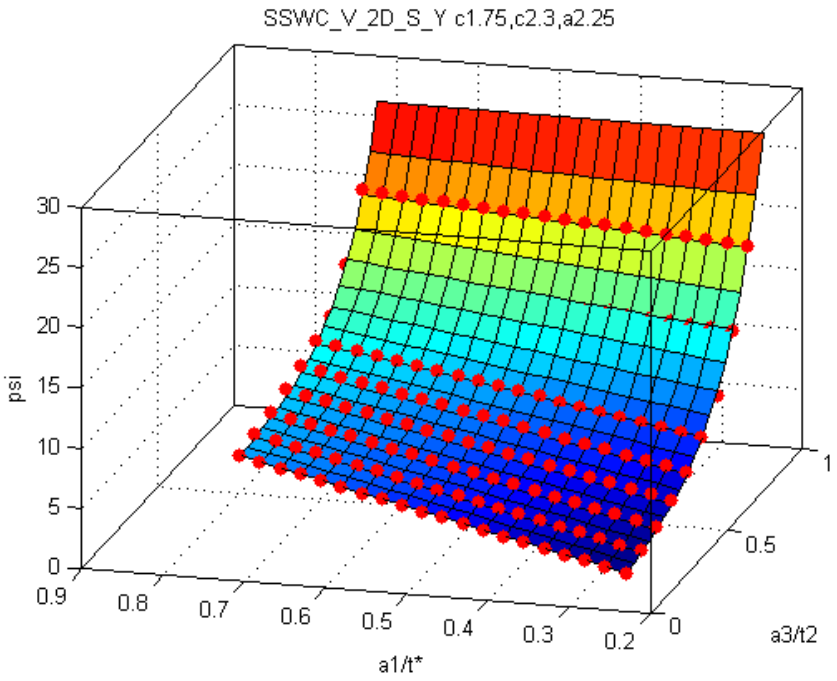

Figure 64: SSWC V-Crack with Width=0.75t, Symmetric General Corrosion Total Width=6t and Depth=0.25t

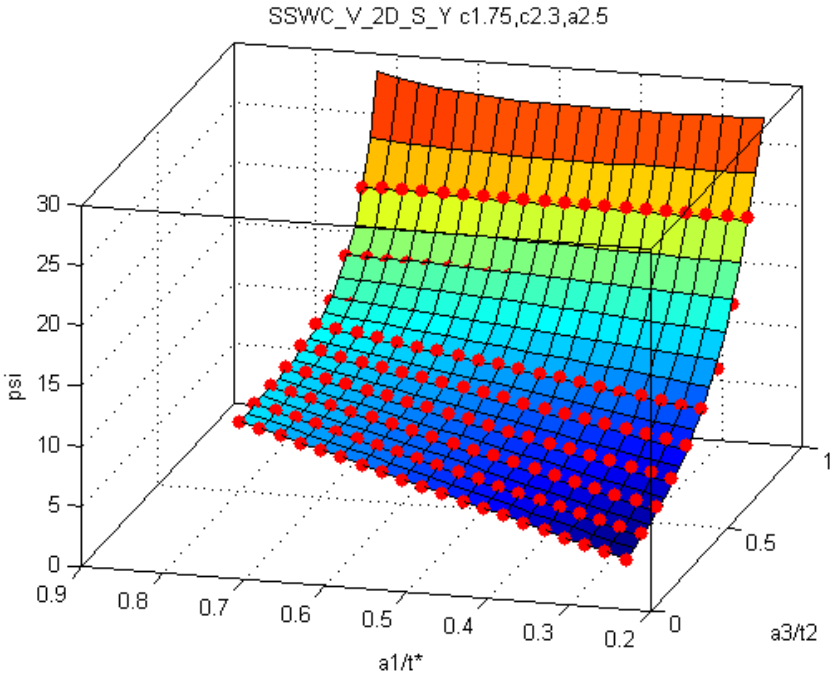

Figure 65: SSWC V-Crack with Width=0.75t, Symmetric General Corrosion Total Width=6t and Depth=0.5t

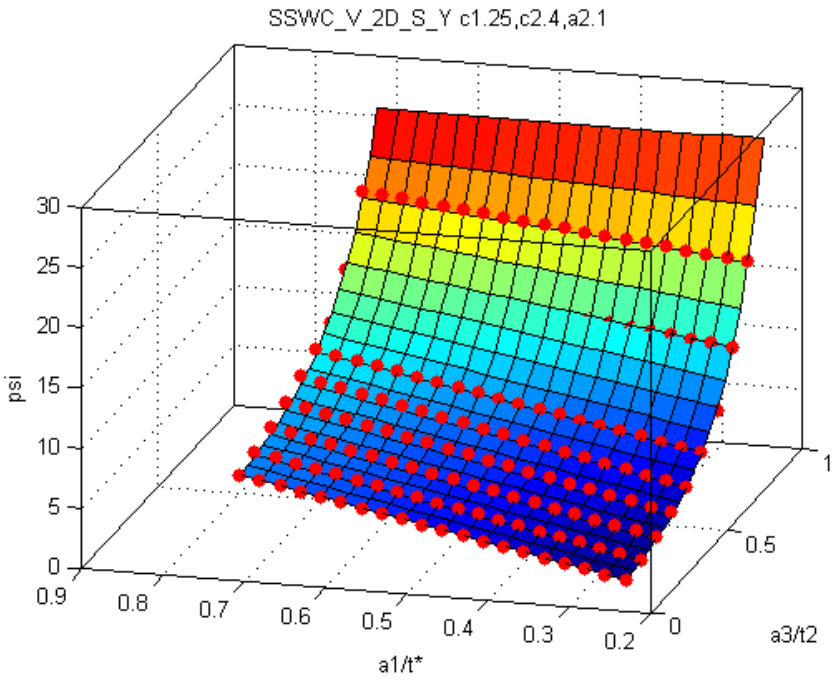

Figure 66: SSWC V-Crack with Width=0.25t, Symmetric General Corrosion Total Width=8t and Depth=0.1t

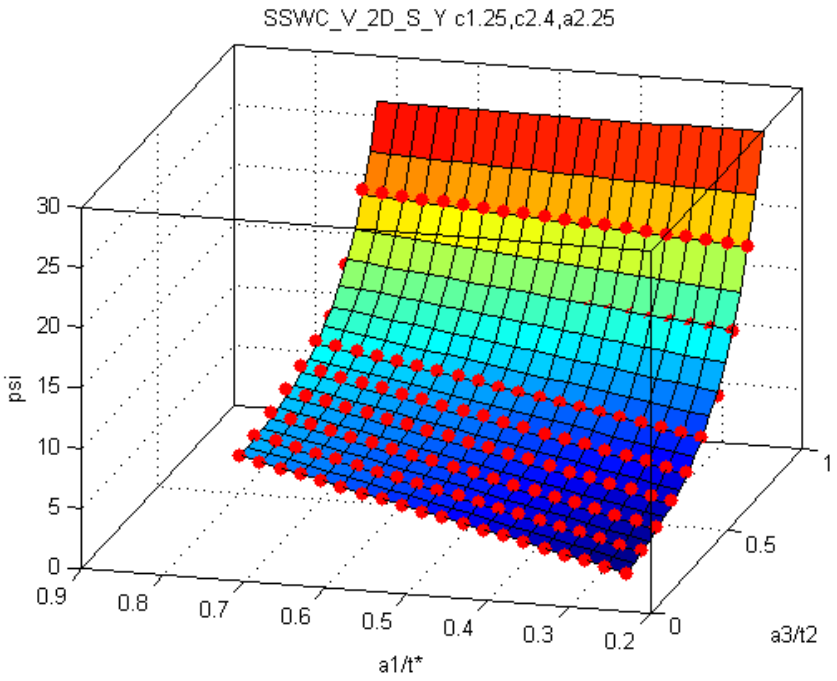

Figure 67: SSWC V-Crack with Width=0.25t, Symmetric General Corrosion Total Width=8t and Depth=0.25t

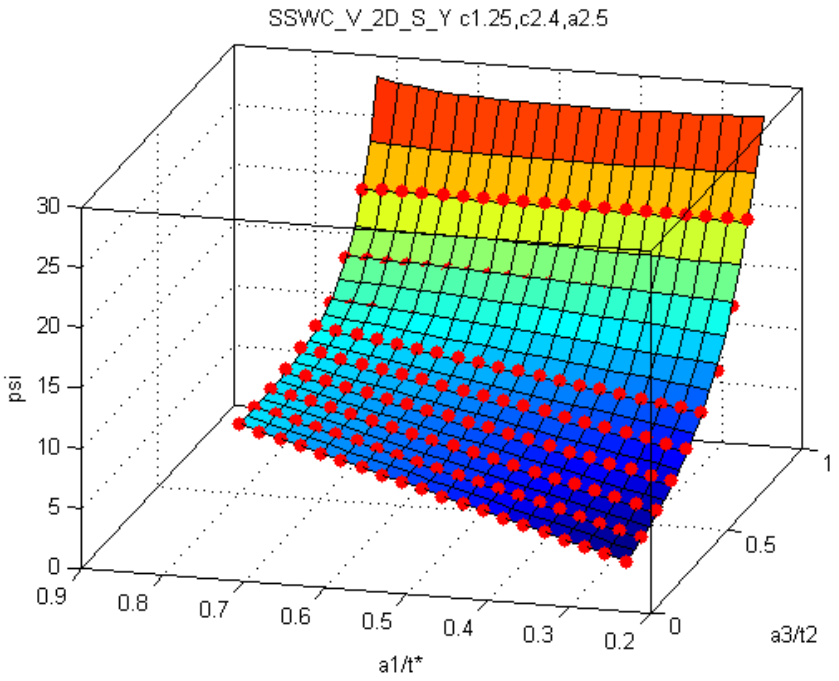

Figure 68: SSWC V-Crack with Width=0.25t, Symmetric General Corrosion Total Width=8t and Depth=0.5t

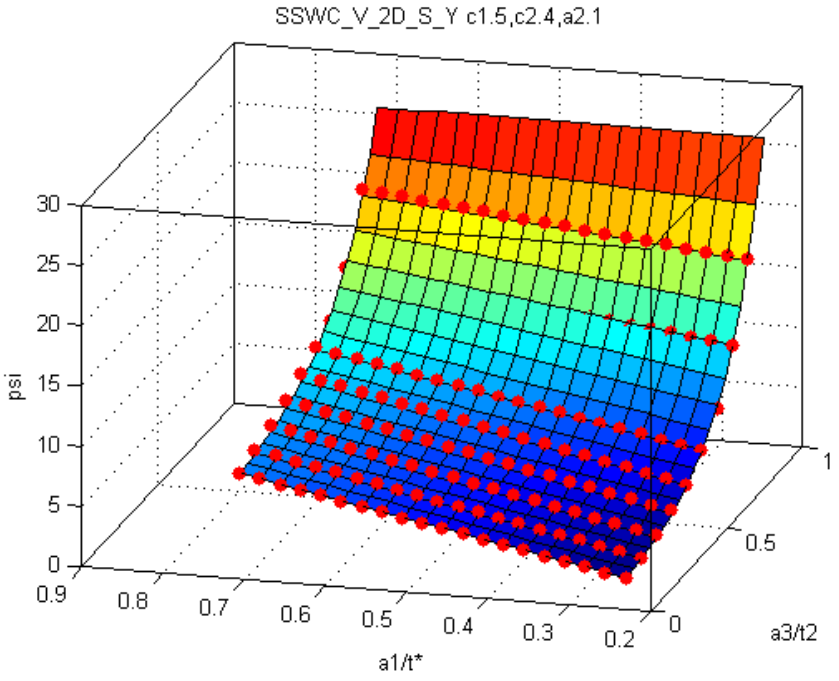

Figure 69: SSWC V-Crack with Width=0.5t, Symmetric General Corrosion Total Width=8t and Depth=0.1t

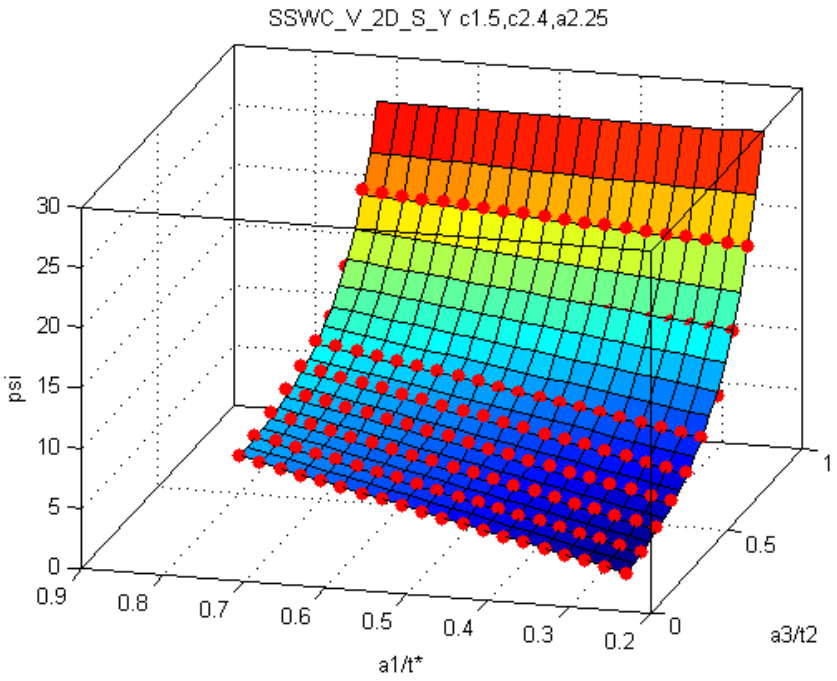

Figure 70: SSWC V-Crack with Width=0.5t, Symmetric General Corrosion Total Width=8t and Depth=0.25t

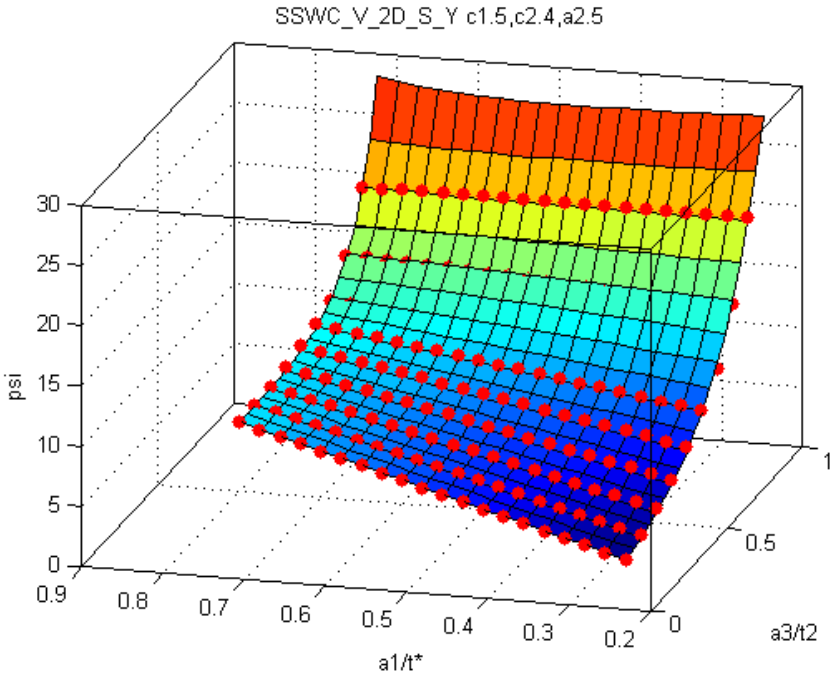

Figure 71: SSWC V-Crack with Width=0.5t, Symmetric General Corrosion Total Width=8t and Depth=0.5t

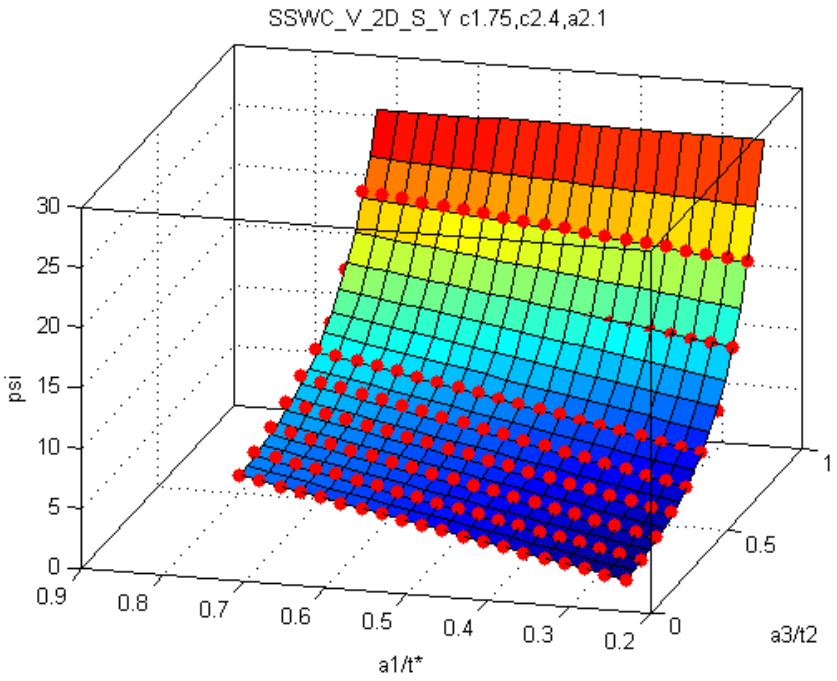

Figure 72: SSWC V-Crack with Width=0.75t, Symmetric General Corrosion Total Width=8t and Depth=0.1t

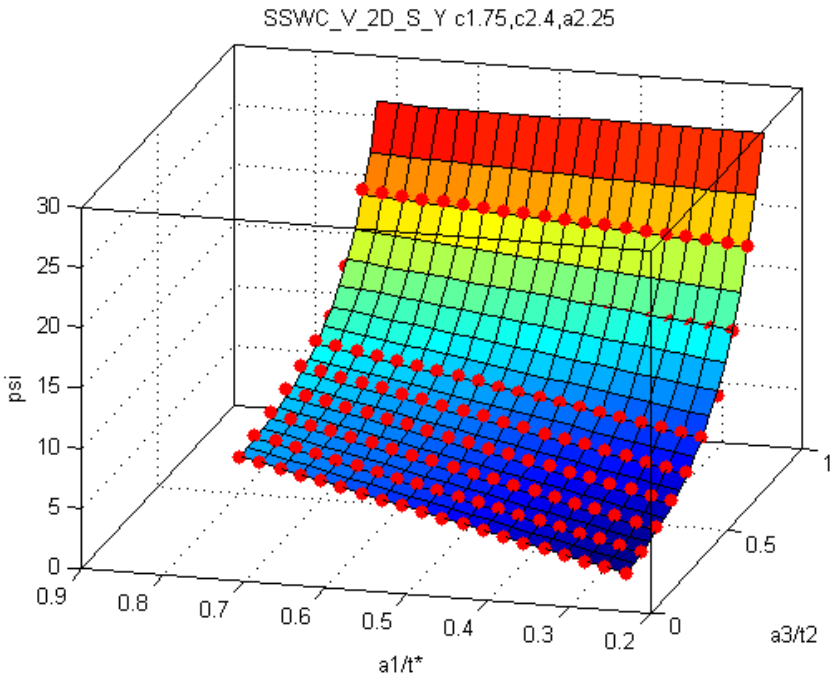

Figure 73: SSWC V-Crack with Width=0.75t, Symmetric General Corrosion Total Width=8t and Depth=0.25t

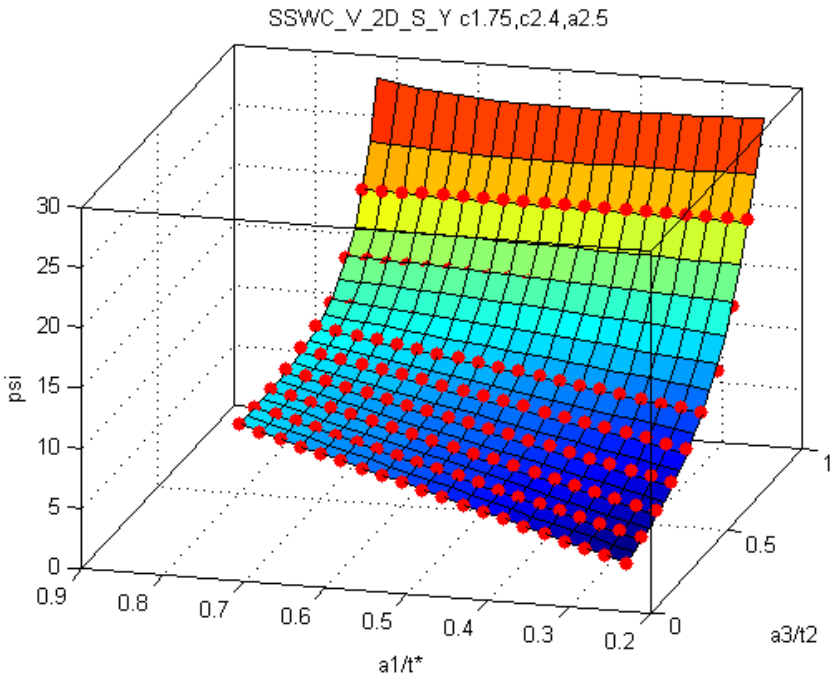

Figure 74: SSWC V-Crack with Width=0.75t, Symmetric General Corrosion Total Width=8t and Depth=0.5t

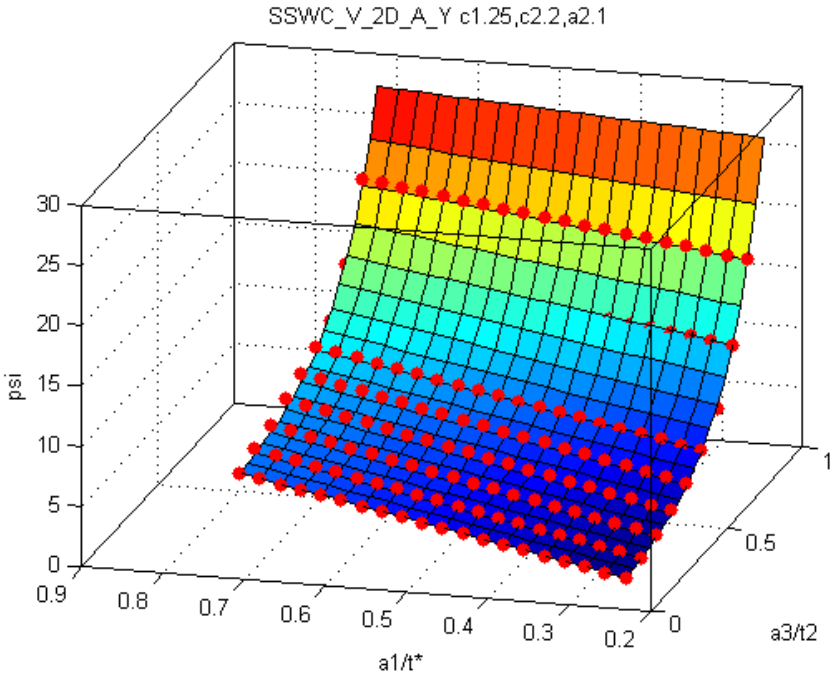

Figure 75: SSWC V-Crack with Width=0.25t, Asymmetric General Corrosion Width=2t in One Direction, Infinite in the Other Direction, and Depth=0.1t

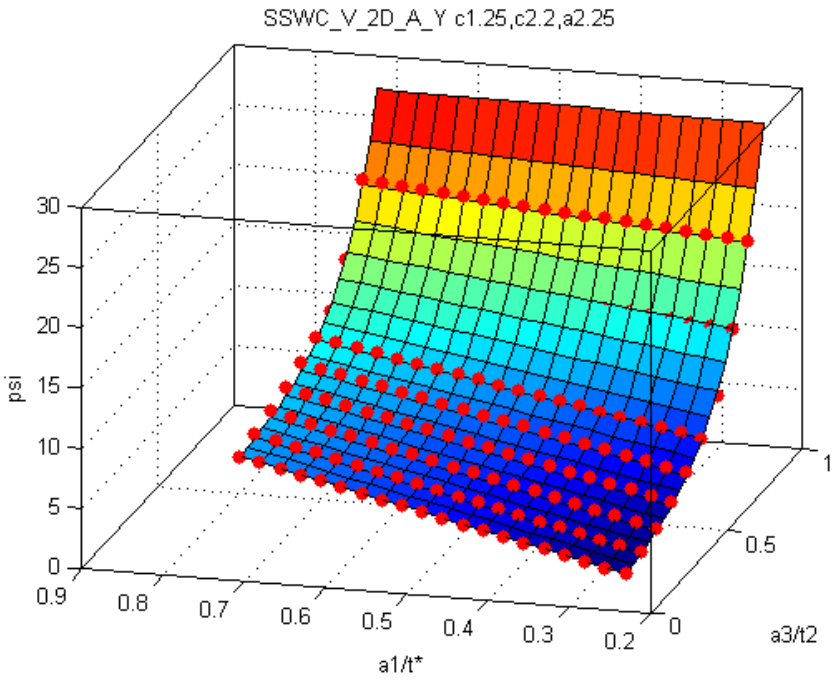

Figure 76: SSWC V-Crack with Width=0.25t, Asymmetric General Corrosion Width=2t in One Direction, Infinite in the Other Direction, and Depth=0.25t

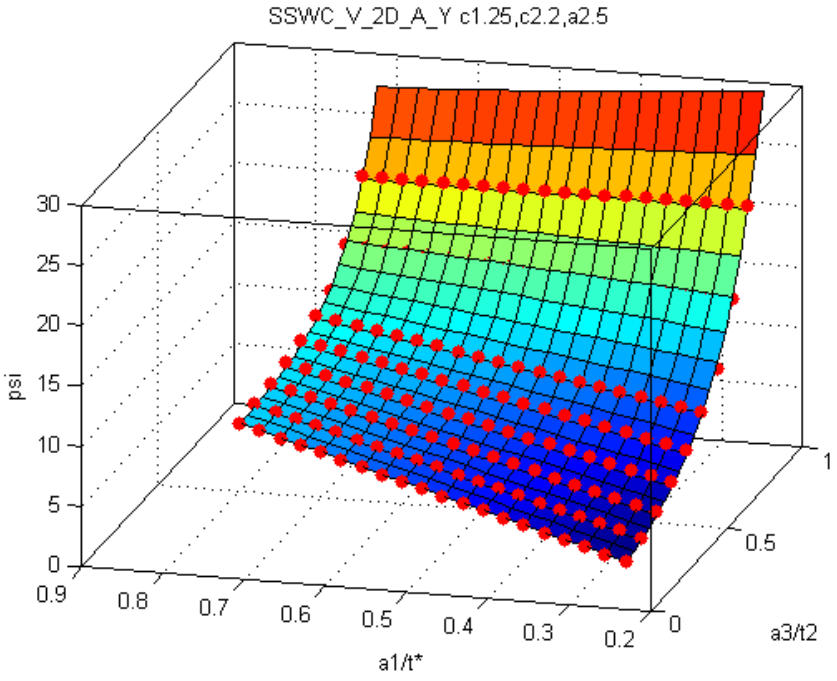

Figure 77: SSWC V-Crack with Width=0.25t, Asymmetric General Corrosion Width=2t in One Direction, Infinite in the Other Direction, and Depth=0.5t

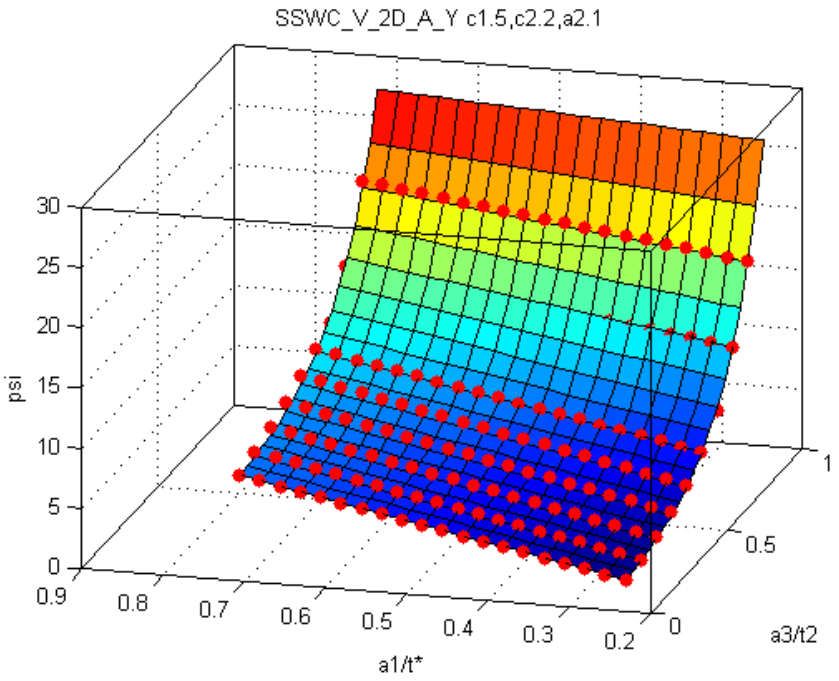

Figure 78: SSWC V-Crack with Width=0.5t, Asymmetric General Corrosion Width=2t in One Direction, Infinite in the Other Direction, and Depth=0.1t

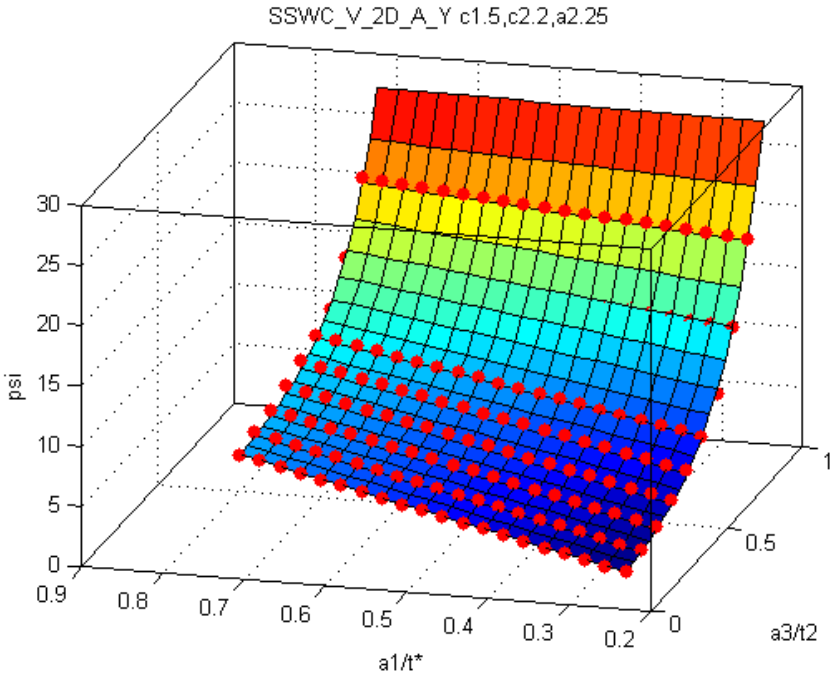

Figure 79: SSWC V-Crack with Width=0.5t, Asymmetric General Corrosion Width=2t in One Direction, Infinite in the Other Direction, and Depth=0.25t

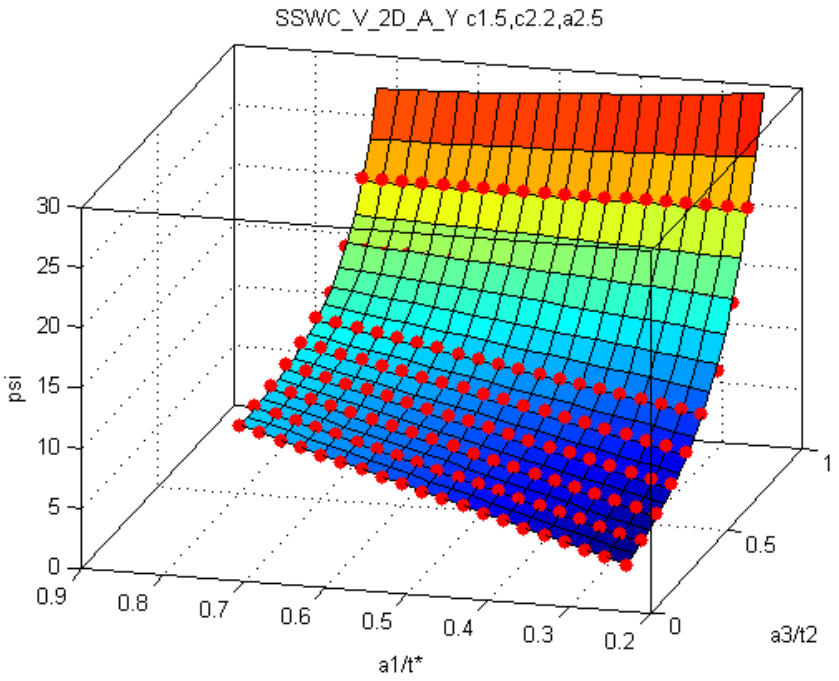

Figure 80: SSWC V-Crack with Width=0.5t, Asymmetric General Corrosion Width=2t in One Direction, Infinite in the Other Direction, and Depth=0.5t

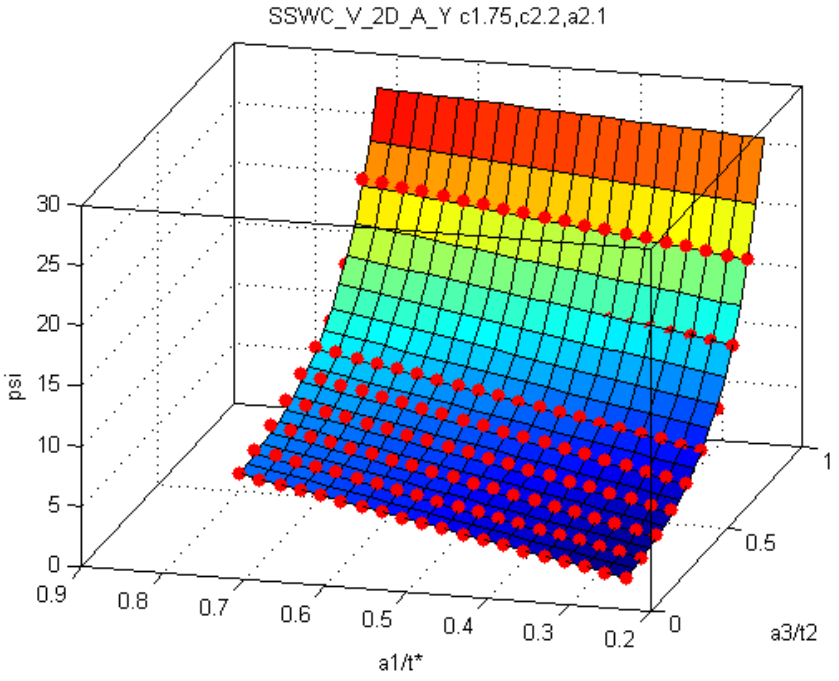

Figure 81: SSWC V-Crack with Width=0.75t, Asymmetric General Corrosion Width=2t in One Direction, Infinite in the Other Direction, and Depth=0.1t

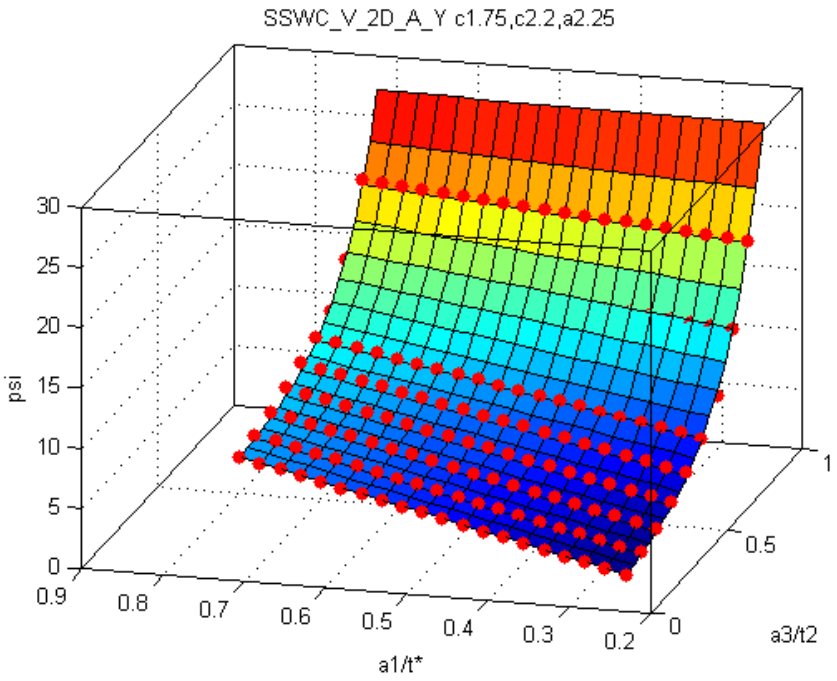

Figure 82: SSWC V-Crack with Width=0.75t, Asymmetric General Corrosion Width=2t in One Direction, Infinite in the Other Direction, and Depth=0.25t

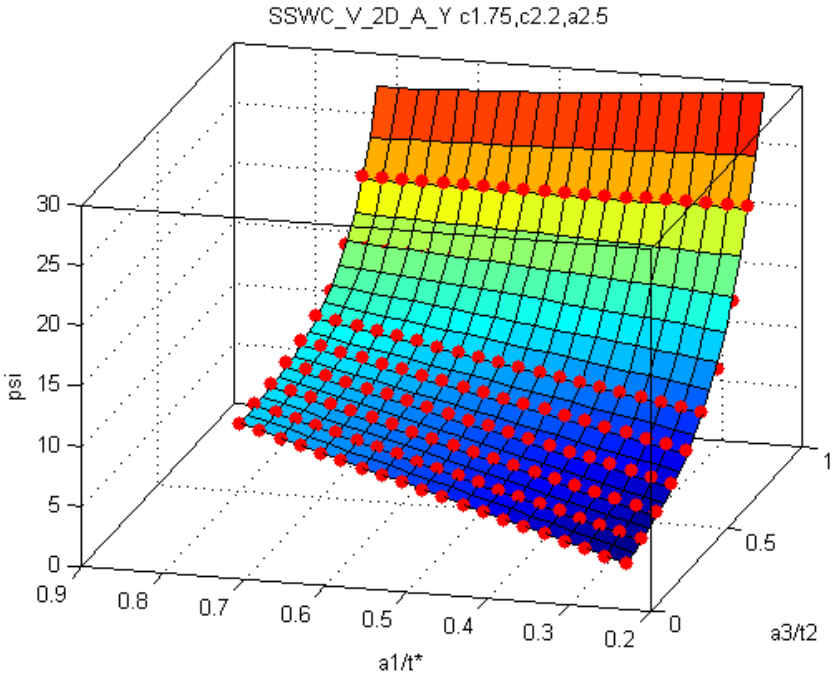

Figure 83: SSWC V-Crack with Width=0.75t, Asymmetric General Corrosion Width=2t in One Direction, Infinite in the Other Direction, and Depth=0.5t

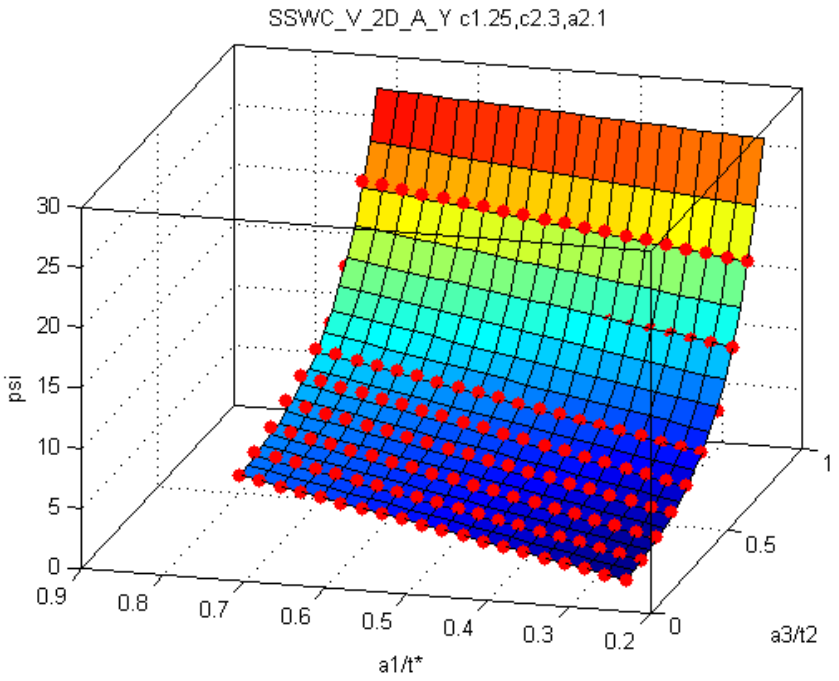

Figure 84: SSWC V-Crack with Width=0.25t, Asymmetric General Corrosion Width=3t in One Direction, Infinite in the Other Direction, and Depth=0.1t

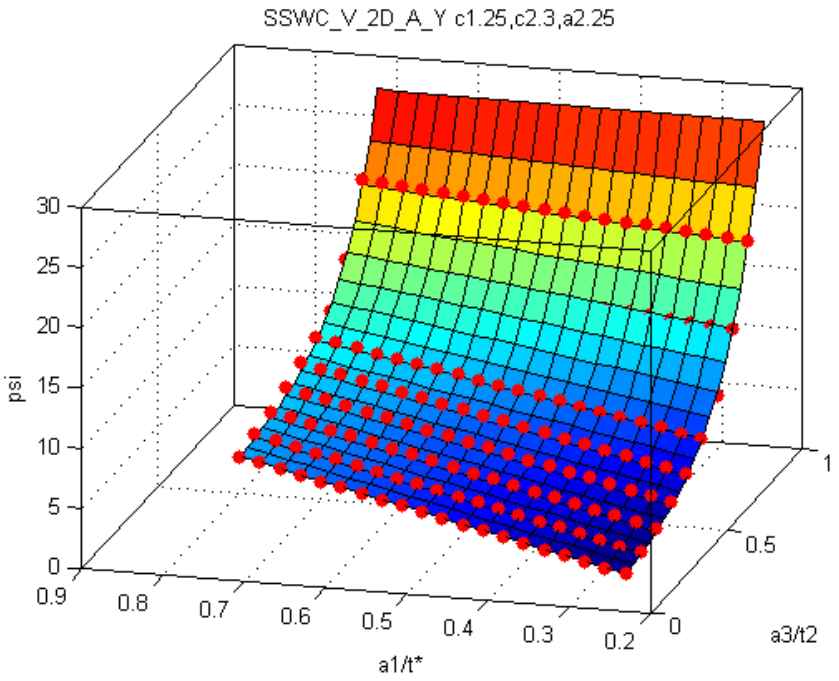

Figure 85: SSWC V-Crack with Width=0.25t, Asymmetric General Corrosion Width=3t in One Direction, Infinite in the Other Direction, and Depth=0.25t

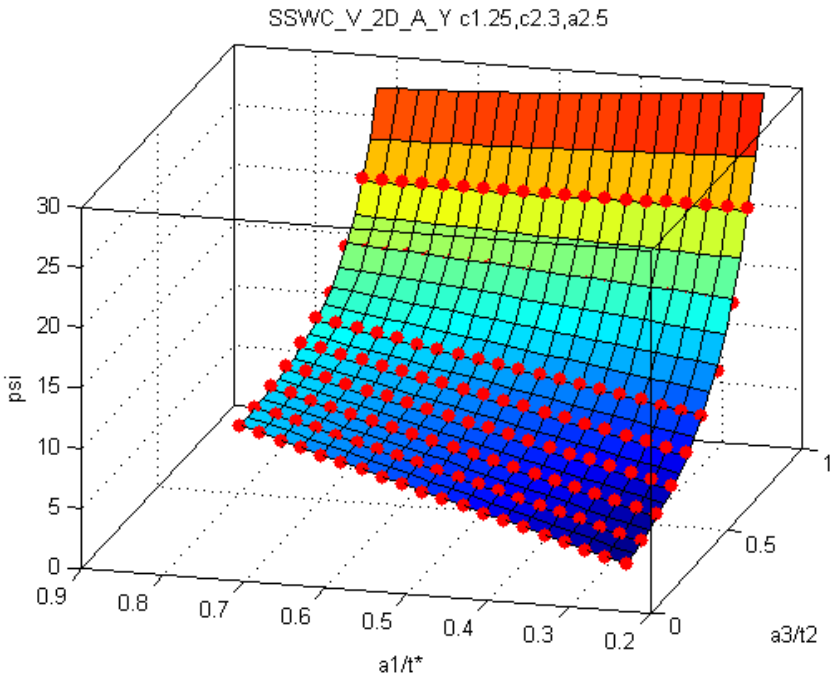

Figure 86: SSWC V-Crack with Width=0.25t, Asymmetric General Corrosion Width=3t in One Direction, Infinite in the Other Direction, and Depth=0.5t

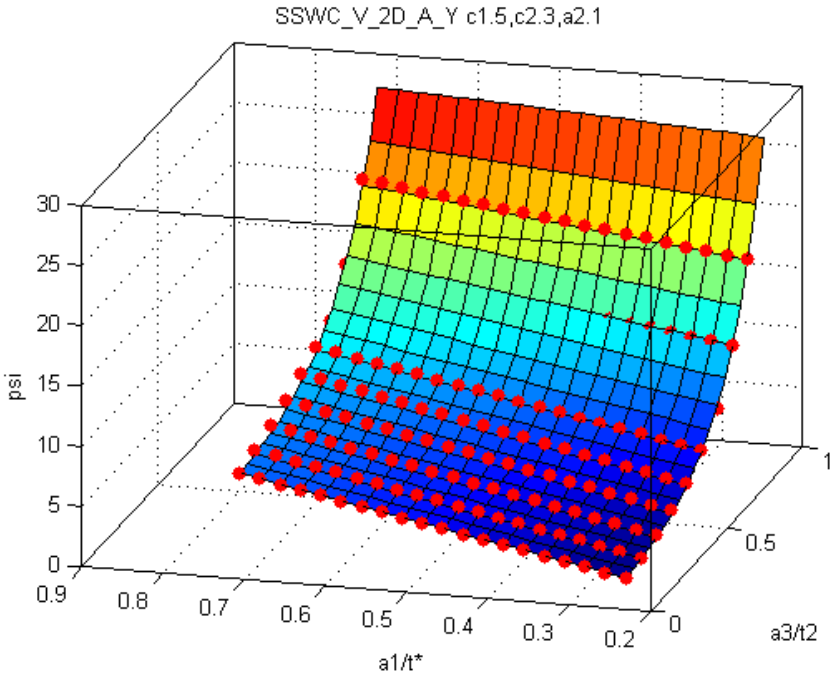

Figure 87: SSWC V-Crack with Width=0.5t, Asymmetric General Corrosion Width=3t in One Direction, Infinite in the Other Direction, and Depth=0.1t

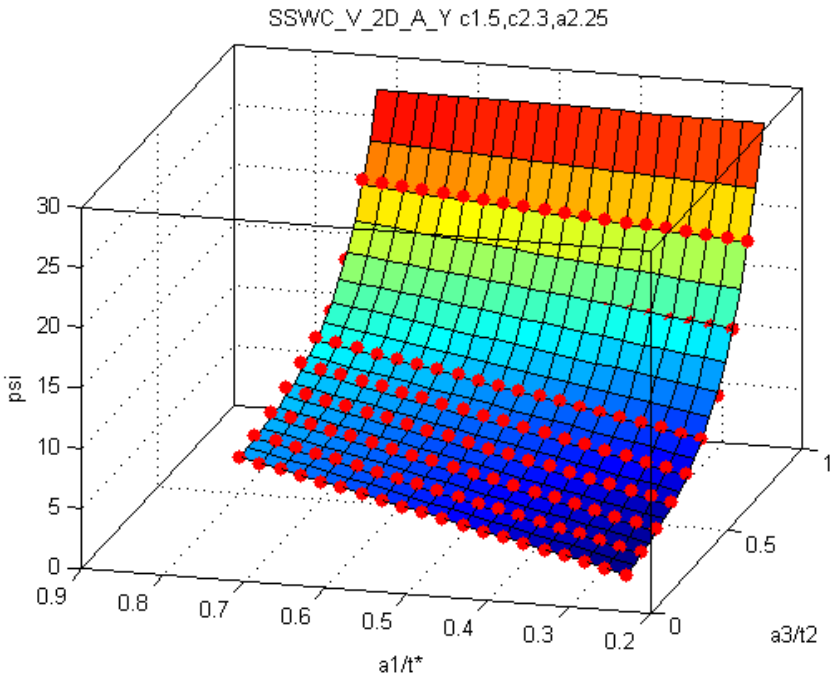

Figure 88: SSWC V-Crack with Width=0.5t, Asymmetric General Corrosion Width=3t in One Direction, Infinite in the Other Direction, and Depth=0.25t

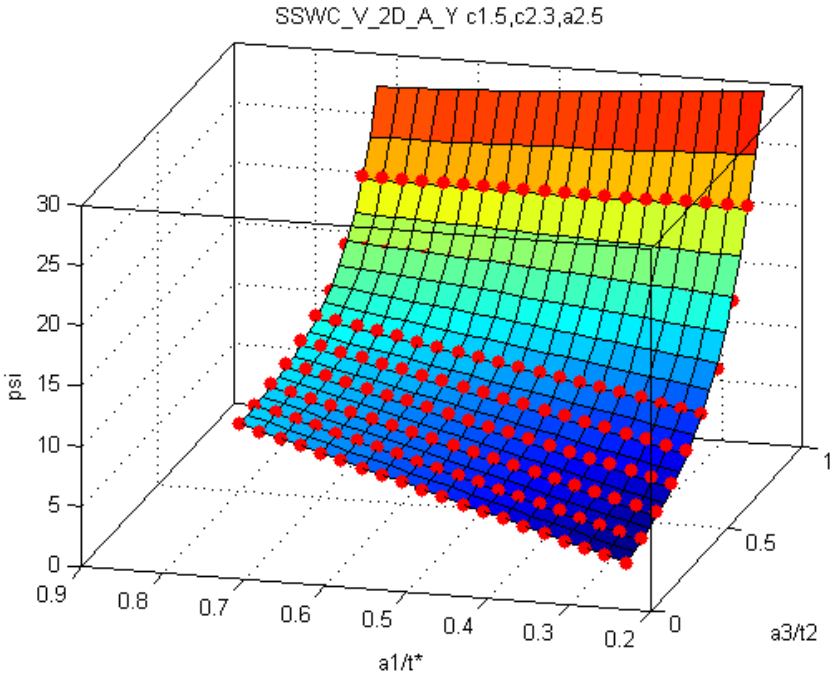

Figure 89: SSWC V-Crack with Width=0.5t, Asymmetric General Corrosion Width=3t in One Direction, Infinite in the Other Direction, and Depth=0.5t

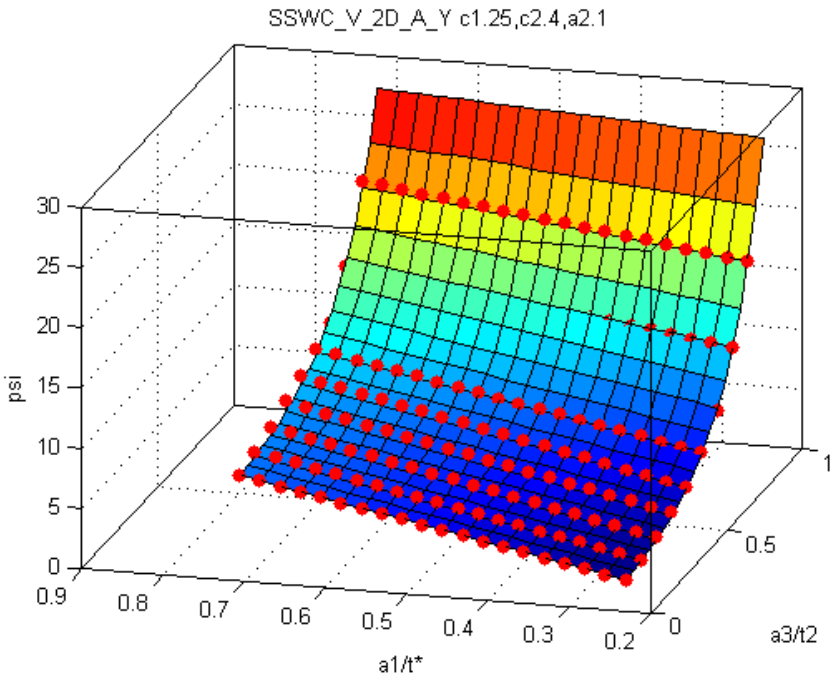

Figure 90: SSWC V-Crack with Width=0.25t, Asymmetric General Corrosion Width=4t in One Direction, Infinite in the Other Direction, and Depth=0.1t

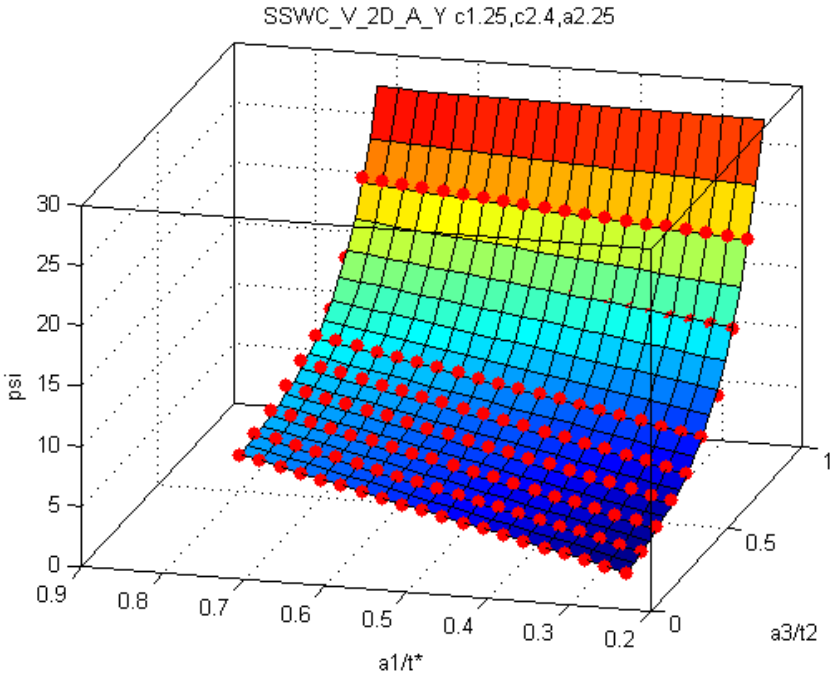

Figure 91: SSWC V-Crack with Width=0.25t, Asymmetric General Corrosion Width=4t in One Direction, Infinite in the Other Direction, and Depth=0.25t

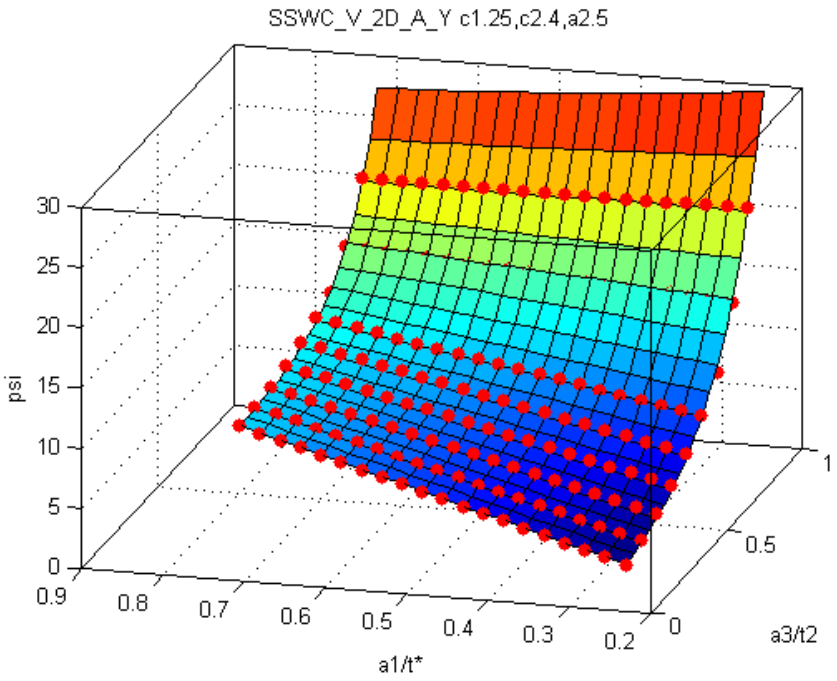

Figure 92: SSWC V-Crack with Width=0.25t, Asymmetric General Corrosion Width=4t in One Direction, Infinite in the Other Direction, and Depth=0.5t

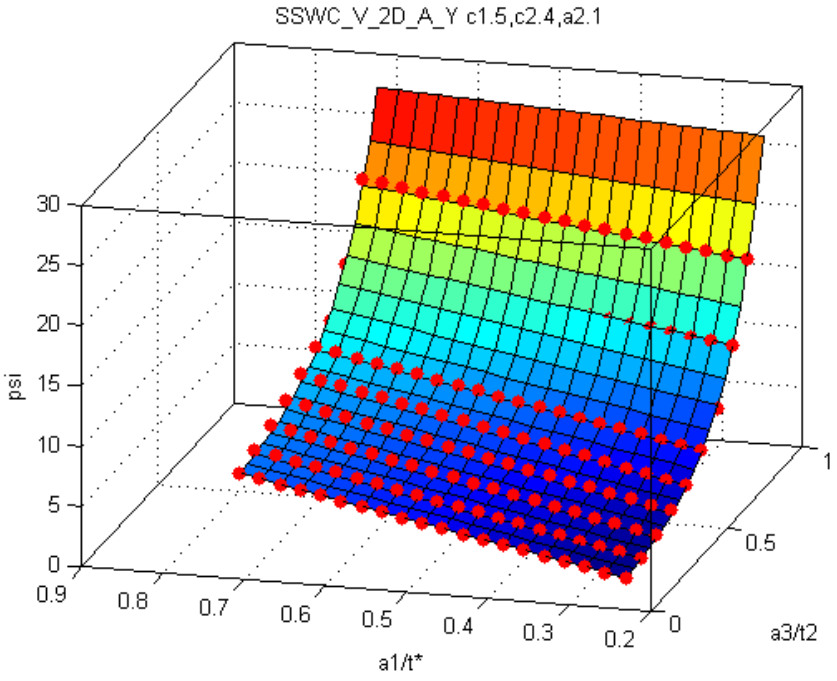

Figure 93: SSWC V-Crack with Width=0.5t, Asymmetric General Corrosion Width=4t in One Direction, Infinite in the Other Direction, and Depth=0.1t

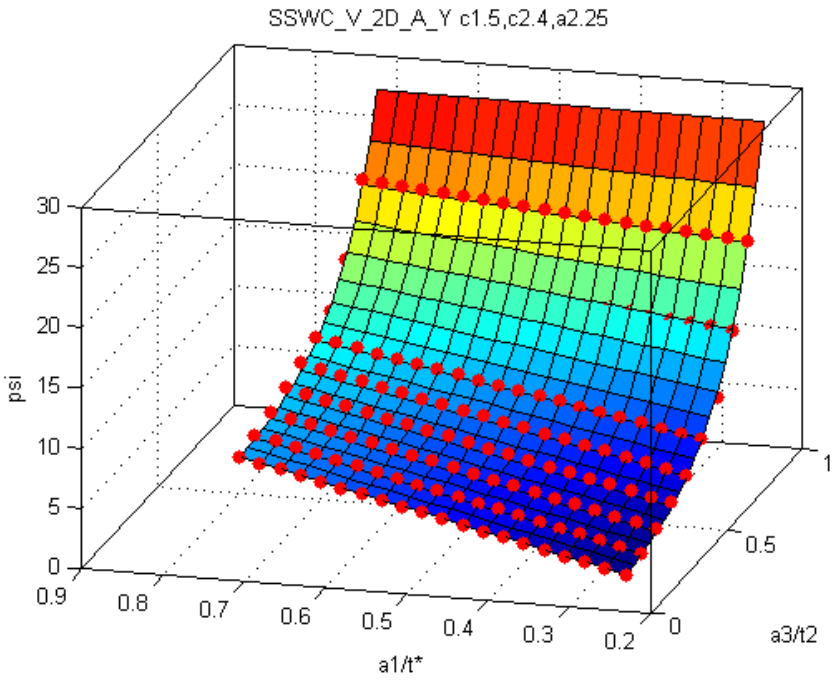

Figure 94: SSWC V-Crack with Width=0.5t, Asymmetric General Corrosion Width=4t in One Direction, Infinite in the Other Direction, and Depth=0.25t

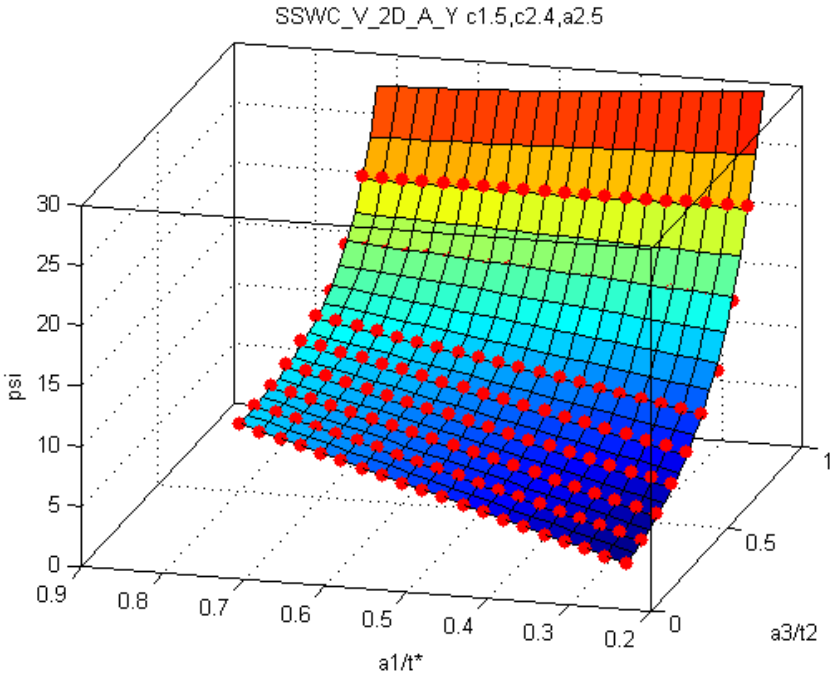

Figure 95: SSWC V-Crack with Width=0.5t, Asymmetric General Corrosion Width=4t in One Direction, Infinite in the Other Direction, and Depth=0.5t

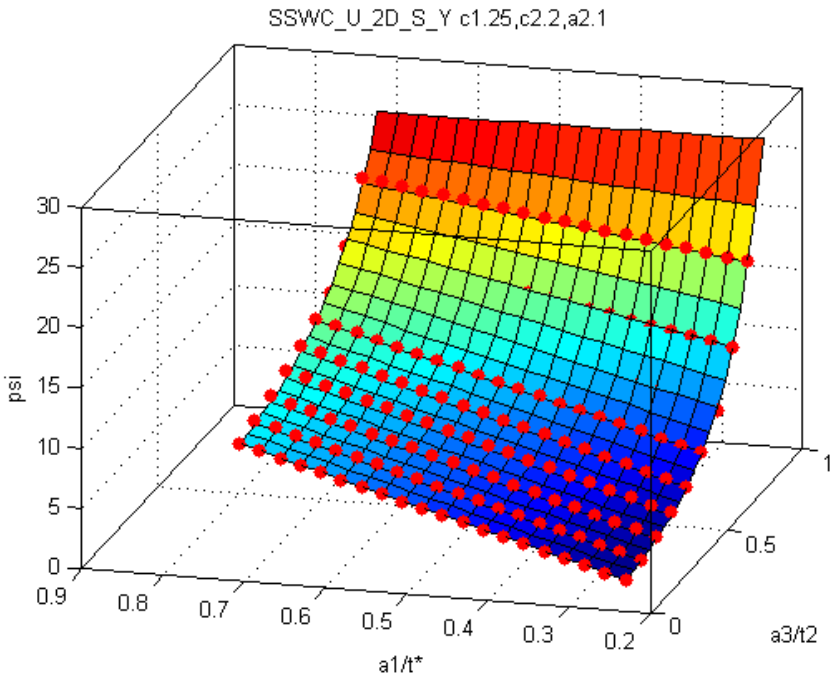

Figure 96: SSWC U-Crack with Width=0.25t, Symmetric General Corrosion Total Width=4t and Depth=0.1t

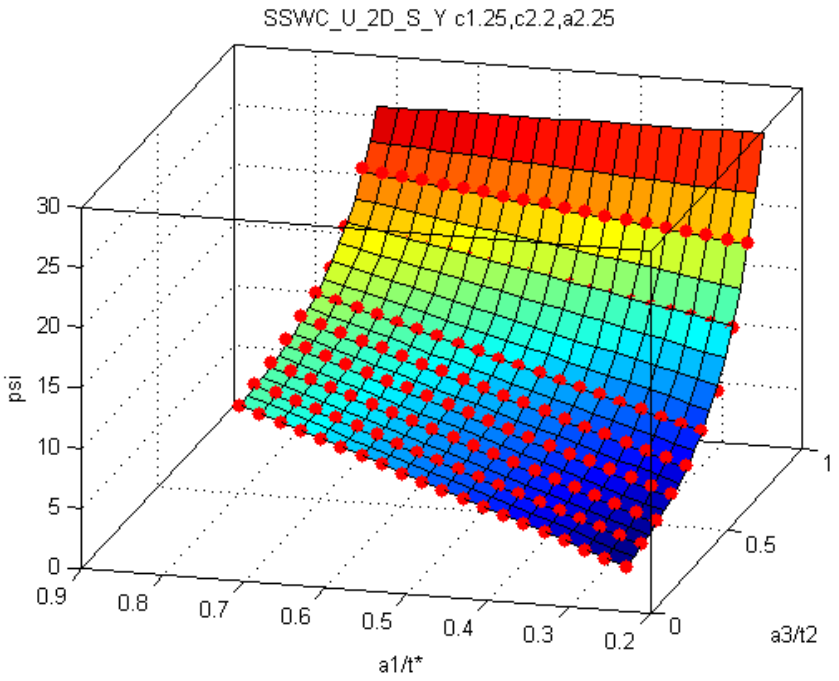

Figure 97: SSWC U-Crack with Width=0.25t, Symmetric General Corrosion Total Width=4t and Depth=0.25t

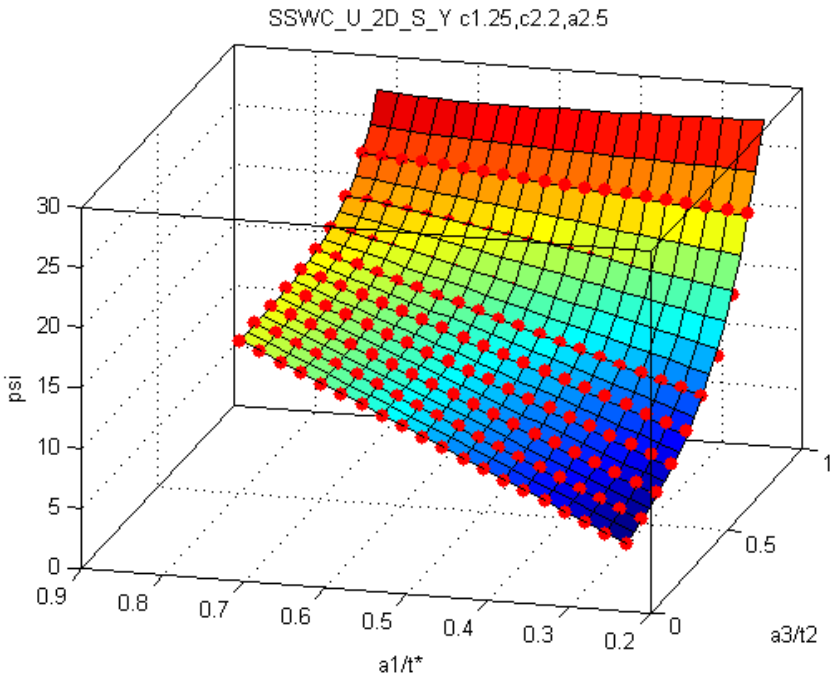

Figure 98: SSWC U-Crack with Width=0.25t, Symmetric General Corrosion Total Width=4t and Depth=0.5t

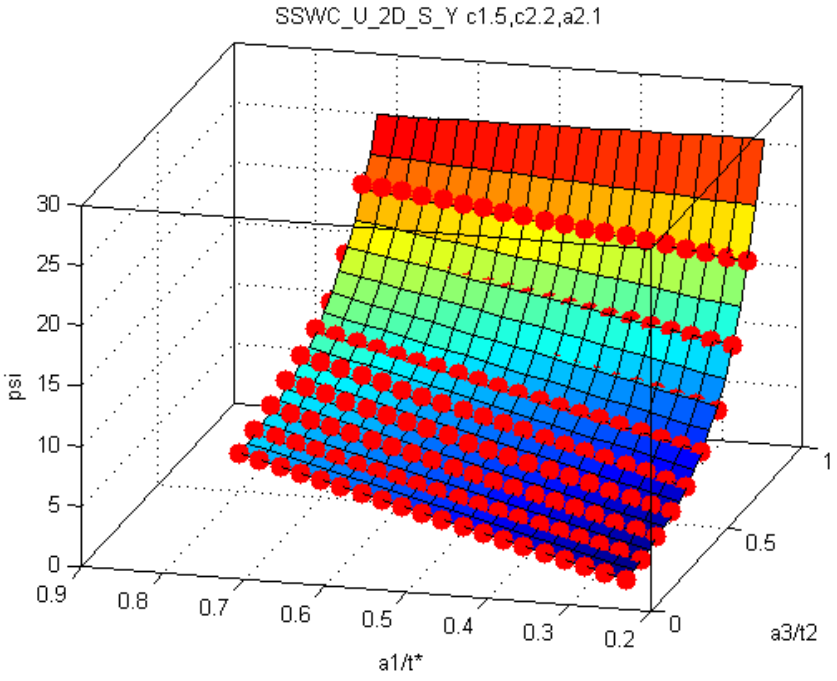

Figure 99: SSWC U-Crack with Width=0.5t, Symmetric General Corrosion Total Width=4t and Depth=0.1t

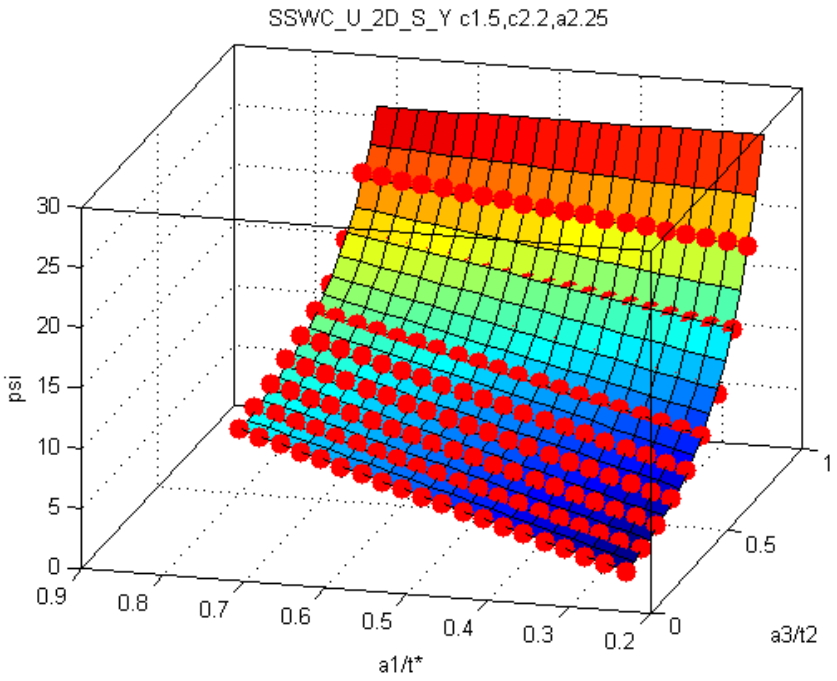

Figure 100: SSWC U-Crack with Width=0.5t, Symmetric General Corrosion Total Width=4t and Depth=0.25t

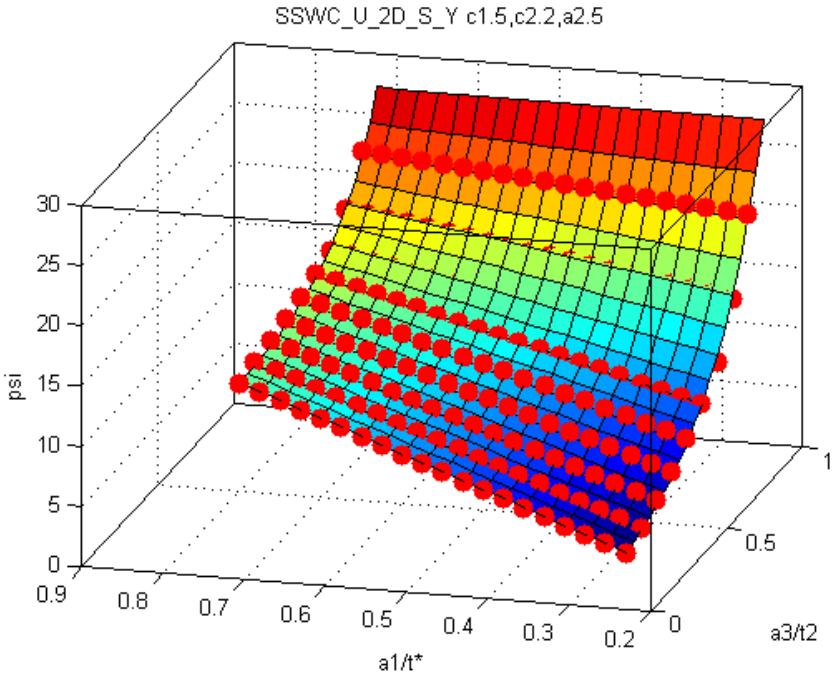

Figure 101: SSWC U-Crack with Width=0.5t, Symmetric General Corrosion Total Width=4t and Depth=0.5t

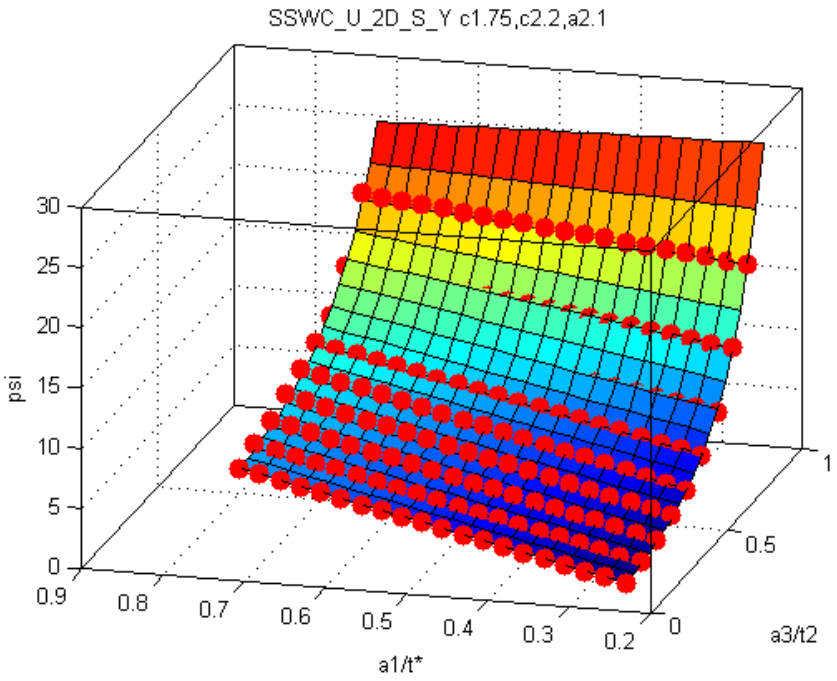

Figure 102: SSWC U-Crack with Width=0.75t, Symmetric General Corrosion Total Width=4t and Depth=0.1t

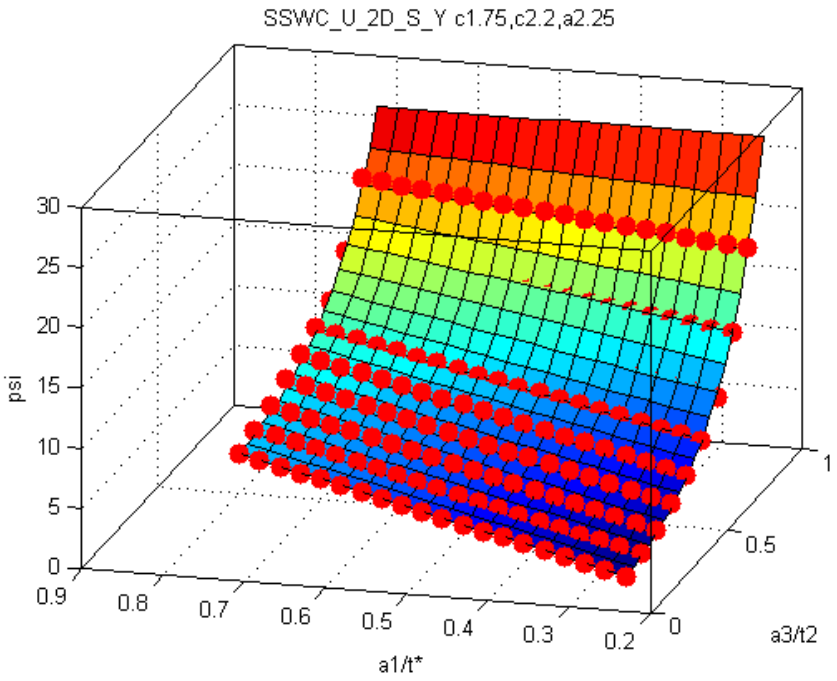

Figure 103: SSWC U-Crack with Width=0.75t, Symmetric General Corrosion Total Width=4t and Depth=0.25t

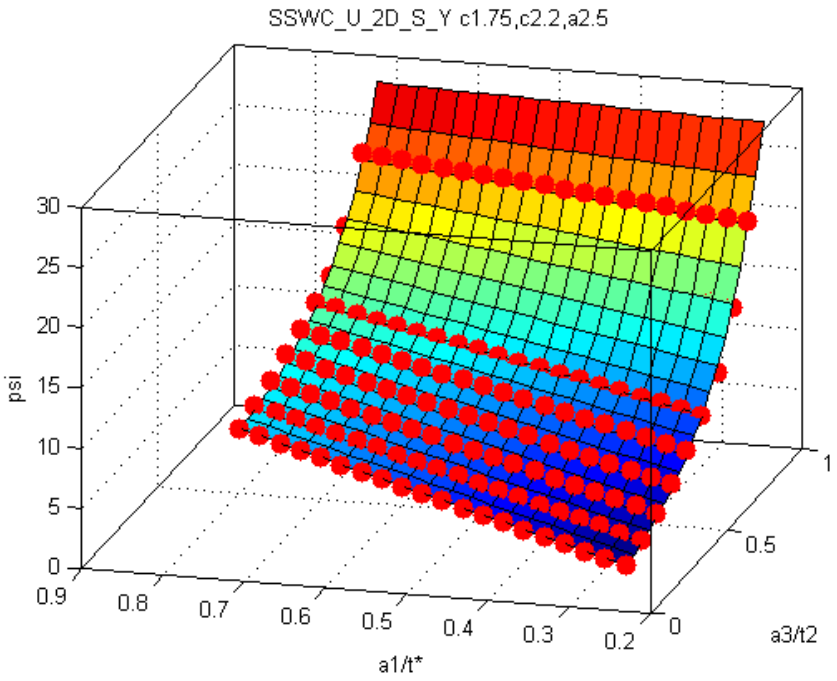

Figure 104: SSWC U-Crack with Width=0.75t, Symmetric General Corrosion Total Width=4t and Depth=0.5t

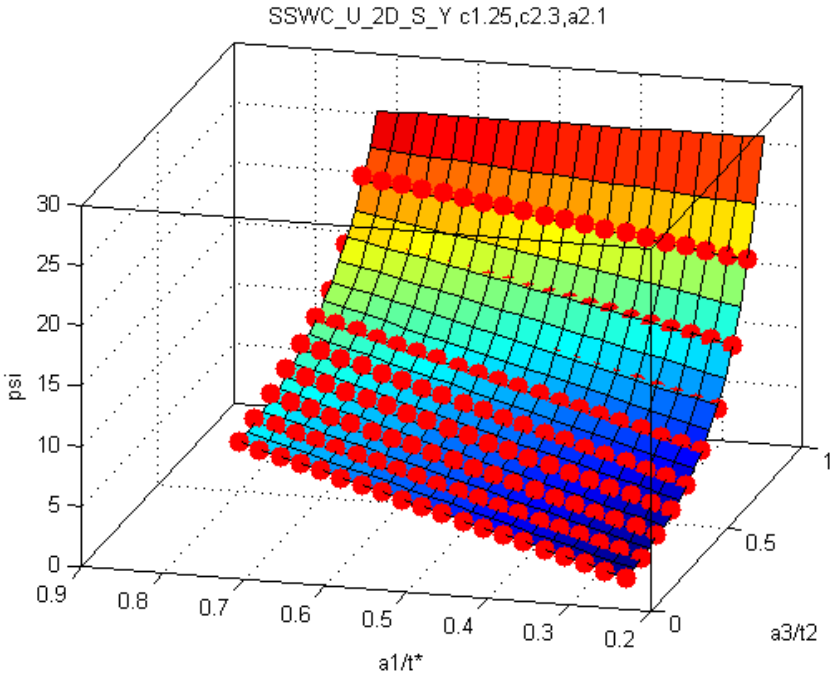

Figure 105: SSWC U-Crack with Width=0.25t, Symmetric General Corrosion Total Width=6t and Depth=0.1t

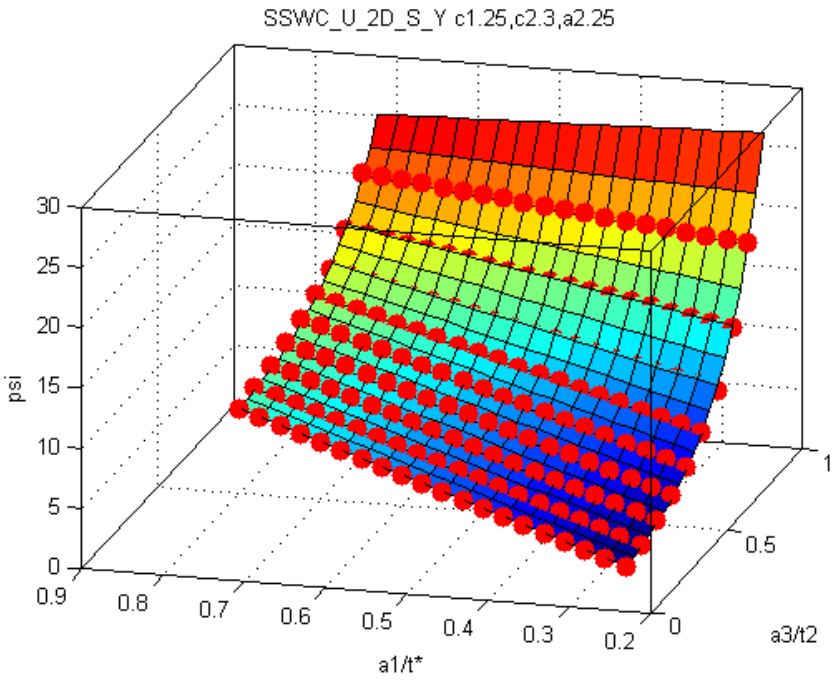

Figure 106: SSWC U-Crack with Width=0.25t, Symmetric General Corrosion Total Width=6t and Depth=0.25t

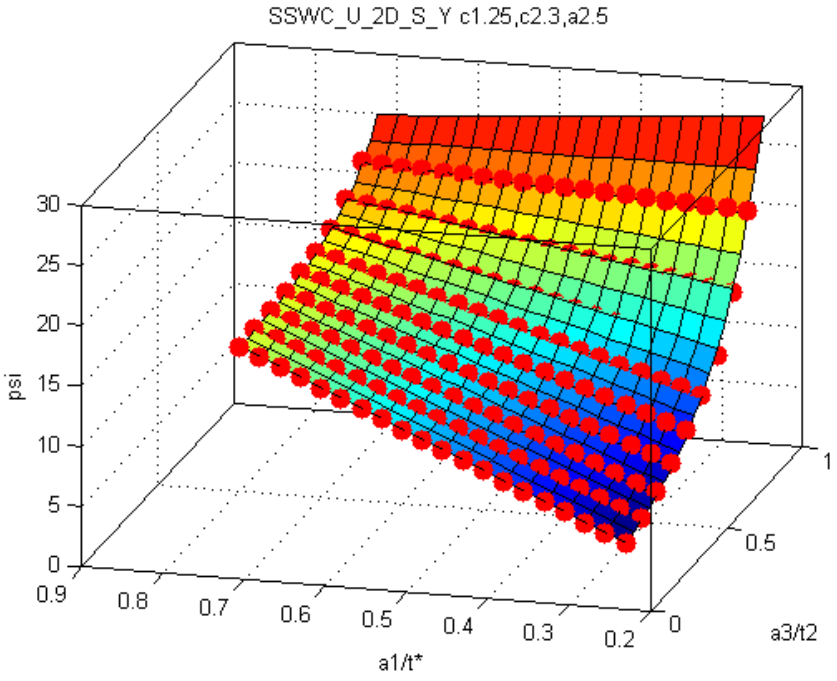

Figure 107: SSWC U-Crack with Width=0.25t, Symmetric General Corrosion Total Width=6t and Depth=0.5t

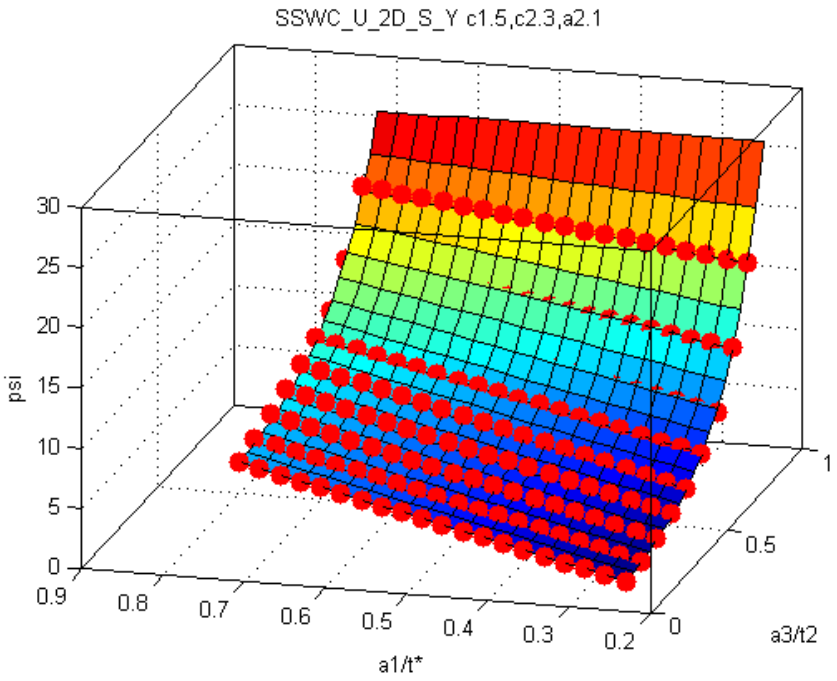

Figure 108: SSWC U-Crack with Width=0.5t, Symmetric General Corrosion Total Width=6t and Depth=0.1t

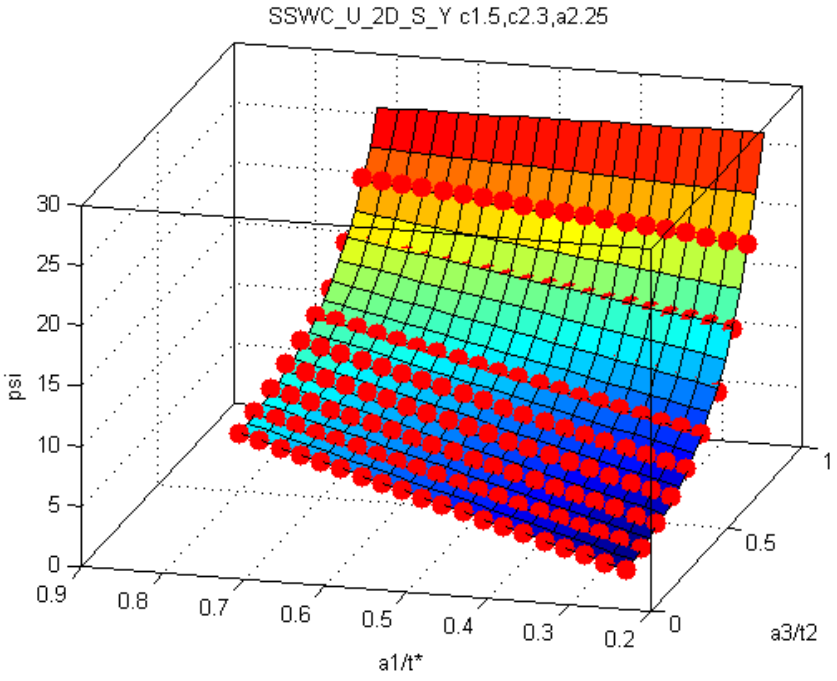

Figure 109: SSWC U-Crack with Width=0.5t, Symmetric General Corrosion Total Width=6t and Depth=0.25t

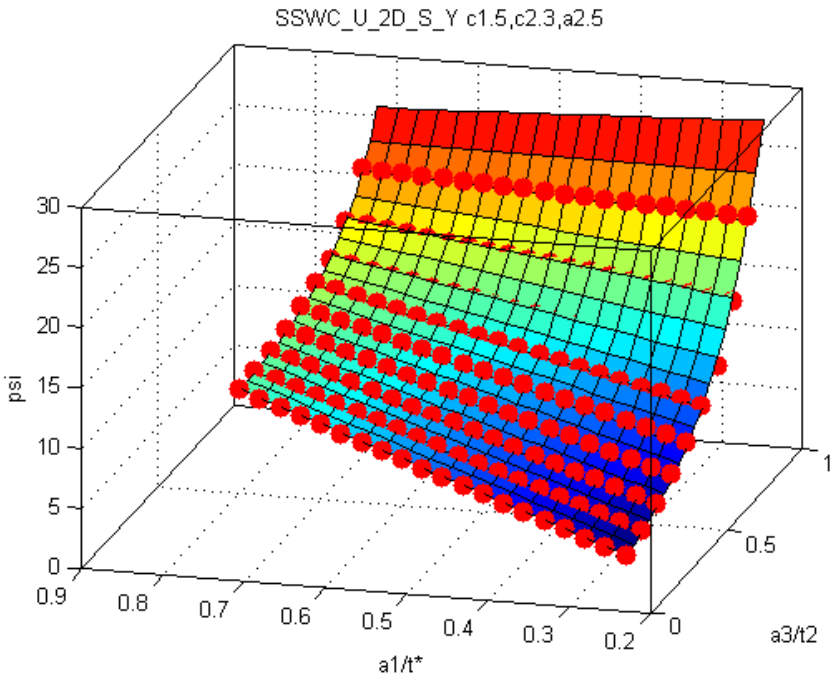

Figure 110: SSWC U-Crack with Width=0.5t, Symmetric General Corrosion Total Width=6t and Depth=0.5t

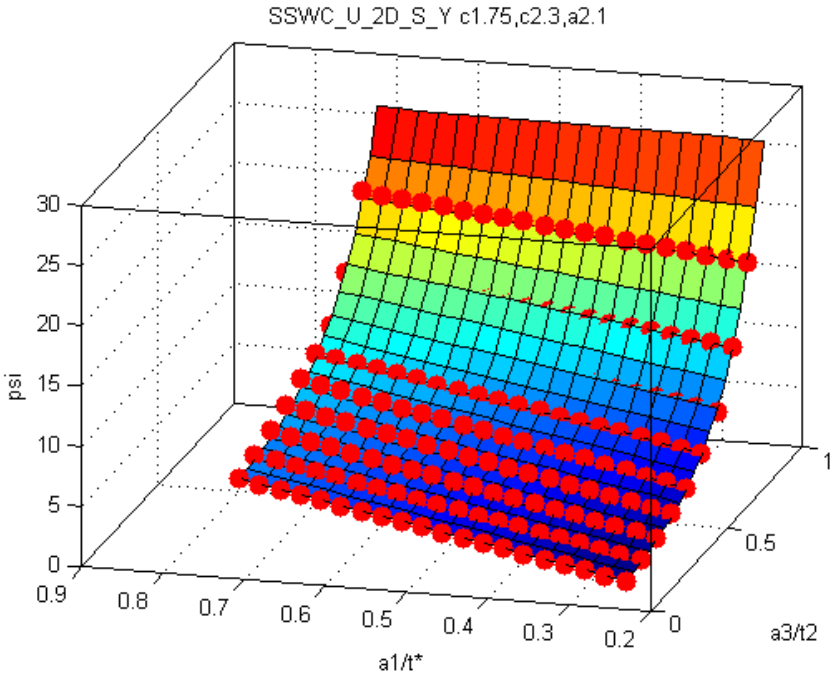

Figure 111: SSWC U-Crack with Width=0.75t, Symmetric General Corrosion Total Width=6t and Depth=0.1t

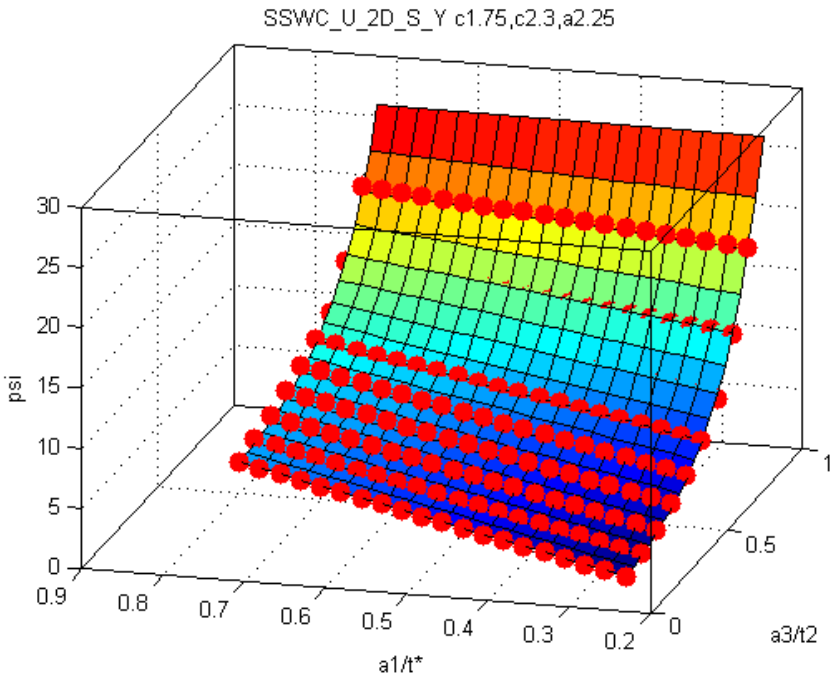

Figure 112: SSWC U-Crack with Width=0.75t, Symmetric General Corrosion Total Width=6t and Depth=0.25t

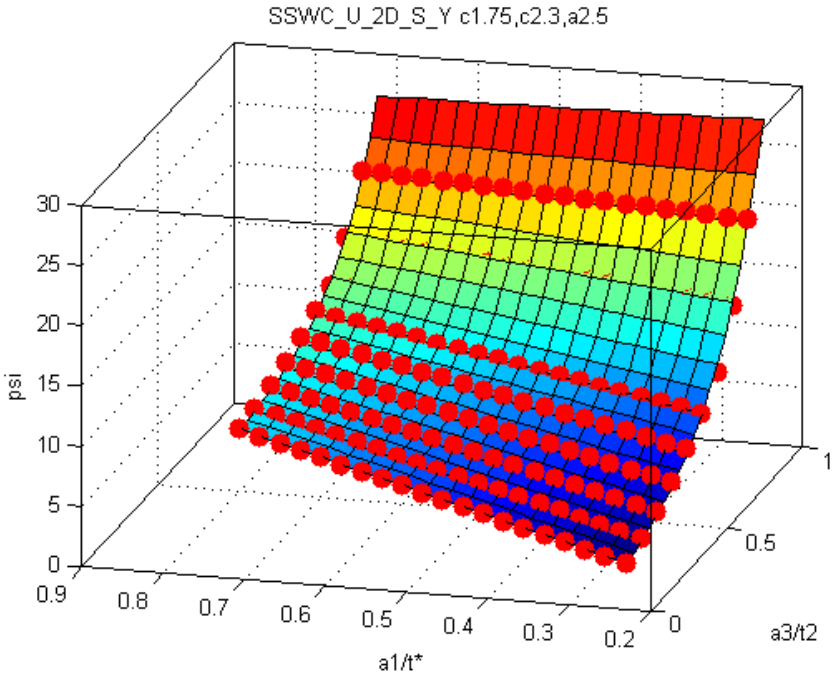

Figure 113: SSWC U-Crack with Width=0.75t, Symmetric General Corrosion Total Width=6t and Depth=0.5t

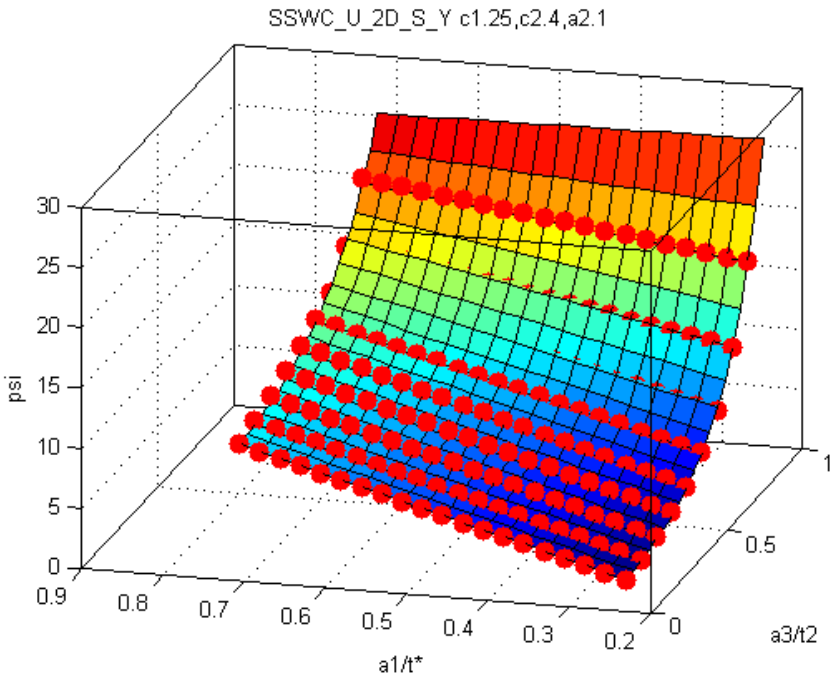

Figure 114: SSWC U-Crack with Width=0.25t, Symmetric General Corrosion Total Width=8t and Depth=0.1t

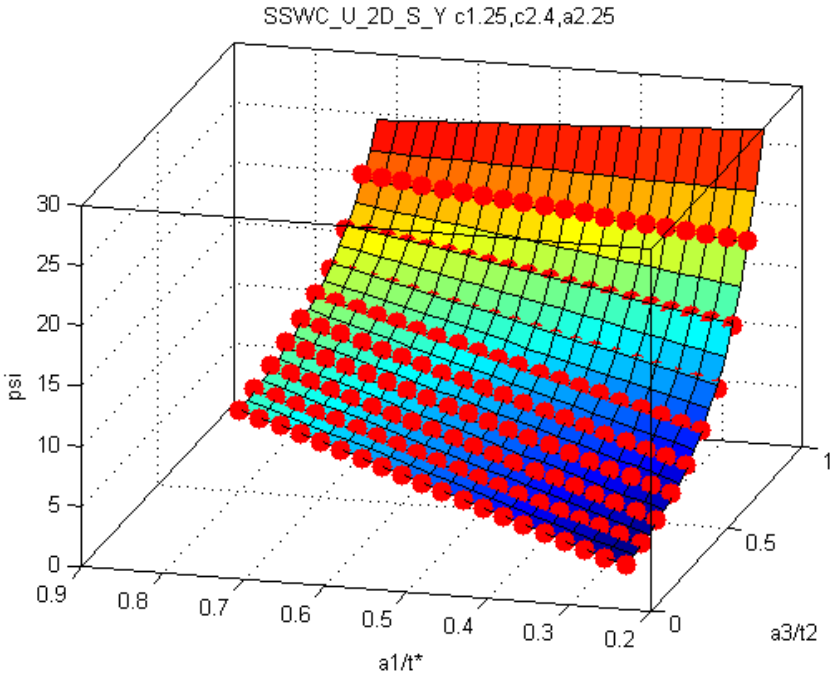

Figure 115: SSWC U-Crack with Width=0.25t, Symmetric General Corrosion Total Width=8t and Depth=0.25t

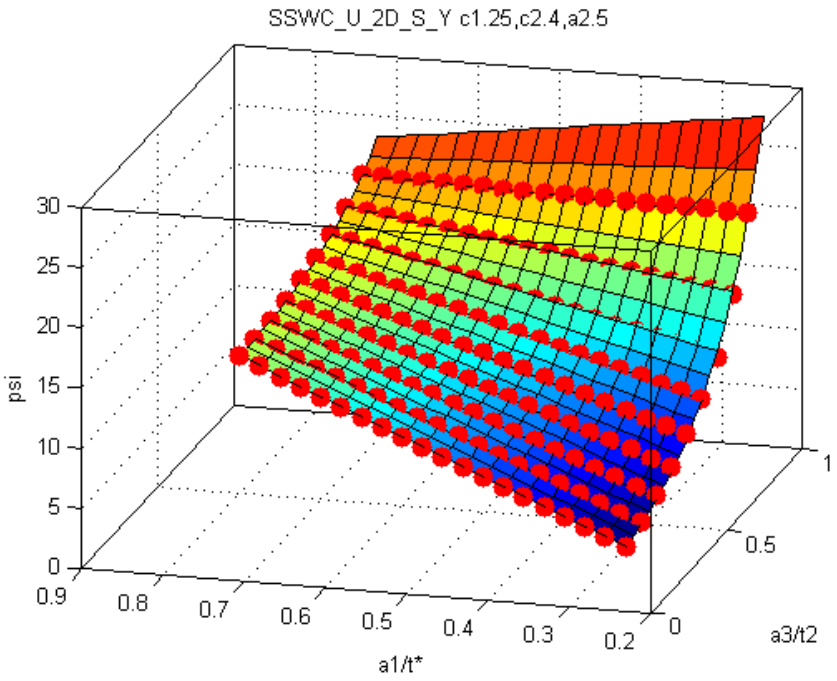

Figure 116: SSWC U-Crack with Width=0.25t, Symmetric General Corrosion Total Width=8t and Depth=0.5t

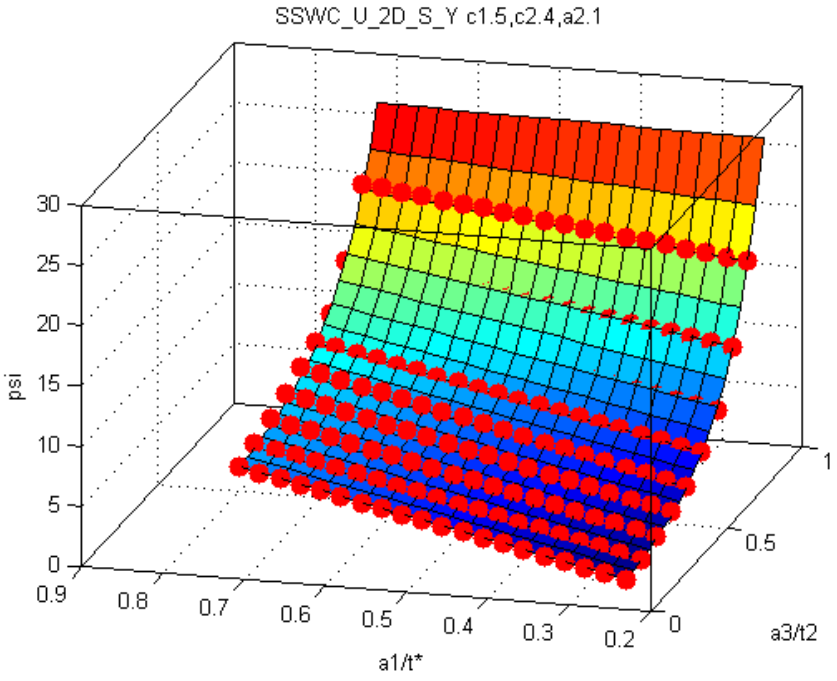

Figure 117: SSWC U-Crack with Width=0.5t, Symmetric General Corrosion Total Width=8t and Depth=0.1t

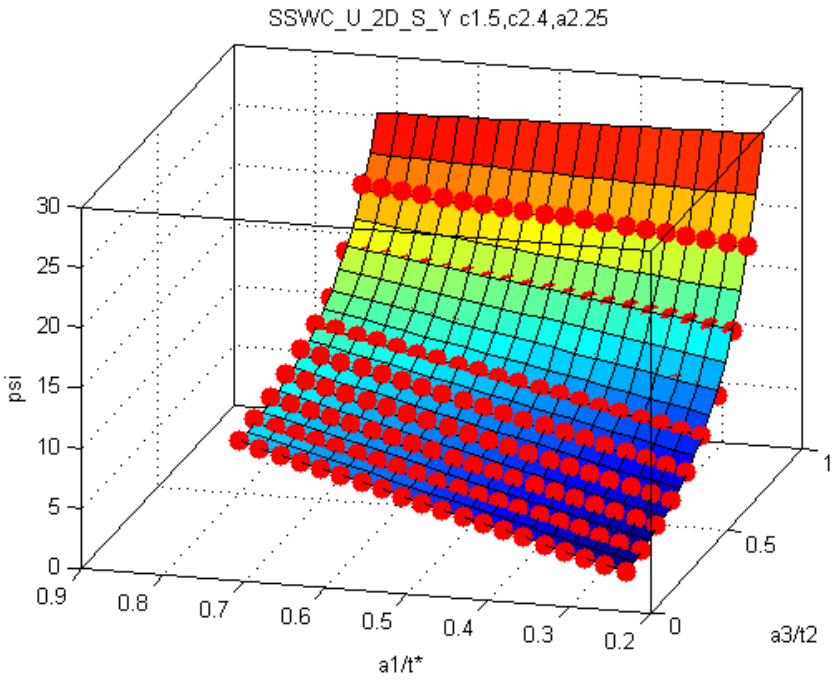

Figure 118: SSWC U-Crack with Width=0.5t, Symmetric General Corrosion Total Width=8t and Depth=0.25t

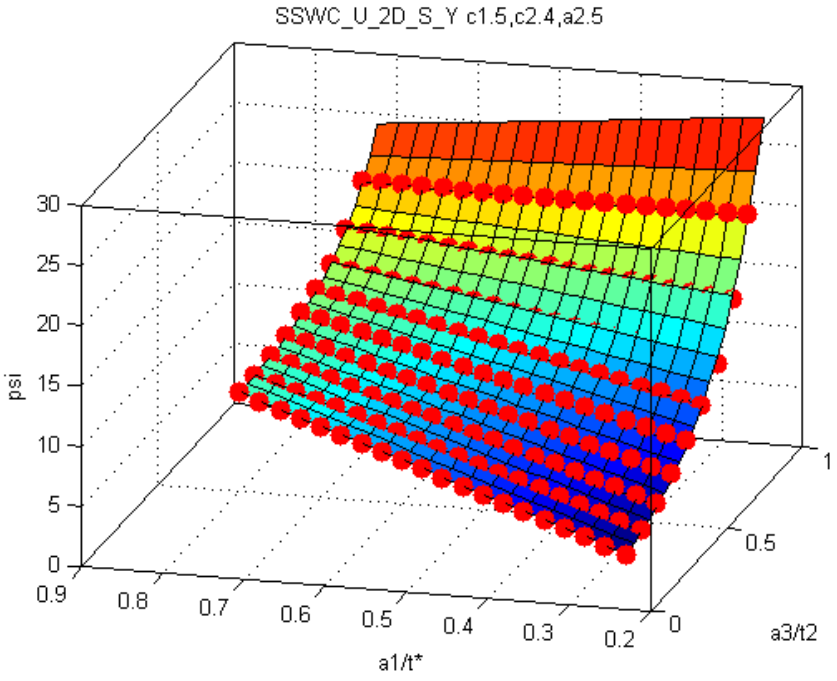

Figure 119: SSWC U-Crack with Width=0.25t, Symmetric General Corrosion Total Width=8t and Depth=0.5t

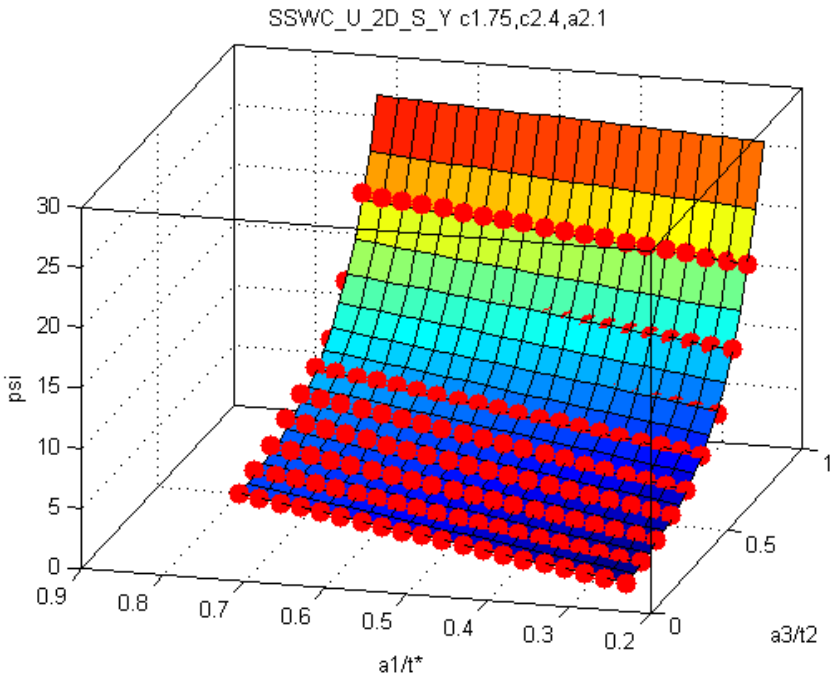

Figure 120: SSWC U-Crack with Width=0.75t, Symmetric General Corrosion Total Width=8t and Depth=0.1t

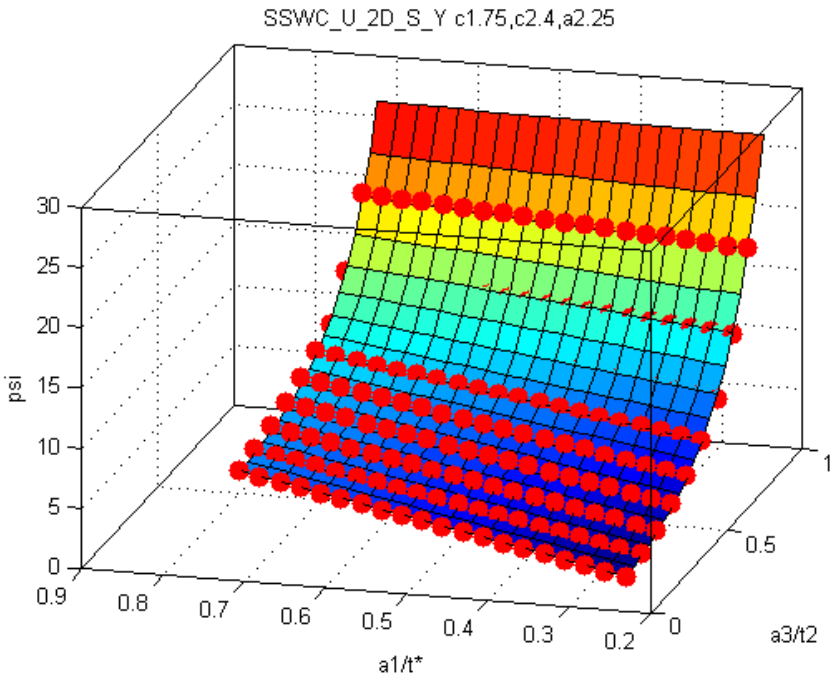

Figure 121: SSWC U-Crack with Width=0.75t, Symmetric General Corrosion Total Width=8t and Depth=0.25t

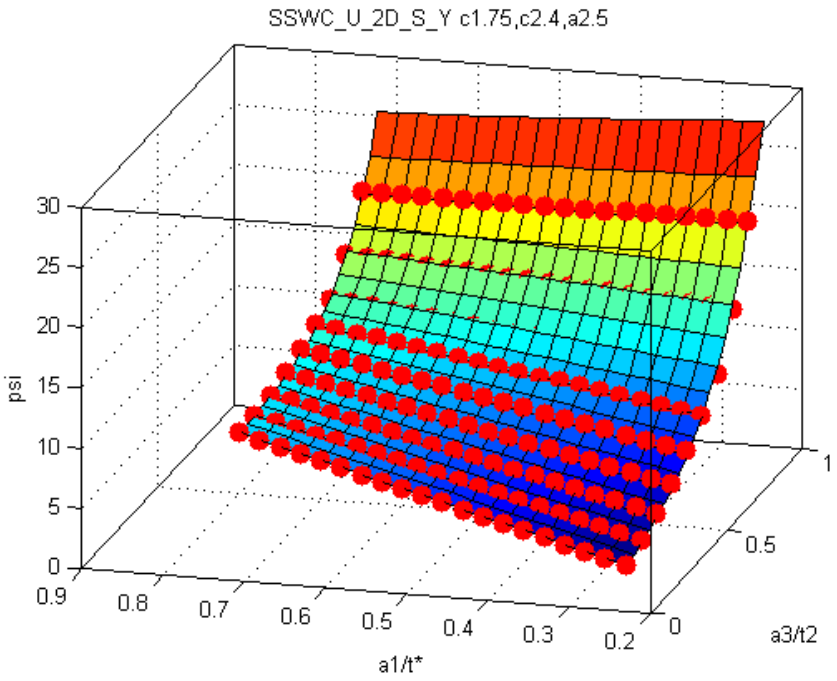

Figure 122: SSWC U-Crack with Width=0.75t, Symmetric General Corrosion Total Width=8t and Depth=0.5t